SPIN PHYSICS AND POLARIZED STRUCTURE FUNCTIONS

Bodo LAMPE[a,b], **Ewald REYA**[c]

[a] *Sektion Physik der Universität München, Theresienstr. 37, D-80333 München, Germany*
[b] *Max-Planck-Institut für Physik, Föhringer Ring 6, D-80805 München, Germany*
[c] *Institut für Physik, Universität Dortmund, D-44221, Dortmund, Germany*

ELSEVIER

AMSTERDAM – LAUSANNE – NEW YORK – OXFORD – SHANNON – TOKYO

ELSEVIER

Physics Reports 332 (2000) 1–163

PHYSICS REPORTS

www.elsevier.com/locate/physrep

Spin physics and polarized structure functions

Bodo Lampe[a,b], Ewald Reya[c,*]

[a]*Sektion Physik der Universität München, Theresienstr. 37, D-80333 München, Germany*
[b]*Max-Planck-Institut für Physik, Föhringer Ring 6, D-80805 München, Germany*
[c]*Institut für Physik, Universität Dortmund, D-44221 Dortmund, Germany*

Received September 1999; editor: W. Weise

Contents

* Corresponding author.
E-mail address: reya@hal1.physik.uni-dortmund.de (E. Reya).

PII: S0370-1573(99)00100-3

Abstract

A review on the theoretical aspects and the experimental results of polarized deep inelastic scattering and of other hard scattering processes is presented. The longitudinally polarized structure functions are introduced and cross section fromulae are given for the case of photon as well as $W^{\pm}$ and Z^0 exchange. Results from the SLAC and CERN polarization experiments are shown and compared with each other as well as their implications for the integrated $g_1(x,Q^2)$ are reviewed. More recent experiments presently underway (like HERMES at DESY) and future projects (like RHIC at BNL, HERA-$\vec{N}$ and a polarized HERA collider at DESY) are discussed too. The QCD interpretation and the LO and NLO Q^2-evolution of g_1, i.e. of the longitudinally polarized parton densities, is discussed in great detail, in particular the role of the polarized gluon density, as well as the expectations for $x \to 0$. Particular emphasis is placed on the first moment of the polarized structure function in various factorization schemes, which is related to the axial anomaly, and on its relevance for understanding the origin of the proton spin. Sum rules (i.e. relations between moments of the structure functions) are derived and compared with recent experimental results. Various other phenomenological applications are discussed as well, in particular the parametrizations of polarized parton densities as obtained from recent data and their evolution in Q^2. Furthermore, jet, heavy quark and direct photon production are reviewed as a sensitive probe of the polarized gluon density, and the physics prospects of the future polarized experiments at RHIC ($\vec{p}\vec{p}$) and a polarized HERA collider ($\vec{e}\vec{p}$) are studied. DIS semi-inclusive asymmetries and elastic neutrino–proton scattering are reviewed, which will help to disentangle the various polarized flavor densities in the nucleon. The status of single- and double-spin asymmetries, and the observation of handedness in the final state, are discussed as well. Structure functions for higher spin hadrons and nuclei are defined and possible nuclear effects on high energy spin physics are reviewed. The theoretical concept of spin-dependent parton distributions and structure functions of the polarized photon is presented and possibilities for measuring them are briefly discussed. Various nonperturbative approaches to understand the origin of the proton spin are reviewed, such as the isosinglet $U_A(1)$ Goldberger–Treiman relation, lattice calculations and the chiral soliton model of the nucleon. The physical interpretation and model calculations of the transverse structure function g_2 are presented, as well as recent twist-3 measurements thereof, and the Burkhardt–Cottingham sum rule is revisited. Finally, the physics of chiral-odd 'transversity' distributions is described and experimental possibilities for delineating them are reviewed, which will be important for a complete understanding of the leading twist-2 sector of the nucleon's parton structure. In the appendix the full two-loop anomalous dimensions and Altarelli–Parisi splitting functions governing the Q^2-evolution of the structure function g_1 are given.

PACS: 13.88. + e

1. Introduction

One of the most fundamental properties of elementary particles is their spin because it determines their symmetry behavior under space-time transformations. The spin degrees of freedom may be used in high-energy experiments to get information on the fundamental interactions which are more precise than those obtained with unpolarized beams. For example, the SLC experiment at SLAC is able to determine $\sin^2\theta_W$ with a higher precision by using polarized e^+e^- beams than current experiments at LEP with unpolarized beams (for a recent review see, e.g., [522]).

Another aspect of polarization is the question how the spin of non-point-like objects like the nucleons is composed of the spins of its constituents, the quarks and gluons. This question can best be answered in high-energy experiments because the quarks and gluons behave as (almost) free particles at energy/momentum-scales $Q \gg \Lambda_{\rm QCD}$. It is possible to attribute numbers $\Delta\Sigma$ and Δg to the quark and gluon spin content of the nucleons which describe their total (integrated) contribution to the nucleon spin in the following sense [381,395,396]:

$$\tfrac{1}{2} = \tfrac{1}{2}\Delta\Sigma + \Delta g + L_z \tag{1.1}$$

where on the left-hand side we have the spin ($+\frac{1}{2}$) of a polarized nucleon state and on the right hand side a decomposition in terms of $\Delta\Sigma(Q^2)$, $\Delta g(Q^2)$ and the relative orbital angular momentum $L_z(Q^2)$ among all the quarks [529,530] and gluons. Furthermore, $\Delta\Sigma = \Delta u + \Delta d + \Delta s + \Delta\bar{u} + \cdots$ can be further decomposed into the contributions from the various quark species which will be discussed in more detail in Sections 4–6.

Unfortunately, the decomposition (1.1) cannot directly be measured in experiments. Instead various other combinations of $\Delta\Sigma$ and Δg appear in experimental observables. The predominant role in the development of understanding the spin structure of nucleons is played by the deep inelastic leptoproduction processes $\ell N \to \ell' X$ (Fig. 1) because of their unique simplicity: The processes are initiated by leptons and are totally inclusive in the hadronic final state. More than 25 years ago Bjorken [118,119] and others [333,253,254] have anticipated the significance of these processes for the understanding of the nucleon spin structure. But only recently, experiments have become precise enough to test some of the theoretical ideas developed so far. Two earlier experiments at SLAC [43,104,105] and CERN [490,77,78] were followed by new results from both

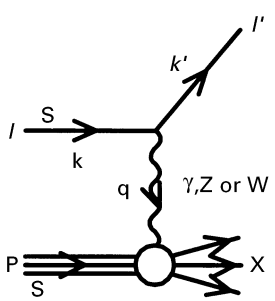

Fig. 1. The basic polarized deep inelastic scattering process.

laboratories in the recent years. Whether or not there is agreement between the new CERN and SLAC data will be discussed in detail and commented in the course of this work. Furthermore, the Hermes experiment which takes place in the DESY-HERA tunnel [207,208,232] has, more recently, also provided us with precision measurements of proton and neutron spin structure functions [12,41].

In Section 2 we summarize all relevant expressions for polarized DIS cross sections and structure functions for neutral and charged electroweak currents. Previous and recent results of longitudinally polarized DIS experiments for $g_1^N(x,Q^2)$ are presented and compared with each other in Section 3. The LO and NLO QCD renormalization group evolution of $g_1(x,Q^2)$ and of longitudinally polarized parton densities $\delta f(x,Q^2)$ are derived in Section 4, as well as their small-x behavior. Section 5 is devoted to the first moment (i.e. total helicities) of longitudinally polarized parton densities and of g_1 in various factorization schemes which is related to the axial anomaly and its relevance for understanding the origin of the proton spin. Here, the Bjorken and Drell–Hearn–Gerasimov sum rules are derived and compared with recent experimental results as well.

Section 6 includes most of the phenomenological aspects relevant for longitudinally polarized processes. We start in Section 6.1 with a brief historical review of 'naive' parton model expectations for polarized parton densities; then we turn to recent developments for determining $\delta f(x,Q^2)$ in LO and NLO from recent data on $g_1^{p,n}(x,Q^2)$ and the implications for their first moments (total helicities). Here we also discuss briefly the present status of the orbital component $L_z = L_q + L_g$ in (1.1), such as the Q^2-evolution equations for $L_{q,g}(Q^2)$ and how one might possibly relate them to measurable observables. In addition, hard processes initiated by doubly (singly) polarized hadron–hadron collisions such as the production of heavy quarks, of large-p_T photons and jets and of Drell–Yan dimuons will be also suitable to measure the polarized parton distributions $\delta f(x,Q^2), f = q, \bar{q}, g$, in particular the gluon distribution $\delta g(x,Q^2)$. Details will be discussed in the various subsections of Section 6. Furthermore, polarized ep and e^+e^- collisions can also shed light on the so far unmeasured polarized parton densities of the photon which are theoretically formulated and discussed in Section 6.12.

Various nonperturbative approaches to understand the origin of the proton spin are presented in Section 7, such as the isosinglet Goldberger–Treiman relation, lattice calculations and the chiral soliton model of the nucleon. Finally structure functions resulting from transverse polarizations are dealt with in Section 8. In Section 8.1 the theoretical concepts and model calculations of the transverse structure function $g_2(x,Q^2)$ are presented as well as recent twist-3 measurements thereof, and the Burkhardt–Cottingham sum rule is revisited. The physics of the chiral-odd 'transversity' distributions is described in Section 8.2 and experimental possibilities for delineating them are reviewed. It should be remembered that a complete understanding of the leading twist-2 parton structure of the nucleon requires, besides the unpolarized and longitudinally polarized parton densities $f(x,Q^2)$ and $\delta f(x,Q^2)$, also the knowledge of the transversity densities $\delta_T q(x,Q^2)$ which are experimentally entirely unknown so far.

The full two-loop polarized Altarelli–Parisi splitting functions $\delta P_{ij}^{(1)}(x)$ and their Mellin n-moments (anomalous dimensions) $\delta P_{ij}^{(1)n}$, governing the Q^2-evolution of $g_1(x,Q^2)$ and $\delta f(x,Q^2)$, are summarized in the appendix.

1.1. Polarization of a Dirac particle

Let us start with a few basic facts about the polarization of a relativistic spin $\frac{1}{2}$ particle. A free Dirac particle of four-momentum p and mass m is described by a four-component spinor $u(p,s)$ which satisfies the equation

$$(\not{p} - m)u(p,s) = 0 \ , \tag{1.2}$$

where $\not{p} = \gamma_\mu p^\mu$. The polarization vector s is a pseudovector which fulfils $s^2 \equiv (s^0)^2 - (\boldsymbol{s})^2 = -1$ and $sp = 0$. The projection operator onto a state with polarization s is known to be

$$P(s) = \tfrac{1}{2}(1 + \gamma_5 \not{s}) \ . \tag{1.3}$$

The transformation properties of s are given in Table 1 where we consider two Dirac particles which move along the z-direction in the lab frame, one of it with transverse and the other one with longitudinal polarization. The transverse polarization vector is not changed when going from the rest frame to the lab frame, but the longitudinal is. The important point to notice is that at high energies $E \gg m$ the product ms_{L} remains finite and converges to p:

$$ms_{\mathrm{L}} \underset{E\to\infty}{\sim} p \ . \tag{1.4}$$

This fact will be used repeatedly in later applications.

2. The polarized structure functions

2.1. Basics of pure photon exchange

First we consider Fig. 1 with photon exchange only. We assume that *both* the incoming lepton *and* the incoming nucleon are polarized (polarization vectors s^μ and S^μ). We shall see below why this is important. The procedure for polarized particles is analogous to the case of unpolarized particles, i.e. the cross section is a product of a leptonic tensor $L_{\mu\nu}$ which is known (cf. Fig. 2) and a hadronic tensor $W^{\mu\nu}$ which can be expanded into Lorentz covariants whose coefficients define the structure functions which are to be measured. In unpolarized $e(\mu)N$ scattering one has the

Table 1
A transverse and a longitudinal polarized Dirac particle in their rest and laboratory frame

	Transverse polarization	Longitudinal polarization
Rest frame $p = (m,0,0,0)$	$s_{\mathrm{T}} = (0,1,0,0)$	$s_{\mathrm{L}} = (0,0,0,1)$
Lab frame $p = (E,0,0,\sqrt{E^2-m^2})$	$s_{\mathrm{T}} = (0,1,0,0)$	$s_{\mathrm{L}} = \frac{1}{m}(\sqrt{E^2-m^2},0,0,E)$

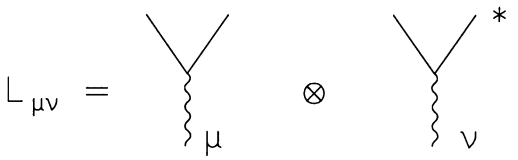

Fig. 2. The definition of the lepton tensor.

well-known functions F_1 and F_2 whereas for polarized particles two additional functions g_1 and g_2 arise:

$$W_{\mu\nu} = \int \mathrm{d}^4x \mathrm{e}^{\mathrm{i}qx} \langle PS|J_\mu(x)J_\nu(0)|PS\rangle$$

$$= W_{\mu\nu}(\text{sym.}) + \mathrm{i}\frac{M}{Pq}\varepsilon_{\mu\nu\rho\sigma}q^\rho\left[S^\sigma g_1(x,Q^2) + \left(S^\sigma - \frac{Sq}{Pq}P^\sigma\right)g_2(x,Q^2)\right] \tag{2.1}$$

$\varepsilon_{\mu\nu\rho\sigma}$ is the totally antisymmetric tensor in four dimensions, $\varepsilon_{0123} = 1$, $\varepsilon_{1023} = -1$, etc., and the polarization vector of the proton is normalized to $S^2 = -1$. Note that there is no analogy $F_{1,2} \leftrightarrow g_{1,2}$ because the contribution of g_2 to the cross section vanishes in the limit of ultra-relativistic on-shell quarks ($S^\sigma \sim P^\sigma$) since there are not enough four vectors available anymore to form an antisymmetric combination in Eq. (2.1). Furthermore $Q^2 = -q^2$ and $x = Q^2/2Pq$ are the usual (Bjorken) variables of the DIS process. It is not entirely trivial to see that (2.1) is the most general form of the antisymmetric hadron tensor. One has to make use of the ε-identity

$$g^{\alpha\beta}\varepsilon^{\mu\nu\rho\sigma} = g^{\alpha\mu}\varepsilon^{\beta\nu\rho\sigma} + g^{\alpha\nu}\varepsilon^{\mu\beta\rho\sigma} + g^{\alpha\rho}\varepsilon^{\mu\nu\beta\sigma} + g^{\alpha\sigma}\varepsilon^{\mu\nu\rho\beta} \tag{2.2}$$

to get rid of tensors like

$$[(p_\mu\varepsilon_{\nu\alpha\beta\rho} - p_\nu\varepsilon_{\mu\alpha\beta\rho})q^\rho + p\cdot q\varepsilon_{\mu\nu\alpha\beta}]S^\alpha p^\beta \ . \tag{2.3}$$

The incoming lepton (Fig. 1) is assumed to be polarized too. Why is that necessary? To see that let us have a look at the lepton tensor

$$L_{\mu\nu} = tr[(1+\gamma_5 \not{s})(\not{k} + m_l)\gamma_\mu(\not{k}' + m_l)\gamma_\nu] \ . \tag{2.4}$$

Obviously, $L_{\mu\nu}$ consists of a part independent of the lepton polarization s^β and a part linear in s^β, the former being symmetric in μ and ν, the latter antisymmetric:

$$L_{\mu\nu} = L_{\mu\nu}(\text{sym.}) + 2\mathrm{i}m_l\varepsilon_{\mu\nu\alpha\beta}q^\alpha s^\beta \ . \tag{2.5}$$

The antisymmetry of the last term is due to the γ_5 in (1.3) and to the vector coupling of the photon to fermions. With the symmetric part alone in Eq. (2.5), g_1 and g_2 cannot be extracted from Eq. (2.1). One needs the antisymmetric part, i.e. the lepton polarization.

From (2.5) it seems that all polarization effects are suppressed at high energy by a factor m_l. However, in the case of longitudinal polarization one has $m_l s^\beta \to k^\beta$ [according to (1.4)] and thus there is no suppression by factors of m_l. In the following we shall always presume the leptons to be longitudinally polarized.

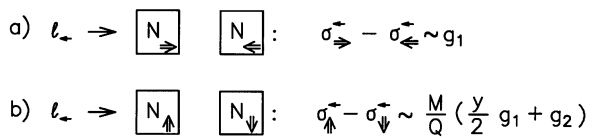

Fig. 3. The basic form of the polarized experiments.

How to measure g_1 and g_2? The cross section $\sigma \sim L_{\mu\nu} W^{\mu\nu}$ will be of the form

$$L_{\mu\nu} W^{\mu\nu} = L_{\mu\nu}\ (\text{sym.})\ W^{\mu\nu}(\text{sym.})\ + L_{\mu\nu}\ (\text{antisym.})\ W^{\mu\nu}\ (\text{antisym.})\ . \tag{2.6}$$

One should try to get rid of the first term in (2.6) because it is the cross section for unpolarized scattering. One possibility is to consider differences of cross sections with nucleons of opposite polarization [161,356,375,63,512] as is depicted in Fig. 3. In both parts of the figure one starts with a beam of high energetic leptons with left-handed helicity (= longitudinally polarized with spin vector antiparallel to the direction of motion). This beam is sent to two nucleon probes with opposite longitudinal polarization, i.e. with their spins along the direction of the lepton beam and opposite to it, and to two probes with opposite transverse polarization. In the difference of the cross sections [part (a) of Fig. 3] the unpolarized structure functions drop out and only g_1 survives (with respect to the suppressed $(2yx^2M^2/Q^2)g_2$ contribution, where $y = Pq/Pk$), i.e. g_1 can in principle be uniquely determined from measuring this difference. Similarly, in the difference of cross sections obtained from part (b) of Fig. 3, the transverse polarization case ($kS = \boldsymbol{k}\cdot\boldsymbol{S} = 0$), the sum $(y/2)g_1 + g_2$ appears. However, there is an overall suppression factor $2xM/\sqrt{Q^2}$, where M is the nucleon mass so that g_2 can be obtained only from rather low-energy experiments. The appearance of this factor has, of course, to do with the transverse polarization. We can take the fact that g_2 appears only in cross sections with transverse polarized nucleons as a hint that it is difficult to accomodate g_2 in the parton model. There is no notion of transversality in the conventional parton model. We shall come back to this 'transverse spin structure function' in Section 8.

2.2. Quantitative formulae for pure photon exchange

To be more specific let us write down the most general cross section difference relevant for polarized deep inelastic fixed target ℓN scattering [375,63,549]:

$$\frac{\mathrm{d}^3[\sigma(\alpha)-\sigma(\alpha+\pi)]}{\mathrm{d}x\,\mathrm{d}y\,\mathrm{d}\phi} = \frac{8\alpha^2}{Q^2}\left\{\cos\alpha\left[\left(1-\frac{y}{2}-\frac{y^2\gamma^2}{4}\right)g_1(x,Q^2)-\frac{y}{2}\gamma^2 g_2(x,Q^2)\right]\right.$$
$$\left. -\ \sin\alpha\cos\phi\gamma\sqrt{1-y-\frac{y^2\gamma^2}{4}}\left[\frac{y}{2}g_1(x,Q^2)+g_2(x,Q^2)\right]\right\}. \tag{2.7}$$

This formula comprehends all information from the antisymmetric part of the tensor Eq. (2.1) where α is the angle between the lepton beam momentum vector $\boldsymbol{k}$ and the nucleon-target polarization vector $\boldsymbol{S}$, ϕ is the angle between the k–S plane and the $k - k'$ lepton scattering plane

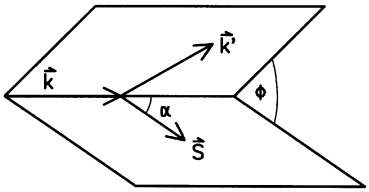

Fig. 4. The geometry of the polarized deep inelastic scattering process in the lab frame.

(cf. Fig. 4), $\gamma = 2Mx/\sqrt{Q^2}$ and a scaling limit has not been taken. From Eq. (2.7) it is obvious that effects associated with g_2 are suppressed (at least) by a factor $2M/\sqrt{Q^2}$ with respect to the leading terms.

More convenient than differences of cross sections are asymmetries

$$A(\alpha) = (\sigma(\alpha) - \sigma(\alpha + \pi))/(\sigma(\alpha) + \sigma(\alpha + \pi)) \tag{2.8}$$

as, for example, the longitudinal asymmetry

$$A_L = (\sigma^{\leftarrow}_{\Rightarrow} - \sigma^{\leftarrow}_{\Leftarrow})/(\sigma^{\leftarrow}_{\Rightarrow} + \sigma^{\leftarrow}_{\Leftarrow}) \tag{2.9}$$

obtained for $\alpha = 0$, and the transverse asymmetry A_T obtained for $\alpha = \pi/2$ and an asymmetric integration over ϕ.

A_L picks up the coefficient of $\cos\alpha$ in Eq. (2.7) whereas A_T picks up the coefficient of $\sin\alpha\cos\phi$. Events with ϕ near $\pi/2$ or $3\pi/2$ (where the nucleon spin is perpendicular to the scattering plane) can be obviously neglected in the determination of A_T; they are not a good measure of $g_2 + yg_1/2$.

The really interesting quantities are the virtual photon asymmetries

$$A_1 = (\sigma_{1/2} - \sigma_{3/2})/(\sigma_{1/2} + \sigma_{3/2}) \tag{2.10}$$

and

$$A_2 = (2\sigma_{TL})/(\sigma_{1/2} + \sigma_{3/2}) \tag{2.11}$$

where $\sigma_{1/2}$ and $\sigma_{3/2}$ are the virtual photoabsorbtion cross sections when the projection of the total angular momentum of the photon–nucleon system along the incident lepton direction is 1/2 and 3/2. Note that $\sigma_T = \frac{1}{2}(\sigma_{1/2} + \sigma_{3/2})$ and that the term σ_{TL} arises from the interference between transverse and longitudinal amplitudes. The significance of these quantities will be clarified in Section 2.3.

A_1 and A_2 can be related, via the optical theorem, to the measured quantities A_L and A_T , or, equivalently, to the structure functions by means of the following relations:

$$A_L = D(A_1 + \eta A_2) \,, \tag{2.12}$$

$$A_T = d(A_2 - \xi A_1) \,, \tag{2.13}$$

with

$$A_1 = (g_1 - \gamma^2 g_2)/F_1 \,, \tag{2.14}$$

$$A_2 = \gamma(g_1 + g_2)/F_1 \,. \tag{2.15}$$

The kinematic factors D, d and η, ξ are defined by

$$D = \frac{y(2-y)}{y^2 + 2(1-y)(1+R)} ,$$
$$\eta = 2\gamma(1-y)/(2-y) ,$$
$$d = D\sqrt{\frac{2\varepsilon}{1+\varepsilon}} ,$$
$$\xi = \eta(1+\varepsilon)/2\varepsilon \tag{2.16}$$

with

$$\varepsilon = (1-y)/(1-y+y^2/2) \tag{2.17}$$

being the degree of transverse polarization of the virtual photon. D and d can be regarded as depolarization factors of the virtual photon. Note that η and ξ are of order $M/\sqrt{Q^2}$. Finally, R is the ratio of cross sections for longitudinally and transversely polarized virtual photons on an unpolarized target, defined by

$$2xF_1(x,Q^2) = F_2(x,Q^2)(1+\gamma^2)/(1+R(x,Q^2)) . \tag{2.18}$$

Note that in the limit $\gamma^2 \equiv 4M^2x^2/Q^2 \ll 1$,

$$R = F_L/2xF_1 \tag{2.19}$$

where $F_L \equiv F_2 - 2xF_1$. Furthermore, in the leading logarithmic order of QCD one arrives asymptotically at the well-known Callan–Gross relation $2xF_1(x,Q^2) = F_2(x,Q^2)$.

2.3. A look at the forward Compton scattering amplitude

Let us now briefly discuss the implications of the optical theorem on polarized DIS. The hadron tensor, Eq. (2.1), is the absorptive part (imaginary part) of the forward Compton scattering amplitude. This amplitude in general has a decomposition into four independent amplitudes which one may choose as

$$\tfrac{1}{2}[T(1+\tfrac{1}{2}\to 1+\tfrac{1}{2}) + T(1-\tfrac{1}{2}\to 1-\tfrac{1}{2})] , \tag{2.20}$$
$$T(0+\tfrac{1}{2}\to 0+\tfrac{1}{2}) , \tag{2.21}$$
$$\tfrac{1}{2}[T(1+\tfrac{1}{2}\to 1+\tfrac{1}{2}) - T(1-\tfrac{1}{2}\to 1-\tfrac{1}{2})] , \tag{2.22}$$
$$T(0+\tfrac{1}{2}\to 1-\tfrac{1}{2}) . \tag{2.23}$$

Their degrees of freedom correspond to the four structure functions F_1, F_2, g_1 and g_2. More precisely, the combinations (2.20)–(2.23) correspond [356,186,357,440] via the optical theorem, to F_1, F_L, $g_1 - \gamma^2 g_2$ and $\gamma(g_1 + g_2)$, respectively.

There are rigorous theoretical limits on the virtual photon asymmetries A_1 and A_2 in Eqs. (2.10) and (2.11) namely

$$|A_1| \le 1, \tag{2.24}$$

$$|A_2| \leq \sqrt{R}\ . \tag{2.25}$$

These inequalities follow from the hermiticity of the electromagnetic current

$$J_\mu = J_\mu^+ \tag{2.26}$$

which implies

$$a_\mu^* a_\nu W^{\mu\nu} \geq 0 \tag{2.27}$$

for any complex vector a_μ. Suitable choices of a_μ lead to the above inequalities.

2.4. Effects of weak currents

Until now we have restricted ourselves to photon exchange only, i.e. to the processes $eN \to eX$, $\mu N \to \mu X$, at momenta $Q \ll m_Z$, and have found two polarized structure functions g_1 and g_2. If we take into account $W^\pm$ and Z exchange, three parity violating polarized structure functions usually called g_3, g_4 and g_5 arise in addition. They will appear, for example, in the scattering of neutrinos on polarized nucleons $\nu N \to \ell' X$ but become also important for the polarized extension of HERA at large values of Q^2. Explicitly, the hadron tensor has the form [218,62,432,571,472–474]

$$\begin{aligned} W_{\mu\nu} = W_{\mu\nu}(S=0) + \frac{M}{Pq}\Bigg\{ & \mathrm{i}\varepsilon_{\mu\nu\rho\sigma} q^\rho S^\sigma g_1 + \mathrm{i}\varepsilon_{\mu\nu\rho\sigma} q^\rho \left(S^\sigma - \frac{Sq}{Pq} P^\sigma \right) g_2 + qS\left(-g_{\mu\nu} + \frac{q_\mu q_\nu}{q^2} \right) g_3 \\ & + \frac{qS}{Pq}\left(P_\mu - \frac{Pq}{q^2} q_\mu \right)\left(P_\nu - \frac{Pq}{q^2} q_\nu \right) g_4 \\ & + \frac{1}{2}\left[\left(P_\mu - \frac{Pq}{q^2} q_\mu \right)\left(S_\nu - \frac{qS}{q^2} q_\nu \right) + \left(P_\nu - \frac{Pq}{q^2} q_\nu \right)\left(S_\mu - \frac{qS}{q^2} q_\mu \right) \right] g_5 \Bigg\}\ . \end{aligned} \tag{2.28}$$

In this expression g_1, g_3 and $g_4 + g_5$ are the 'longitudinal' structure functions which survive in the high energy limit, and g_2 and $g_4 - g_5$ are the transverse ones. The appearance of symmetric tensors which are linear in S^μ is due to the axial vector component of the $W^\pm$ and Z couplings to fermions. Notice that terms proportional to q^μ or q^ν can be dropped in the definition of $W_{\mu\nu}$ because they give no contribution in the limit $m_l/E \to 0$ when contracted with the appropriate lepton tensors $L_{\mu\nu}$.

If one considers longitudinally polarized nucleons ($S^\mu \sim P^\mu$), the structure functions g_2 and $g_4 - g_5$ are clearly not of interest. The cross section difference $\sigma^{\leftarrow}_{\Rightarrow} - \sigma^{\leftarrow}_{\Leftarrow}$ of part (a) of Fig. 3 will measure a linear combination [63,218,62] of g_1, g_3 and $g_4 + g_5$ with coefficients depending on the vector and axial vector couplings of the W/Z to the lepton.

Let us first consider *neutrino* nucleon scattering. Here the lepton tensor is the same for the polarized and the unpolarized case:

$$L_{\mu\nu}(\text{long. pol.}) = L_{\mu\nu}(\text{unpol.}) = 2(k'_\mu k_\nu + k'_\nu k_\mu - g_{\mu\nu} k k' + \mathrm{i}\varepsilon_{\mu\nu\alpha\beta} k^\alpha k'^\beta) \tag{2.29}$$

because the νW^+-interaction is $V-A$ so that the neutrino is forced to be left-handed. As a result

$$L_{\mu\nu}(\text{long. pol.})W^{\mu\nu}(\text{long.pol.}) = L_{\mu\nu}(\text{unpol.})W^{\mu\nu}(\text{unpol.})|_{F_3\to g_1, F_1\to g_3, F_2\to g_4+g_5} \ , \tag{2.30}$$

i.e. one can formally get the polarization cross section $(\sigma^{\leftarrow}_{\Rightarrow} - \sigma^{\leftarrow}_{\Leftarrow})^{\nu N}$ by taking the well-known $\nu N \to l^- X$ cross section for unpolarized beams and replace the unpolarized structure functions F_i by the polarized ones (here $g_i \equiv g_i^{\nu N}$ and $F_i \equiv F_i^{\nu N}$ are the structure functions specific to νN-scattering):

$$\frac{\mathrm{d}^2(\sigma^{\leftarrow}_{\Rightarrow} - \sigma^{\leftarrow}_{\Leftarrow})^{\nu N}}{\mathrm{d}x\,\mathrm{d}y} = \frac{G_F^2 s}{2\pi}\frac{1}{(1+Q^2/m_W^2)^2}\left\{y\left(1-\frac{y}{2}-\frac{xyM}{2E}\right)xg_1^{\nu N} - \frac{x^2yM}{E}g_2^{\nu N}\right.$$
$$\left. + \ y^2x\left(1+\frac{xM}{E}\right)g_3^{\nu N} + \left(1-y-\frac{xyM}{2E}\right)\left[\left(1+\frac{xM}{E}\right)g_4^{\nu N} + g_5^{\nu N}\right]\right\}, \tag{2.31}$$

where $s = 2ME$ in the nucleon's rest frame. In contrast, if the nucleon is transversely polarized one finds

$$\mathrm{d}(\sigma^{\leftarrow}_{\Uparrow} - \sigma^{\leftarrow}_{\Downarrow})^{\nu N} \sim L_{\mu\nu}(\text{long. pol.})W^{\mu\nu}(\text{transv. pol.}) \ , \tag{2.32}$$

i.e.

$$\frac{\mathrm{d}^2(\sigma^{\leftarrow}_{\Uparrow} - \sigma^{\leftarrow}_{\Downarrow})^{\nu N}}{\mathrm{d}x\,\mathrm{d}y} = \frac{MG_F^2}{16\pi^2}\frac{1}{(1+Q^2/m_W^2)^2}\sqrt{xyM[2(1-y)E-xyM]}\left\{-2xy\left(\frac{y}{2}g_1^{\nu N}+g_2^{\nu N}\right)\right.$$
$$\left. + \ xy^2g_3^{\nu N} + \left(1-y-\frac{xyM}{2E}\right)g_4^{\nu N} - \frac{y}{2}g_5^{\nu N}\right\}. \tag{2.33}$$

To obtain this result one should make use of the relations $kS = 0$ (transverse polarization), $PS = 0, kP = Pq/y$, $2kq = q^2, P^2 = k^2 = 0$ and $x = Q^2/2Pq$. In Eq. (2.33) we recognize the term $\sim (y/2)g_1 + g_2$ which was mentioned already earlier for the case of pure γ-exchange. Note that the transverse cross section is suppressed by M/Q with respect to the longitudinal cross section in (2.31).

The corresponding cross section for antineutrinos, $\bar{\nu}N \to l^+X$ (W^- exchange) can be obtained by reversing the sign of g_1 and g_2 in Eqs. (2.31) and (2.33). Note that, to get a nonvanishing effect, one must have $kS = 0$ but $qS \neq 0$.

In Sections 4 and 6 a physical (parton model) interpretation will be given for the structure functions g_1, g_3 and $g_4 + g_5$. It should be stressed that until today no satisfactory physical model exists for the 'transverse' structure functions g_2 and $g_4 - g_5$.

We now turn to neutral and charged current interactions initiated by charged *leptons*, since neutrino-induced reactions on polarized targets are not very realistic, because large nucleon targets are difficult to polarize. For sufficiently large Q^2, charged (and neutral) current exchange occurs in $l^\pm$-induced processes as well. As will become clear later, such an experiment would yield some very important information on the polarized parton densities and will therefore hopefully be carried out in the next century.

One has separate cross sections for charged and neutral current exchange. For the charged current processes, $lN \to \nu N$ one can take over the results from above, Eqs. (2.31) and (2.33). For the neutral current the cross section consists of three terms, for γ-, for Z-exchange and for γ-Z-interference,

$$\mathrm{d}\sigma \sim \eta^{\gamma\gamma} L^{\gamma\gamma}_{\mu\nu} W^{\mu\nu\gamma\gamma} + \eta^{\gamma Z} L^{\gamma Z}_{\mu\nu} W^{\mu\nu\gamma Z} + \eta^{ZZ} L^{ZZ}_{\mu\nu} W^{\mu\nu ZZ} \,, \tag{2.34}$$

where

$$L^{\gamma\gamma}_{\mu\nu} = 2(k'_\mu k_\nu + k'_\nu k_\mu - g_{\mu\nu} k k' - \mathrm{i}\lambda \varepsilon_{\mu\nu\alpha\beta} k^\alpha k'^{\,\beta}) \,, \tag{2.35}$$

$$L^{\gamma Z}_{\mu\nu} = (v_l - \lambda a_l) L^{\gamma\gamma}_{\mu\nu} \,, \tag{2.36}$$

$$L^{ZZ}_{\mu\nu} = (v_l - \lambda a_l)^2 L^{\gamma\gamma}_{\mu\nu} \tag{2.37}$$

$v_l = -\frac{1}{2} + 2s^2_W$ and $a_l = -\frac{1}{2}$ are the Z–l^--couplings and $\lambda = \pm 1$ is the helicity of the incoming lepton. Furthermore, we have defined

$$\eta^{\gamma\gamma} = 1 \,, \tag{2.38}$$

$$\eta^{\gamma Z} = \frac{G_F m_Z^2}{2\sqrt{2}\pi\alpha} \frac{1}{(1 + Q^2/m_Z^2)^2} \,, \tag{2.39}$$

$$\eta^{ZZ} = \left(\frac{G_F m_Z^2}{2\sqrt{2}\pi\alpha} \frac{1}{(1 + Q^2/m_Z^2)^2} \right)^2 . \tag{2.40}$$

Note that $G_F m_Z^2/2\sqrt{2}\pi\alpha = 1/4 s^2_W c^2_W \approx 1.4$ and $2ME = s$. All three hadron tensors $W^{\gamma\gamma}$, $W^{\gamma Z}$ and W^{ZZ} have an expansion of the form of Eq. (2.28), but of course for $W^{\gamma\gamma}$ one has $g^{\gamma\gamma}_3 = g^{\gamma\gamma}_4 = g^{\gamma\gamma}_5 = 0$ due to parity conservation. All in all, there are 12 free independent polarized structure functions, among them seven ($g^{\gamma\gamma}_1$, $g^{\gamma Z}_1$, g^{ZZ}_1, $g^{\gamma Z}_3$, g^{ZZ}_3, $g^{\gamma Z}_{4+5}, g^{ZZ}_{4+5}$) with and five without a parton model interpretation.

The neutral current cross section for longitudinally polarized leptons is given by [62]

$$\begin{aligned} \frac{\mathrm{d}^2\sigma^{lN}_{\mathrm{NC}}}{\mathrm{d}x\,\mathrm{d}y}(\lambda, S = S_{\mathrm{L}}) = 4\pi ME y \frac{\alpha^2}{Q^4} \sum_{i=\gamma\gamma, ZZ, \gamma Z} \eta^i C^i \Bigg\{ & 2xy\, F^i_1 + \frac{2}{y}\left(1 - y - \frac{xyM}{2E}\right)(F^i_2 + g^i_5) \\ & - 2\lambda x\left(1 - \frac{y}{2}\right) F^i_3 - 2\lambda x\left(2 - y - \frac{xyM}{E}\right) g^i_1 - \frac{2}{y}\left(1 + \frac{xM}{E}\right)\left(1 - y - \frac{xyM}{2E}\right) g^i_4 \\ & + 4\lambda \frac{x^2 M}{E} g^i_2 + 2xy\left(1 + \frac{xM}{E}\right) g^i_3 \Bigg\} \end{aligned} \tag{2.41}$$

where, for negatively charged leptons,

$$C^{\gamma\gamma} = 1, \quad C^{\gamma Z} = v_l - \lambda a_l, \quad C^{ZZ} = (v_l - \lambda a_l)^2 \tag{2.42}$$

and for positively charged leptons one simply replaces a_l by $-a_l$. Notice that when the lepton flips its helicity, λ changes sign, and when the nucleon flips its spin, all terms containing a polarized

structure function $g_{1,2,3,4,5}$ also change sign. Upon averaging over λ and S one obtains the unpolarized cross section

$$\frac{\mathrm{d}^2\sigma^{\ell N}_{\mathrm{NC}}}{\mathrm{d}x\,\mathrm{d}y}(\mathrm{unp.}) = \frac{1}{4}\sum_{\lambda,S}\frac{\mathrm{d}^2\sigma^{\ell N}_{\mathrm{NC}}}{\mathrm{d}x\,\mathrm{d}y}(\lambda,S) = 4\pi MEy\frac{\alpha^2}{Q^4}\sum_i \eta^i C^i\left\{2xyF_1^i + \frac{2}{y}\left(1-y-\frac{xyM}{2E}\right)F_2^i\right\}, \quad (2.43)$$

where we have again used $s = 2ME$ appropriate for a fixed nucleon target in its rest frame. Alternatively, $\mathrm{d}^2\sigma/\mathrm{d}x\,\mathrm{d}Q^2$ can be simply obtained from $\mathrm{d}^2\sigma/\mathrm{d}x\,\mathrm{d}Q^2 = (1/sx)\mathrm{d}^2\sigma/\mathrm{d}x\,\mathrm{d}y$.

In the case of nucleons with transverse polarization, i.e. with a spin orthogonal to the lepton direction (z-axis) at an angle α to the x-axis, one has

$$\begin{aligned}\frac{\mathrm{d}^3\sigma^{\ell N}_{\mathrm{NC}}}{\mathrm{d}x\,\mathrm{d}y\,\mathrm{d}\phi}(\lambda, S = S_{\mathrm{T}}) = 2MEy\frac{\alpha^2}{Q^4}\sum_i \eta^i C^i\Bigg\{&2xy\,F_1^i + \frac{2}{y}\left(1-y-\frac{xyM}{2E}\right)F_2^i - 2\lambda x\left(1-\frac{y}{2}\right)F_3^i \\ &+ \frac{\sqrt{xyM[2(1-y)E - xyM]}}{E}\cos(\alpha-\phi) \\ &\times\left[-2\lambda x g_1^i - 4\lambda\frac{x}{y}g_2^i + \frac{1}{y}g_5^i + \frac{2}{y^2}\left(1-y-\frac{xyM}{2E}\right)g_4^i - 2xg_3^i\right]\Bigg\}. \end{aligned} \quad (2.44)$$

To experimentally unravel the whole set of independent structure functions one should make use of leptons of opposite charges and/or polarizations, in which cases the structure functions enter with different weights. Furthermore, use can be made of the propagator structure $1/(1 + Q^2/m_Z^2)^{0,1,2}$, so that one can separate the $\gamma\gamma$, γZ and ZZ components by measurements at different Q^2-values. We shall come back to these processes in Section 6.7 where the parton model interpretation and some phenomenological applications will be given.

3. Polarized deep inelastic scattering (PDIS) experiments

3.1. Results from old SLAC experiments

After the famous Stern–Gerlach discovery it became possible to produce and use polarized atomic beams. However, experiments with polarized *lepton* beams are a fairly recent development because before 1972 it was not possible to produce a polarized electron beam. In 1972 physicists from the Yale university succeeded in polarizing electrons by photoionization from polarized alkali atoms. This was used afterwards for elastic scattering experiments between polarized electrons and polarized atoms. As time went by, beam energies increased from the eV level to the level where deep inelastic experiments can be performed.

This is – in short – the prehistory of the SLAC experiments. The CERN experiments followed another route. They used polarized muons from high energetic pions. These muons are automatically polarized because of the weak V–A nature of the decay.

But let us start with SLAC. High energetic electrons from a polarized alkali source were used in the SLAC experiment E80 which took place in 1976 [43,104]. The electrons in this experiment with

energies between 6 and 13 GeV, scattered off a polarized butanol target, were detected by the 8 GeV spectrometer built for all DIS experiments at SLAC. Average beam and target polarizations of experiment E80 were rather high (50% resp. 60%). In the butanol target only the hydrogen atoms contribute to the polarized scattering because carbon and oxygen are spin-0 nuclei. Therefore, the effective target polarization is reduced by a 'dilution factor' $f = \frac{10}{74}$ (= ratio of number of hydrogen nucleons over total number of nucleons). This dilution effect together with other nuclear uncertainties is a problem of all present experiments. The HERMES experiment [207,208] at DESY is using a hydrogen (as well as deuterium or ^{3}He) gas target [12,41] in which this problem is absent.

The main deficiency of the E80 experiment was that its polarized source was rather limited in beam current. Nevertheless, it was possible to select about two million scattered electron events and to determine the asymmetry A_1, Eq. (2.10), for the proton for several x values between 0.1 and 0.5, and rather low values of Q^2 (about 2 GeV^2). The asymmetry turned out to be rather large, in rough agreement with expectations based on the quark-parton model [43,104].

The desire to reduce higher twist effects motivated a second SLAC experiment in 1983 (E130) [105]. This experiment was run at an electron beam energy of about 23 GeV. The beam polarization was increased to about 80% and a new Möller polarimeter was built which allowed for continuous beam polarization measurements during the experiment. The detector was improved as well so that the kinematic coverage extended in x from 0.2 to 0.65 and in Q^2 from 3.5 to 10 GeV^2. The experiment concentrated on measurements of rather high x values and consequently collected only about one million events.

In Fig. 5 the results for the proton asymmetry A_1^p are shown for E80 and E130 together. Their average of [105]

$$\Gamma_1^p(\langle Q^2\rangle \simeq 4\,\mathrm{GeV}^2) = 0.17 \pm 0.05 \quad (\mathrm{SLAC\ E80, E130}) \tag{3.1}$$

is in good agreement with the value ($\frac{5}{9}$) of the static SU(6) quark model [357,186,440] and the Ellis–Jaffe 'sum rule' [333,253,254] to be discussed in Section 5. Here we have defined the 'first moment' of g_1 by

$$\Gamma_1^{p,n}(Q^2) \equiv \int_0^1 g_1^{p,n}(x, Q^2)\,\mathrm{d}x\ . \tag{3.2}$$

However, the result (3.1) is plagued by a large error whose main source comes from the extrapolation into the unmeasured x ranges, in particular as $x \to 0$. We shall see that a discrepancy with the CERN data exists which originates from data taken at small x (between 0.01 and 0.1).

3.2. The CERN experiments

The CERN PDIS experiments were started as an addendum [490,77,78,549] to the unpolarized EMC deep inelastic muon-nucleon experiments. A polarized beam source of muons with energies $E_\mu = 100$–200 GeV was available to hit a polarized ammonia (NH_3) target. Due to the high muon energy, x-values as low as 0.01 could be reached.

The results from this experiment which was meant to supplement the SLAC data at small-x and to confirm the Ellis–Jaffe 'sum rule' [333,253,254] came as a major surprise. Actually, they

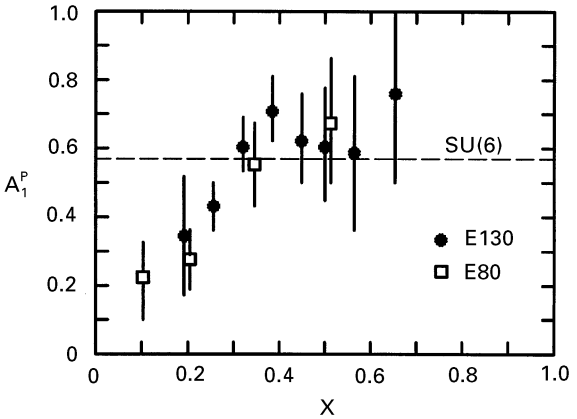

Fig. 5. The spin asymmetry of the proton from the 'old' SLAC data from 1976 and 1983 [365]. In the naive SU(6) model one has $A_1^p = \frac{5}{9}$ and $A_1^n = 0$ [186].

confirmed the SLAC measurements in the common large-x region but found too small asymmetries in the small-x region, in disagreement with the expectations of Gourdin, Ellis and Jaffe and the naive quark parton model.

The high energetic muon beam is a low-luminosity beam because it is a secondary beam from the semileptonic decay of pions which are produced in proton collisions. Its main advantage is its high energy which not only allows to enter the small-x region but also guarantees higher Q^2-values in the region of intermediate-x and a corresponding suppression of possible higher twist effects. In the rest system of the pions the emitted muons are 100% left-handed, due to the V–A nature of the decay. In the laboratory frame the muons have a degree of polarization which depends on the ratio E_μ/E_π. For the EMC experiment the beam was selected such that the polarization of the muon beam was about 80%. The muon beam polarization was determined from the muon event distribution via a Monte Carlo study of muon production – an indirect and not really satisfactory method.

The ammonia target was quite large, with a length of about 2 m, and separated into two halves with opposite polarization. On the average only a fraction f, the dilution factor, of the target protons were polarized. The polarization of the target could be determined as a function of its length (by NMR coils placed along the target).

The scattered muons were detected by a well-established muon tracking spectrometer. It was possible to reconstruct the muon scattering vertex to determine that half of the target in which the scattering took place. The target spins were reversed (once per week) 11 times in the experiment. Changes in the spectrometer acceptance from one spin reversal to another was the main systematic uncertainty in the experiment.

In Fig. 6 the combined results from SLAC and CERN on the structure function g_1^p are presented. The low values of the asymmetries at small-x translate into low values for the proton structure function and a low value for its first moment [490,77,78]

$$\Gamma_1^p(\langle Q^2\rangle) = 0.126 \pm 0.010 \pm 0.015 \quad (\mathrm{EMC, SLAC})\,, \tag{3.3}$$

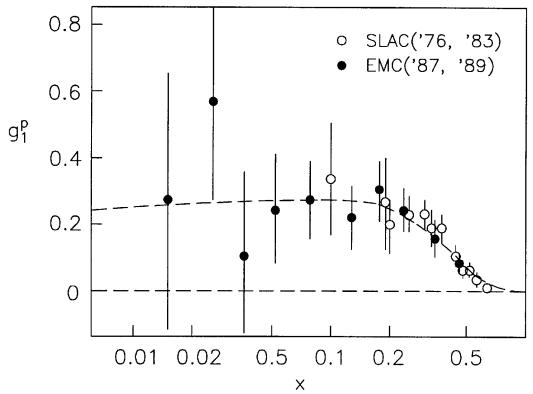

Fig. 6. Combined results of SLAC and EMC on g_1^p [78]. The dashed curve is an EMC parametrization of the data.

where the first is the statistical and the second is the systematic error which includes, as always, uncertainties from Regge extrapolations to $x \to 0$; the average values of Q^2 are $\langle Q^2 \rangle = 10.7\,\mathrm{GeV}^2$ (EMC) and $\langle Q^2 \rangle = 4\,\mathrm{GeV}^2$ (SLAC). It should be emphasized that almost all of $\int_0^1 g_1^p\,\mathrm{d}x$ stems from the region $x \geq 0.01$ which gives [490,77,78], instead of (3.3),

$$\int_{0.01}^{1} g_1^p(x,\langle Q^2 \rangle)\,\mathrm{d}x \simeq 0.123\ . \tag{3.4}$$

If, on the contrary, one does not combine the EMC and SLAC measurements, the EMC asymmetry measurements alone imply similar results, namely [490,77,78]

$$\Gamma_1^p(\langle Q^2 \rangle = 10.7\,\mathrm{GeV}^2) = 0.123 \pm 0.013 \pm 0.019 \quad \text{(EMC)}\ . \tag{3.5}$$

The surprising EMC result triggered a second CERN experiment with polarization, the so-called SMC experiment [25,23,549,29]. Instead of ammonia a polarized butanol target has been used. In butanol the only polarized nucleons are the protons ($\simeq 12\%$) and deuterons ($\simeq 19\%$). The goal of this experiment was to infer information about the neutron from the difference $g_1^d - g_1^p$. Butanol allows for a much more rapid spin reversal than ammonia, this way reducing the large systematic uncertainty from the varying detector acceptance. With the alcohol targets, spin reversals took one hour and were implemented every 8 h.

The main improvement of the SMC experiment was in the measurement of the beam polarization. It was obtained from the energy spectrum of positrons from muon decay. The positron energy spectrum is rather sensitive to the muon beam polarization and provides a direct measurement.

In Figs. 7 and 8 the SMC results for A_1^d and g_1^d are shown which are plotted as a function of $\ln x$ to make the small-x results more transparent. For x less than 0.1 the results are compatible with zero although with rather limited statistics. The theoretically more interesting longitudinally polarized neutron structure function $g_1^n(x, Q^2)$ can be obtained via the relation

$$g_1^d(x, Q^2) = \tfrac{1}{2}[g_1^p(x, Q^2) + g_1^n(x, Q^2)](1 - \tfrac{3}{2}w_D) \tag{3.6}$$

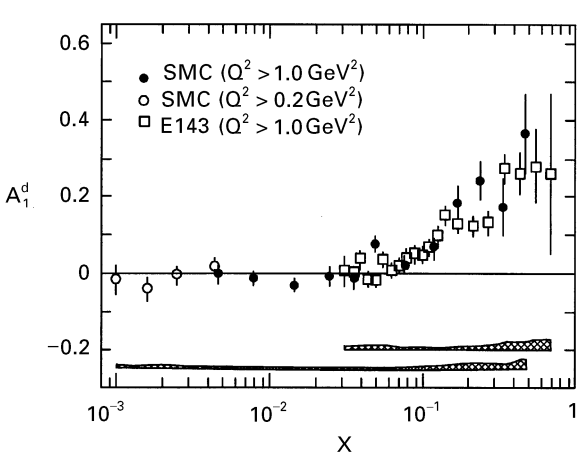

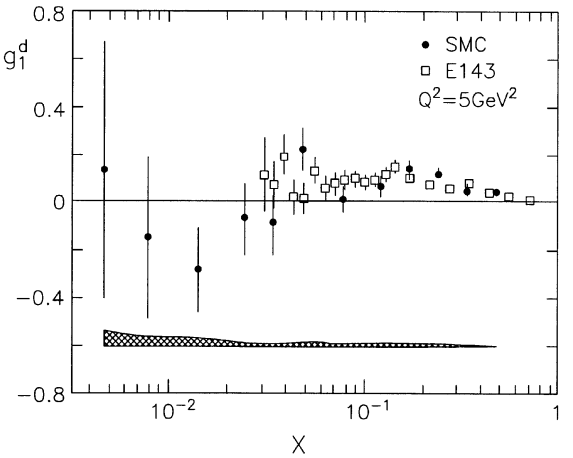

Fig. 7. The virtual photon–deuteron cross section asymmetry as measured by SMC [23] and compared to the SLAC E143 data [3]. Only statistical errors are shown. The size of the systematic errors is indicated by the shaded area.

Fig. 8. g_1^d deduced from A_1^d in Fig. 7 evolved to a common $Q^2 = 5\,\mathrm{GeV}^2$ [23]. Only statistical errors are shown. The size of the systematic errors is indicated by the shaded area.

where $w_D(\simeq 0.058)$ accounts for the D-state admixture in the deuteron wave function [25]. The resulting [26] $g_1^n(x, Q^2 = 5\,\mathrm{GeV}^2)$ is shown in Fig. 9 where the 'old' EMC [490,77,78] and SLAC [43,104,105] data have been used for g_1^p, all reevaluated at $Q^2 = 5\,\mathrm{GeV}^2$ under the assumption that the asymmetries $A_1^{d,p}$ are independent of Q^2. (This latter assumption is theoretically questionable, at least in the small-x and larger-Q^2 region where no data exist so far, as will be discussed in Section 6.) Also shown in Fig. 9 are the SLAC (E142) data [65], to be discussed next, which agree with the SMC results in the x region of overlap. The SMC results of Fig. 9 imply [25]

$$\Gamma_1^n(Q^2 = 5\,\mathrm{GeV}^2) = -0.08 \pm 0.04 \pm 0.04 \quad \text{(SMC)} \tag{3.7}$$

which still deviates from the Ellis–Jaffe expectation -0.002 ± 0.005.

More recently, SMC has also measured $g_1^p(x, Q^2)$ [17,18,24] shown in Figs. 10 and 11, which results in

$$\Gamma_1^p(Q^2 = 10\,\mathrm{GeV}^2) = 0.136 \pm 0.013 \pm 0.011 \quad \text{(SMC)}\,. \tag{3.8}$$

This result increases to [17,18,24]

$$\Gamma_1^p(Q^2 = 5\,\mathrm{GeV}^2) = 0.141 \pm 0.011 \quad \text{(SMC, EMC, SLAC)} \tag{3.9}$$

if the 'old' EMC and SLAC measurements are included which led to (3.3). Eq. (3.9) represents, for the time being, probably the best estimate of the full first moment ($0 \le x \le 1$) of $g_1^p(x, Q^2)$ at $Q^2 = 5$ to $10\,\mathrm{GeV}^2$. All the above results are still significantly below the Gourdin–Ellis–Jaffe [333,253,254] expectation (assuming a vanishing total polarization of strange sea quarks in the LO-QCD parton model expression for Γ_1 in, e.g., Eq. (5.14) below) of about 0.18 ± 0.01 which will be discussed in more detail in Sections 5 and 6.1.

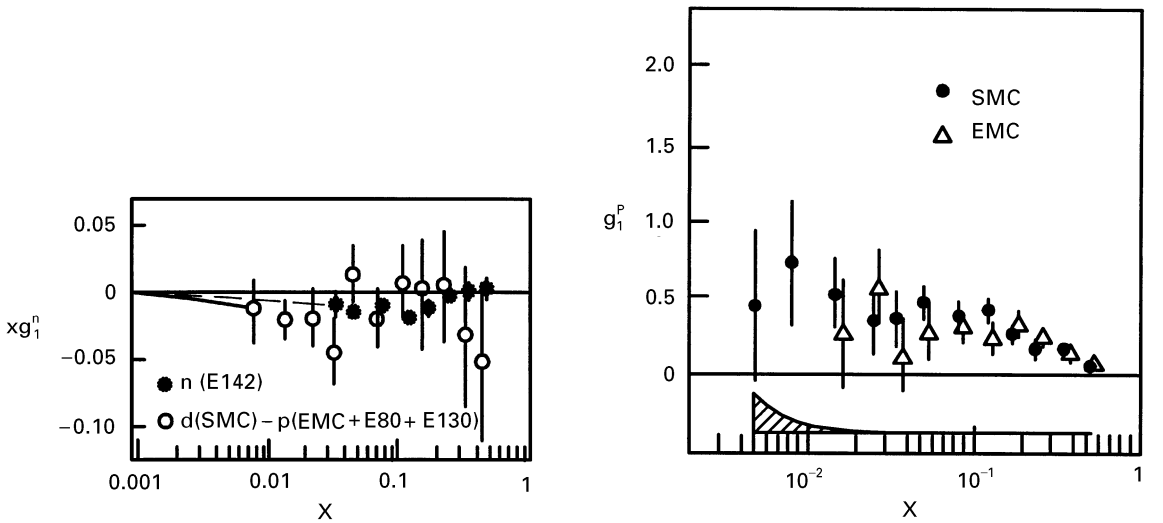

Fig. 9. g_1^n as a function of x at $Q^2 = 5\,\mathrm{GeV}^2$. The full circles are the data from the SLAC E142 experiment. The dashed and solid curves show the extrapolations to low x using the E142 data and using the combined data, respectively [26].

Fig. 10. SMC/EMC results for g_1^p at the average Q^2 for each x bin [17,18,28]. Only statistical errors are shown. The size of the systematic errors is indicated by the shaded area.

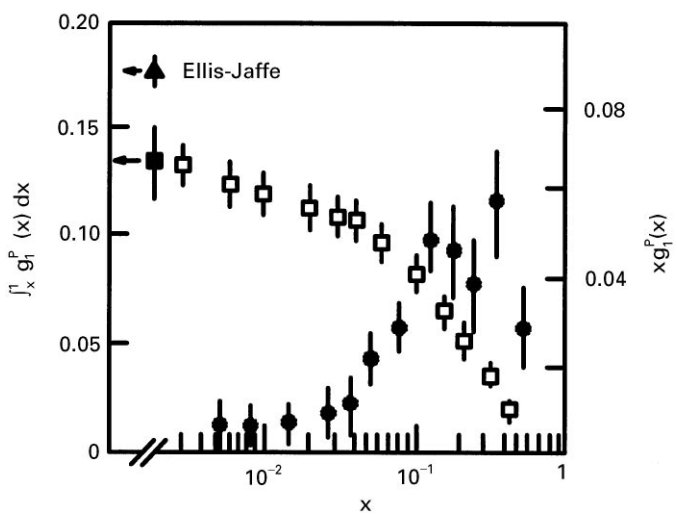

Fig. 11. The solid circles show the SMC results for g_1^p as a function of x, at $Q_0^2 = 10\,\mathrm{GeV}^2$. The open boxes show the integral from x to 1 (left-hand axis). Only statistical errors are shown. The solid square shows the result for the first moment (integral from 0 to 1), with statistical and systematic errors combined in quadrature [17,18].

SMC [27,30] and HERMES [13] have also presented semi-inclusive $\pi^{\pm}$ measurements which give direct access to the polarized valence densities $\delta u_v(x,Q^2)$ and $\delta d_v(x,Q^2)$. More details will be discussed in Section 6.5.

Due to the use of (longitudinally) polarized high current electron beams, measurements of $g_1^{p,n}(x,Q^2)$ with much higher statistics are obtained from the latest round of SLAC experiments (although at significantly lower values of Q^2 due to the lower beam energy) to which we turn now.

3.3. The new generation of SLAC experiments

The SLAC E142 experiment [65] used a different electron source than the old SLAC experiments [43,104,105] relying on developments on solid-state GaAs cathodes. They were able to produce high current electron beam pulses with energies 19.4, 22.7 and 25.5 GeV and through that a rather high statistics experiment. Altogether, 300 million events could be collected. In addition, reversal of beam spin direction could be implemented randomly.

The target was polarized ^{3}He. From the measurements on ^{3}He the neutron structure function can be directly inferred because the polarization effects from the two protons inside the helium compensate each other, due to the Pauli principle. This is true to the extent that the helium nucleus is in its S-state. The probability for this is about 90%. The remaining 10% probability with which the two proton spins are parallel can be corrected for.

There is another nuclear uncertainty at low Q^2 ($\langle Q^2\rangle \simeq 2\,\mathrm{GeV}^2$), namely the possible exchange of mesons (ρ's and π's) which is a bit more dangerous for ^{3}He than for the deuteron because ^{3}He has a larger binding energy per nucleon than d. Furthermore, its magnetic moment is a worse approximation to the free neutron than μ_d is to $\mu_p + \mu_n$.

The ^{3}He target is polarized by optical pumping. Circularly polarized near infrared laser light illuminates the target cell with ^{3}He and rubidium vapor. The outer shell electrons in the rubidium become polarized and transfer their polarization to the ^{3}He nucleus via spin exchange collisions. Once achieved, the polarization of the ^{3}He is rather stable. The entire target chamber was placed in a constant magnetic field which holds the ^{3}He spins in a fixed orientation. Target spin reversal was achieved several times per day and used to reduce the systematic error.

The results for g_1^n are shown in Fig. 12 and can be compared with the more recent SLAC E143 experiment [3] in Fig. 13. These experiments span the Q^2-range $1 < Q^2 < 10\,\mathrm{GeV}^2$, corresponding to $0.029 < x < 0.8$ at their respective energies, where the E143 polarized electron beam energies refer to 9.7, 16.2 and 29.1 GeV. The E143 data for g_1^n in Fig. 13 imply [3]

$$\Gamma_1^n(\langle Q^2\rangle = 2\,\mathrm{GeV}^2) = -0.037 \pm 0.008 \pm 0.011 \quad \text{(E143)} \tag{3.10}$$

compared with $-0.022 \pm 0.007 \pm 0.009$ from the E142 data [65]. These results are consistent with the less accurate SMC measurement in (3.7). The E143 experiment [3,4] uses a deuterated ammonia (ND_3) target, polarized by dynamic nuclear polarization in a 4.8 T magnetic field, in order to check the SMC experiment at lower Q^2. The comparison of their measured asymmetries $A_1^d(x,Q^2)$ in Fig. 7 demonstrates that these two experiments are consistent with each other although it should be kept in mind that the Q^2-value of SMC is about twice as large, for each specific x-bin, as of E143; the average Q^2 of the latter experiment varies from $1.3\,\mathrm{GeV}^2$ (at low x) to $9\,\mathrm{GeV}^2$ (at high x). A comparison of the integral of g_1^n, $\int_x^1 g_1^n(x',Q^2)\,\mathrm{d}x'$, for each x-bin as lower integration limit is shown in Fig. 14 which eventually (as $x \to 0$) leads to the full 'first moment' of

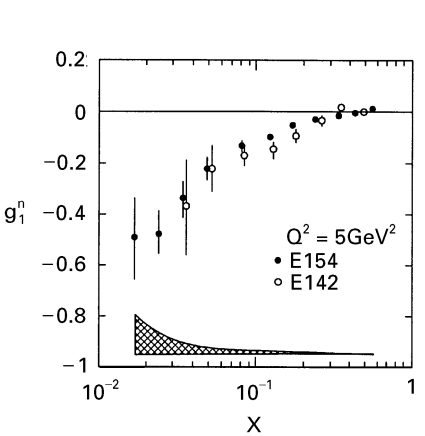

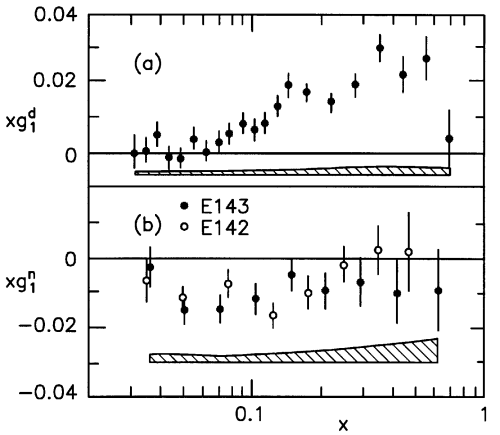

Fig. 12. Result for g_1^n at $Q^2 = 5\,\mathrm{GeV}^2$ from SLAC (E142) [65]. The most recent SLAC (E154) results are also shown for comparison [7].

Fig. 13. xg_1 for (a) the deuteron at $Q^2 = 3\,\mathrm{GeV}^2$ and (b) the neutron at $Q^2 = 2\,\mathrm{GeV}^2$ as measured by E142 and E143 [3]. Systematic errors are indicated by the shaded bands.

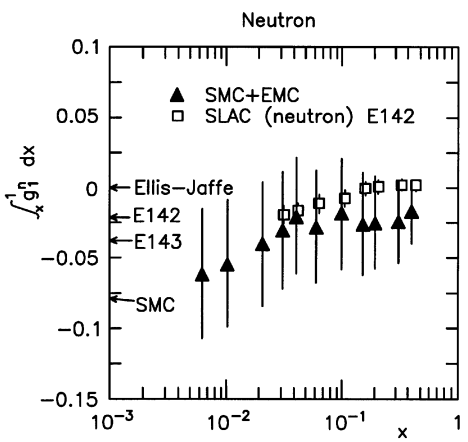

Fig. 14. Comparison between SLAC and CERN of the integral of g_1^n at the average Q^2 of the respective experiments.

g_1^n as stated in Eqs. (3.7) and (3.10). The results shown in Fig. 14 are particularly interesting because they clearly demonstrate that the difference between SLAC and SMC/EMC comes mainly from the small-x region, $x < 0.03$, where SLAC has no data points and thus has to fully rely on assumptions about the behavior of g_1 as $x \to 0$.

Furthermore the E143 experiment used also an ammonia target [2] in order to check, at lower Q^2, the SMC/EMC proton measurements for g_1^p. Their results are again compatible with the ones

Table 2
Experimental results for the g_1-integrated quantity $\Gamma_1(Q^2)$ in Eq. (3.2)

Experiment	$\Gamma_1(Q^2/\mathrm{GeV}^2)$	Reference
EMC, SLAC	$\Gamma_1^p(10.7) = 0.126 \pm 0.010 \pm 0.015$	[77,78]
SMC	$\Gamma_1^p(10) = 0.136 \pm 0.013 \pm 0.011$	[17,18,24]
E143	$\Gamma_1^p(3) = 0.127 \pm 0.004 \pm 0.010$	[2]
SMC	$\Gamma_1^n(10) = -0.063 \pm 0.024 \pm 0.013$	[20]
SMC	$\Gamma_1^n(5) = -0.08 \pm 0.04 \pm 0.04$	[25]
SMC	$\Gamma_1^n(5) = -0.048 \pm 0.022$	[24]
E142	$\Gamma_1^n(2) = -0.022 \pm 0.007 \pm 0.009$	[65]
E143	$\Gamma_1^n(2) = -0.037 \pm 0.008 \pm 0.011$	[3]
E154	$\Gamma_1^n(5) = -0.041 \pm 0.004 \pm 0.006$	[7]

of SMC in the x-region of overlap and give [2]

$$\Gamma_1^p(Q^2 = 3\,\mathrm{GeV}^2) = 0.127 \pm 0.004 \pm 0.010 \quad \text{(E143)} \tag{3.11}$$

to be compared with Eqs. (3.3)–(3.5) and (3.8). Since the latter SMC result/estimate (3.8) holds at $Q^2 = 10\,\mathrm{GeV}^2$, it is more appropriate to calculate the integral at $Q^2 = 3\,\mathrm{GeV}^2$, assuming $g_1^p/F_1^p \simeq A_1^p$ to be independent of Q^2, which gives $0.122 \pm 0.011 \pm 0.011$, instead of Eq. (3.8), and compares better with the E143 result (3.11). These various consistent measurements imply that by now, after 20 years of having performed polarized deep inelastic experiments, we have available a rather reliable and sufficiently precise result for $\int_0^1 g_1^p(x, Q^2)\,\mathrm{d}x$ which is confidently more than two standard deviations *below* the Ellis–Jaffe–Gourdin sum rule expectation (no polarized strange sea [333,253,254]) of $\Gamma_1^p(Q^2 = 3\,\mathrm{GeV}^2)_{\mathrm{EJ}} = 0.160 \pm 0.006$ [2]. We shall come back to this point in Section 5.

The integrated quantities $\Gamma_1^{p,n}(Q^2)$ which resulted from all polarization experiments discussed and performed thus far [574] are finally summarized in Table 2.

There are several new experiments at SLAC (see e.g. [366]), the experiments E154 [7] and E155 [66] with a ^{3}He target [365] and an ammonia target [71], respectively, which run at 50 GeV beam energy and which are the follow-up experiments to E142 and E143. Clearly, with SLAC statistics, these measurements will provide us with a powerful test of the larger Q^2 and small x ($\gtrsim 0.01$) dependence of the spin structure functions $g_1^{p,n}$, as can be seen from the comparison with the first results of E154 with E142 in Fig. 12.

3.4. Future polarization experiments

The HERMES experiment [207,208,89,12,41], being a fixed target experiment, takes place in the HERA tunnel with a longitudinally polarized electron beam of about 30 GeV incident on a polarized H, D or ^{3}He gas jet target. Although this experiment is performed at a similarly low energy as present SLAC measurements, the novel technique of polarized gas-jet target technology is expected to allow for high-precision measurements since the target atoms are present as pure atomic species and hence almost no dilution of the asymmetry occurs in the scattering from unpolarized target

material. The main advantages: HERMES will use a pure proton gas target in a thin wall storage cell, so that the dilution factor will be close to one and there is almost no background from windows effects. The thin targets will still provide very good statistics because the beam current is enormous. Even a measurement of the structure function g_2 is conceivable. Finally, the spectrometer allows for multiparticle identification and thereby measurements of semiinclusive cross sections from which additional information on valence, sea and strange quark polarization can be obtained. In addition, polarized internal gas targets allow for a rapid reversal of the target spin [207,208] which will be crucial for understanding and minimizing systematic errors. This rapid spin reversal will be also crucial for measuring *directly neutron* asymmetries by using a ^{3}He gas target where spins of the two protons are practically in opposite directions and thus the ^{3}He target acts as an effective neutron target. Actual data taking has started in 1995/96 and the accessible kinematic region ($0.02 \leq x \leq 0.8$, $1 \leq Q^2 \leq 10\,\mathrm{GeV}^2$) will be similar to the one of present SLAC experiments. It is intended to measure $g_1^{p,n,d}$ and $g_2^{p,n,d}$ and in particular semi-inclusive asymmetries $A_{p,n}^{\pi}$ from $\vec{e}\vec{p}\,(\vec{n}) \to e\pi X$ which allows to extract separately the polarized valence quark densities $\delta d_v(x,Q^2)$ and $\delta u_v(x,Q^2)$. More details will be discussed in Section 6.

New experiments like COMPASS [106,486] (consisting partly of the former SMC) and HERMES [355] have been proposed for measuring semi-inclusive (D-mesons, etc.) reactions in deep inelastic $\vec{\mu}\vec{p}(\vec{d})$ scattering at 100–200 GeV $\vec{\mu}$-beam energies and 27.5 GeV $\vec{e}$-beam energies, respectively. These will be dedicated experiments for measuring, among other things, the polarized gluon distribution $\delta g(x,Q^2)$ which plays a predominant role in understanding the nucleon spin structure and which so far is experimentally entirely unknown. It will be deduced from the production of heavy quarks (like charm) via the fusion process $\vec{\gamma}^*\vec{g} \to c\bar{c}$ responsible for open charm production which is one of the most promising and cleanest processes for extracting $\delta g(x,Q^2)$ since it occurs already in the leading order (LO) of QCD with no light quark contributions present (see Section 6.2). It is expected to achieve a sensitivity for $\delta g/g$ of about 15%. Note, however, that this cross section is *not* sensitive to the 'anomalous' (= first moment) part of the polarized gluon density, because the first moment contribution of polarized gluons to heavy quark production vanishes. These issues will be discussed in detail in Sections 5 and 6.

So far we have concentrated on deep inelastic $\vec{l}\vec{N}$ reactions. Purely hadronic reactions are presently being studied at the Fermilab Spin Physics Facility which consists of a 200 GeV longitudinally polarized proton or antiproton beam incident on a fixed polarized proton target [14,584]. Apart from the non-uniquely polarized pentanol target, the beam energy is rather low for a purely hadronic reaction ($\sqrt{s} = 19.4\,\mathrm{GeV}$). Nevertheless, first measurements resulted in a small, almost vanishing longitudinal spin asymmetry $A_{\mathrm{LL}}^{\pi^0}$ for inclusive π^0-production at small $p_{\mathrm{T}}^{\pi^0}$ (between 1 and 4 GeV). This measurement is naively more consistent with a small polarized gluon component in the proton than with a large one, but has a very large error. An updated result is being prepared by E-704 as well as results on the totally inclusive polarized cross section and polarized hyperon, direct photon and J/ψ production [21,22]. All of these have limited statistics and thus will be of very limited use for perturbative QCD interpretations. Using the 200 GeV proton beam, E-704 have also measured transverse single-spin asymmetries in inclusive pion production, $p^{\uparrow} + p \to \pi^{0\pm} + X$ and found appreciable asymmetries [16]. More details will be discussed in Section 6.8.

On the other hand, there is the upcoming very promising experimental spin program of the Relativistiv Heavy Ion Collider (RHIC) Spin Collaboration (RSC) [148,585] at the Brookhaven

National Laboratory, to which many of the E-704 physicists have switched. At RHIC *both* proton beams, with an average energy of 250 GeV each, will be polarized, using the 'Siberian snake' concept [216,217,425,514], to an expected polarization of about 70%. Due to the high luminosity of the order of $\sim 10^{32}\,\mathrm{cm}^{-2}\,\mathrm{s}^{-2}$ (corresponding to an integrated luminosity of about $800\,\mathrm{pb}^{-1}$) the polarized RHIC pp collisions will play a decisive role in measuring the polarized gluon density. This can be achieved either via heavy quark production ($\vec{g}\vec{g} \to Q\bar{Q}$, etc.) or via direct photon production ($\vec{g}\vec{q} \to \gamma q$, etc.). The latter process is particularly promising, and a sensitivity of about 5% is expected for $\delta g/g$. The theory of these processes will be discussed in Section 6. Of course, polarization asymmetries for semi-inclusive pion production and jet production will be also measured, in particular for $W^{\pm}$ and Z production which give access to the various polarized quark densities δu, $\delta\bar{u}$, δd and $\delta\bar{d}$ separately (cf. Section 6). Furthermore, transversity distributions (see Section 8.2) will also be accessible. Some other theoretical aspects of RHIC are discussed in [136].

The build-up of the RSC experiment is depicted in Fig. 15. The protons are taken from a polarized H^- source and are succesively accelerated by a LINAC, a Booster and the Alternating Gradient Synchrotron (AGS) to an energy of 24.6 GeV. In the AGS a 'partial snake' is built in to maintain the polarization. A successful partial snake test has been carried out in 1994 by the E880

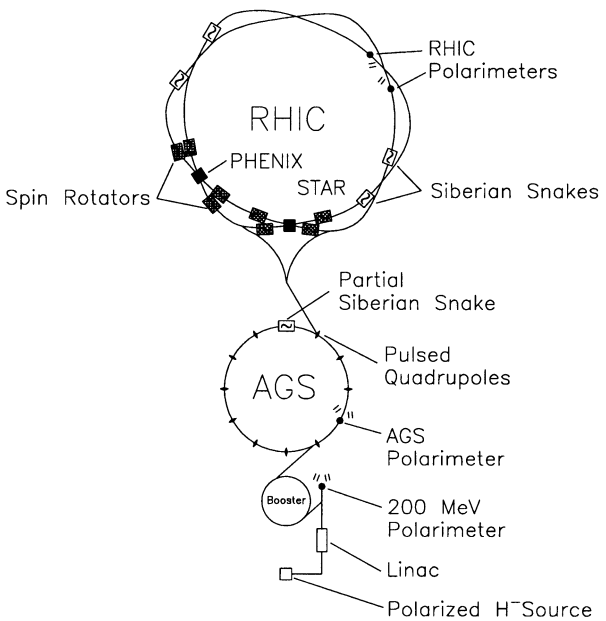

Fig. 15. The built-up of the RHIC collider.

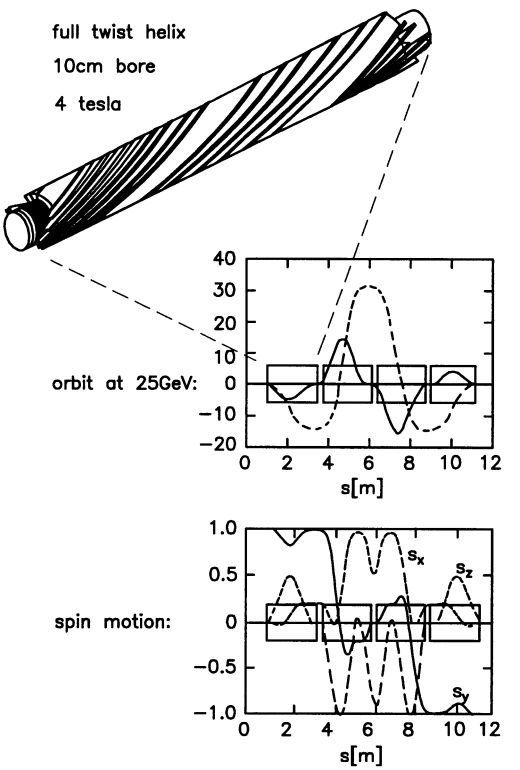

Fig. 16. The layout of a Siberian snake.

collaboration [120,364,329]. Within the RHIC tunnel two full Siberian snakes will be installed, more precisely four split Siberian snakes, two per ring, 180° apart. This is expected to be complete in 2000, at which time the PHENIX [334] and STAR [348] detectors should also be completed. First data taking is scheduled for 2000 as well.

For the nonexperts we include here a qualitative description of how a 'Siberian snake' works. Siberian snakes [216,217] are localized spin rotators distributed around the ring to overcome the effects of depolarizing resonances. For spin manipulations on protons at high energy, one should use transverse magnetic fields, because the impact of longitudinal fields disappears at high energy. In a transverse B-field the spin of the high energy protons rotates $\kappa_p\gamma$ times faster than motion ($\gamma = E/m$ and $\kappa_p = 1.79$ is the anomalous magnetic moment of the proton). During acceleration, a depolarizing resonance is crossed if this product is equal to an integer or equals the frequency with which spin-perturbing magnetic fields are encountered. A Siberian snake turns the spin locally by an angle δ ($\delta = 180^\circ$ for a full snake, $\delta \neq 0$ for a partial snake) so that the would-be resonance condition is violated. For the two full Siberian snakes in the RHIC collider the number of 360° spin rotations per turn is $\frac{1}{2}$, i.e. the resonance condition can never be met. The evolution of the spin and orbit motion in the snake area are shown in Fig. 16.

Coming back to the future of polarized experiments, we note that the possibility of polarized protons is also being considered at HERA. The concept for HERA is in principle very similar to RHIC, the role of the AGS being taken by DESYIII and PETRA which successively accelerate the protons to 40 GeV [123]. There have been further Workshops on the future (spin) physics at HERA [369,124] where the option of polarized high energy protons (besides polarized electrons) at HERA has been discussed. We refer to the proceedings of these Workshops for extensive discussions of this topic [123,124,369]. Of particular interest would be a fully polarized HERA ($\vec{e}\vec{p}$) collider. Such a $\vec{e}\vec{p}$ collider would be unique for studying 'small-x' ($x \lesssim 10^{-3}$) physics of $g_1(x, Q^2)$ and $\delta f(x, Q^2)$, $f = q, \bar{q}, g$ which will be discussed in the next section, in particular Section 4.4; it will give access to the experimentally entirely unknown (partonic) structure functions of a *resolved* polarized photon to be discussed in Section 6.12; and last, but not least, it will enable measurements of the electroweak spin structure functions [124] in Section 2.4, as will be discussed in more detail in Section 6.7. Another experiment ('HERA-$\vec{N}$') utilizing an internal polarized fixed nucleon target in the 820 GeV HERA proton beam has also been examined, see also [423] and references therein. Conceivably, this would be the only place where to study high-energy nucleon–nucleon spin physics besides the dedicated RHIC spin program. An internal polarized nucleon target offering unique features such as polarization above 80% and no or small dilution, can be safely operated in a proton ring at high densities up to 10^{14} atoms/cm^2 [547]. As long as the polarized target is used in conjunction with an unpolarized proton beam, the physics scope of HERA-$\vec{N}$ would be focussed to 'Phase I', i.e. measurements of single-spin asymmetries (to be discussed in Section 6.8). Once polarized protons should become available later, the same set-up would be readily available to measure a variety of double-spin asymmetries. These 'Phase II' measurements would constitute an alternative fixed target approach to similar physics which will be accessible to the collider experiments STAR and PHENIX at the low end of the RHIC energy scale ($\sqrt{s} \simeq 50$ GeV).

Furthermore, there are several polarized low energy ($E^{e^-}_{\text{beam}} \lesssim 5$ GeV) facilities, such as AmPS-NIKHEF, MIT-Bates, CEBAF-Newport News, ELSA-Bonn and MAMI-Mainz, some of which are already operating and will provide us with low-energy precision measurements of $\vec{e}\vec{N}$ reactions. The interested reader is referred to the respective review articles in [264].

4. The structure function g_1 and polarized parton distributions

4.1. The quark parton model to leading order of QCD

The parton model is a very useful tool for the understanding of hadronic high-energy reactions. This is due to its simplicity and comprehensiveness as well as to its universality, i.e. applicability to any hadronic process. In the form of the QCD improved parton model it has had tremendous successes in the understanding of unpolarized scattering. One is therefore tempted to apply it to processes with polarized particles as well.

In the following we will assume that the nucleon is longitudinally polarized. The notion of transversality is difficult to adopt in the parton model, only at the price of losing many of its virtues. The main aim of this section is to represent the polarized structure functions in terms of 'polarized' parton densities, in a similar fashion as the spin-averaged structure functions can be represented in terms of spin-averaged parton densities. For definiteness, let us consider the process $\mu p \to \mu X$ at scales $Q^2 \ll m_{W,Z}^2$ (only photon exchange needed), with a proton of positive longitudinal polarization (= right-handed helicity). Within this reference proton there are (massless) partons with positive and negative helicity which carry a fraction x of the proton momentum and to whom one can associate quark densities $q_+(x,Q^2)$ and $q_-(x,Q^2)$. The difference

$$\delta q(x,Q^2) = q_+(x,Q^2) - q_-(x,Q^2) \tag{4.1}$$

measures how much the parton of flavor q 'remembers' its parent proton polarization. Similarly, one may define

$$\delta\bar{q}(x,Q^2) = \bar{q}_+(x,Q^2) - \bar{q}_-(x,Q^2) \tag{4.2}$$

for antiquarks. Note that the ordinary, spin-averaged parton densities are given by

$$q(x,q^2) = q_+(x,Q^2) + q_-(x,Q^2) \tag{4.3}$$

and

$$\bar{q}(x,Q^2) = \bar{q}_+(x,Q^2) + \bar{q}_-(x,Q^2)\ . \tag{4.4}$$

In the quark parton model, to leading order (LO) in QCD, g_1 can be written as a linear combination of δq and $\delta\bar{q}$ [266,54,45],

$$g_1(x,Q^2) = \frac{1}{2}\sum_q e_q^2[\delta q(x,Q^2) + \delta\bar{q}(x,Q^2)]\ , \tag{4.5}$$

where e_q are the electric charges of the (light) quark-flavors $q = u,d,s$. Notice that in the case of spin-averaged structure functions $F_{1,2}$ the negative helicity densities $q_-, \bar{q}_-$ enter with an opposite sign, e.g. $F_1(x,Q^2) = \frac{1}{2}\sum_q e_q^2(q + \bar{q})$. This has to do with the opposite charge conjugation property of γ_μ and $\gamma_\mu\gamma_5$. In the case of the polarized νN structure functions g_3, etc., the situation is reversed. There the $\delta\bar{q}(x,Q^2)$ enter with a negative sign, $g_3 \sim \delta q - \delta\bar{q}$, cf. Section 6; and for the unpolarized νN structure function F_3 one has $F_3 \sim q - \bar{q}$.

Furthermore, Eq. (4.5) can be decomposed into a flavor nonsinglet (NS) and singlet (S) component

$$g_1(x,Q^2) = g_{1,\mathrm{NS}}(x,Q^2) + g_{1,\mathrm{S}}(x,Q^2)\ , \tag{4.6}$$

where

$$g_{1,\mathrm{NS}} = \frac{1}{2}\sum_q (e_q^2 - \langle e^2\rangle)(\delta q + \delta\bar{q}) \tag{4.7}$$

with $\langle e^2\rangle = (1/f)\sum_q e_q^2$ (e.g. for $f = 3$ light u, d, s flavors $\langle e^2\rangle = \frac{2}{9}$) and

$$g_{1,\mathrm{S}} = \frac{1}{2}\langle e^2\rangle\sum_q (\delta q + \delta\bar{q}) \equiv \frac{1}{2}\langle e^2\rangle\delta\Sigma\ . \tag{4.8}$$

In the last equation we have defined the singlet combination (sum of) quarks and antiquarks by

$$\delta\Sigma(x,Q^2) = \sum_q [\delta q(x,Q^2) + \delta\bar{q}(x,Q^2)]\ , \tag{4.9}$$

where the sum usually runs over the light quark-flavors $q = u, d, s$, since the heavy quark contributions $(c, b, \dots)$ have preferrably to be calculated perturbatively from the intrinsic light quark (u, d, s) and gluon (g) partonic-constituents of the nucleon which will be discussed in Section 6.2.

The QCD scale-violating Q^2-dependence of the above structure functions and parton distributions is inherently introduced dynamically due to gluon radiation $(q \to qg)$ and gluon-initiated $(g \to q\bar{q})$ subprocesses depicted, to LO, in Fig. 17. To the leading logarithmic order (LO), these Q^2-corrections have been calculated in [54,36,37,520]. The next-to-leading order NLO (two-loop) results (Wilson coefficients and in particular splitting functions) have recently been calculated [478,568,569] and will be discussed in detail in Section 4.2. One of the main ingredients from QCD (or, more generally, from any strongly interacting quantum field theory) is the appearance of gluon distributions in the nucleon in the form $\delta g(x,Q^2)$ which is the longitudinally polarized gluon density, probed at a scale Q^2, and is defined as follows. Assume that in our reference proton of positive helicity the gluons have momenta of the form $p_g = E(1,0,0,1)$ [in the Breit-frame $P = (\sqrt{P^2 + M^2}, 0, 0, P)$, $q = (0,0,0,-Q)$ in which $E = xP$]. The two possible polarization vectors of the gluon are $\varepsilon_g^\mu = (1/\sqrt{2})(0, 1, \pm \mathrm{i}, 0)$ which correspond to positive and negative circular polarization. To each state of polarization one can attribute a gluon density, $g_+(x,Q^2)$ and

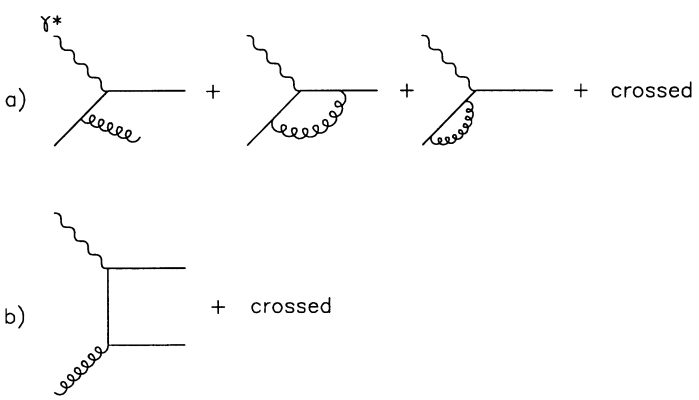

Fig. 17. The parton subprocesses $\gamma^* q \to gq$ and $\gamma^* g \to q\bar{q}$.

$g_-(x,Q^2)$. The ordinary, spin-averaged gluon density is given by $g(x,Q^2) = g_+ + g_-$, whereas δg is defined as

$$\delta g(x,Q^2) = g_+(x,Q^2) - g_-(x,Q^2)\ . \tag{4.10}$$

Since the individual parton distributions with definite helicity $f_\pm(x,Q^2), f = q, \bar{q}, g$, in Eqs. (4.1)–(4.4) and (4.10) are by definition positive definite, their difference δf has to satisfy the general positivity constraints

$$|\delta f(x,Q^2)| \leq f(x,Q^2)\ . \tag{4.11}$$

In LO the gluon distribution does *not directly* contribute to the structure function $g_1(x,Q^2)$ in (4.5), but only indirectly via the Q^2-evolution equations. Furthermore, it is a pure flavor-*singlet*, as is $\delta\Sigma(x,Q^2)$ in (4.9), because each massless quark flavor u,d,s is produced by gluons at the same rate.

The LO Q^2-evolution (or renormalization group) equations are as follows. Only flavor-nonsinglet (valence) combination $\delta q_{\rm NS}$ [$= \delta u - \delta\bar{u}, \delta d - \delta\bar{d}$, $(\delta u + \delta\bar{u}) - (\delta d + \delta\bar{d})$, $(\delta u + \delta\bar{u}) + (\delta d + \delta\bar{d}) - 2(\delta s + \delta\bar{s})$, etc.], i.e. sea- and gluon-contributions cancel, evolve in the *same* way in LO:

$$\frac{\mathrm{d}}{\mathrm{d}t}\delta q_{\rm NS}(x,Q^2) = \frac{\alpha_s(Q^2)}{2\pi}\delta P^{(0)}_{\rm NS}\otimes\delta q_{\rm NS}\ , \tag{4.12}$$

where $t = \ln Q^2/Q_0^2$, with Q_0 being the appropriately chosen reference scale at which $\delta q_{\rm NS}$ is determined (mainly from experiment), and

$$\frac{\alpha_s(Q^2)}{4\pi} \simeq \frac{1}{\beta_0 \ln Q^2/\Lambda^2_{\rm LO}} \tag{4.13}$$

with $\beta_0 = 11 - \frac{2}{3}f$ and f is the number of active flavors. The convolution ($\otimes$) is given by

$$(P\otimes q)(x,Q^2) = \int_x^1 \frac{\mathrm{d}y}{y} P\left(\frac{x}{y}\right) q(y,Q^2) \tag{4.14}$$

which goes over into a simple ordinary product if one considers Mellin n-moments to be discussed later. The LO NS splitting function,

$$\delta P^{(0)}_{\rm NS}(x) = \delta P^{(0)}_{qq}(x) \equiv P^{(0)}_{q_+q_+} - P^{(0)}_{q_-q_+}\ , \tag{4.15}$$

where $P_{q_\pm q_+}$ corresponds to transitions from a quark q_+ with positive helicity to a quark $q_\pm$ with positive/negative helicity, is given by [54]

$$\delta P^{(0)}_{qq}(x) = P^{(0)}_{qq}(x) = C_F\left(\frac{1+x^2}{1-x}\right)_+ \tag{4.16}$$

with $C_F = 4/3$. The fact that $\delta P^{(0)}_{qq}$ turns out to be equal to the unpolarized splitting function $P^{(0)}_{qq}$, i.e.

$$P^{(0)}_{q_-q_+}(x) = 0 \tag{4.17}$$

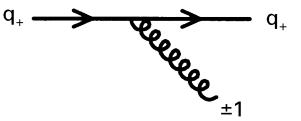

Fig. 18. The leading-order splitting process $q \to qg$.

in Eq. (4.15), is a consequence of helicity conservation, i.e. the fact that no transition between quarks of opposite helicity are allowed in massless perturbative QCD – at least to leading order. In suitable (chirality respecting) regularization schemes this statement, i.e. Eq. (4.17), can be generalized to higher orders as we shall see later. The LO diagram is shown in Fig. 18: The conservation of the quark helicity is a consequence of the vector-like coupling between quarks and gluons. Furthermore, since the gluon has spin $+1$ or -1, a finite angular momentum between the quark and gluon is always produced in such a process. Finally, the convolution (4.14) with the $(\,)_+$ distribution [54] in (4.16) can be easily calculated using

$$\int_x^1 \frac{\mathrm{d}y}{y} f\left(\frac{x}{y}\right)_+ g(y) = \int_x^1 \frac{\mathrm{d}y}{y} f\left(\frac{x}{y}\right)\left[g(y) - \frac{x}{y}g(x)\right] - g(x)\int_0^x \mathrm{d}y f(y)\ . \tag{4.18}$$

In contrast to (4.12), the LO Q^2-evolution equations in the flavor-singlet section are *coupled* integro-differential equations,

$$\frac{\mathrm{d}}{\mathrm{d}t}\begin{pmatrix}\delta\Sigma(x,Q^2)\\ \delta g(x,Q^2)\end{pmatrix} = \frac{\alpha_s(Q^2)}{2\pi}\begin{pmatrix}\delta P_{qq}^{(0)} & 2f\delta P_{qg}^{(0)}\\ \delta P_{gq}^{(0)} & \delta P_{gg}^{(0)}\end{pmatrix}\otimes\begin{pmatrix}\delta\Sigma\\ \delta g\end{pmatrix} \tag{4.19}$$

with $\delta P_{qq}^{(0)}(x)$ given by Eq. (4.16). The remaining longitudinally polarized splitting functions are defined, in analogy to (4.15),

$$\delta P_{AB}^{(0)}(x) \equiv P_{A_+B_+}^{(0)} - P_{A_-B_+}^{(0)} \tag{4.20}$$

with $A, B = q, g$, which fulfil $P_{A_\mp B_-}^{(0)} = P_{A_\pm B_+}^{(0)}$ due to parity invariance of the strong interactions (QCD). The spin-averaged splitting functions are given by the sum $P_{AB}^{(0)}(x) = P_{A_+B_+}^{(0)} + P_{A_-B_+}^{(0)}$. Note that $\delta\Sigma$ refers to the *sum* of all quark flavors and antiflavors and therefore the factor $2f$ in front of $\delta P_{qg}^{(0)}$ in (4.19). Besides $\delta P_{qq}^{(0)}$ in (4.16), the remaining polarized LO splitting function in (4.19) are given by [54]

$$\begin{aligned}
\delta P_{qg}^{(0)}(x) &= T_R[x^2 - (1-x)^2] = T_R(2x-1)\ ,\\
\delta P_{gq}^{(0)}(x) &= C_F\frac{1-(1-x)^2}{x} = C_F(2-x)\ ,\\
\delta P_{gg}^{(0)}(x) &= C_A\left\{(1+x^4)\left(\frac{1}{x} + \frac{1}{(1-x)_+}\right) - \frac{(1-x)^3}{x} + \left(\frac{11}{6} - \frac{f}{9}\right)\delta(1-x)\right\}\ ,
\end{aligned} \tag{4.21}$$

with $T_R = \frac{1}{2}$ and $C_A = N_c = 3$. The advantage of introducing the single set of differences of parton distributions $(\delta\Sigma, \delta g)$ in (4.19), instead of using the individual positive and negative helicity densities $q_\pm$ and $g_\pm$ in (4.1) and (4.10), is that they evolve *in*dependently in Q^2 of the set of the conventional unpolarized densities (Σ, g) where $\Sigma \equiv \sum_f (q + \bar{q})$. This is in contrast to the individual densities $q_\pm$ and $g_\pm$ of definite helicity. The evolution equations (4.12) and (4.19) can be solved numerically by iteration directly in Bjorken-x space. In many cases it is, however, more convenient and physically more transparent to work in Mellin n-moment space where the LO as well as the NLO evolution equations can be solved analytically to a given (consistent) perturbative order in α_s. This is due to the fact that for moments, defined by

$$f^n(Q^2) \equiv \int_0^1 x^{n-1} f(x, Q^2)\, \mathrm{d}x \ , \tag{4.22}$$

the convolution (4.14) appearing in (4.12) and (4.19) factorizes into simple ordinary products:

$$\begin{aligned} \int_0^1 \mathrm{d}x\, x^{n-1} f \otimes g &\equiv \int_0^1 \mathrm{d}x\, x^{n-1} \int_x^1 \frac{\mathrm{d}y}{y} f(y) g\left(\frac{x}{y}\right) \\ &= \int_0^1 \mathrm{d}x\, x^{n-1} \int_0^1 \mathrm{d}y\, \mathrm{d}z\, \delta(x - zy) f(y) g(z) = f^n g^n \ . \end{aligned} \tag{4.23}$$

In moment space the LO nonsinglet and singlet evolution equations (4.12) and (4.19) are thus simply given by

$$\frac{\mathrm{d}}{\mathrm{d}t} \delta q_{\mathrm{NS}}^n(Q^2) = \frac{\alpha_s(Q^2)}{2\pi} \delta P_{qq}^{(0)n} \delta q_{\mathrm{NS}}^n(Q^2) \ , \tag{4.24}$$

$$\frac{\mathrm{d}}{\mathrm{d}t} \begin{pmatrix} \delta\Sigma^n(Q^2) \\ \delta g^n(Q^2) \end{pmatrix} = \frac{\alpha_s(Q^2)}{2\pi} \begin{pmatrix} \delta P_{qq}^{(0)n} & 2f\delta P_{qg}^{(0)n} \\ \delta P_{gq}^{(0)n} & \delta P_{gg}^{(0)n} \end{pmatrix} \begin{pmatrix} \delta\Sigma^n(Q^2) \\ \delta g^n(Q^2) \end{pmatrix} , \tag{4.25}$$

where the $\delta P_{ij}^{(0)n}$ are simply the nth moment of Eqs. (4.16) and (4.21):

$$\begin{aligned} \delta P_{qq}^{(0)n} &= \frac{4}{3}\left[\frac{3}{2} + \frac{1}{n(n+1)} - 2S_1(n)\right] , \\ \delta P_{qg}^{(0)n} &= \frac{1}{2}\frac{n-1}{n(n+1)} \ , \\ \delta P_{gq}^{(0)n} &= \frac{4}{3}\frac{n+2}{n(n+1)} \ , \\ \delta P_{gg}^{(0)n} &= 3\left[\frac{11}{6} + \frac{4}{n(n+1)} - 2S_1(n)\right] - \frac{2f}{32} \ . \end{aligned} \tag{4.26}$$

Here $S_1(n) \equiv \sum_{j=1}^n 1/j = \psi(n+1) + \gamma_E$, $\psi(n) \equiv \Gamma'(n)/\Gamma(n)$ and $\gamma_E = 0.577216$.

The evolution equations (4.24) and (4.25) in n-moment space are usually referred to as LO renormalization group (RG) equations which were originally derived [181,155,420,338,

339,295,212,267,288] from the operator product (light-cone) expansion for unpolarized structure functions (for reviews see, for example, [45,492,509]). The moments $\delta P_{ij}^{(0)n}$ are called (or, more precisely, related[1] to the) 'anomalous dimensions' because they determine the logarithmic Q^2-dependence of the moments of parton distributions and thus of g_1 as we shall see later.

The solution of the simple NS equation (4.24) is straightforward:

$$\delta q_{\rm NS}^n(Q^2) = L^{-(2/\beta_0)\delta P_{qq}^{(0)n}} \delta q_{\rm NS}^n(Q_0^2) \tag{4.27}$$

with $L(Q^2) \equiv \alpha_s(Q^2)/\alpha_s(Q_0^2)$, β_0 being defined after (4.13) and $\delta q_{\rm NS}^n(Q_0^2)$ is the appropriate NS-combination of polarized parton densities fixed (mainly) from experiment at a chosen input scale Q_0^2. The solution of the coupled singlet evolution equations (4.25) is formally similar to (4.27):

$$\begin{pmatrix} \delta\Sigma^n(Q^2) \\ \delta g^n(Q^2) \end{pmatrix} = L^{-(2/\beta_0)\delta\hat{P}^{(0)n}} \begin{pmatrix} \delta\Sigma^n(Q_0^2) \\ \delta g^n(Q_0^2) \end{pmatrix}, \tag{4.28}$$

where $\delta\hat{P}^{(0)n}$ denotes the 2×2 singlet matrix of splitting functions in Eq. (4.25). The treatment of this exponentiated matrix follows the standard diagonalization technique, see e.g. [338,339], where one projects onto the larger and smaller eigenvalues $\lambda_\pm^n$ of $\delta\hat{P}^{(0)n}$ with the help of the 2×2 projection matrices $\hat{P}_\pm$ given by

$$\hat{P}_\pm \equiv \pm \frac{\delta\hat{P}^{(0)n} - \lambda_\mp^n 1}{\lambda_+^n - \lambda_-^n} \tag{4.29}$$

with

$$\lambda_\pm^n = \frac{1}{2}[\delta P_{qq}^{(0)n} + \delta P_{gg}^{(0)n} \pm \sqrt{(\delta P_{qq}^{(0)n} - \delta P_{gg}^{(0)n})^2 + 8f\delta P_{qg}^{(0)n}\delta P_{gq}^{(0)n}}\,] \,. \tag{4.30}$$

The projection matrices $\hat{P}_\pm$ have the usual properties $\hat{P}_\pm^2 = \hat{P}_\pm$, $\hat{P}_+\hat{P}_- = \hat{P}_-\hat{P}_+ = 0$ and $\hat{P}_+ + \hat{P}_- = 1$. Since $\delta\hat{P}^{(0)n} = \lambda_+^n\hat{P}_+ + \lambda_-^n\hat{P}_-$, the matrix expression in (4.28) can be explicitly calculated using

$$f(\delta\hat{P}^{(0)n}) = f(\lambda_+^n)\hat{P}_+ + f(\lambda_-^n)\hat{P}_- \,, \tag{4.31}$$

i.e.

$$L^{-(2/\beta_0)\delta\hat{P}^{(0)n}} = L^{-(2/\beta_0)\lambda_+^n}\hat{P}_+ + L^{-(2/\beta_0)\lambda_-^n}\hat{P}_- \,. \tag{4.32}$$

Thus the solution of (4.28) is explicitly given by

$$\delta\Sigma^n(Q^2) = [\alpha_n\delta\Sigma^n(Q_0^2) + \beta_n\delta g^n(Q_0^2)]L^{-(2/\beta_0)\lambda_-^n} + [(1-\alpha_n)\delta\Sigma^n(Q_0^2) - \beta_n\delta g^n(Q_0^2)]L^{-(2/\beta_0)\lambda_+^n} \,, \tag{4.33}$$

[1] The anomalous dimensions $\delta\gamma^n$, being usually defined as an expansion in $\alpha_s/4\pi$, $\delta\gamma^n = (\alpha_s/4\pi)\delta\gamma^{(0)n} + (\alpha_s/4\pi)^2\delta\gamma^{(1)n} + \cdots$, in terms of the LO (one-loop) $\delta\gamma^{(0)n}$ and NLO (two-loop) $\delta\gamma^{(1)n}$ expressions, are related to the δP^n via $\delta P_{ij}^{(0)n} = -\frac{1}{4}\delta\gamma_{ij}^{(0)n}$ and $\delta P_{ij}^{(1)n} = -\frac{1}{8}\delta\gamma_{ij}^{(1)n}$, where the two-loop splitting functions $\delta P_{ij}^{(1)}$ will become important for the NLO evolutions to be discussed in Section 4.2.

$$\delta g^n(Q^2) = \left[(1-\alpha_n)\delta g^n(Q_0^2) + \frac{\alpha_n(1-\alpha_n)}{\beta_n}\delta\Sigma^n(Q_0^2)\right]L^{-(2/\beta_0)\lambda_-^n} + \left[\alpha_n\delta g^n(Q_0^2) - \frac{\alpha_n(1-\alpha_n)}{\beta_n}\delta\Sigma^n(Q_0^2)\right]L^{-(2/\beta_0)\lambda_+^n} \tag{4.34}$$

with

$$\alpha_n = (\delta P_{qq}^{(0)n} - \lambda_+^n)/(\lambda_-^n - \lambda_+^n)\ , \tag{4.35}$$

$$\beta_n = 2f\delta P_{qg}^{(0)n}/(\lambda_-^n - \lambda_+^n)\ . \tag{4.36}$$

Once the parton distributions are fixed at a specific input scale $Q^2 = Q_0^2$, mainly by experiment and/or theoretical model constraints, their evolution to any $Q^2 > Q_0^2$ is uniquely predicted by the QCD-dynamics due to the uniquely calculable 'anomalous dimensions' $\delta P_{ij}^{(0)n}$ in LO of α_s. Of course a LO calculation by itself is in general not sufficient since neither the Λ-parameter in $\alpha_s(Q^2)$ can be unambiguously defined nor can one prove the perturbative reliability of the results which requires at least a NLO analysis, to which we will turn in the next subsections.

To obtain the x-dependence of structure functions and parton distributions, usually required for practical purposes, from the above n-dependent exact analytical solutions in Mellin-moment space, one has to perform a numerical integral in order to invert the Mellin transformation in (4.22) according to

$$f(x,Q^2) = \frac{1}{\pi}\int_0^\infty \mathrm{d}z\ \mathrm{Im}[\mathrm{e}^{\mathrm{i}\varphi}x^{-c-z\mathrm{e}^{\mathrm{i}\varphi}}f^{n=c+z\mathrm{e}^{\mathrm{i}\varphi}}(Q^2)]\ , \tag{4.37}$$

where the contour of integration, and thus the value of c, has to lie to the right of all singularities of $f^n(Q^2)$ in the complex n-plane, i.e., $c > 0$ since according to Eq. (4.26) the dominant pole of *all* δP_{ij}^n is located at $n = 0$. For all practical purposes one may choose $c \approx 1$, $\varphi = 135^\circ$ and an upper limit of integration, for any Q^2, of about $5 + 10/\ln x^{-1}$, instead of ∞, which suffices to guarantee accurate and stable numerical results [314,316]. Note that it is advantageous to use $\varphi > \pi/2$ in (4.37) because then the factor $x^{-z\exp(\mathrm{i}\varphi)}$ dampens the integrand for increasing values of z which allows for a reduced upper limit in the numerical integration; this is in contrast to the standard mathematical choice $\varphi = \pi/2$ which corresponds to a contour parallel to the imaginary axis.

4.2. Higher-order corrections to g_1

The LO results discussed so far originated from calculating the logarithmic $O(\alpha_s)$ contributions of the parton subprocesses $\gamma^* q \to gq$ and $\gamma^* g \to q\bar{q}$ (Fig. 17) to the zeroth-order 'bare' term $\gamma^* q \to q$ of g_1 [45,54]:

$$g_1(x,Q^2) = \frac{1}{2}\sum_{q,\bar{q}} e_q^2\left\{\delta q_0(x) + \frac{\alpha_s(Q^2)}{2\pi}\int_x^1 \frac{\mathrm{d}y}{y}\delta q_0(y)\left[t\delta P_{qq}^{(0)}\left(\frac{x}{y}\right) + \delta f_q\left(\frac{x}{y}\right)\right]\right\} + \frac{1}{2}\left(\sum_{q,\bar{q}} e_q^2\right)\frac{\alpha_s(Q^2)}{2\pi}\int_x^1 \frac{\mathrm{d}y}{y}\delta g_0(y)\left[t\delta P_{qg}^{(0)}\left(\frac{x}{y}\right) + \delta f_g\left(\frac{x}{y}\right)\right], \tag{4.38}$$

where $\delta q_0, \delta g_0$ denote the unphysical and unrenormalized (i.e. scale independent) bare parton distributions and the function δf_q and δf_g are sometimes called 'constant terms' or 'coefficient functions' because they are related to the $\ln Q^2$-independent terms and to the Wilson coefficients usually introduced within the framework of the operator product expansion. In the leading logarithmic order (LO) one assumes the dominance of the universal $t = \ln Q^2/Q_0^2$ terms which are independent of the regularization scheme adopted, in contrast to $\delta f_{q,g}$.

Eq. (4.38) as it stands is physically meaningless since Q_0^2 is an entirely arbitrary scale which, among other things, serves as an effective cutoff for the emitted parton-k_T (or angular) phase space integration in order to avoid collinear (mass) singularities when the emitted partons in Fig. 17 are along the intitial quark/gluon direction ($k_T = 0$ or $\theta = 0$). Therefore, only the *variation* with Q^2 can be uniquely predicted for the physical and renormalized (i.e. scale dependent) 'dressed' quark distribution,

$$\delta q(x, Q^2) \equiv \delta q_o(x) + \frac{\alpha_s(Q^2)}{2\pi} t(\delta q_0 \otimes \delta P_{qq}^{(0)} + \delta g_0 \otimes \delta P_{qg}^{(0)}) \tag{4.39}$$

and similarly for a suitably defined 'dressed' polarized gluon density $\delta g(x, Q^2)$. These redefinitions result in the RG evolution equations (4.12) and (4.19) [54].

In NLO, i.e. if one goes beyond the leading logarithmic order, the 'finite' terms $\delta f_{q,g}$ in (4.38) have to be included, as well as the contributions of the two-loop splitting functions $\delta P_{ij}^{(1)}(x)$. These additional quantities have the unpleasant feature that they depend on the regularization scheme adopted. For calculational convenience one often chooses dimensional regularization and the 't Hooft-Veltman prescription for γ_5 [362,141,163]. In $D = 4 - 2\varepsilon$ dimensions one obtains for the diagrams in Fig. 17 [478,503,565,566,128,466,259]

$$\begin{aligned} g_1(x, Q^2) = \frac{1}{2}\sum_{q,\bar{q}} e_q^2 \{ & \delta q_0(x) \\ & + \frac{\alpha_s(Q^2)}{2\pi} \int_x^1 \frac{\mathrm{d}y}{y} \delta q_0(x) \left[\left(\ln \frac{Q^2}{\mu^2} - \frac{1}{\varepsilon} + \gamma_E - \ln 4\pi \right) \delta P_{qq}^{(0)}\left(\frac{x}{y}\right) + \delta C_q\left(\frac{x}{y}\right) \right] \Bigg\} \\ & + \frac{1}{2}\left(\sum_{q,\bar{q}} e_q^2 \right) \frac{\alpha_s(Q^2)}{2\pi} \int_x^1 \frac{\mathrm{d}y}{y} \delta g_0(y) \left[\left(\ln \frac{Q^2}{\mu^2} - \frac{1}{\varepsilon} + \gamma_E - \ln 4\pi \right) \delta P_{qg}^{(0)}\left(\frac{x}{y}\right) + \delta C_g\left(\frac{x}{y}\right) \right], \end{aligned} \tag{4.40}$$

where the dimensional regularization mass parameter μ is usually chosen to equal Q, and

$$\delta C_q(z) = \frac{4}{3}\left[(1+z^2)\left(\frac{\ln(1-z)}{1-z} \right)_+ - \frac{3}{2}\frac{1}{(1-z)_+} - \frac{1+z^2}{1-z}\ln z + 2 + z - \left(\frac{9}{2} + \frac{\pi^2}{3} \right)\delta(1-z) \right], \tag{4.41}$$

$$\delta C_g(z) = \frac{1}{2}\left[(2z-1)\left(\ln \frac{1-z}{z} - 1 \right) + 2(1-z) \right]. \tag{4.42}$$

The $(\ )_+$ distribution is, as usual, defined by

$$\int_0^1 \mathrm{d}x \frac{f(x)}{(1-x)_+} \equiv \int_0^1 \mathrm{d}x \frac{f(x) - f(1)}{1-x} \tag{4.43}$$

and Eq. (4.18) is again useful for calculating the convolutions.

The unphysical 'bare' quark and gluon densities δq_0 and δg_0 in (4.40) have to be redefined in order to get rid of the singularities present (for $\varepsilon = 0$). The renormalized 'dressed' quark distribution is defined by

$$\delta q(x,Q^2) \equiv \delta q_0(x) + \frac{\alpha_s(Q^2)}{2\pi}\left(\ln\frac{Q^2}{\mu^2} - \frac{1}{\varepsilon} + \gamma_E - \ln 4\pi\right)(\delta q_0 \otimes \delta P_{qq}^{(0)} + \delta g_0 \otimes \delta P_{qg}^{(0)}) \tag{4.44}$$

and there is a similar equation for the redefined gluon density. Eq. (4.44) refers to the 'modified minimal subtraction' ($\overline{\text{MS}}$) factorization scheme since also the combination $\gamma_E - \ln 4\pi$, being just a mathematical artifact of the phase space in $4 - 2\varepsilon$ dimensions, has been absorbed, together with $-1/\varepsilon$, into the definition of $\delta q(x,Q^2)$. Besides dimensional regularization one has of course the possibility to use masses of quarks and/or gluons to regulate the divergences. However, in those schemes NLO calculations become usually far more cumbersome. Furthermore, one obtains results for δC_q and δC_g which differ from the ones in (4.41) and (4.42). This, however, is not a fundamental problem. It can be traced to a difference in the definition of parton densities and NLO splitting functions $\delta P_{ij}^{(1)}$ in the various schemes. We shall come back to this point at the end of Section 4.3 and in Section 5.

It should be mentioned that the straightforward $\overline{\text{MS}}$ result for δC_g in (4.42), which gives rise to a vanishing 'first moment'

$$\Delta C_g \equiv \int_0^1 \mathrm{d}z\, \delta C_g(z) = \tfrac{1}{2}[-1+1] = 0\ , \tag{4.45}$$

has been a matter of dispute during the past years [55,241,158,282,242,56,381,112,564,46,50,47,128, 283,284,466,259,531,103,165,510,511,370]. This vanishing is caused by the second term $+2(1-z)$ in square brackets of $\delta C_g(z)$ in (4.42) which derives from the soft nonperturbative collinear region where $k_{\mathrm{T}}^2 \sim m_q^2 \ll \Lambda^2$ [462,565,566,460]; therefore it appears to be reasonable that this term should be absorbed, besides the $\delta P_{qg}^{(0)}$ piece in (4.40), into the definition of the light (nonperturbative) quark distribution $\delta q(x, Q^2 = Q_0^2)$ in (4.44). This implies that, instead of $\delta C_g(z)$ in (4.42), we have

$$\delta\tilde{C}_g(z) = \frac{1}{2}(2z-1)\left(\ln\frac{1-z}{z} - 1\right) \tag{4.46}$$

which has a nonvanishing first moment $\Delta\tilde{C}_g = -\frac{1}{2}$, in contrast to (4.45). It should be mentioned that a first moment of $-\frac{1}{2}$ for the Wilson coefficient of the gluon can be obtained *without any subtractions* in the so-called off-shell scheme, to be discussed at the end of Section 4.3 and in Section 5. This scheme therefore *directly* reproduces the ABJ anomaly contribution to the first moment of g_1. For more details see Section 5. However, from a technical point of view the off-shell scheme is somewhat impractical, because two-loop splitting functions are very difficult to calculate in this scheme, and only the $\overline{\text{MS}}$ results (4.41) and (4.42) comply with the NLO($\overline{\text{MS}}$) result [478,568,569] for the two-loop splitting functions $\delta P_{ij}^{(1)}(x)$ to be discussed next.

Within the $\overline{\text{MS}}$ factorization scheme the NLO contributions to $g_1(x,Q^2)$ are finally given by

$$g_1(x,Q^2) = \frac{1}{2}\sum_q e_q^2\left\{\delta q(x,Q^2) + \delta\bar{q}(x,Q^2) + \frac{\alpha_s(Q^2)}{2\pi}[\delta C_q \otimes (\delta q + \delta\bar{q}) + 2\delta C_g \otimes \delta g]\right\}. \tag{4.47}$$

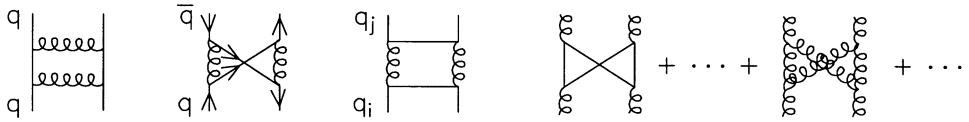

Fig. 19. Diagrams relevant for two-loop splitting functions.

The NLO parton densities $\delta f(x,Q^2), f = q, \bar{q}, g$, evolve according to the NLO evolution equations where the (scheme dependent) two-loop splitting functions $\delta P_{ij}^{(1)}(x)$ enter and to which we now turn.

In NLO the evolution equations (4.12) and (4.19) have to be generalized since, in contrast to the LO in α_s, the $O(\alpha_s^2)$ two-loop splitting functions $\delta P_{ij}^{(1)}$ allow for transitions between quarks and antiquarks and among the different quark flavors as illustrated in Fig. 19. The situation is completely analogous to the unpolarized, i.e. spin-averaged case [45,212,267,288]. The NLO flavor non-singlet renormalization group equations read

$$\frac{\mathrm{d}}{\mathrm{d}t}\delta q_{\mathrm{NS}\pm}(x,Q^2) = \delta P_{\mathrm{NS}\pm} \otimes \delta q_{\mathrm{NS}\pm} \tag{4.48}$$

where

$$\delta P_{\mathrm{NS}\pm} = \frac{\alpha_s(Q^2)}{2\pi}\delta P_{qq}^{(0)}(x) + \left(\frac{\alpha_s(Q^2)}{2\pi}\right)^2 \delta P_{\mathrm{NS}\pm}^{(1)}(x)\ , \tag{4.49}$$

and

$$\frac{\alpha_s(Q^2)}{4\pi} \simeq \frac{1}{\beta_0 \ln Q^2/\Lambda^2} - \frac{\beta_1 \ln\ln Q^2/\Lambda^2}{\beta_0^3 (\ln Q^2/\Lambda^2)^2} \tag{4.50}$$

with $\beta_1 = 102 - \frac{38}{3}f$ (e.g. $\beta_0 = 9$, $\beta_1 = 64$ for the $f = 3$ light active flavors). There are two different, independent NS evolution equations in NLO because of the additional transitions between different, non-diagonal flavors ($u \to d$, $u \to \bar{s}$, etc.) and $q\bar{q}$-mixing ($u \to \bar{u}$, etc.) which start at 2-loop (α_s^2) order as illustrated in Fig. 19. Thus, opposite to the situation of unpolarized (spin-averaged) parton distributions [212,314], $\delta q_{\mathrm{NS}+}$ corresponds to the NS combinations $\delta u - \delta\bar{u} \equiv \delta u_v$ and $\delta d - \delta\bar{d} \equiv \delta d_v$, while $\delta q_{\mathrm{NS}-}$ corresponds to the combinations $\delta q + \delta\bar{q}$ appearing in the NS expressions $(\delta u + \delta\bar{u}) - (\delta d + \delta\bar{d})$ and $(\delta u + \delta\bar{u}) + (\delta d + \delta\bar{d}) - 2(\delta s + \delta\bar{s})$. The required 2-loop splitting functions $\delta P_{\mathrm{NS}\pm}^{(1)}(x)$ in (4.49) are the same [414,586] as the unpolarized ones,[2] $\delta P_{\mathrm{NS}\pm}^{(1)} = P_{\mathrm{NS}\pm}^{(1)}$ in the (chirality conserving) $\overline{\mathrm{MS}}$ regularization scheme [212,267] – similarly to the LO splitting function in Eq. (4.16). The NLO flavor-*singlet* Q^2-evolution equations are similar to the LO ones in (4.19):

$$\frac{\mathrm{d}}{\mathrm{d}t}\begin{pmatrix}\delta\Sigma(x,Q^2)\\ \delta g(x,Q^2)\end{pmatrix} = \delta\hat{P}\otimes\begin{pmatrix}\delta\Sigma\\ \delta g\end{pmatrix} \tag{4.51}$$

[2] More explicitly, $P_{\mathrm{NS}\pm}^{(1)}(x)$ is given, in the notation of [212] by $P_{\mathrm{NS}\pm}^{(1)} = P_{(\pm)}^{(1)} = P_{qq}^{(1)} \pm P_{q\bar{q}}^{(1)}$ according to Eqs. (4.8), (4.35) and (4.50)–(4.55) of [212], which are summarized in the appendix.

with $\delta\Sigma$ being defined in (4.9), and

$$\delta\hat{P} = \frac{\alpha_s(Q^2)}{2\pi}\delta\hat{P}^{(0)}(x) + \left(\frac{\alpha_s(Q^2)}{2\pi}\right)^2 \delta\hat{P}^{(1)}(x) \,, \tag{4.52}$$

where the LO 2×2 matrix $\delta\hat{P}^{(0)}$ of singlet splitting functions is as in Eq. (4.19) and the NLO 2-loop singlet matrix is given by

$$\delta\hat{P}^{(1)}(x) = \begin{pmatrix} \delta P_{qq}^{(1)} & 2f\delta P_{qg}^{(1)} \\ \delta P_{gq}^{(1)} & \delta P_{gg}^{(1)} \end{pmatrix} . \tag{4.53}$$

The calculation of all these NLO singlet splitting functions $\delta P_{ij}^{(1)}(x)$, $i,j = q,g$, has been recently completed in the $\overline{\text{MS}}$ factorization scheme [478,568,569][3] and is summarized in the appendix. As in the LO case, the independent NS evolution equations (4.48) and the coupled singlet equations (4.51) can be solved numerically by iteration directly in Bjorken-x space in order to calculate $g_1(x,Q^2)$ in (4.47) to NLO. It will, however, be more convenient and physically more transparent to work in Mellin n-moment space where the evolution equations can be solved analytically.

In moment space the NLO evolution equations (4.48) and (4.51) are simply given by

$$\frac{\mathrm{d}}{\mathrm{d}t}\delta q_{\text{NS}\pm}^n(Q^2) = \left[\frac{\alpha_s}{2\pi}\delta P_{\text{NS}}^{(0)n} + \left(\frac{\alpha_s}{2\pi}\right)^2 \delta P_{\text{NS}\pm}^{(1)n}\right]\delta q_{\text{NS}\pm}^n(Q^2) \,, \tag{4.54}$$

$$\frac{\mathrm{d}}{\mathrm{d}t}\begin{pmatrix}\delta\Sigma^n(Q^2)\\ \delta g^n(Q^2)\end{pmatrix} = \left[\frac{\alpha_s}{2\pi}\delta\hat{P}^{(0)n} + \left(\frac{\alpha_s}{2\pi}\right)^2 \delta\hat{P}^{(1)n}\right]\begin{pmatrix}\delta\Sigma^n(Q^2)\\ \delta g^n(Q^2)\end{pmatrix} \tag{4.55}$$

with the moments of the LO splitting functions given in (4.26) and the moments of the NLO($\overline{\text{MS}}$) flavor-NS splitting function $\delta P_{\text{NS}\pm}^{(1)n}$ are again equal to the unpolarized ones.[4] The moments of the NLO($\overline{\text{MS}}$) flavor-singlet splitting functions $\delta P_{ij}^{(1)n}$ appearing in $\delta\hat{P}^{(1)n}$, as defined in (4.52), have also been presented in [478]; however, in a form which is not adequate for analytic continuation in n as required for a (numerical) Mellin inversion to Bjorken-x space. The appropriate NLO($\overline{\text{MS}}$) anomalous dimensions can be found in [309] [5] and are summarized in the appendix. The more complicated matrix equation (4.55) can be easily solved in a compact form by introducing [288] an evolution matrix (obvious n-dependencies are suppressed)

$$\hat{E}(Q^2) = \left(1 + \frac{\alpha_s(Q^2)}{2\pi}\hat{U}\right)L^{-(2/\beta_0)\delta\hat{P}^{(0)n}} \,, \tag{4.56}$$

---

[3] These are given by Eqs. (3.65)–(3.68) of [478] where $\delta P_{qq}^{(1)} = \delta P_{\text{NS}-}^{(1)} + \delta P_{PS,qq}^{(1)}$ with $\delta P_{PS,qq}^{(1)}$ being given by Eq. (3.65) of [478]. Note, however, that the $\delta P_{ij}^{(1)}$ have been defined relative to $(\alpha_s/4\pi)^2$ in [478], cf. footnote 1, and that the factor $2f$ in (4.53) has been absorbed into the definition of $\delta P_{qg}^{(1)}$ in [478].

[4] In the notation of [267], the 'anomalous dimensions' (see footnote 1) are given by $\delta P_{\text{NS}\pm}^{(1)n} = -\gamma_{\text{NS}}^{(1)n}(\eta = \pm 1)/8$ with $\gamma_{\text{NS}}^{(1)n}(\eta)$ given by Eq. (B.18) of [267] which are summarized in the appendix.

[5] In the notation of [478,309], $\delta P_{ij}^{(1)n} = -\delta\gamma_{ij}^{(1)n}/8$ with $\delta\gamma_{ij}^{(1)n}$ being given by Eqs. (A.2)–(A.6) of [309]. Moreover, $2f\delta P_{qg}^{(1)n} = -\delta\gamma_{qg}^{(1)n}/8$ since the factor $2f$ has been absorbed into the definition of $\delta\gamma_{qg}^{(1)n}$ in [478,309].

defined as the solution of the equation [cf. (4.51)]

$$\frac{\mathrm{d}}{\mathrm{d}t}\hat{E} = \delta\hat{P}^n\hat{E} \tag{4.57}$$

with $L(Q^2) \equiv \alpha_s(Q^2)/\alpha_s(Q_0^2)$, the NLO α_s being given in (4.50), and where $\hat{U}$ accounts for the 2-loop contributions as an extension of the LO expression (4.28). It satisfies [288]

$$[\hat{U}, \delta\hat{P}^{(0)n}] = \tfrac{1}{2}\beta_0\hat{U} + \hat{R} \tag{4.58}$$

with $\hat{R} \equiv \delta\hat{P}^{(1)n} - (\beta_1/2\beta_0)\delta\hat{P}^{(0)n}$, which yields

$$\hat{U} = -\frac{2}{\beta_0}(\hat{P}_+\hat{R}\hat{P}_+ + \hat{P}_-\hat{R}\hat{P}_-) + \frac{\hat{P}_-\hat{R}\hat{P}_+}{\lambda_+^n - \lambda_-^n - \frac{1}{2}\beta_0} + \frac{\hat{P}_+\hat{R}\hat{P}_-}{\lambda_-^n - \lambda_+^n - \frac{1}{2}\beta_0} \tag{4.59}$$

where the projectors $\hat{P}_\pm$ and $\lambda_\pm^n$ are given in (4.29) and (4.30). The singlet solutions are then given by

$$\begin{pmatrix}\delta\Sigma^n(Q^2)\\ \delta g^n(Q^2)\end{pmatrix} = \left\{L^{-(2/\beta_0)\delta\hat{P}^{(0)n}} + \frac{\alpha_s(Q^2)}{2\pi}\hat{U}L^{-(2/\beta_0)\delta\hat{P}^{(0)n}} - \frac{\alpha_s(Q_0^2)}{2\pi}L^{-(2/\beta_0)\delta\hat{P}^{(0)n}}\hat{U}\right\} \times \begin{pmatrix}\delta\Sigma^n(Q_0^2)\\ \delta g^n(Q_0^2)\end{pmatrix} + \mathrm{O}(\alpha_s^2)\,, \tag{4.60}$$

where the remaining matrix expressions can be explicitly calculated using Eq. (4.31).

For the flavor nonsinglet evolution equations (4.54), which do not involve any matrices, Eq. (4.58) simply reduces to $U_{\mathrm{NS}} = -(2/\beta_0)R_{\mathrm{NS}}$ and (4.60) obviously reduces to

$$\delta q_{\mathrm{NS}\pm}^n(Q^2) = \left\{1 + \frac{\alpha_s(Q^2) - \alpha_s(Q_0^2)}{2\pi}\left(-\frac{2}{\beta_0}\right)\left(\delta P_{\mathrm{NS}\pm}^{(1)n} - \frac{\beta_1}{2\beta_0}\delta P_{qq}^{(0)n}\right)\right\} \times L^{-(2/\beta_0)\delta P_{qq}^{(0)n}}\delta q_{\mathrm{NS}\pm}^n(Q_0^2) + \mathrm{O}(\alpha_s^2)\,. \tag{4.61}$$

These analytic solutions (4.60) and (4.61) in n-moment space can now be inverted to Bjorken-x space by numerically performing the integral in (4.37). The final predictions for $g_1(x, Q^2)$ can then be calculated according to (4.47). Alternatively, one can use directly the moment solutions (4.60) and (4.61) and insert them into the nth moment of (4.47),

$$g_1^n(Q^2) = \frac{1}{2}\sum_q e_q^2\left\{\left(1 + \frac{\alpha_s}{2\pi}\delta C_q^n\right)[\delta q^n(Q^2) + \delta\bar{q}^n(Q^2)] + \frac{\alpha_s}{2\pi}2\delta C_g^n\delta g^n(Q^2)\right\}, \tag{4.62}$$

where [415]

$$\delta C_q^n = \frac{4}{3}\left[-S_2(n) + (S_1(n))^2 + \left(\frac{3}{2} - \frac{1}{n(n+1)}\right)S_1(n) + \frac{1}{n^2} + \frac{1}{2n} + \frac{1}{n+1} - \frac{9}{2}\right] \tag{4.63}$$

is the nth moment of $\delta C_q(z)$ in Eq. (4.41) with $S_1(n)$ given after (4.26) and $S_2(n) \equiv \sum_{j=1}^n 1/j^2 = (\pi^2/6) - \psi'(n+1)$ where $\psi'(n) = \mathrm{d}^2 \ln \Gamma(n)/\mathrm{d}n^2$. The nth moment of $\delta C_g(z)$ in Eq. (4.42) is

$$\delta C_g^n = \frac{1}{2}\left[-\frac{n-1}{n(n+1)}(S_1(n) + 1) - \frac{1}{n^2} + \frac{2}{n(n+1)}\right] \tag{4.64}$$

which gives rise to the vanishing first ($n = 1$) moment, $\delta C_g^1 = 0$. On the other hand, in the factorization scheme of Eq. (4.46) we have

$$\delta\tilde{C}_g^n = \delta C_g^n - \frac{1}{2}\frac{2}{n(n+1)} \tag{4.65}$$

i.e. $\delta\tilde{C}_g^1 = -\frac{1}{2}$. With these expressions at hand one can now obtain $g_1(x, Q^2)$ from Eq. (4.62) by performing a *single* numerical integration according to (4.37). It should be remembered that a theoretically consistent NLO analysis can be conveniently performed within the common $\overline{\text{MS}}$ factorization scheme where all $\delta P_{ij}^{(1)}$ are known [478,568,569], using $\delta C_{q,g}$ of Eqs. (4.63) and (4.64). This is particularly relevant for the parton distributions which have to satisfy the fundamental positivity constraints (4.11) at any value of x and scale Q^2, as calculated by the unpolarized and polarized evolution equations, within the *same* factorization scheme.

From the above solutions (4.60)–(4.62) it becomes apparent that, as usual, a NLO analysis requires two-loop $O(\alpha_s^2)$ splitting functions $\delta P_{ij}^{(1)}$ and one-loop $O(\alpha_s)$ Wilson coefficient, i.e. partonic cross sections, δC_i. Furthermore, in any realistic analysis beyond the LO, the coefficient and splitting functions are not uniquely defined to the extent that it is a mere matter of a theorist's convention of how much of the NLO corrections are attributed to δC_i and how much to $\delta P_{ij}^{(1)}$ [see, for example, the discussion which led to Eq. (4.46)]. This is usually referred to as 'renormalization/factorization scheme convention'. What is, however, important is that, to a given perturbative order in α_s, any physically directly measurable quantity must be *in*dependent of the convention chosen ('scheme independence') and that the convention dependent terms appear only beyond this order in α_s considered which are perturbatively (hopefully) small. The requirements of convention independence of our NLO analysis can be easily derived [288,302] from Eqs. (4.60)–(4.62): Choosing a different factorization scheme in the NS sector ($\delta C_{\text{NS}} = \delta C_q$) according to

$$\delta C_{\text{NS}}^n \to \delta C_{\text{NS}}^{\prime n} = \delta C_{\text{NS}}^n + \Delta_{\text{NS}}^n \ , \tag{4.66}$$

this change has to be compensated, to $O(\alpha_s^2)$, by an appropriate change of $\delta P_{\text{NS}}^{(1)}$,

$$\delta P_{\text{NS}}^{(1)n} \to \delta P_{\text{NS}}^{(1)\prime n} = \delta P_{\text{NS}}^{(1)n} + \frac{\beta_0}{2}\Delta_{\text{NS}}^n \ . \tag{4.67}$$

Similarly in the singlet sector, where we have to deal with 2×2 matrices, a change of the factorization scheme

$$\delta\hat{C}^n \to \delta\hat{C}^{\prime n} = \delta\hat{C}^n + \hat{\Delta}^n \tag{4.68}$$

implies [288,302]

$$\delta\hat{P}^{(1)n} \to \delta\hat{P}^{(1)\prime n} = \delta\hat{P}^{(1)n} + (\beta_0/2)\hat{\Delta}^n - [\hat{\Delta}^n, \delta\hat{P}^{(0)n}] \tag{4.69}$$

in order to guarantee convention (scheme) independence to order α_s^2. The upper row of $\delta\hat{C}$ corresponds to our fermion (quark) $\delta C_{qq} \equiv \delta C_q$ and gluon $\delta C_{qg} \equiv \delta C_g$ Wilson coefficients in an obvious notation. To keep the treatment as symmetric as possible we introduced in addition hypothetical Wilson coefficients δC_{gq} and δC_{gg} in the lower row of $\delta\hat{C}$ which do *not* directly

contribute to deep inelastic lepton-hadron scattering and indeed drop out from the final results relevant for g_1. In general, the transformation of splitting functions in (4.69) and of the gluon density is *not* fixed by the change of the physical first row coefficient functions alone since the lower row of $\hat{\Delta}^n$ remains undetermined. This is partly in contrast to the unpolarized situation [288,302,314] where the energy-momentum conservation constraint (for $n = 2$) may be used together with the assumption of its analyticity in n.

From these results it is clear that a consistent, i.e. factorization scheme independent NLO analysis of $g_1(x, Q^2)$ in (4.62) requires the knowledge of *all* polarized two-loop splitting functions $\delta P_{ij}^{(1)n}$ [or $\delta P_{ij}^{(1)}(x)$], besides the coefficient functions $\delta C_{q,g}^n$ [or $\delta C_{q,g}(x)$]. Such an analysis can be conveniently performed in the common $\overline{\text{MS}}$ factorization scheme where all $\delta P_{ij}^{(1)n}$ are known [478,568,569] – a situation very similar to the unpolarized case.

One could of course choose to work within a different factorization scheme, in particular one which leads to (4.46) and (4.65), as for example in the chirally invariant (CI) or JET scheme [174,176,446,482], or any other specific scheme. In this case, however, one has for consistency reasons to calculate *all* polarized NLO quantities ($\delta C_i, \delta P_{ij}^{(1)n}$, etc.), and not just their first ($n = 1$) moments, in these specific schemes *as well as* also NLO subprocesses of purely hadronic reactions to which the NLO (polarized/unpolarized) parton distributions are applied to. So far, complete NLO calculations have only been performed in the $\overline{\text{MS}}$ scheme.

4.3. Operator product expansion for g_1

The phenomena discussed so far in the QCD improved parton model can also be understood in the framework of the operator product expansion (OPE). In contrast to the QCD parton model, which is universally valid, the OPE is designed exclusively to the understanding of deep inelasic lepton nucleon scattering. One starts with an expansion of the Fourier transform of the time ordered product of two currents, i.e., the virtual Compton amplitude

$$T_{\mu\nu} = \mathrm{i}\int \mathrm{d}^4x\, \mathrm{e}^{\mathrm{i}qx} T(J_\mu(x) J_\nu(0)) \tag{4.70}$$

near the light-cone $x^2 \sim 1/Q^2 \approx 0$, i.e. in powers of $1/Q^2$, and is led to a description of the moments of structure functions in terms of anomalous dimensions, Wilson coefficients and matrix elements. The OPE has been used very successfully to derive results for unpolarized scattering [338,339,295,492,509], and results for polarized scattering exist as well [36,37,520,414,478]. The particular feature of *polarized* DIS is the appearance of antisymmetric ($\mu \leftrightarrow \nu$) terms in the expansion of $T_{\mu\nu}$. We shall start with a discussion of the structure function g_1 for the case of photon exchange. The analysis of g_2 is complicated by the appearance of transverse effects and will be discussed in Section 8. We may then assume longitudinal polarization $P_\sigma = MS_\sigma$ of the proton. One has

$$\begin{aligned} &T_{\mu\nu} \text{ (antisymm., em. current)} \\ &= \mathrm{i}\varepsilon_{\mu\nu\lambda\sigma} q^\lambda \sum_{n=1,3,5,\ldots} \left(\frac{2}{Q^2}\right)^n q_{\mu_1} \ldots q_{\mu_{n-1}} \sum_{i=0}^{9} R_i^{\sigma\mu_1\ldots\mu_{n-1}} E_i^n(Q^2/\mu^2, \alpha_s)\,, \end{aligned} \tag{4.71}$$

where

$$R_i^{\sigma\mu_1\cdots\mu_{n-1}} = \mathrm{i}^{n-1}\bar{\psi}\gamma_5\gamma^{\{\sigma}D^{\mu_1}\cdots D^{\mu_{n-1}\}}\lambda_i\psi \tag{4.72}$$

with $i = 0,\ldots,8$; $n = 1,3,5,\ldots$ and

$$R_9^{\sigma\mu_1\cdots\mu_{n-1}} = \mathrm{i}^{n-1}\varepsilon^{\alpha\beta\gamma\{\sigma}G_{\beta\gamma}D^{\mu_1}\cdots D^{\mu_{n-2}\}}G_\alpha^{\mu_{n-1}} \tag{4.73}$$

with $n = 3,5,7,\ldots$ are the relevant operators, λ_i are the Gell–Mann matrices (λ_0 = unit matrix) and $\{\}$ denotes symmetrization on the indices $\sigma\mu_1\ldots\mu_{n-1}$. In order to obtain operators of definite twist and spin, the appropriate subtraction of trace-terms is always implied. R_{1-8} are the nonsinglet and R_0 and R_9 the singlet contributions. For each $n = 3,5,7,\ldots$ there are 8 NS operators and two singlet operators. For $n = 1$ (the first moment case) there are 8 NS operators $\bar{\psi}\gamma_5\gamma_\sigma\lambda_{1-8}\psi$ but only one singlet operator $\bar{\psi}\gamma_5\gamma_\sigma\psi$, the axial vector singlet current. This operator is of particular interest because it carries the triangle anomaly. Through this anomaly the gluon enters the scene, via $\delta\tilde{C}_g$ in Eqs. (4.46) and (4.65) even though formally no gluon operator R_9 exists for $n = 1$. The case of the first moment will be discussed in great detail in Section 5.

We shall denote the matrix elements of the operators R_i by M_i ($S_\sigma = P_\sigma/M$):

$$\langle PS|R_i^{\sigma\mu_1\cdots\mu_{n-1}}|PS\rangle = -M_i^n S^{\{\sigma}P^{\mu_1}\cdots P^{\mu_{n-1}\}}\,. \tag{4.74}$$

Furthermore, the imaginary part of $\langle PS|T_{\mu\nu}|PS\rangle$ is related to the hadronic tensor $W_{\mu\nu}$ in Eq. (2.1) which determines the cross section and contains the structure functions [181,338,339,295,492]. Therefore, through the optical theorem, g_1 can be related to the E_i^n and the matrix elements M_i^n:

$$\int_0^1 \mathrm{d}x\, x^{n-1}g_1(x,Q^2) = \frac{1}{2}\sum_i M_i^n E_i^n(Q^2/\mu^2,\alpha_s) \tag{4.75}$$

for $n = 1,3,5,\ldots$ Notice that the knowledge of the moments for $n = 1,3,5,\ldots$ together with the fact that g_1 is even in $x \leftrightarrow -x$ completely determines g_1 by analytic continuation. The functions E_i^n, the 'Wilson coefficients', have a Q^2-dependence which is determined by the anomalous dimensions $\delta\gamma^n$ defined in Section 4.2 namely

$$E_i^n(Q^2/\mu^2,\alpha_s) = \sum_j E_j^n(1,\alpha_s(Q^2))T\exp\left(-\int_{\alpha_s(\mu^2)}^{\alpha_s(Q^2)}\frac{\delta\gamma^n(\alpha_s)}{2\beta(\alpha_s)}\,\mathrm{d}\alpha_s\right)_{ij} \tag{4.76}$$

where μ is the renormalization point. T indicates 'time' ordering,

$$T\exp\int_a^b f(x)\mathrm{d}x = 1 + \int_a^b f(x)\mathrm{d}x + \int_a^b \mathrm{d}x\int_x^b \mathrm{d}y f(x)f(y) + \cdots\,. \tag{4.77}$$

When one expands Eq. (4.76) in powers of α_s, it turns out that the two-loop β-function and anomalous dimensions enter the first-order correction. This will be shown explicitly in Eq. (4.80). Those two-loop quantities as well as the first-order Wilson coefficients are in general scheme and convention dependent. By scheme dependence we mean a dependence on the regularization procedure as well as on the renormalization prescription. But this dependence cancels in the combination which enters Eq. (4.83) below, i.e. it cancels in the prediction for the physical quantities. This is complementary to what we said about different definitions of quark densities in Section 4.2 and is exactly analogous to what happens in unpolarized scattering [288,509,302].

Comparing (4.75) and (4.62) there is a one-to-one correspondence between the OPE and the parton model description. The matrix elements M_i^n correspond to the moments of suitable combinations of parton densities δq, $\delta\bar{q}$ and δg. For example,

$$M_8^n = \frac{1}{18}\int_0^1 \mathrm{d}x\, x^{n-1}[\delta u + \delta\bar{u} + \delta d + \delta\bar{d} - 2(\delta s + \delta\bar{s})] \ . \tag{4.78}$$

The anomalous dimensions of the OPE govern the Q^2-evolution of the parton densities and the Wilson coefficients arise as the 'constant terms' discussed in Eq. (4.40). This correspondence holds for general n. For $n = 1$ there is the peculiar situation that only one singlet operator exists whereas in the parton model there are two degrees of freedom, the first moment of $\delta\Sigma$ and the first moment of δg. Therefore, the translation between the two schemes is somewhat more subtle for $n = 1$ than for general n and will be discussed in detail in Section 5.

For each $n = 3, 5, \ldots$ the anomalous dimension matrix $\delta\gamma^n$ decomposes into a 2×2 singlet and a 8×8 nonsinglet block. Let us first discuss the nonsinglet part in some detail. In the nonsinglet block the operators are multiplicatively renormalizable with effectively one anomalous dimension $\delta\gamma_{\mathrm{NS}}^n$, proportional to the moment of the evolution kernel δP_{NS} introduced in the last section (see footnote 1). It can be expanded in powers of α_s

$$\delta\gamma_{\mathrm{NS}}^n = \frac{\alpha_s}{4\pi}\delta\gamma_{\mathrm{NS}}^{(0)n} + \left(\frac{\alpha_s}{4\pi}\right)^2 \delta\gamma_{\mathrm{NS}}^{(1)n} + \mathrm{O}(\alpha_s^3) \ , \tag{4.79}$$

where $\delta\gamma_{\mathrm{NS}}^{(0,1)n}$ are given by the moments of the quantities $\delta P_{qq}^{(0)}$ and $\delta P_{\mathrm{NS}-}^{(1)}$ introduced in Eq. (4.49). They are identical to the analogous quantities in unpolarized scattering. More precisely, one has $\delta\gamma_{\mathrm{NS}}^{(0)n} = -4\delta P_{qq}^{(0)n}$ and $\delta\gamma_{\mathrm{NS}}^{(1)n} = -8\delta P_{\mathrm{NS}-}^{(1)n}$ (see footnotes 1 and 4) because of the use of 4π instead of 2π in the expansion parameter. $\delta P_{\mathrm{NS}+}^{(1)}$ plays no role for g_1 but is only important for g_3 and $g_4 + g_5$ in (2.28) (cf. Section 6.7). Since the OPE method provides only the values of the even or odd moments depending on the crossing parity of the particular structure functions, only specific NS splitting functions ($\delta P_{\mathrm{NS}-}^{(1)}$ or $\delta P_{\mathrm{NS}+}^{(1)}$) are allowed in the evolution kernel. This is in contrast to the more general parton model method discussed before, which makes no restriction on the value of n. In other words, the parton model formulae, besides reproducing the OPE results, provide also the analytic continuation of the OPE results to those values of n which are artificially forbidden in the OPE.

Inserting Eq. (4.79) into (4.76) one obtains

$$\begin{aligned} &T\exp\left(-\int_{\alpha_s(\mu^2)}^{\alpha_s(Q^2)} \frac{\delta\gamma_{\mathrm{NS}}^n(\alpha_s)}{2\beta(\alpha_s)}\mathrm{d}\alpha_s\right) \\ &\quad = \left(\frac{\alpha_s(Q^2)}{\alpha_s(\mu^2)}\right)^{\delta\gamma_{\mathrm{NS}}^{(0)n}/2\beta_0}\left(1 + \frac{\alpha_s(Q^2)-\alpha_s(\mu^2)}{4\pi}\left(\frac{\delta\gamma_{\mathrm{NS}}^{(1)n}}{2\beta_0} - \frac{\beta_1\,\delta\gamma_{\mathrm{NS}}^{(0)n}}{2\beta_0^2}\right) + \mathrm{O}(\alpha_s^2)\right), \end{aligned} \tag{4.80}$$

where we have used

$$\frac{\beta(\alpha_s)}{\alpha_s} = -\beta_0\frac{\alpha_s}{4\pi} - \beta_1\left(\frac{\alpha_s}{4\pi}\right)^2 \tag{4.81}$$

with $\beta_0 = 11 - \frac{2}{3}f$ and $\beta_1 = 102 - \frac{38}{3}f$ as in the previous section. This makes explicit that the two-loop anomalous dimensions and β-function enter the NLO one-loop analysis of cross sections, i.e. Wilson coefficients.

The Wilson coefficient has the form

$$E^n(1, \alpha_s(Q^2)) = 1 + \frac{\alpha_s}{2\pi}\delta C^n_{\rm NS} + {\rm O}(\alpha_s^2) \tag{4.82}$$

with $\delta C^n_{\rm NS}$ given by Eq. (4.63) in the $\overline{\rm MS}$-scheme.

One can combine the above expansions to obtain

$$\int_0^1 {\rm d}x\, x^{n-1} g_{1,{\rm NS}}(x, Q^2) = \left(\frac{\alpha_s(Q^2)}{\alpha_s(\mu^2)}\right)^{\delta\gamma^{(0)n}_{\rm NS}/2\beta_0} \left\{1 + \frac{\alpha_s(Q^2)}{2\pi}\delta C^n_{\rm NS} + \frac{\alpha_s(Q^2) - \alpha_s(\mu^2)}{4\pi} \times \left(\frac{\delta\gamma^{(1)n}_{\rm NS}}{2\beta_0} - \frac{\beta_1 \delta\gamma^{(0)n}_{\rm NS}}{2\beta_0^2}\right)\right\} \frac{1}{2}\sum_i M_i^n(\mu^2) \tag{4.83}$$

which should be compared with Eqs. (4.61) and (4.62). This equation shows how the $\mathrm{O}(\alpha_s)$ Wilson coefficient $\delta C^n_{\rm NS}$ and the anomalous dimensions combine with the matrix element to form the nth moment of g_1. As discussed earlier, the scheme dependence of the quantities $\delta C^n_{\rm NS}$ and $\delta\gamma^{(1)n}_{\rm NS}$ must cancel in the combination in Eq. (4.83) because it gives a physical observable.

Similar features arise in the singlet sector and in higher orders although the formalism becomes more complicated. In the singlet sector the anomalous dimensions form a nondiagonal 2×2 matrix and there are two coefficients, one for the quark type operator R_0 and the other one for the gluon operator R_9. To first order α_s the coefficient for the quark type operator is the same as for the nonsinglet operators, and is of the form

$$E^n_q(1, \alpha_s(Q^2)) = 1 + (\alpha_s/2\pi)\delta C^n_q + {\rm O}(\alpha_s^2) \tag{4.84}$$

with δC^n_q given again by Eq. (4.63). The coefficient for the gluon operator is of the form

$$E^n_g(1, \alpha_s(Q^2)) = (\alpha_s/2\pi)\delta C^n_g + {\rm O}(\alpha_s^2) \tag{4.85}$$

with δC^n_g given in the $\overline{\rm MS}$ scheme by Eq. (4.64). The singlet anomalous dimension matrix has an expansion

$$\delta\gamma^n_{\rm S} = \frac{\alpha_s}{4\pi}\delta\gamma^{(0)n}_{\rm S} + \left(\frac{\alpha_s}{4\pi}\right)^2 \delta\gamma^{(1)n}_{\rm S} + {\rm O}(\alpha_s^3) \tag{4.86}$$

where $\delta\gamma^n_{\rm S}$, $\delta\gamma^{(0)n}_{\rm S}$ and $\delta\gamma^{(1)n}_{\rm S}$ are 2×2 matrices with indices $ij = qq, qg, gq, gg$. With these expansions one can now calculate the singlet part of $\int_0^1 {\rm d}x\, x^{n-1} g_1(x, Q^2)$, using the one-to-one correspondence between the parton model densities and the OPE matrix elements, with the same methods as described after Eq. (4.55). The result is exactly analogous to Eqs. (4.60) and (4.62). An alternative to present this somewhat cumbersome matrix result is the following. If one goes to a basis of the quark and gluon matrix elements, in which $\delta\gamma^{(0)n}_{\rm S}$ is a diagonal matrix, one can calculate the exponential

matrix

$$T\exp\left(-\int_{\alpha_s(\mu^2)}^{\alpha_s(Q^2)}\frac{\delta\gamma_{\rm S}^n(\alpha_s)}{2\beta(\alpha_s)}{\rm d}\alpha_s\right)=\begin{pmatrix}\delta E_{++} & \delta E_{+-}\\ \delta E_{-+} & \delta E_{--}\end{pmatrix} \tag{4.87}$$

with

$$\delta E_{\pm\pm}=\left(\frac{\alpha_s(Q^2)}{\alpha_s(\mu^2)}\right)^{\delta\gamma_\pm^{(0)n}/2\beta_0}\left\{1+\frac{\alpha_s(Q^2)-\alpha_s(\mu^2)}{4\pi}\left(\frac{\delta\gamma_{\pm\pm}^{(1)n}}{2\beta_0}-\frac{\beta_1\delta\gamma_\pm^{(0)n}}{2\beta_0^2}\right)\right\} \tag{4.88}$$

$$\delta E_{\pm\mp}=\frac{\delta\gamma_{\pm\mp}^{(1)n}}{\delta\gamma_\pm^{(0)n}-\delta\gamma_\mp^{(0)n}-2\beta_0}\left\{\frac{\alpha_s(\mu^2)}{4\pi}\left(\frac{\alpha_s(Q^2)}{\alpha_s(\mu^2)}\right)^{\delta\gamma_\pm^{(0)n}/2\beta_0}-\frac{\alpha_s(Q^2)}{4\pi}\left(\frac{\alpha_s(Q^2)}{\alpha_s(\mu^2)}\right)^{\delta\gamma_\mp^{(0)n}/2\beta_0}\right\}, \tag{4.89}$$

where $\delta\gamma_\pm^{(0)n}=-4\lambda_\pm^n$ are the eigenvalues of $\delta\gamma_{\rm S}^{(0)n}$ [cf. Eq. (4.30)], and $\delta\gamma_{\rm S}^{(1)n}$ is assumed to be of the form

$$\delta\gamma_{\rm S}^{(1)n}=\begin{pmatrix}\delta\gamma_{++}^{(1)n} & \delta\gamma_{+-}^{(1)n}\\ \delta\gamma_{-+}^{(1)n} & \delta\gamma_{--}^{(1)n}\end{pmatrix} \tag{4.90}$$

in the new basis.

The first-order Wilson coefficients and the two-loop anomalous dimensions are scheme dependent. However, for consistent schemes the scheme dependence must be such that the predictions for the physical quantities, the moments of g_1, are scheme independent. This implies that the combinations of coefficients and anomalous dimensions, which appear in the representation of g_1, are scheme independent as discussed at the end of the previous section. For example, from Eq. (4.83) we see that $2\delta C_{\rm NS}^n+(\gamma_{\rm NS}^{(1)n}/2\beta_0)$ must be a scheme-independent combination. A similar scheme-independent combination exists in the singlet sector. In the following we want to compare some results for $\delta C_{{\rm NS},q,g}^n$ and $\delta\gamma_{\rm NS,S}^{(1)n}$ in various schemes. Note that the first-order anomalous dimensions $\delta\gamma^{(0)n}$ [given in Eq. (4.26)] as well as the β-function coefficients β_0 and β_1 are scheme independent. In all schemes singular collinear pole contributions arise, which are to be factorized into the quark distributions. The various schemes are:

- The $\overline{\rm MS}$ scheme in dimensional regularization using the reading point method [419] for the treatment of γ_5 (γ_5 is appearing due to the projector on the quark's helicity). In this scheme the factorized singular terms in the coefficients are of the form $\delta\gamma^{(0)n}(-1/\varepsilon-\ln 4\pi+\gamma_E)$.

  The reading point method is the more systematic generalization of the CFH [163] γ_5-prescription, i.e. a totally anticommuting γ_5, in which the γ^*q-vertex is defined to be the starting point, from which the Dirac trace is read. From the calculational point of view this scheme is the most tractable one, because no extra mass parameters or counter terms have to be introduced. Indeed, it is this scheme, for which all coefficients δC_i^n are known and all anomalous dimensions $\delta\gamma_{ij}^{(1)n}$ have been recently calculated for the first time [478]. The coefficients are given in Eqs. (4.63) and (4.64) and the two-loop anomalous dimensions are given in [478,309] as described in footnotes 3 and 5. It is interesting to note that for the first moment ($n=1$)

$$\delta C_{\rm NS}^1=\delta C_q^1=-\tfrac{3}{2}C_F=-2\,, \tag{4.91}$$

$$\delta C_g^1=0\,, \tag{4.92}$$

and

$$\delta\gamma_{\rm NS-}^{(1)1} = 0\ , \tag{4.93}$$

$$\delta\gamma_{qq}^{(1)1} = 24C_F\frac{f}{2}, \tag{4.94}$$

where $\delta\gamma_{\rm NS-}^{(1)} \equiv \gamma_{\rm NS}^{(1)}$ ($\eta = -1$) (see footnote 4). The relation (4.91) implies that the correction to the Bjorken sum rule is saturated by $\delta C_{\rm NS}^1$, i.e. $\delta\gamma_{\rm NS-}^{(1)1} = 0$ in Eq. (4.83) due to (4.93). The relation (4.94) implies that in this scheme the quark contribution to the first moment of g_1 is not conserved (Q^2-dependent). It will be shown in Section 5 that this implies that in this scheme there is no gluon contribution to the first moment of g_1, i.e. $\delta C_g^1 = 0$ as made explicit in Eq. (4.92). The *same* results for δC_i^n and $\delta\gamma_{ij}^{(1)n}$ are obtained [478] if one adopts the HVBM [362,141] method for treating the γ_5 matrix in $D \neq 4$ dimensions, *provided* an additional renormalization constant (counter term) [437] is introduced in order to guarantee the conservation of the NS axial vector operators R_{1-8} in (4.72). It is mandatory to keep these NS axial vector currents conserved [414] due to the absence of gluon-initiated triangle γ_5-anomalies in the flavor nonsinglet sector which *dictates* the vanishing of $\delta\gamma_{\rm NS-}^{(1)1}$.

It should be noted, however, when using 'naively' the original HVBM prescription for the treatment of γ_5 one obtains [578,567] a result for $\delta C_{\rm NS}^n = \delta C_q^n$ which implies for the first moment $\delta C_q^1 = -\frac{7}{2}C_F$ which is different than the one in Eq. (4.91). This corresponds, however, to a nonzero value for $\delta\gamma_{\rm NS-}^{(1)1}$ [on account of the scheme invariance of $2\delta C_{\rm NS}^1 + (\delta\gamma_{\rm NS-}^{(1)1}/2\beta_0) = -3C_F$, using Eqs. (4.91) and (4.93)] in contradiction to the conservation of the NS axial vector current.

- The regularization with (on-shell) massless quarks and off-shell gluons. From the calculational point of view this scheme is difficult, because the gluon off-shellness is difficult to handle in two loops, and consequently the $\delta\gamma_{ij}^{(1)n}$ are not known for general n. However, this scheme is rather meaningful physically for polarized DIS, because it corresponds best to the notion of constituent quarks [56,50,47,511] as will be discussed in detail in Section 5. Furthermore, it avoids the fundamental difficulties with γ_5 present in dimensional regularization. The Wilson coefficients in this scheme are given by [177,413]

$$\delta C_q^n = C_F\Bigg[-\frac{9}{4} - \frac{3}{2n} + \frac{3}{n+1} + \frac{2}{n^2} - \frac{1}{(n+1)^2} + \left(\frac{3}{2} - \frac{1}{n(n+1)}\right)S_1(n) + (S_1(n))^2 - 3S_2(n)\Bigg], \tag{4.95}$$

$$\delta C_g^n = 2T_R\left[\frac{1}{n} - \frac{2}{n+1} - \frac{1}{n^2} + \frac{2}{(n+1)^2}\right], \tag{4.96}$$

where, as previously, $S_k(n) \equiv \sum_{j=1}^n 1/j^k$. In particular one has

$$\delta C_{\rm NS}^1 = \delta C_q^1 = -2\ , \tag{4.97}$$

$$\delta C_g^1 = -\tfrac{1}{2} \tag{4.98}$$

and [50]

$$\delta\gamma_{\mathrm{NS}^-}^{(1)1} = \delta\gamma_{qq}^{(1)1} = 0 \ . \tag{4.99}$$

These results correspond to a nonvanishing gluon contribution to the first moment of g_1 and to conserved, i.e. Q^2-independent, first moments of the polarized quark densities.

A theoretically consistent NLO analysis of polarized structure functions and parton distributions cannot be performed for the time being, apart from their first ($n = 1$) moments since it would require the knowledge of all $\delta\gamma_{ij}^{(1)n}$, or equivalently of $\delta\gamma_{ij}(x)$, in this particular regularization/factorization scheme.

Just as the $\overline{\mathrm{MS}}$ scheme the off-shell scheme naturally fulfills $\delta C_q^1 = -2$. This implies that the coefficient alone saturates the Bjorken sum rule and reproduces the standard correction factor $1 - (\alpha_s/\pi)$ for the first moment of the singlet contribution.

- The regularization with massive quarks. Some of the collinear singularities in the coefficient functions can be regularized by introducing a quark mass. The remaining singularities are again regularized by a nonzero offshellness/mass of the gluon. For example, for the Wilson coefficient of the quark field one obtains to one-loop order [557]

$$\delta C_q^n = C_F\Bigg[-\frac{5}{2} - \frac{5}{2n} + \frac{2}{n+1} + \frac{1}{n^2} - \frac{2}{(n+1)^2} + \left(\frac{7}{2} + \frac{1}{n(n+1)}\right) S_1(n) - 3S_2(n) - (S_1(n))^2 \Bigg] . \tag{4.100}$$

For the first moment this yields $\delta C_q^1 = -\frac{7}{2}C_F$, i.e. not directly the expected correction to the Bjorken sum rule (cf. Section 5 for more explanations on the scheme dependence of the first moment).

Although this scheme is not very tractable in a two-loop calculation, and for the light quarks is usually not considered very physical, its results are sometimes interesting for comparative reasons. For example, in [50] it was shown that the difference $\delta\gamma_{qq}^{(1)1}$(massive quarks)–$\delta\gamma_{qq}^{(1)1}$(massless quarks) is of such a form that it cancels the corresponding change in δC_g^1 so that a scheme independent result arises (for more details see Section 5).

In the case of heavy quarks ($m_q^2 \gg \Lambda_{\mathrm{QCD}}^2$) a calculation with quark masses has to be done, but then the quark mass is not just a regulator (O(m)-terms to be neglected), but has a real physical meaning [577,311]. The heavy quark contribution to PDIS will be discussed in detail in Section 6.

- Keeping the incoming parton (quark or gluon) off-shell is another possibility to renormalize; δC_q is then given by [414,557]

$$\delta C_q^n = C_F\Bigg[-\frac{3}{2n} + \frac{2}{n+1} + \frac{2}{n^2} - \frac{2}{(n+1)^2} + \frac{3}{2}S_1(n) - 4S_2(n) \Bigg] \tag{4.101}$$

and δC_g^n is as in Eq. (4.96). The first moments are again as in Eqs. (4.97) and (4.98), and the ones for the quark anomalous dimensions are given by Eq. (4.99). Again the anomalous dimensions for arbitrary n are not known.

4.4. The behavior of $g_1(x,Q^2)$ at small x

The behavior of g_1 at small x is an important issue because the experimental determination of the first moment of $g_1(x,Q^2)$, as defined in Eq. (3.2), depends on it rather strongly. Therefore it has an influence on tests of the fundamental Bjorken sum rule [118,119] and of the Gourdin–Ellis–Jaffe expectations for $\Gamma_1^{p,n}$, which will be discussed in detail in Section 5, and also on the question how large the contribution from the various parton species to the proton spin is, cf. Eq. (1.1). Due to the very different polarized and unpolarized splitting functions (except for $\delta P_{qq}^{(0)n} = P_{qq}^{(0)n}, \delta P_{\mathrm{NS}\pm}^{(1)n} = P_{\mathrm{NS}\pm}^{(1)n}$) one expects different Q^2 evolutions of $g_1(x,Q^2)$ and $F_{1,2}(x,Q^2)$, respectively, and thus different small-x predictions for these two cases especially in the medium to small-x region ($x < 0.2$) dominated by polarized flavor-singlet contributions $\delta\Sigma$ and δg. According to our results in the two previous subsections, e.g. Eqs. (4.28) and (4.60), these quantum field theoretic renormalization group predictions depend on the input densities $\delta\Sigma(x,Q_0^2)$ and $\delta g(x,Q_0^2)$ to be fixed mainly by experiment. Unfortunately, the present polarization experiments [77,78,25,17,18,20,65,2–4] with their scarce statistics constrain these singlet input densities rather weakly, see, e.g. [52,53,293,313,309], in particular $\delta g(x,Q_0^2)$ remains almost entirely arbitrary, which is in constrast to unpolarized structure functions (see, e.g., [315,318,319]). One therefore has, for the time being, to rely on theoretical prejudices and guesses.

There is a suggestion from Regge theory for the small-x behavior of g_1. Under the assumption that there is no spin-dependent diffractive scattering, one may assume that the $a_1(1260)$ trajectory dominates the Regge asymptotics [143,255] and obtains

$$g_1(x,Q_0^2) \underset{x\to 0}{\sim} x^{-\alpha_{a_1}(0)}, \qquad -0.5 \lesssim \alpha_{a_1}(0) \lesssim 0\ , \tag{4.102}$$

where $\alpha_{a_1}(0)$ is the intercept of the degenerate $a_1(1260), f_1(1285)$ and $f_1(1420)$ Regge trajectories. The scale Q_0^2 where this asymptotic expectation is supposed to hold is entirely unrestricted by Regge arguments. A naive guess would be that $g_1(x,Q_0^2)$ should behave more or less like a constant as $x \to 0$ ($g_1 \sim x^0$), to be compared with a fit [143,255] to the EMC data [77,78], which has been done for the region $x < 0.2$ and yields $g_1^p(x,Q^2) \sim x^{0.07^{+0.32}_{-0.42}}$. The main uncertainty lies of course in the value of $Q^2 = Q_0^2$ where this Regge behavior is implemented. If, for example, we implement Eq. (4.102) at a scale $Q_0^2 \simeq 1\,\mathrm{GeV}^2$ then, according to the QCD evolution, $g_1^p(x,Q^2)$ as well as $\delta q(x,Q^2)$, $\delta\bar{q}(x,Q^2)$ and $\delta g(x,Q^2)$ derived from it will be steeper as $x \to 0$ than in Eq. (4.102) at $Q^2 > 1\,\mathrm{GeV}^2$, e.g. at $Q^2 \simeq 10\,\mathrm{GeV}^2$ relevant for some recent experiments [77,78,25,17,18,20]. The only somewhat reliable conclusion we can draw from this is that g_1 and thus δq_v, $\delta\bar{q}$ and δg will *not* diverge at the same strength as $x \to 0$ as the unpolarized structure functions F_1 and F_2/x since $q_v \sim x^{-\alpha_\rho(0)} \sim x^{-1/2}$ and $\bar{q}, g \sim x^{-\alpha_P(0)} \sim x^{-1}$. The divergence of the unpolarized structure functions for $x \to 0$ is driven by the $1/x$ singularity of the vacuum (Pomeron) exchange which is *not* present in $\delta q_v(x,Q^2)$, $\delta\bar{q}(x,Q^2)$ and $\delta g(x,Q^2)$.

Accepting a particular input behavior at $Q^2 = Q_0^2$, the perturbative QCD prediction at $Q^2 > Q_0^2$ for the singlet sector follows from Eqs. (4.28)–(4.36) and (4.60). Even in the small-x limit one has to resort to the full solutions of the evolution equations since the 'leading pole' or 'asymptotic $1/x$' approximation [248,113,192,87] to the polarized splitting functions is quantitatively (and partly even qualitatively) *not* appropriate [313,294], at least for x-values of experimental relevance,

$x \gtrsim 10^{-3}$. For qualitative purposes it is nevertheless instructive to recall the leading pole (in n) or asymptotic $1/x$ approximation, presented here in LO for simplicity. In polarized scattering *all* $\delta P_{ij}^{(0)}$ in Eqs. (4.21) and (4.26) are less singular as $x \to 0$ than in unpolarized scattering: $\delta P_{ij}^{(0)n} \sim 1/n$ [$\delta P_{ij}^{(0)}(x) \sim$ const.] as compared to $P_{gi}^{(0)n} \sim 1/n - 1$ [$P_{gi}^{(0)}(x) \sim 1/x$] and $P_{qi}^{(0)n} \sim 1/n$ [$P_{qi}^{(0)}(x) \sim$ const.]. This complicates the situation to some extent because polarized quark and gluon densities contribute at the same level. Thus the 2×2 matrix of splitting functions in Eq. (4.25), required for the LO solution (4.28), reduces to

$$\delta \hat{P}^{(0)n} \underset{x \to 0}{\sim} \frac{1}{n} \begin{pmatrix} C_F & -2fT_R \\ 2C_F & 4C_A \end{pmatrix} \tag{4.103}$$

with $C_F = \frac{4}{3}$, $T_R = \frac{1}{2}$, $C_A = 3$. We first diagonalize this matrix and obtain for the eigenvalues [cf. (4.30)]

$$\lambda_{\pm}^{n} = \frac{1}{n} \bar{\lambda}_{\pm}, \qquad \bar{\lambda}_{\pm} = \frac{1}{2} \left(\frac{40}{3} \pm \frac{32}{3} \sqrt{1 - \frac{3f}{32}} \right). \tag{4.104}$$

For $f = 3$ active flavors we have $\bar{\lambda}_{+} = 11.188 \gg \bar{\lambda}_{-} = 2.145$. This means that the second term in Eq. (4.31) which involves the λ_{-}^{n} renormalization group exponent is subleading as $x \to 0$ and we obtain approximately

$$\begin{pmatrix} \delta\Sigma^n(Q^2) \\ \delta g^n(Q^2) \end{pmatrix} \simeq \frac{1}{\bar{\lambda}_{+} - \bar{\lambda}_{-}} \begin{pmatrix} C_F - \bar{\lambda}_{-} & -2fT_R \\ 2C_F & 4C_A - \bar{\lambda}_{-} \end{pmatrix} \begin{pmatrix} \delta\Sigma^n(Q_0^2) \\ \delta g^n(Q_0^2) \end{pmatrix} \mathrm{e}^{(2/\beta_0)(\bar{\lambda}_{+}/n)\xi}, \tag{4.105}$$

where $\xi = \xi(Q^2) \equiv \ln L^{-1} = \ln[\alpha_s(Q_0^2)/\alpha_s(Q^2)]$. Approximately the same result can be obtained, if one uses just the dominant $\delta P_{gg}^{(0)}$ contribution $4C_A$ and neglects the remaining entries in (4.103): In that case one has $\bar{\lambda}_{+} = 4C_A = 12$ and $\bar{\lambda}_{-} = 0$, i.e. a sufficiently accurate approximation [192]. Assuming the input densities to be flat in x as $x \to 0$ [cf. Eq. (4.102)], $\delta\Sigma(x, Q_0^2) \sim$ const. and $\delta g(x, Q_0^2) \sim$ const., i.e. $\delta\Sigma^n(Q_0^2) \sim 1/n$ and $\delta g^n(Q_0^2) \sim 1/n$, Eq. (4.105) can be easily Mellin-inverted, cf. (4.37), on account of [299,467,215]

$$\delta f(x, Q^2) = \frac{1}{2\pi \mathrm{i}} \int_{c-\mathrm{i}\infty}^{c+\mathrm{i}\infty} \mathrm{d}n\, x^{-n} \delta f^n(Q^2) \sim \frac{1}{2\pi \mathrm{i}} \int_{c-\mathrm{i}\infty}^{c+\mathrm{i}\infty} \mathrm{d}n\, x^{-n} \frac{1}{n} \mathrm{e}^{a/n} = I_0 \left(2\sqrt{a \ln \frac{1}{x}} \right). \tag{4.106}$$

Using the asymptotic expression for the modified Bessel function $I_0(z) \sim \mathrm{e}^z/\sqrt{2\pi z} - \mathrm{O}(1/z)$ for large z, we arrive at the 'double leading log' (DLL) formula

$$\delta\Sigma(x, Q^2), \delta g(x, Q^2) \underset{x \to 0}{\sim} C_{\Sigma, g} \exp \left[2\sqrt{\frac{2}{\beta_0} \bar{\lambda}_{+} \xi(Q^2) \ln \frac{1}{x}} \right] \tag{4.107}$$

where all (partly unknown) constants are lumped into $C_{\Sigma,g}$. This gives the dominant $x \to 0$ behavior of the singlet component $g_{1,\mathrm{S}}$ of $g_1 = g_{1,\mathrm{NS}} + g_{1,\mathrm{S}}$ which dominates g_1 because the nonsinglet part (4.27) leads, analogously to the above derivation using $\delta P_{qq}^{(0)n} \sim C_F/n$, to

$$\delta q_{\mathrm{NS}}(x, Q^2) \underset{x \to 0}{\sim} C_{\mathrm{NS}} \exp \left[2\sqrt{\frac{2}{\beta_0} C_F \xi(Q^2) \ln \frac{1}{x}} \right] \tag{4.108}$$

which is again subleading since $\bar{\lambda}_+ \gg C_F$. These results illustrate that for example a positive δg input ($C_g > 0$) drives $\delta\Sigma(x,Q^2)$ negative as $x \to 0$ and Q^2 increases, due to the negative large matrix element $-2fT_R$ in (4.105). Therefore g_1^p is eventually driven negative as well for $x \lesssim 10^{-3}$ and $Q^2 > 1\,\mathrm{GeV}^2$ [87,48]. Thus, estimates of small-x contributions to the first moment $\Gamma_1(Q^2)$ of $g_1(x,Q^2)$ using Regge extrapolations alone will be unreliable, underestimating their size, for a positive δg, and sometimes even giving them the wrong sign [48,87].

Eq. (4.107) may be compared with the asymptotic $1/x$ behavior of the unpolarized structure function $F_{1,2}(x,Q^2)$: Assuming that the gluon with $P_{gg}^{(0)n} \sim 2C_A/(n-1)$ dominates the evolution of the singlet quark combination $\Sigma = q + \bar{q}$, the quantity which couples directly to $F_{1,2}$, one obtains the standard DLL result [299,467,215]

$$xg(x,Q^2) \underset{x\to 0}{\sim} \exp\left[2\sqrt{\frac{2}{\beta_0}2C_A\xi(Q^2)\ln\frac{1}{x}}\right] \tag{4.109}$$

which is in principle similar to the result in Eq. (4.107) but has an additional factor $1/x$ in front due to the dominant vacuum (Pomeron) exchange allowed for spin-averaged structure functions as discussed at the beginning of this subsection.

This relatively simple exercise demonstrates explicitly that $A_1(x,Q^2)$ in Eq. (2.14) will *not* be independent of Q^2 in the small-x region, as commonly assumed [490,77,78,25,17,18,20,65,2,3] for extracting $g_1(x,Q^2)$ [because $\bar{\lambda}_+ \simeq 4C_A > 2C_A$ according to Eqs. (4.107) and (4.109)], i.e.

$$A_1(x,Q^2) \simeq \frac{g_1(x,Q^2)}{F_1(x,Q^2)} \simeq 2x\frac{g_1(x,Q^2)}{F_2(x,Q^2)} \underset{x\to 0}{\sim} x\exp\left\{2(\sqrt{2}-1)\sqrt{\frac{2}{\beta_0}2C_A\xi(Q^2)\ln\frac{1}{x}}\right\}. \tag{4.110}$$

Note that $A_1(x,Q^2) \sim const.$ as $x \to 1$ due to $\delta P_{qq}^{(0)n} = P_{qq}^{(0)n}$ and $\delta P_{\mathrm{NS}\pm}^{(1)n} = P_{\mathrm{NS}\pm}^{(1)n}$ which dominate in the large-x region. It should, however, be emphasized that the above asymptotic results in (4.107) and (4.108) are *not* even qualitatively sufficient for x as low as 10^{-3} when compared with the exact LO/NLO results for A_1 [313,294,309]. They might become relevant for $x \lesssim 10^{-4}$, depending on the input densities [313,294]. In contrast to the unpolarized $F_{1,2}(x,Q^2)$, measurements of $g_1(x,Q^2)$ in the small-x region will be far more difficult due to $A_1(x,Q^2) \simeq 2xg_1/F_2 \to 0$ as $x \to 0$ according to (4.110). Here, a fully polarized HERA $\vec{e}\vec{p}$ collider [123,124,369] would be of great help to delineate the small-x behavior of g_1 which is expected to be entirely different in QCD [48,87,551,276,224,28] as compared to naive Regge extrapolations in (4.102) as discussed above after Eq. (4.108).

In addition, the evolution of parton distributions $f(x,Q^2)$ involve in general convolutions $P\otimes f$, see e.g. Eqs. (4.12), (4.14) and (4.19), which are sensitive to the shape of these distributions in the large-x region, even for $(P\otimes f)(x \to 0)$. This can be easily envisaged by considering according to Eq. (4.102), for example,

$$f(x) = x^{-\alpha}(1-x)^a = x^{-\alpha}\sum_{n=0}^{a}\binom{a}{n}x^n \tag{4.111}$$

which implies for the convolution, using $P(x) = 1/x^p$ with $p \geq 0$,

$$(P\otimes f)(x\to 0) \simeq \frac{1}{x^p}\sum_n\binom{a}{n}\frac{1}{n+p-\alpha} - \frac{x^{-\alpha}}{p-\alpha} + \mathrm{O}(x^{p-\alpha}). \tag{4.112}$$

Thus, because of the remaining a-dependence, the behavior of $P\otimes f$ in the small-x limit is closely correlated with the distributions in the *large-x* region! A more detailed quantitative analysis can be found in [294]. Therefore the mere knowledge of $P(x)$ and $f(x,Q^2)$ as $x\to 0$ is insufficient to predict the small-x behavior of $g_1(x,Q^2)$. It is thus apparent that reliable results can only be obtained by performing *full* LO and/or NLO analyses as described in the previous Sections 4.1 and 4.2 [313,309]. Anyway, the scale-violating Q^2-dependence of $A_1(x,Q^2)$ is a general and specific feature of perturbative QCD as soon as gluon and sea densities become relevant. This is due to the very different polarized and unpolarized splitting functions $\delta P_{ij}^{(0,1)}$ and $P_{ij}^{(0,1)}$, respectively (except for $x\to 1$ as discussed above, after Eq. (4.110)).

Finally, we turn to the more speculative nonperturbative approach to the small-x behavior of g_1. The result in Eq. (4.102) is obtained if there is no spin dependence in diffractive scattering. The possibility of spin-dependent diffractive scattering has been examined in [192,102] where it has been shown that a logarithmic rise of g_1 at small x could in principle be induced

$$g_1(x,Q^2)\underset{x\to 0}{\sim}\ln(1/x) \tag{4.113}$$

with the scale Q^2 being entirely unspecified. An explicit calculation [102], being based on the exchange of two nonperturbative gluons, has manifested this $\ln x$ behavior, i.e. $g_1\sim 2\ln(1/x)-1$. The behavior in Eq. (4.113) is by no means compelling but it shows that there is a considerable amount of theoretical uncertainty, at least as far as the nonperturbative input distributions are concerned. A numerical analysis shows that this leads to an uncertainty in the determination of the first moment, defined in Eq. (3.2), typically about 10% [192]. This can be seen by taking the present experimental results with cut values $x\gtrsim 0.01$, cf. Eq. (3.4), and fitting Eqs. (4.102) and (4.113) in the small-x region.

Even extreme double-logarithmic contributions $g_1\sim\ln^2(1/x)$ are conceivable and, in fact, claimed to be present at $x\ll 1$ [192,263,93,94], which are not included in the usual RG evolution equation. More precisely, in a simple ladder approach one has for each (except for the first) power of α_s terms of the form $(\alpha_s\ln^2(1/x))^2$. Summing up to arbitrary order in α_s one obtains $g_1\sim(1/x)^{c_1\sqrt{\alpha_s}}$. This is to be contrasted to the unpolarized structure function F_1 for which one gets in this approach $F_1\sim(1/x)^{c_2\alpha_s}$. The latter result is obtained by resumming single logarithms of $1/x$ where double logarithms are not present in the unpolarized case. Numerically, the exponent $c_1\sqrt{\alpha_s}$ turns out to be larger than 1 for the singlet contribution to g_1. Therefore in this approach the first moment of g_1 does not exist. This probably signals a breakdown of the approximation used and suggests that other, yet unknown, terms in addition to the logarithms of x have to be summed as well.

A recent more detailed and consistent analysis [126,125] has demonstrated, however, that such more singular terms are not present in the flavor nonsinglet contribution to g_1 because potentially large $\ln^n x$ contributions get cancelled by similar singular terms in the Wilson coefficients. Such a conclusion cannot be reached for the singlet contribution to g_1 since less singular terms of the NNLO (3-loop) singlet splitting functions have not yet been calculated [127].

5. The first moment of g_1

5.1. The first moment and the gluon contribution

Quantities of particular significance are the first moments of polarized parton distributions $\delta f(x,Q^2)$,

$$\Delta f(Q^2) \equiv \int_0^1 \mathrm{d}x\, \delta f(x,Q^2), \quad f = q, \bar{q}, g \tag{5.1}$$

since they enter the fundamental spin relation Eq. (1.1). According to Eqs. (4.1) and (4.2), $\Delta(q+\bar{q})$ is the net number of right-handed quarks of flavor q inside a right-handed proton and thus $\frac{1}{2}\Delta\Sigma(Q^2)$, cf. Eq. (4.9), is a measure of how much all quark flavors contribute to the spin of the proton. Similarly, $\Delta g(Q^2)$ in (1.1) represents the total gluonic contribution to the spin of the nucleon. Later we shall try to answer the important question of how much these first moments contribute numerically to the spin of the proton. The present experimental results on the first moment $\Gamma_1(Q^2) \equiv \int_0^1 \mathrm{d}x\, g_1(x,Q^2)$, defined in Eq. (3.2) and reviewed in Section 3, have a better statistics than $g_1(x,Q^2)$ itself, just because $\Gamma_1(Q^2)$ is an average. It should, however, be kept in mind that the determination of $\int_0^1 \mathrm{d}x\, g_1(x,Q^2)$ relies on theoretical assumptions concerning the extrapolations for $x \to 0$ and $x \to 1$ since the actual (x,Q^2) dependent data extend only over a limited range of x.

Let us first study the scale (Q^2) dependence of $\Delta\Sigma(Q^2)$ and $\Delta g(Q^2)$ in LO. The $n=1$ moment of the singlet evolution equations in (4.25) is given by

$$\begin{aligned}\frac{\mathrm{d}}{\mathrm{d}t}\begin{pmatrix}\Delta\Sigma(Q^2)\\ \Delta g(Q^2)\end{pmatrix} &= \frac{\alpha_s(Q^2)}{2\pi}\begin{pmatrix}\Delta P_{qq}^{(0)}, & 2f\Delta P_{qg}^{(0)}\\ \Delta P_{gq}^{(0)}, & \Delta P_{gg}^{(0)}\end{pmatrix}\begin{pmatrix}\Delta\Sigma(Q^2)\\ \Delta g(Q^2)\end{pmatrix} + \mathcal{O}(\alpha_s^2)\\ &= \frac{\alpha_s(Q^2)}{2\pi}\begin{pmatrix}0, & 0\\ 2, & \dfrac{\beta_0}{2}\end{pmatrix}\begin{pmatrix}\Delta\Sigma(Q^2)\\ \Delta g(Q^2)\end{pmatrix} + \mathcal{O}(\alpha_s^2)\end{aligned} \tag{5.2}$$

according to Eq. (4.26) , and $\beta_0 = \frac{1}{3}(11N_c - 2f)$ is the coefficient appearing in the renormalization group equation for $\alpha_s, \mathrm{d}\alpha_s/\mathrm{d}t = -\beta_0\alpha_s^2/4\pi + \mathcal{O}(\alpha_s^3)$, with $N_c = 3$ and $f = 3$ for the relevant 'light' u,d,s flavors. The Q^2-independence of $\Delta\Sigma$ is trivial due to $\Delta P_{qq}^{(0)} = \Delta P_{qg}^{(0)} = 0$ which holds also for each NS combination in (4.24) due to $\mathrm{d}/\mathrm{d}t\, \Delta q_{\mathrm{NS}}(Q^2) = 0 + \mathcal{O}(\alpha_s^2)$. Thus the total polarization of each (anti)quark flavor is *conserved*, i.e. Q^2-independent in LO: $\Delta^{(-)}q\,(Q^2) = \text{const}$. The vanishing of $\Delta P_{qg}^{(0)}$ can be understood as follows: assume that a gluon of positive helicity $+1$ splits into a $q\bar{q}$ pair. Then the helicity of the quark will always be $+\frac{1}{2}$ and that of the antiquark $-\frac{1}{2}$, and therefore $\Delta P_{qg}^{(0)} = 0$. (Note that in this process angular momentum is produced.) $\Delta P_{qq} = 0$ is a consequence of $\delta P_{qq}^{(0)}(x) = P_{qq}^{(0)}(x)$ together with the so-called Adler sum rule [32] which says that the number of quarks of a certain flavor inside the proton is Q^2-independent. In chirality-preserving regularization schemes the Q^2-independence of $\Delta^{(-)}q$ holds true even beyond the leading order. Furthermore, Eqs. (5.2) imply for $\alpha_s\Delta g$

$$\frac{\mathrm{d}}{\mathrm{d}t}[\alpha_s(Q^2)\Delta g(Q^2)] = 0 + \mathcal{O}(\alpha_s^2) \tag{5.3}$$

and thus $\alpha_s(Q^2)\Delta g(Q^2) \simeq$ const., i.e. Q^2-independent in LO [431,304,305,55], but not in higher orders. This is a rather peculiar property of the $n = 1$ moment of $\delta g(x, Q^2)$ and derives formally from the appearance of β_0 in $\Delta P_{gg}^{(0)}$. Therefore the product $\alpha_s \Delta g$ behaves more like an object of order $\mathcal{O}(1)$, although strictly speaking it refers to a combination which enters only in NLO, and any contribution $\sim \alpha_s \Delta g$ to $\Gamma_1(Q^2)$ could be in principle potentially large, irrespective of the value of Q^2. From the theoretical point of view it is important to note that $\alpha_s(Q^2)\Delta g(Q^2)$ becomes Q^2-dependent beyond the LO. However, for practical purposes the Q^2-dependence is too small to distinguish $\Delta\Sigma$ and $\alpha_s(Q^2)\Delta g(Q^2)$ by examining this Q^2-dependence.

In the LO-QCD parton model one has, using the $SU(3)$ flavor decomposition Eq. (4.6),

$$\Gamma_1^{p,n}(Q^2) = \tfrac{1}{2}(\pm \tfrac{1}{6}A_3 + \tfrac{1}{18}A_8 + \tfrac{2}{9}A_0) , \tag{5.4}$$

where

$$A_3 = \Delta u + \Delta\bar{u} - \Delta d - \Delta\bar{d} , \tag{5.5}$$

$$A_8 = \Delta u + \Delta\bar{u} + \Delta d + \Delta\bar{d} - 2(\Delta s + \Delta\bar{s}) , \tag{5.6}$$

$$A_0 \equiv \Delta\Sigma = \sum_q (\Delta q + \Delta\bar{q}) = A_8 + 3(\Delta s + \Delta\bar{s}) , \tag{5.7}$$

with A_i being related to $M_i^{n=1}$ in Eq. (4.75) in an obvious way. As discussed above, the two flavor nonsinglet combinations ($A_{3,8}$) and the singlet $A_0 \equiv \Delta\Sigma$ are independent of Q^2 in LO QCD. As discussed already in Section 4.3 (in particular after Eq. (4.94)), the NS combinations have to remain Q^2-independent, i.e. conserved to any order in α_s due to the absence of the gluon-initiated γ_5-anomaly in the NS sector. This is in contrast to the singlet component A_0 which can and will become Q^2-dependent beyond the LO, depending of course on the specific factorization scheme chosen (e.g. due to the nonvanishing $\Delta\gamma_{qq}^{(1)}$ in (4.94) in the $\overline{\text{MS}}$ scheme). The fundamental conserved NS quantities A_3 and A_8 can be fixed by the Gamov–Teller part of the (flavor changing) octet hyperon β-decays (F, D values) [529,530,63]:

$$A_3 = F + D = g_A/g_V = 1.2573 \pm 0.0028 , \tag{5.8}$$

$$A_8 = 3F - D = 0.579 \pm 0.025 \tag{5.9}$$

with the F, D values taken from [480,191]. It should be noted that the result for A_3 relies only on the fundamental $SU(2)$ isospin symmetry, i.e. is obtained just from the neutron β-decay. In order to obtain A_8 one has, however, to extend the phenomenological analysis of the g_A/g_V ratios to the full $SU(3)$ baryon octet, the spin $\frac{1}{2}$ hyperons p, n, Λ, $\Sigma^{0,\pm}$ and $\Xi^{0,-}$. The β-decay of some of these baryons or, more precisely, the transition of strange into nonstrange components, can be used to get information about A_8. Thus the main assumptions used are $SU(3)_f$ symmetry and the approximation of massless quarks – both are not very precise but are to some extent reasonable. Then the hyperon transition matrix elements of the octet of the axial vector currents are of the general form

$$\langle H_j PS|J_{5\mu}^i|H_k PS\rangle = S_\mu(-if_{ijk}F + d_{ijk}D) , \tag{5.10}$$

where the hyperons are denoted by H_i, $i = 1, \ldots, 8$ ($H_1 = \Sigma^0$, etc.) and f_{ijk} and d_{ijk} are the totally antisymmetric and symmetric $SU(3)$ group constants, respectively. The expression (5.10) is completely fixed by the two constants F and D, with a recent experimental fit resulting in [480,191]

$$F = 0.459 \pm 0.008, \quad D = 0.798 \pm 0.008 \,, \tag{5.11}$$

i.e. $F/D = 0.575 \pm 0.016$, which gives A_8 in Eq. (5.9). Moreover, Eqs. (5.8) and (5.9), together with (5.5) and (5.6), allow to express $\Delta(u + \bar{u})$ and $\Delta(d + \bar{d})$ in terms of $\Delta(s + \bar{s})$:

$$\Delta u + \Delta\bar{u} = \tfrac{1}{2}(A_8 + A_3) + \Delta s + \Delta\bar{s} = 0.92 + \Delta s + \Delta\bar{s} \,, \tag{5.12}$$

$$\Delta d + \Delta\bar{d} = \tfrac{1}{2}(A_8 - A_3) + \Delta s + \Delta\bar{s} = -0.34 + \Delta s + \Delta\bar{s} \,. \tag{5.13}$$

The crude assumption $\Delta s = \Delta\bar{s} = 0$ essentially corresponds to the so-called Ellis–Jaffe sum rule to be discussed below. A finite $\Delta s = \Delta\bar{s} \neq 0$ (as likely to be the case experimentally) obviously implies significant changes of the total polarizations carried by u und d quarks in Eqs. (5.12) and (5.13). Apart from contributing differently to the nucleon's spin, such changes of $\Delta(u + \bar{u})$ and $\Delta(d + \bar{d})$ from their 'canonical' values $\frac{1}{2}(A_8 \pm A_3)$ in (5.12) and (5.13) may be of astrophysical relevance [249–252,336] as well as of substantial consequences for, e.g., laboratory searches of supersymmetric dark matter candidates, and for the flux of neutrinos from supersymmetric dark matter annihilation in the sun (which will be reduced due to the reduced photino/neutralino trapping rate in the sun).

The constraint equations (5.8) and (5.9) are the ones used in most analyzes performed so far and we shall refer to them as the $SU(3)_f$ symmetric 'standard' scenario. While the validity of (5.8) is unquestioned since it depends merely on the fundamental $SU(2)_f$ isospin rotation ($u \leftrightarrow d$) between charged and neutral axial currents, the constraint Eq. (5.9) depends critically on the assumed $SU(3)_f$ flavor symmetry between hyperon decay matrix elements of the flavor changing charged weak axial currents and the neutral ones relevant for $\Delta f(Q^2)$. Although there are some arguments in favor of this latter full $SU(3)_f$ symmetry [545], there are serious objections to it [529,530,407,64,449], i.e. to the constraint Eq. (5.9). We shall come back to these $SU(3)_f$ symmetry breaking effects later.

Inserting the constraints Eqs. (5.8) and (5.9) into Eq. (5.4) gives, using (5.7),

$$\begin{aligned} \Gamma_1^{p,n} &= \pm\frac{1}{12}(F + D) + \frac{5}{36}(3F - D) + \frac{1}{3}(\Delta s + \Delta\bar{s}) \\ &= \left\{ \begin{matrix} 0.185 \pm 0.004 \\ -0.024 \pm 0.004 \end{matrix} \right\} + \frac{1}{3}(\Delta s + \Delta\bar{s}) \,, \end{aligned} \tag{5.14}$$

where the contribution from the strange sea remains unknown since the flavor changing (NS) hyperon β-decay data cannot constrain the singlet quantity $A_0 \equiv \Delta\Sigma$ in Eq. (5.7). *Assuming* naively $\Delta s = \Delta\bar{s} = 0$, Eq. (5.14) gives

$$\Gamma_{1,\mathrm{EJ}}^{p} \simeq 0.185 \tag{5.15}$$

which is the so-called Ellis–Jaffe 'sum rule' originally derived in [333,253,254]. This 'naive' theoretical expectation lies, however, significantly *above* present measurements (cf. Table 2). This

fact is usually referred to as the 'spin crisis' or more appropriately 'spin surprise' since a sizeable negative polarization of the strange sea is required [304,305,252,249] in Eq. (5.14) ($\Delta s = \Delta\bar{s} \simeq -0.05$ to -0.1) in order to *reduce* $\Gamma_{1,\mathrm{EJ}}^p$, i.e. to reduce significantly the singlet contribution $\Delta\Sigma$ in (5.7) relative to A_8; thus $\frac{1}{2}\Delta\Sigma \ll \frac{1}{2}$, i.e. the quark flavors seem to contribute marginally to the spin of the proton, Eq. (1.1), which is surprising indeed! Alternatively, a negative polarization of the light sea quarks ($\Delta\bar{u} \simeq \Delta\bar{d} < 0$, keeping $\Delta s = \Delta\bar{s} = 0$) could also account for a suppression of $\Delta\Sigma$ in Eq. (5.7) when $SU(3)_f$ symmetry-breaking effects are taken into account [450,451,448], i.e. when the constraint Eq. (5.9) does not hold anymore; or a negative $\alpha_s\Delta g$ contribution to $\Delta\Sigma$ could equally account for the required reduction [55,241] of A_0 in Eq. (5.7). The latter scenario of a large gluon contribution will be discussed in detail below. More detailed quantitative analyses and results will be discussed in Section 6. Here it suffices to remark that one does not expect intuitively a large total polarization of strange sea quarks due to the fact that it is easier for a gluon to create a nonstrange 'light' pair ($u\bar{u}$, $d\bar{d}$) than a heavier strange pair – a situation very similar to the unpolarized broken $SU(3)$ sea [315,318,319] as observed by neutrino-nucleon scattering experiments [10,277,496].

It is perhaps also interesting to compare the above results with the expectations of a (nonperturbative) 'constituent' quark model [357,186,440]. The constituent models generally fulfil $\Delta\Sigma = 1$, i.e. the entire nucleon spin is saturated by valence quark spins. Among the conventional 'extreme' constituent models, the static $SU(6)$ model [357,186,440] is the most favorable, because it is able to explain some of the static properties of nucleons. For example, the $SU(6)$ model explains the measured ratio μ_n/μ_p to be about $-\frac{2}{3}$ (experimental value $= -0.685$).[6]

However, it fails to predict $g_A/g_V \simeq 1.26$ correctly but gives $g_A/g_V = \frac{5}{3}$. Since g_A/g_V is the triplet ingredient of $\int_0^1 g_1(x,Q^2)\,\mathrm{d}x$ one suspects that $SU(6)$ will fail for $\int_0^1 g_1(x,Q^2)\,\mathrm{d}x$ as well.

In a static picture of the nucleon, in which the nucleon consists purely of valence quarks, its wave function can be found by counting all possible antisymmetric combinations of three quark states. If there is negligible L_z in the system, one quark spin is always antiparallel to the other two. The proton can then be described by a wave function which is a member of a 56-plet of $SU(6)$, and the probabilities to find u_+, u_-, d_+ and d_- in the proton turn out to be 5/3,1/3,1/3 and 2/3, respectively. For the neutron the role of u and d are to be interchanged. Thus $\Delta u = 4/3$, $\Delta d = -1/3$ and $\Delta\bar{u} = \Delta\bar{d} = \Delta s = \Delta\bar{s} = 0$, i.e.

$$A_3^{SU(6)} = \tfrac{5}{3}, \quad A_8^{SU(6)} = A_0^{SU(6)} = 1 \tag{5.16}$$

[6] It is instructive to remind the reader that constituent quark models may be used to represent the nucleon magnetic moments μ_N in terms of quark magnetic moments $\mu_q = e/2\hat{m}_q$ where $\hat{m}_q$ is the constituent quark mass, e.g. $\hat{m}_u = 336$ MeV [95,408,168,360]. This fact can be used to derive the successful relation $\mu_n/\mu_p = -\frac{2}{3}$. Writing $\mu_p = \mu_u(u_+ - u_-) + \mu_d(d_+ - d_-) + \mu_s(s_+ - s_-)$ it is even possible to include strange quark contributions [95,408,360]. However, a real understanding of Γ_1^p within constituent models will never be possible. The reason for this is that in magnetic moments antiquarks count with opposite sign than in Γ_1^p. Constituent quark models are able to account for antiquarks but informations from magnetic moment measurements cannot be used to get informations on Γ_1^p because in magnetic moments combinations $\Delta q - \Delta\bar{q} = q_+ - q_- - \bar{q}_+ + \bar{q}_-$ enter, whereas Γ_1^p is determined by combinations $\Delta q + \Delta\bar{q} = q_+ - q_- + \bar{q}_+ - \bar{q}_-$.

so that

$$\Gamma_1^{p,SU(6)} = \tfrac{5}{54}, \quad \Gamma_1^{n,SU(6)} = 0 \ . \tag{5.17}$$

These numbers deviate only by about 30% in the NS sector from the experimental results, Eqs. (5.8) and (5.9), but the difference is huge in the singlet sector $A_0 \ll A_0^{SU(6)} = 1$ – again a rather surprising result. It should be kept in mind, however, that constituent quarks are strictly nonperturbative objects which cannot be reached by perturbative evolutions in contrast to partonic quarks which should rather be identified with the current quark content of hadrons.

It should, however, be kept in mind that in relativistic quark models such as the MIT-Bag Model, the Cloudy Bag Model or the Nambu–Jona–Lasinio model, the static SU(6) expectations in (5.16) are significantly reduced, bringing them close to their physical, i.e. experimental values (for a recent review, see [101]).

The NLO corrections to Eq. (5.4) in the $\overline{\rm MS}$ scheme can be directly read off Eq (4.62):

$$\Gamma_1^{p,n}(Q^2) = \left(1 - \frac{\alpha_s(Q^2)}{\pi}\right)\left[\pm \frac{1}{12}A_3 + \frac{1}{36}A_8 + \frac{1}{9}\Delta\Sigma(Q^2)\right], \tag{5.18}$$

where we used Eqs. (4.91) and (4.92); the NS combinations $A_{3,8}$ remain Q^2-independent due to the vanishing of $\Delta\gamma_{\rm NS-}^{(1)}$ in (4.93) in contrast to the singlet combination $A_0(Q^2) \equiv \Delta\Sigma(Q^2)$ since $\Delta\gamma_{qq}^{(1)} \neq 0$ in (4.94). The total polarizations of the parton distributions themselves evolve according to Eqs. (4.54) and (4.55) with $n = 1$ and the LO $\Delta P_{ij}^{(0)}$ given in Eq. (5.2) and the NLO $\Delta P_{ij}^{(1)}$ given by [478] (see footnotes 4 and 5)

$$\begin{aligned}
&\Delta P_{\rm NS-}^{(1)} = 0, \qquad \Delta P_{\rm NS+}^{(1)} \approx -0.3197 \ , \\
&\Delta P_{qq}^{(1)} = -2f, \qquad \Delta P_{qg}^{(1)} = 0 \ , \\
&\Delta P_{gq}^{(1)} = \frac{1}{3}\left(59 - \frac{2f}{3}\right), \qquad \Delta P_{gg}^{(1)} = \frac{\beta_1}{4}
\end{aligned} \tag{5.19}$$

where again $\beta_1 = 102 - \frac{38}{3}f$. Note that $\Delta g(Q^2)$ in Eq. (4.62) does *not* contribute to Γ_1 in (5.18) in the $\overline{\rm MS}$ factorization since here the first moment decouples due to $\Delta C_g \equiv \delta C_g^{n=1} = 0$, cf. (4.92). It should be emphasized, however, that an actual analysis of present data which are available only in a limited x-range requires *all* moments in (4.62) where $\delta g^n(Q^2)$, or equivalently $\delta g(x, Q^2)$, represent an important contribution to $g_1(x, Q^2)$ as we shall see in Section 6. Furthermore such an analysis is, for the time being, possible only in the $\overline{\rm MS}$ scheme where *all* two-loop $\delta P_{ij}^{(1)}$ are known [478,568,569], unless one allows for transformations (4.69) to other factorization schemes. Moreover, since the polarized and unpolarized parton densities originate from the *same* densities of definite positive and negative helicities, $\delta f = f_+ - f_-$ and $f = f_+ + f_-$ according to Eqs. (4.1)–(4.4) and (4.10), it is also desirable to remain within the factorization scheme commonly used in all present NLO analyzes of unpolarized deep inelastic/hard processes – which is the $\overline{\rm MS}$ scheme. This is of particular importance for a consistent implementation of the fundamental positivity constraints (4.11).

For completeness it should be mentioned that the NLO($\overline{\text{MS}}$) result in Eq. (5.18) has been extended to even higher orders [438]:

$$\Gamma_1^{p,n}(Q^2) = \left(\pm\frac{1}{12}A_3 + \frac{1}{36}A_8 \right)\left(1 - \frac{\alpha_s(Q^2)}{\pi} - 3.5833\left(\frac{\alpha_s(Q^2)}{\pi}\right)^2\right) + \frac{1}{9}\Delta\Sigma(Q^2)\left(1 - \frac{\alpha_s(Q^2)}{\pi} - 1.0959\left(\frac{\alpha_s(Q^2)}{\pi}\right)^2\right) \tag{5.20}$$

for $f = 3$ light flavors. The evolution of $\Delta\Sigma(Q^2)$ involves now, in contrast to the NLO result (5.18), two- *and* three-loop anomalous dimensions of the singlet axial current [438]. The Q^2 corrections to the NS coefficient function for the $A_{3,8}$ contributions have been calculated [439] even to $\mathcal{O}(\alpha_s^3)$. This is relevant for the (nonsinglet) Bjorken sum rule to be discussed in Section 5.4.

Although a complete NLO analysis for all moments is usually performed in the $\overline{\text{MS}}$ scheme, there is a factorization scheme for the *first* moment, which is closer to the constituent quark picture Eq. (5.16); it allows, at least in principle, for larger contributions of $\Delta\Sigma$ to the spin sum rule (1.1). This is the scheme corresponding to Eq. (4.46), or the off-shell scheme resulting in Eqs. (4.97) and (4.98), where Eq. (4.62) yields

$$\Gamma_1^{p,n}(Q^2) = \left(1 - \frac{\alpha_s(Q^2)}{\pi}\right)\left(\pm\frac{1}{12}A_3 + \frac{1}{36}A_8 + \frac{1}{9}\Delta\Sigma_{\text{off}}\right) - \frac{1}{9}f\frac{\alpha_s(Q^2)}{2\pi}\Delta g(Q^2)$$
$$= \left(1 - \frac{\alpha_s(Q^2)}{\pi}\right)\left(\pm\frac{1}{12}A_3 + \frac{1}{36}A_8 + \frac{1}{9}A_0(Q^2)\right) + \mathcal{O}(\alpha_s^2) \tag{5.21}$$

for $f = 3$ light quark flavors and where the singlet contribution is now given by

$$A_0(Q^2) = \Delta\Sigma_{\text{off}} - f\frac{\alpha_s(Q^2)}{2\pi}\Delta g(Q^2) \tag{5.22}$$

in contrast to the identification (5.7) which appears also in (5.18). Here, $\Delta\Sigma_{\text{off}}$ is different from the quantity $\Delta\Sigma(Q^2)$ appearing in (5.18) and is Q^2 *in*dependent due to the vanishing of $\Delta\gamma_{qq}^{(1)}$ in (4.99). Whether this conserved $\Delta\Sigma_{\text{off}}$ is used to define the actual polarized quark densities or alternatively the 'renormalized' nonconserved quantity $\Delta\Sigma(Q^2) \equiv A_0(Q^2)$, is a matter of theoretical convention (choice of factorization scheme) or 'intuitive' physical interpretation [46,47,510,511] as shall be discussed below. It should be remembered that only the *products* $\Delta C_i A_i$ and $\Delta C_g \Delta g$ in Eq. (5.21) are renormalization convention *in*dependent quantities to the $\mathcal{O}(\alpha_s^2)$ considered, which can therefore be meaningfully related to physical, i.e. experimental measurements. In this sense the second line in Eq. (5.21) is identical to the first one since the NNLO terms $\mathcal{O}(\alpha_s^2)$ are disregarded. It is this latter expression which has been frequently used for first moment analyses in the past, for example in [56,52,53,293]. It should be again mentioned that in these (non-$\overline{\text{MS}}$) factorization schemes only the $n = 1$ moments of splitting functions (anomalous dimensions) have been calculated so far to which we will now turn.

Originally, NLO contributions to the first moment $\Gamma_1(Q^2)$ have been calculated by Kodaira [413] with the help of the operator product expansion near the light cone using an off-shell

factorization scheme with all external lines kept off-shell ($p^2 < 0$) and assuming massless quarks and gluons. They have been confirmed and substantially reinterpreted in the framework of the QCD-based parton model in recent years [55,241,158,50]. The upshot of the result in the off-shell scheme is that Eq. (5.4) goes over to

$$\Gamma_1^{p,n}(Q^2) = \left(\pm \frac{1}{12} A_3 + \frac{1}{36} A_8 \right) \left(1 - \frac{\alpha_s(Q^2)}{\pi} \right) + \frac{1}{9} A_0 \left[1 - \frac{\alpha_s(Q^2)}{\pi} \left(1 - \frac{2f}{\beta_0} \right) \right], \tag{5.23}$$

where $A_0 \equiv A_0(Q^2)[1 - (\alpha_s(Q^2)/\pi)(2f/\beta_0)]$ and $A_0(Q^2)$ is given by (5.22) for $f = 3$ light quark flavors. This result fixes the effect of the quarks and gluons and incorporates all scaling violations up to next-to-leading order. Remember that all the $\Delta^{(-)}q$ in $\Delta\Sigma$ are Q^2 independent quantities due to Eq. (4.99).

Several remarks are in order: the decomposition of $A_0(Q^2)$ into a quark and a gluon contribution, Eq. (5.22), was not known to Kodaira [413] because he worked in the framework of the OPE where the basic objects, and in particular the singlet part $A_0(Q^2)$, are matrix elements. The decomposition becomes only apparent in the QCD parton model where the gluon term is induced by the photon-gluon fusion process in Fig. 17. The coefficient $f = 3$ of Δg in Eq. (5.22) is the number of light quarks because heavy quarks (with masses much larger than $\Lambda_{\rm QCD}$) can be shown to yield a vanishing first moment contribution [577,433,311]. This is a consequence of the matrix element calculation which will be discussed in Section 5.3.

The factors $1 - (\alpha_s(Q)/\pi)$ in Eq. (5.23) arise from the Wilson coefficient of the quarks, both for the nonsinglet and singlet contribution. The fact that $\Delta\Sigma$ and Δg appear in a factorized form in Eq. (5.22) has to do with the fact that for the singlet there is only one operator. Thus the expansion of the RG exponent is formally the same as for the nonsinglet case in (4.80) or (4.83) which contributes $(\alpha_s/4\pi)(\Delta\gamma_{qq}^{(1)}/2\beta_0) = (\alpha_s/\pi)(2f/\beta_0)$ in the OPE scheme used by Kodaira [413], using $\Delta\gamma_{qq}^{(0)} = 0$. Since this two-loop term $\sim 2f/\beta_0$ in Eq. (5.23) has been explicitly factored out from the (fermionic) singlet matrix element, according to Kodaira's original calculation [413], the A_0 in Eq. (5.23) [but not $A_0(Q^2)$] is Q^2-*in*dependent in this specific way of writing. The A_0 in Eq. (5.23) should in fact depend on the renormalization (input) scale μ. This dependence has been suppressed here but will be made explicit later [cf. Eq. (5.53)]. Note that the term $\sim 2f/\beta_0$ does not arise in the nonsinglet part in (5.23), but is inherently a singlet contribution and a two-loop effect of the triangle anomaly (Fig. 20).

It is evident from the above results and discussions that the representation Eq. (5.22) of $A_0(Q^2)$ in terms of $\Delta\Sigma$ and Δg depends on the regularization scheme, despite the fact that the remaining Q^2-dependent corrections in Eq. (5.23) are scheme independent. The appearance of the gluon in (5.22), with the $-\alpha_s/2\pi$ coefficient as calculated directly from the photon–gluon fusion diagram in Fig. 17 using an off-shell regularization, could account for the reduction of the singlet contribution to $\Gamma_1(Q^2)$ [55,241,158] required by experiment as discussed in particular after Eq. (5.15). For example, the recent experimental average result for Γ_1^p in (3.9) at $Q^2 = 5$ to $10\,\mathrm{GeV}^2$ implies, using Eq. (5.21) together with (5.8) and (5.9) for $A_{3,8}$,

$$A_0(Q^2) \equiv \Delta\Sigma_{\rm off} - 3\frac{\alpha_s(Q^2)}{2\pi}\Delta g(Q^2) = 0.27 \pm 0.13 \tag{5.24}$$

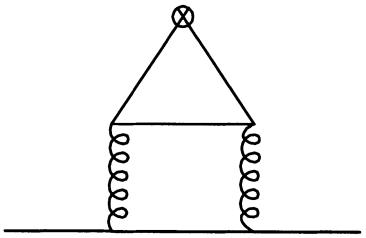

Fig. 20. The two-loop triangle diagram which contributes to the singlet $\Delta\gamma_{qq}^{(1)}$.

at $Q^2 = 5$ to $10\,\mathrm{GeV}^2$.[7] Making the extreme and equally naive assumption that $\Delta s = \Delta\bar{s} = 0$ and disregarding any effects due to flavor $SU(3)_f$ breaking, one obtains a large $\Delta\Sigma = A_8 + 3(\Delta s + \Delta\bar{s}) = A_8 = 0.579 \pm 0.025$ according to Eqs. (5.7) and (5.9). If one wants to keep a large and conserved $\Delta\Sigma \simeq 0.6$ and at the same time reduce the Ellis–Jaffe prediction (5.15) to the experimental measurement in Eq. (3.9), a value

$$\Delta g(Q^2 = 10\,\mathrm{GeV}^2) = 3.4 \pm 1.5 \tag{5.25}$$

is required by Eq. (5.24). This number is obtained with the NLO $\alpha_s(10\,\mathrm{GeV}^2)/\pi = 0.061$ for $\Lambda_{\overline{\mathrm{MS}}} = 0.2\,\mathrm{GeV}$. Similar results have been obtained recently by QCD-fits performed directly by the experimental E154 and SMC groups [9,224,31], for example, who arrived at $\Delta g(5\,\mathrm{GeV}^2) \simeq 1.7 \pm 1.1$ although it is difficult to estimate the total error on Δg for the time being. Realistically, however, there is no reason for a vanishing total helicity of strange quarks and one expects a combination of *both* effects ($\Delta g \neq 0$ and $\Delta s = \Delta\bar{s} \neq 0$), probably with additional flavor $SU(3)_f$ breaking effects, to account for the required singlet suppression in Eq. (5.24). As we shall see in the next section, present data are far too scarce for distinguishing or confirming the various scenarios. Before turning to a discussion of more detailed (x, Q^2) dependent analyses of present experiments, let us concentrate on a few theoretical aspects concerning the total helicities (first moments) of quarks and gluons for the remainder of this section.

As already mentioned above, it is a matter of theoretical convention to interpret $\Delta\Sigma$ as the actual total helicity of the singlet quark densities or effectively the entire singlet expression (5.22)

$$\Delta\Sigma(Q^2) \equiv \Delta\Sigma_{\mathrm{off}} - 3\frac{\alpha_s(Q^2)}{2\pi}\Delta g(Q^2) \tag{5.26}$$

which, in contrast to $\Delta\Sigma_{\mathrm{off}}$, is Q^2-dependent and effectively has to be interpreted as the singlet contribution entering the $\overline{\mathrm{MS}}$ result (5.18). The real question then arises is which $\Delta\Sigma$ enters, for example, Eq. (1.1). Intuitive arguments have been forwarded [46,47,510,50,434] in favor of the *conserved* Q^2-independent $\Delta\Sigma_{\mathrm{off}}$ in Eq. (5.26): in this case the flavor singlet quark contribution can be kept sizeable, $\Delta\Sigma_{\mathrm{off}} = A_8 \simeq 0.6$ (still assuming $\Delta s = \Delta\bar{s} = 0$), as compared to the (constituent)

[7] For consistency note that (5.24) implies, via Eq. (5.21), for the neutron $\Gamma_1^n(Q^2) = -0.055 \pm 0.014$ in agreement with the neutron measurements in Table 2.

static $SU(6)$ prediction in (5.16),

$$\Delta\Sigma_{\rm off} \simeq 0.6 \lesssim \Delta\Sigma^{SU(6)} = 1 \tag{5.27}$$

in complete analogy to the flavor nonsinglet sector where, using Eqs. (5.8), (5.9) and (5.12),

$$A_3 \simeq 1.26 \lesssim A_3^{SU(6)} = \tfrac{5}{3}, \quad A_8 \simeq 0.58 \lesssim A_8^{SU(6)} = 1 \ . \tag{5.28}$$

In *both* cases there are only 30–40% reductions from the static $SU(6)$ expectations which are attributed to helicity nonconservation induced at low-energy scales by finite quark mass effects which break chirality and thus the symmetry in the nonperturbative region which creates a difference in the initial values for the perturbative QCD evolution [46,47]. Note that only for *conserved* quantities one expects, in the absence of chirality breaking effects, constituent and parton results to coincide. The reduction of $A_{3,8}$ from their static $SU(6)$ values in (5.28) can be theoretically understood in terms of relativistic binding effects within the framework of relativistic quark models [101]. Furthermore, the choice of a Q^2-independent $\Delta\Sigma_{\rm off}$ fulfills the requirement of what might be called an 'extended' Adler sum rule or an 'extended' baryon (Gross Llewellyn–Smith) sum rule. The usual (unpolarized) Adler [32] and baryon [337] sum rules measure the isospin of the target nucleon and the sum of the baryon number and strangeness of the nucleon, respectively. On the parton level there appear in both cases first moment expressions $\int_0^1 {\rm d}x[q(x,Q^2) - \bar{q}(x,Q^2)]$ whose differences and sums over different quark flavors are independent of Q^2. Specifically, it follows that the number of quarks of a certain flavor inside the nucleon is 'conserved', i.e. Q^2-independent, to any order in α_s. The 'extended' Adler and baryon sum rules extend this statement to the conservation of the number of quarks of a certain helicity, i.e. $\int_0^1 {\rm d}x[\delta q(x,Q^2) + \delta\bar{q}(x,Q^2)]$, to be independent of Q^2. The difference in sign of the antiquark contributions has to do with the opposite charge conjugation properties of the vector and axial-vector current.

Unfortunately, our present ignorance of all moments of two-loop splitting functions $\delta P_{ij}^{(1)n}$, or equivalently of $\delta P_{ij}^{(1)}(x)$, calculated in the off-shell scheme prevents us from a detailed (x,Q^2) dependent analysis of present data, in contrast to the $\overline{\rm MS}$ regularization/factorization scheme where such an analysis has been performed. In the $\overline{\rm MS}$ scheme one is confronted with a less plausible large difference between the singlet sector

$$\Delta\Sigma(Q^2) \equiv A_0(Q^2) \simeq 0.3 \ll A_0^{SU(6)} = 1 \ , \tag{5.29}$$

at $Q^2 = 5$ to $10\,{\rm GeV}^2$ according to (5.24), and the nonsinglet quantities in (5.28).

5.2. The first moment and the anomaly

In the OPE approach the possible decomposition, Eq. (5.22), into quark and gluon was not realized because the fundamental quantities of the OPE are not parton densities but matrix elements of certain operators between proton states. $\langle PS\,|\,\bar{q}\gamma_\mu\gamma_5 q\,|\,PS\rangle$ are the matrix elements relevant for the total helicities, i.e. for the first moment of g_1 [529,530]. More precisely, in the framework of the operator product expansion one obtains the result Eq. (5.23) with A_0, A_3 and A_8 defined by

$$A_3 S_\mu = \langle PS|\bar{\psi}\gamma_\mu\gamma_5\lambda_3\psi|PS\rangle \ , \tag{5.30}$$

$$A_8 S_\mu = \sqrt{3}\langle PS|\bar{\psi}\gamma_\mu\gamma_5\lambda_8\psi|PS\rangle \,, \tag{5.31}$$

$$A_0 S_\mu = \langle PS|\bar{\psi}\gamma_\mu\gamma_5\psi|PS\rangle \,, \tag{5.32}$$

where $\psi = (u,d,s)^{\mathrm{T}}$ and λ_a are the Gell–Mann matrices, $a = 1,\ldots,8$. Longitudinal polarization $S^\sigma \sim P^\sigma$ of the proton is assumed throughout this section. In the naive quark parton model one has the identity

$$(\Delta q + \Delta\bar{q})S_\mu \overset{\text{naive}}{=} \langle PS|\bar{q}\gamma_\mu\gamma_5 q|PS\rangle \tag{5.33}$$

between the first moments $\Delta q + \Delta\bar{q}$ ($q = u,d,s$) and the matrix elements. However, one should note that $j^5_\mu = \bar{\psi}\gamma_\mu\gamma_5\psi$ which appears in Eq. (5.32) is the axial vector singlet current which is not conserved, $\partial^\mu j^5_\mu \neq 0$, but is 'anomalous' in the sense of Adler [33] and Bell and Jackiw [108]

$$\partial^\mu j^5_\mu = \frac{f}{2}\frac{\alpha_s}{2\pi}\varepsilon^{\mu\nu\alpha\beta}G^a_{\alpha\beta}G^a_{\mu\nu} \,. \tag{5.34}$$

The appearance of the gluon field strength $G_{a\mu\nu}$ in this equation is the reason why Eqs. (5.22) and (5.32) are not in contradiction and instead of Eq. (5.33) one has (in the particular factorization scheme called the off-shell scheme)

$$\left(\Delta q + \Delta\bar{q} - \frac{\alpha_s}{2\pi}\Delta g\right)S_\mu = \langle PS|\bar{q}\gamma_\mu\gamma_5 q|PS\rangle \,. \tag{5.35}$$

The anomaly enters in one-loop order through the diagram in Fig. 21, which, in the gluon off-shell scheme, determines the (Wilson) coefficient $-\frac{1}{2}$ of $2(\alpha_s/2\pi)\Delta g$, and in two-loop order through the diagram in Fig. 20 from which Kodaira [413] has obtained his anomalous dimension.

$\Delta q + \Delta\bar{q}$ and $-(\alpha_s/2\pi)\Delta g$ appear with the same coefficient in Eq. (5.35) because there is only one operator for the first moment singlet contribution. For the gluon there is no direct operator, but only a representation of Δg

$$\langle PS|K^\mu|PS\rangle = -S^\mu\Delta g \tag{5.36}$$

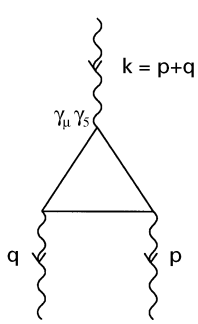

Fig. 21. Triangle anomaly diagram giving rise to Eqs. (5.34) and (5.40).

in terms of the gauge-dependent current

$$K_\mu = \tfrac{1}{2}\varepsilon^{\mu\nu\rho\sigma} A^a_\nu (G^a_{\rho\sigma} - \tfrac{1}{3} g_s f_{abc} A^b_\rho A^c_\sigma) \tag{5.37}$$

whose divergence is

$$\partial^\mu K_\mu = \tfrac{1}{2}\varepsilon^{\mu\nu\alpha\beta} G^a_{\alpha\beta} G^a_{\mu\nu} \tag{5.38}$$

(so that $j^5_\mu - f(\alpha_s/2\pi)K_\mu$ is conserved).

An explicit computation by Forte [274,275] of $\langle PS|(\alpha_s/2\pi)K^\mu|PS\rangle$ in (5.36) has revealed that $(\alpha_s/2\pi)\Delta g = (\alpha_s/2\pi)\Delta g' + \Omega$ where $\Delta g'$ corresponds to the perturbatively calculable hard piece of the anomaly which may be identified with the usual (perturbative) partonic definition used thus far; the remaining gluon-topological Chern–Simons (instantonic) piece Ω is the soft nonperturbative contribution to the triangle anomaly [274,275,100,101] which does not correspond to a hard (large-k_T) subprocess and thus should be absorbed into the definition of the conserved total quark polarization, i.e. $\Delta\Sigma_{\rm off} - f(\alpha_s/2\pi)\Delta g = (\Delta\Sigma_{\rm off} - f\Omega) - f(\alpha_s/2\pi)\Delta g' \equiv \Delta\Sigma' - f(\alpha_s/2\pi)\Delta g'$. This leaves us formally with our original expression (5.26) with both terms being now separately gauge invariant. The term $-f\Omega$ may be interpreted as an additional sea polarization induced by instantonic effects. A first attempt [458] to evaluate $\langle PS|(\alpha_s/2\pi)K^\mu|PS\rangle$ on a (small) lattice yielded the bound $3|(\alpha_s/2\pi)\Delta g' + \Omega| < 0.05$. This surprisingly small result can obviously not be used to extract some information about $\Delta g'$.

It should be noted that Eq. (5.35) is really a representation of (chiral invariant) massless QCD. If fermion masses are introduced, the anomaly Eq. (5.34) is modified according to

$$\partial^\mu j^5_\mu = 2\mathrm{i}\bar{\psi}\gamma_5 M\psi + \frac{f}{2}\frac{\alpha_s}{2\pi}\varepsilon^{\mu\nu\alpha\beta} G^a_{\alpha\beta} G^a_{\mu\nu} \tag{5.39}$$

where $M = \mathrm{diag}(m_u, m_d, m_s)$ is the fermion mass matrix. The mass term in this equation is able to conceal the effect of the anomalous term under certain circumstances. To examine this effect, we write down the anomaly equation, Eq. (5.39), in momentum space for the case of one fermion with mass m

$$(p+q)^\alpha \Gamma^{\mu\nu}_\alpha(p,q) = 2m\Gamma^{\mu\nu}(p,q) - (\alpha_s/\pi)\varepsilon^{\mu\nu\alpha\beta} p_\alpha q_\beta \ . \tag{5.40}$$

Here $\Gamma^{\mu\nu}_\alpha(p,q)$ is the triangle diagram (cf. Fig. 21) and

$$\Gamma^{\mu\nu}(p,q) = m\frac{\alpha_s}{\pi}\varepsilon^{\mu\nu\alpha\beta} p_\alpha q_\beta \int_0^1 \mathrm{d}x \int_0^{1-x} \frac{\mathrm{d}y}{m^2 - (p+q)^2 xy} \ . \tag{5.41}$$

the contribution from the mass term. If $(p+q)^2 \le m^2$, the two terms on the right-hand side of Eq. (5.40) (i.e. the anomalous contribution and the mass contribution) cancel each other, up to terms of order $(p+q)^2/m^2$, so that the anomaly is concealed.

A similar effect occurs in Eq. (5.35) if one includes the quark mass. Namely, the anomalous gluon term $\sim \Delta g$ disappears and one formally recovers the naive Eq. (5.33). Thus the contribution to g_1 from the anomaly is hidden in the massive theory (as well as in the $\overline{\rm MS}$ subtraction scheme). This result will be derived in detail in the next section.

The anomaly induces a point-like interaction between the axial-vector current and the gluons because the amplitude $\Gamma^{\alpha\mu\nu}(p,q)$ does not depend on the momentum transfer $p-q$ when $m=0$. Furthermore, it is known that the anomaly is not affected by higher order corrections [34] and it has been argued [363] that this is true even beyond perturbation theory. This leads us to believe that the identification, Eq. (5.35), remains true in higher orders, at least in suitable chirality preserving schemes like the gluon off-shell scheme.

5.3. Detailed derivation of the gluon contribution

The most straightforward way to derive the gluon contribution is the QCD parton model. In the following we shall only consider the flavor singlet piece of g_1 because the gluon contributes only to the singlet. In the QCD parton model the evolution of the first moments of the polarized quark and gluon density is given by

$$\frac{\mathrm{d}}{\mathrm{d}t}\begin{pmatrix}\Delta\Sigma\\ \Delta\Gamma\end{pmatrix}=\left(\frac{\alpha_s(t)}{2\pi}\right)^2\begin{pmatrix}\Delta P_{qq}^{(1)} & \Delta P_{qg}^{(2)}\\ \Delta P_{gq}^{(0)} & \Delta P_{gg}^{(1)}-\dfrac{\beta_1}{4}\end{pmatrix}\begin{pmatrix}\Delta\Sigma\\ \Delta\Gamma\end{pmatrix}+\mathrm{O}(\alpha_s^3)\ . \tag{5.42}$$

This is an extension of Eq. (5.2) to second order in α_s, in which the two-loop contribution β_1 to the β function arises, cf. Eq. (4.50), because instead of Δg we have introduced the product $\Delta\Gamma=(\alpha_s(t)/2\pi)\Delta g$ (see the discussion in Section 5.1). In Eq. (5.42) we have used quantities $\Delta P_{ij}^{(k)}$ which are the first moments of $\delta P_{ij}^{(k)}$ defined in Eq. (4.52)

$$\Delta P_{ij}=\int_0^1 \mathrm{d}x\,\delta P_{ij}(x)=\Delta P_{ij}^{(0)}+\frac{\alpha_s}{2\pi}\Delta P_{ij}^{(1)}+\left(\frac{\alpha_s}{2\pi}\right)^2\Delta P_{ij}^{(2)}+\mathrm{O}(\alpha_s^3)\ . \tag{5.43}$$

They are related to the corresponding anomalous dimensions by the usual factors of $-\frac{1}{4}$ and $-\frac{1}{8}$ in the one- and two-loop case (see footnote 1).

As is well known, for a complete discussion of first-order effects the knowledge of second-order ($k=1$) anomalous dimensions is mandatory. These second-order (two-loop) anomalous dimensions depend on the calculational (i.e. regularization) scheme. For example, it is not true in general that $\Delta P_{qq}^{(1)}=\Delta P_{qg}^{(2)}=0$. However, some specific (chirality preserving) schemes have this property, so that $\Delta\Sigma$ is constant in Q^2 and the generalized Adler sum rule holds. Note furthermore that in deriving the evolution equation (5.42) we have used $\Delta P_{qg}^{(1)}=0$: $\Delta P_{qg}^{(1)}$ has to vanish on general grounds in any scheme [55,407], since the gauge-invariant axial current j_μ^5 is multiplicatively renormalizable and therefore cannot mix with the gauge-dependent current K_μ in Eq. (5.37).

In the QCD parton model it is well known how to calculate the contribution of Δg to $\Gamma_{1,S}=\int_0^1 \mathrm{d}x\,g_{1,S}$. Namely, one just has to calculate the diagrams in Fig. 17b and take the first moment. We call the amplitude squared corresponding to these diagrams $\Omega_{\mu\nu\rho\sigma}$. It has four indices, μ,ν for the photon, and ρ, σ for the gluon. To get the contribution proportional to Δg in Eqs. (5.22) and (5.23) one has to contract it with $\varepsilon^{\mu\nu\alpha\beta}p_\alpha q_\beta\times\varepsilon^{\rho\sigma\gamma\delta}p_\gamma q_\delta$ because $\varepsilon^{\rho\sigma\gamma\delta}p_\gamma q_\delta$ is proportional to the difference of products of gluon polarization tensors $\varepsilon_{\rho_+}\varepsilon^*_{\sigma_+}-\varepsilon_{\rho_-}\varepsilon^*_{\sigma_-}$ of gluons with positive and negative helicity. This one can see, for example, in the Breit frame where $p=E_g(1,0,0,1)$ is the gluon momentum and $q=(0,0,0,-Q)$. In this frame the polarization tensors are $\varepsilon_\pm=(1/\sqrt{2})(0,1,\pm i,0)$.

To calculate the diagrams or, more precisely, the coefficient of the $\Delta\Gamma$ contribution to $\Gamma_{1,S}$ it is more appropriate to go to the c.m.s. of the photon and gluon in which

$$\begin{aligned} q &= (q_0, 0, 0, -p_1)\ , \\ p &= (p_0, 0, 0, p_1)\ , \\ k &= (k_o, 0, k_1 \sin\theta, k_1 \cos\theta)\ , \\ p' &= (p'_0, 0, -k_1 \sin\theta, -k_1 \cos\theta)\ , \end{aligned} \tag{5.44}$$

where

$$\begin{aligned} q_0 &= \sqrt{p_1^2 - Q^2}, \qquad p_0 = \sqrt{p_1^2 - P^2}, \\ p_1 &= \sqrt{\frac{(pq)^2 - P^2Q^2}{s}}, \qquad k_1 = p'_0 = k_0 = \frac{\sqrt{s}}{2}\ . \end{aligned} \tag{5.45}$$

Note that $s = (p+q)^2$ and the fraction of momentum of the gluon which is carried by the intermediate quark in Fig. 17b is given by $z = Q^2/(s+Q^2)$. This is the quantity with respect to which the first moment has to be taken. A phase space integration over the production angle θ is also necessary.

In Eq. (5.45) a gluon off-shellness $P^2 = -p^2$ has been introduced. It is needed for regularization purposes because although the final result turns out to be finite, singular expressions arise in intermediate steps of the calculation (from the collinear region $\theta \to 0$). In the off-shell sheme ($P^2 \neq 0$) the coefficient of $\Delta\Gamma$ in Eq. (5.22) turns out to be

$$\begin{aligned} &f\int_0^1 \mathrm{d}z(1-2z)\int_{-1}^{1} \mathrm{d}\cos\theta \frac{1}{4}\left(2 - \frac{1}{u} - \frac{1}{t} + P^2\frac{z^2}{Q^2}\left(\frac{1}{u^2} + \frac{1}{t^2}\right)\right) \\ &\quad = f\int_0^1 \mathrm{d}z(2z-1)\ln\frac{Q^2(1-z)}{P^2 z} = -f + 0(P^2)\ , \end{aligned} \tag{5.46}$$

where

$$\begin{aligned} u &= -(p-p')^2\frac{z}{Q^2} \approx \frac{1}{2}(1+\cos\theta) + P^2\frac{z^2}{Q^2}\ , \\ t &= -(k-p)^2\frac{z}{Q^2} \approx \frac{1}{2}(1-\cos\theta) + P^2\frac{z^2}{Q^2}\ , \end{aligned} \tag{5.47}$$

and $f = 3$ is the number of light quarks. In Eq. (5.46) terms like P^2/u or P^2/t which do not contribute in the limit $P^2 \to 0$ have been left out. However, the terms $\sim P^2/u^2$ and $\sim P^2/t^2$ are important. After integration over θ a term $\sim \Delta P_{qg} \ln P^2$ arises which drops out because the first moment of $\delta P_{qg}^{(0)} = \frac{1}{2}(2z-1)$ vanishes. There is an overall factor of f because each quark flavor can be produced.

Instead of P^2 a quark mass m may be introduced to regulate the collinear singularity ('on-shell scheme'). This is the more appropriate procedure for heavy quarks (c and b) but less useful for the

light quarks (u, d and s). In that scheme one has instead of Eq. (5.45)

$$\begin{aligned} q_0 &= \sqrt{p_1^2 - Q^2}, \qquad p_0^2 = p_1^2 = (pq)^2/s \,, \\ k_0 &= p_0' = \sqrt{s}/2, \qquad k_1 = (\sqrt{s}/2)\sqrt{1 - 4m^2/s} \,. \end{aligned} \tag{5.48}$$

The coefficient of $\Delta\Gamma$ is now

$$\int_0^1 \mathrm{d}z \int_{-1}^1 \mathrm{d}\cos\theta \left(\frac{1}{2}(2z-1)\left(\frac{1}{1-\beta\cos\theta} + \frac{1}{1+\beta\cos\theta} - 1 \right) + \frac{2m^2(1-z)}{s}\left(\frac{1}{(1-\beta\cos\theta)^2} + \frac{1}{(1+\beta\cos\theta)^2} \right) \right) = \mathrm{O}(m^2) \,, \tag{5.49}$$

where $\beta = \sqrt{1 - (4m^2/s)}$. This time the effect of the double pole term in Eq. (5.49) $\sim 2m^2/s$ is such that there is no gluon contribution (for small quark masses $m \to 0$).

If used for the light quarks, Eq. (5.49) seems to be in contradiction with Eq. (5.18) because they seem to imply, at some conveniently chosen input scale $Q^2 = \mu^2$, two different relations between the axial vector singlet current matrix element and $\Delta\Sigma$ and $\Delta\Gamma$ namely

$$A_0(\mu^2) = \begin{cases} \Delta\Sigma_{\mathrm{on}}(\mu^2) & \text{on-shell scheme} \,, \\ \Delta\Sigma_{\mathrm{off}} - f\Delta\Gamma(\mu^2) & \text{off-shell scheme} \,. \end{cases} \tag{5.50}$$

$\Delta\Gamma$ is scale independent in first order but picks up a scale dependence in higher orders. It is well known, for example, from the calculation of QCD corrections to unpolarized structure functions, that different regularization schemes can lead to different results. Usually, this is interpreted in such a way that the use of different regularization schemes corresponds to different definitions of the quark density. In our case this means that one has to deal with two different $\Delta\Sigma$'s which are denoted by $\Delta\Sigma_{\mathrm{on}}$ and $\Delta\Sigma_{\mathrm{off}}$ in Eq. (5.50). Going from the second to the first relation in Eq. (5.50) means that one absorbs the gluon contribution into a redefinition of $\Delta\Sigma_{\mathrm{off}}$. The obtained result, $\Delta\Sigma_{\mathrm{on}}$, corresponds to the one in the conventional $\overline{\mathrm{MS}}$ scheme in Eq. (5.18) where $\Delta\Gamma(\mu^2)$ does not explicitly occur due to $\Delta C_g = 0$ in Eq. (4.92). Although in principle it is a mere matter of convention to choose a particular factorization scheme the use of the off-shell scheme (where a potentially large gluon contribution exists) has the advantage that $\Delta\Sigma_{\mathrm{off}}$ is conserved, i.e. scale independent, as will be shown below. This way the Adler sum rule [32] is extended to higher orders of polarized scattering. Furthermore, for the case of the light quarks (u, d, s with $m < \Lambda_{\mathrm{QCD}}$) the massless scheme might be more physical because it could be related to the notion of constituent quarks [46,511]. To really understand why the two definitions in Eq. (5.50) do not contradict each other, one must write down the full result for the first moment of the singlet component of g_1 in Eq. (4.6), $\int_0^1 \mathrm{d}x\, g_{1,S}$, in both schemes and compare it with Kodaira's original result, cf. Eq. (5.23) [413]. In order to do this it should be noted that $\int_0^1 \mathrm{d}x\, g_{1,S}$ is a physical observable and therefore the prediction for it must be scheme independent. The physical prediction is always a product of coefficient functions, anomalous dimensions and the parton densities/matrix elements, i.e.

$$\int_0^1 \mathrm{d}x\, g_{1,S}(x, Q^2) = \frac{1}{9} C_{\mathrm{off}}(Q) E_{\mathrm{off}}(Q, \mu) \begin{pmatrix} \Delta\Sigma_{\mathrm{off}} \\ \Delta\Gamma(\mu) \end{pmatrix} \tag{5.51}$$

$$= \frac{1}{9} C_{\text{on}}(Q) E_{\text{on}}(Q,\mu) \begin{pmatrix} \Delta\Sigma_{\text{on}}(\mu) \\ \Delta\Gamma(\mu) \end{pmatrix} \tag{5.52}$$

$$= \frac{1}{9} C_{\text{Kodaira}}(Q) E_{\text{Kodaira}}(Q,\mu) A_0(\mu) \tag{5.53}$$

in the three schemes to be compared, with

$$C_{\text{Kodaira}} = 1 + \frac{\alpha_s(Q)}{2\pi}\left(-\frac{3}{2} C_F \right) \tag{5.54}$$

and

$$E_{\text{Kodaira}} = 1 + \frac{\alpha_s(\mu) - \alpha_s(Q)}{\pi\beta_0}\left(-\frac{3}{2} C_F f \right) \tag{5.55}$$

are taken from the work of Kodaira [413] which was done with massless quarks and off-shell gluons. For simplicity we work below the charm threshold so that $f = 3$. Furthermore [50],

$$C_{\text{off}} = (1, -f) + \frac{\alpha_s(Q)}{2\pi}\left(-\frac{3}{2} C_F, c_{\Gamma_{\text{off}}} \right), \tag{5.56}$$

$$E_{\text{off}} = 1 + \frac{\alpha_s(\mu) - \alpha_s(Q)}{\pi\beta_0} \begin{pmatrix} 0 & 0 \\ \frac{3}{2} C_F & \Delta P^{(1)}_{gg,\text{off}} - \frac{\beta_1}{4} \end{pmatrix}. \tag{5.57}$$

Here $c_{\Gamma_{\text{off}}}$ is a second-order correction to the first-order gluon photon-fusion process (Fig. 17b). Eq. (5.50) and the entry $-\frac{3}{2} C_F$ in Eq. (5.56) give rise to the QCD correction factor $1 - \alpha_s(Q)/\pi$ in the coefficient of A_0 in Eq. (5.23). Both $c_{\Gamma_{\text{off}}}$ and $\Delta P^{(1)}_{gg,\text{off}}$ can be determined by comparison with Kodaira's result, Eqs. (5.54) and (5.55), i.e. by the consistency requirement Eqs. (5.51)–(5.53), which yields [50] $\Delta P^{(1)}_{gg,\text{off}} - \beta_1/4 = -f\Delta P^{(0)}_{gq} = -2f$. The form of the matrix in Eq. (5.57) is quite remarkable, in particular the vanishing of the entries in the first row. According to Eq. (5.42) this corresponds to

$$\Delta P^{(1)}_{qq,\text{off}} = 0 \tag{5.58}$$

and

$$\Delta P^{(2)}_{qg,\text{off}} = 0\ . \tag{5.59}$$

Note that the vanishing of $\Delta P^{(0)}_{qq}$ and $\Delta P^{(0)}_{qg}$ is explicit from Eq. (4.26) and the vanishing of $\Delta P^{(1)}_{qg}$ has been proven by [55]. In [55] the entry $\Delta P^{(1)}_{gg,\text{off}} - \beta_1/4$ was called $\gamma^{(2)}_{gg}$. Eqs. (5.58) and (5.59) go a step further, saying that in a suitable chirality conserving regularization scheme, $\Delta\Sigma$ is a conserved (i.e. Q^2-independent) quantity beyond the leading order, in fact to any order. It is well known that in massless perturbative QCD the chiral symmetry is unbroken to any order. Eqs. (5.58) and (5.59) show that the off-shell scheme realizes this fact in the most intuitive way by forbidding chirality flip interactions to any order of perturbation theory. As we shall see in the following this fact is also intimately related to the reasonable treatment of the ABJ anomaly in the off-shell scheme. The anomaly term $-f$ in C_{off}, Eq. (5.56), will be shown to correspond – via the consistency requirement, Eqs. (5.51)–(5.53) – to a conserved $\Delta\Sigma$ and vice versa.

Eqs. (5.58) and (5.59) can be derived, for example, from the consistency requirement, Eqs. (5.51)–(5.53). To see that let us evaluate the products $C_{\rm off}E_{\rm off}(\Delta\Sigma_{\rm off},\Delta\Gamma)^{\rm T}$ and $C_{\rm Kodaira}E_{\rm Kodaira}A_0$ appearing in Eqs. (5.51) and (5.53):

$$
\begin{aligned}
&C_{\rm off}(Q)E_{\rm off}(Q,\mu)\begin{pmatrix}\Delta\Sigma_{\rm off}(\mu)\\ \Delta\Gamma(\mu)\end{pmatrix}\\
&=\left[1-\frac{3}{2}C_F\frac{\alpha_s(\mu)}{2\pi}+\frac{\alpha_s(\mu)-\alpha_s(Q)}{\pi\beta_0}\left(\Delta P^{(1)}_{qq,\rm off}-f\Delta P^{(0)}_{gq}+\frac{3}{2}C_F\frac{\beta_0}{2}\right)\right]\Delta\Sigma_{\rm off}(\mu)\\
&\quad+\left\{-f+c_{\Gamma_{\rm off}}\frac{\alpha_s(\mu)}{2\pi}+\frac{\alpha_s(\mu)-\alpha_s(Q)}{\pi\beta_0}\right.\\
&\quad\left.\times\left[\Delta P^{(2)}_{qg,\rm off}-f\left(\Delta P^{(1)}_{gg}-\frac{\beta_1}{4}\right)-c_{\Gamma_{\rm off}}\frac{\beta_0}{2}\right]\right\}\Delta\Gamma(\mu)+{\rm O}(\alpha_s^2),
\end{aligned}
\tag{5.60}
$$

$$
\begin{aligned}
C_{\rm Kodaira}(Q)E_{\rm Kodaira}(Q,\mu)A_0(\mu)&=\left[1-\frac{3}{2}C_F\frac{\alpha_s(\mu)}{2\pi}+\frac{\alpha_s(\mu)-\alpha_s(Q)}{\pi\beta_0}\left(-\frac{3}{2}C_Ff+\frac{3}{2}C_F\frac{\beta_0}{2}\right)\right]\\
&\quad\times[\Delta\Sigma_{\rm off}(\mu)-f\Delta\Gamma(\mu)]+{\rm O}(\alpha_s^2)\ .
\end{aligned}
\tag{5.61}
$$

By comparison one obtains (among other things)

$$
\Delta P^{(1)}_{qq,\rm off}-f\Delta P^{(0)}_{gq}=-\frac{3}{2}C_Ff\ .
\tag{5.62}
$$

Because of the unambiguously determined leading order $\Delta P^{(0)}_{gq}=3/2C_F$, the right-hand side of (5.62) (= Kodaira's anomalous dimension) is saturated by the second term on the left-hand side, so that one arrives at Eq. (5.58). Thus $\Delta\Sigma_{\rm off}(\mu)$ is scale independent, i.e. conserved.

Until now we have discussed only the scheme dependence of the coefficient of Δg in Eq. (5.22). It turns out that other quantities differ in the on-shell scheme from their corresponding counterparts in the off-shell scheme as well. Therefore, we make a general ansatz

$$
C_{\rm on}(Q)=(1,0)+\frac{\alpha_s(Q)}{2\pi}(C_{\Sigma_{\rm on}},c_{\Gamma_{\rm on}})\ ,
\tag{5.63}
$$

$$
E_{\rm on}(Q,\mu)=1+\frac{\alpha_s(\mu)-\alpha_s(Q)}{\pi\beta_0}\begin{pmatrix}\Delta P^{(1)}_{qq,\rm on} & \Delta P^{(2)}_{qg,\rm on}\\ \frac{3}{2}C_F & \Delta P^{(1)}_{gg,\rm on}-\dfrac{\beta_1}{4}\end{pmatrix}
\tag{5.64}
$$

for the coefficients and anomalous dimensions in the on-shell scheme. The entry $\Delta P^{(0)}_{gq}=\frac{3}{2}C_F$ in the anomalous dimension matrix is scheme independent. Due to the consistency requirement, Eqs. (5.51)–(5.53), for the physical observable there must be a transformation matrix

$$
M(Q)=\begin{pmatrix}1+\dfrac{\alpha_s(Q)}{2\pi}m_{11} & -f\\ 0 & 1\end{pmatrix}
\tag{5.65}
$$

such that

$$
C_{\rm on}(Q)=C_{\rm off}(Q)M^{-1}(Q)\ ,
\tag{5.66}
$$

$$E_{\rm on}(Q,\mu) = M(Q)E_{\rm off}(Q,\mu)M^{-1}(\mu)\ , \tag{5.67}$$

$$\begin{pmatrix}\Delta\Sigma_{\rm on}\\ \Delta\Gamma(\mu)\end{pmatrix} = M(\mu)\begin{pmatrix}\Delta\Sigma_{\rm off}(\mu)\\ \Delta\Gamma(\mu)\end{pmatrix}\ . \tag{5.68}$$

$\Delta\Gamma$ is not redefined at the order at which we are working; ergo the two entries 0 and 1 in the second row of $M(Q)$. Eqs. (5.66)–(5.68) can be used to calculate m_{11} as well as the complete set of quantities in $C_{\rm on}$ and $E_{\rm on}$. One simply has to work out the matrix expressions in Eqs. (5.66)–(5.68). Equivalently, these quantities can be derived by using the transformations, Eqs. (4.68) and (4.69), of Section 4.2 for $n = 1$ (with the transition from Δg to $\Delta\Gamma$ to be carried out). Here we do not want to bother with all the details of the transition to the on-shell scheme, but concentrate on one particular aspect, the non-conservation of $\Delta\Sigma_{\rm on}(\mu)$ which becomes explicit in the result [50]

$$\Delta P^{(1)}_{qq,{\rm on}} = -\tfrac{3}{2}C_F f \tag{5.69}$$

which makes clear that $\Delta\Sigma_{\rm on}(\mu)$ is not a conserved but a scale dependent quantity (in contrast to $\Delta\Sigma_{\rm off}$). This result follows from the consistency requirement, Eq. (5.67) (by comparison with the off-shell scheme) but also from the consistency requirement, Eqs. (5.52) and (5.53) (by comparison with Kodaira's result), in a similar fashion as $\Delta P^{(1)}_{qq,{\rm off}} = 0$ was derived in Eq. (5.58).

All of the above considerations were carried out in a decent but rather abstract way by imposing the condition of the scheme independence of a physical observable. An explicit check of the truthfulness of the whole approach was made in Ref. [50] where the relation (5.69) was reproven by an explicit two-loop calculation in the on-shell scheme (massive quarks). The main point was to show that the diagrams in Fig. 22 give rise to a nonvanishing anomalous dimension when calculated in the scheme with massive quarks, and a vanishing anomalous dimension in the off-shell scheme. More precisely, the matrix element corresponding to Fig. 22 is of the form

$$ME(\text{Fig. 22}) = \Delta P^{(1){\rm ND}}_{qq}\ln\frac{Q^2}{\mu^2} + \text{const}\ . \tag{5.70}$$

after integration over the appropriate phase space [50]. Here ND denotes 'nondiagonal' transitions between quarks of different flavors q and q' (cf. Fig. 22). It was shown in [50] that $\Delta P^{{\rm ND}(1)}_{qq',{\rm on}} = -\tfrac{3}{2}C_F f$ for any masses m and m' of the quarks q and q', whereas in the off-shell scheme $\Delta P^{(1){\rm ND}}_{qq',{\rm off}} = 0$. In other words, the change in $\Delta P^{(1)}_{qq'}$ when going from the off-shell to the on-shell scheme is entirely due to non-diagonal flavor transitions. In this way a completely consistent picture arises, in which results of the off-shell scheme can be transformed to any other scheme and vice versa. Note that diagram Fig. 22 can be obtained from Fig. 20 by cutting.

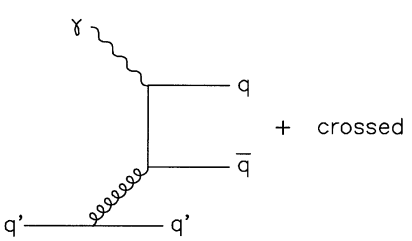

Fig. 22. DIS process involving non diagonal transitions between quarks of different flavors.

Most important among the other schemes is of course the $\overline{\rm MS}$ scheme, because the two-loop anomalous dimensions are now known for *all* moments [478,568,569]. The results for the first moment were already given in Section 4.3. Here we recollect them for the convenience of the reader. One has, according to Eqs. (4.91)–(4.94) (see footnote 4)

$$C_{\overline{\rm MS}}(Q) = (1,0) + \frac{\alpha_s(Q)}{2\pi}\left(-\frac{3}{2}C_F, c_{\Gamma_{\overline{\rm MS}}}\right), \tag{5.71}$$

$$E_{\overline{\rm MS}} = 1 + \frac{\alpha_s(\mu)-\alpha_s(Q)}{\pi\beta_0}\begin{pmatrix} -\frac{3}{2}C_F f & 0 \\ \frac{3}{2}C_F & \Delta P^{(1)}_{gg,\overline{\rm MS}} - \dfrac{\beta_1}{4}\end{pmatrix}, \tag{5.72}$$

where $c_{\Gamma_{\overline{\rm MS}}} = \frac{3}{2}C_F f$, which will contribute only in NNLO α_s^2 and $\Delta P^{(1)}_{gg,\overline{\rm MS}} - \beta_1/4 = 0$ can be also obtained from consistency by comparison with Kodaira's result, namely from

$$\int_0^1 {\rm d}x\, g_1^S(x,Q^2) = \frac{1}{9}C_{\overline{\rm MS}}(Q)E_{\overline{\rm MS}}(Q,\mu)\begin{pmatrix}\Delta\Sigma_{\overline{\rm MS}}(\mu)\\ \Delta\Gamma(\mu)\end{pmatrix} = \frac{1}{9}C_{\rm Kodaira}(Q)E_{\rm Kodaira}(Q,\mu)A_0(\mu)\ , \tag{5.73}$$

in agreement with the results in Eq. (5.19). It should be noted that the entry 0 in Eq. (5.71) corresponds to a vanishing ΔC_g in Eq. (4.62) or (4.85), i.e. to the fact that Δg decouples from $\Gamma_{1,S}^{p,n}$ in the $\overline{\rm MS}$ scheme, as well as in the on-shell scheme according to Eq. (5.63).

It is now instructive, after these many technical details, to summarize the NLO evolution equations for the first moments of the flavor singlet quantities in the different schemes. In the $\overline{\rm MS}$ and on-shell schemes we have

$$\frac{\rm d}{{\rm d}t}\Delta\Sigma(Q^2)_{\overline{\rm MS},{\rm on}} = \left(\frac{\alpha_s(Q^2)}{2\pi}\right)^2(-2f)\Delta\Sigma(Q^2)_{\overline{\rm MS},{\rm on}}\ , \tag{5.74}$$

$$\frac{\rm d}{{\rm d}t}\Delta\Gamma(Q^2)_{\overline{\rm MS},{\rm on}} = \left(\frac{\alpha_s(Q^2)}{2\pi}\right)^2 2\Delta\Sigma(Q^2)_{\overline{\rm MS},{\rm on}}\ , \tag{5.75}$$

with the singlet contribution A_0 to $\Gamma_1^{p,n}$ being given by $A_0(Q^2) = \Delta\Sigma(Q^2)_{\overline{\rm MS},{\rm on}}$. In the off-shell scheme we have obtained

$$\frac{\rm d}{{\rm d}t}\Delta\Sigma(Q^2)_{\rm off} = 0\ , \tag{5.76}$$

$$\frac{\rm d}{{\rm d}t}\Delta\Gamma(Q^2)_{\rm off} = \left(\frac{\alpha_s(Q^2)}{2\pi}\right)^2[2\Delta\Sigma_{\rm off} - 2f\Delta\Gamma(Q^2)_{\rm off}] \tag{5.77}$$

with the singlet contribution now being given by $A_0(Q^2) = \Delta\Sigma_{\rm off} - f\Delta\Gamma(Q^2)_{\rm off}$ as was already anticipated in Eq. (5.50). Due to the Q^2-independence of $\Delta\Sigma_{\rm off}$, Eq. (5.76), these latter two RG equations can be combined into one simple evolution equation for the singlet combination A_0:

$$\frac{\rm d}{{\rm d}t}[\Delta\Sigma - f\Delta\Gamma(Q^2)]_{\rm off} = \left(\frac{\alpha_s(Q^2)}{2\pi}\right)^2(-2f)[\Delta\Sigma - f\Delta\Gamma(Q^2)]_{\rm off}\ . \tag{5.78}$$

Recalling

$$\frac{\mathrm{d}\alpha_s}{\mathrm{d}t} = -\beta_0\frac{\alpha_s^2}{4\pi} - \beta_1\frac{\alpha_s^3}{(4\pi)^2}\,, \tag{5.79}$$

the solutions of the above RG equations are straightforward. In the $\overline{\mathrm{MS}}$ and in the on-shell scheme, Eqs. (5.74) and (5.75) give

$$\Delta\Sigma(Q^2)_{\overline{\mathrm{MS}},\mathrm{on}} = \left\{1 - \frac{2f}{\beta_0}\frac{\alpha_s(\mu^2)-\alpha_s(Q^2)}{\pi} + \mathrm{O}(\alpha_s^2)\right\}\Delta\Sigma(\mu^2)_{\overline{\mathrm{MS}},\mathrm{on}} \tag{5.80}$$

$$\Delta\Gamma(Q^2)_{\overline{\mathrm{MS}},\mathrm{on}} = \Delta\Gamma(\mu^2)_{\overline{\mathrm{MS}},\mathrm{on}} - \frac{2f}{\beta_0}\left[\frac{\alpha_s(\mu^2)-\alpha_s(Q^2)}{\pi} + \mathrm{O}(\alpha_s^2)\right]\Delta\Sigma(\mu^2)_{\overline{\mathrm{MS}},\mathrm{on}} \tag{5.81}$$

with an appropriately chosen input scale $Q_0^2 = \mu^2$ and $\beta_0 = 11 - 2f/3$. In the off-shell scheme, Eqs. (5.76)–(5.78) give

$$\Delta\Sigma(Q^2)_{\mathrm{off}} = \Delta\Sigma(\mu^2)_{\mathrm{off}} \equiv \Delta\Sigma = \text{const.}\,, \tag{5.82}$$

$$\Delta\Gamma(Q^2)_{\mathrm{off}} = \left\{1 - \frac{2f}{\beta_0}\frac{\alpha_s(\mu^2)-\alpha_s(Q^2)}{\pi} + \mathrm{O}(\alpha_s^2)\right\}\Delta\Gamma(\mu^2)_{\mathrm{off}} + \frac{2}{\beta_0}\frac{\alpha_s(\mu^2)-\alpha_s(Q^2)}{\pi}\Delta\Sigma\,. \tag{5.83}$$

As an illustrative application of these results, let us estimate dynamically $\Delta g(Q^2)$ in the off-shell scheme according to Eq. (5.83) [306,428,307]. The necessary input at $Q^2 = \mu^2$, i.e. the boundary condition, can be deduced from the unpolarized *valence-like* gluon and sea input densities (i.e. $xg(x,\mu^2) \sim x^a(1-x)^b$ with $a > 0$, etc.) which are thus integrable, i.e. their $n = 1$ moments $g(\mu^2) \equiv \int_0^1 g(x,\mu^2)\,\mathrm{d}x$, etc., exist (only) at $Q^2 = \mu^2$ with the result $g(\mu^2) \approx 1$ and $s(\mu^2) \approx 0$ at $\mu^2 \approx 0.3\,\mathrm{GeV}^2$ [315,318,319]. This allows for a parameter-free as well as perturbatively stable calculation of structure functions in the small-x region ($x \leq 10^{-2}$, at $Q^2 > \mu^2$) which is entirely based on QCD dynamics and agrees with all present measurements obtained at DESY-HERA [319]. Thus, the positivity constraints (4.11) imply

$$|\Delta g(\mu^2)| \leq g(\mu^2) \approx 1, \qquad |\Delta s(\mu^2)| \leq s(\mu^2) \approx 0\,. \tag{5.84}$$

Using therefore $\Delta\Sigma \approx A_8$, with A_8 being given in (5.9), Eq. (5.83) yields [307]

$$-2.6 \lesssim \Delta g(Q^2)_{\mathrm{off}} \lesssim 3.9 \tag{5.85}$$

for $Q^2 = 10\,\mathrm{GeV}^2$, which is compatible with Eq. (5.25). Here we have used $\beta_0 = 9$ for $f = 3$ light quark flavors and $\alpha_s(\mu^2)/2\pi = 0.108$ and $\alpha_s\,(10\,\mathrm{GeV}^2)/2\pi = 0.0304$ in NLO. It is also interesting to note that on rather general heuristic grounds based on the intrinsic bound-state dynamics of the nucleon, counting rules, consistency constraints for g_-/g_+ and $\Delta g/g$ as $x \to 1$ and $x \to 0$, one expects [145] the total gluon helicity to be sizeable, $\Delta g \approx 1.2$. Note, however, that the scale μ remains undetermined in such considerations, in contrast to the RG based result in Eq. (5.85).

In the $\overline{\mathrm{MS}}$ as well as in the on-shell scheme where the full first moment Δg decouples from $A_0(Q^2)$ and $\Delta\Sigma(Q^2)$ is not conserved, cf. Eq. (5.80), the experimentally required suppression of A_8 in Eq. (5.7), as required by the constraint (5.24), can be achieved either by $\Delta s = \Delta\bar{s} < 0$ or by

$\Delta\bar{u} \approx \Delta\bar{d} < 0$ in a $SU(3)_f$ broken scenario. A detailed (x, Q^2) dependent analysis of present polarization data will be presented in Section 6. Despite the fact that Δg decouples from A_0, the polarized gluon density $\delta g(x, Q^2)$ will in future play an important part in analyzing presently available data for $x \geq 5 \times 10^{-3}$ which give rise to a sizeable Δg as well.

As already mentioned in Section 3.4 and to be discussed in more detail in Section 6, the best information on $\delta g(x, Q^2)$ will come from heavy quark production in polarized $\vec{e}\vec{p}$ via $\vec{\gamma}^*\vec{g} \to c\bar{c}$ (with no light quark contribution present in LO), or in polarized $\vec{p}\vec{p}$ collisions at the RHIC facility via the dominant $\vec{g}\vec{g} \to c\bar{c}$ subprocess; in the latter case also the production of direct photons should offer a good possibility to extract information about the magnitude of $\Delta g(Q^2)$. Alternatively, $\delta g(x, Q^2)$ could be determined from the Q^2-dependence of g_1 if HERA is run with a polarized proton beam.

5.4. The Bjorken sum rule

Sum rules are relations for moments of the structure functions. The most important and fundamental sum rule for polarized scattering is the Bjorken sum rule which was derived in 1966 from SU(6)⊗SU(6) current algebra [118,119]. It describes a relationship between spin-dependent DIS and the weak coupling constant defined in neutron β-decay

$$\int_0^1 \mathrm{d}x[g_1^p(x, Q^2) - g_1^n(x, Q^2)] = \frac{1}{6}\frac{g_\mathrm{A}}{g_\mathrm{V}} \tag{5.86}$$

where g_A and g_V are the vector and axial vector couplings measured in nuclear β-decay

$$\mathscr{L}_{\beta\text{-decay}} = -\frac{G_F}{\sqrt{2}}\cos\theta_\mathrm{c}\left[\bar{p}\gamma_\mu\left(1 - \frac{g_\mathrm{A}}{g_\mathrm{V}}\gamma_5\right)n\right][\bar{e}\gamma^\mu(1-\gamma_5)\nu]\,. \tag{5.87}$$

Here θ_c is the Cabibbo angle and $g_\mathrm{A}/g_\mathrm{V} = 1.2573 \pm 0.0028$ in Eq. (5.8) is known to high precision.

It is not difficult to prove the Bjorken sum rule with the help of the knowledge which was collected in Section 5.1. Qualitatively, it arises as follows: $g_\mathrm{A}/g_\mathrm{V}$ gives the strength at which the axialvector transformation from up to down quark in the proton takes place. In DIS this is measured by $\Delta(u + \bar{u}) - \Delta(d + \bar{d})$. Indeed, from Eqs. (5.5), (5.30) and (5.87) one sees that one simply has to show

$$_p\langle PS|\bar{\psi}\gamma_\mu\gamma_5\lambda_3\psi|PS\rangle_p = (g_\mathrm{A}/g_\mathrm{V})S_\mu\ . \tag{5.88}$$

One can use the isospin symmetry to apply the Wigner–Eckhart theorem

$$_p\langle PS|\bar{\psi}\gamma_\mu\gamma_5\lambda_3\psi|PS\rangle_p = {}_p\langle PS|\bar{\psi}\gamma_\mu\gamma_5\lambda_+\psi|PS\rangle_n\ , \tag{5.89}$$

where $|\rangle_p$ and $|\rangle_n$ denote the proton and neutron states. From Eq. (5.89) one gets

$$_p\langle PS|\bar{u}\gamma_\mu\gamma_5 d|PS\rangle_n = (g_\mathrm{A}/g_\mathrm{V})S_\mu \tag{5.90}$$

which completes the proof of the Bjorken sum rule.

This sum rule is so very fundamental because it relies only on isospin invariance, i.e. on a $SU(2)_f$ symmetry between up- and down-quarks, cf. Eq. (5.89). The Bjorken sum rule is an asymptotic result which relates low- and high-Q^2 quantities. This originates from the fact that, apart from finite

$O(\alpha_s)$ corrections, the l.h.s. of Eq. (5.86) $\Gamma_1^p(Q^2) - \Gamma_1^n(Q^2) = \frac{1}{6}A_3 = \frac{1}{6}(\Delta u + \Delta\bar{u} - \Delta d - \Delta\bar{d})$ is just the nonsinglet isospin-3 component in Eq. (5.4) which does not renormalize due to the vanishing of $\Delta P_{qq}^{(0)}$ and $\Delta P_{\mathrm{NS}-}^{(1)}$ in (5.19). Thus it is generally believed that the Bjorken sum rule gets only moderate QCD corrections. For example, the perturbative QCD corrections are given by the nonsinglet Wilson coefficient ΔC_{NS} in (5.20) and known to be small. In addition, there are probably nonperturbative higher-twist (HT) corrections, so that instead of (5.86) we have in general

$$\int_0^1 \mathrm{d}x[g_1^p(x,Q^2) - g_1^n(x,Q^2)] = \frac{1}{6}\frac{g_{\mathrm{A}}}{g_{\mathrm{V}}}\Delta C_{\mathrm{NS}}(Q^2) + \frac{c_{HT}}{Q^2} \tag{5.91}$$

with [414,415,439]

$$\Delta C_{\mathrm{NS}} = 1 - \frac{\alpha_s(Q^2)}{\pi} - 3.5833\left(\frac{\alpha_s(Q^2)}{\pi}\right)^2 - 20.2153\left(\frac{\alpha_s(Q^2)}{\pi}\right)^3, \tag{5.92}$$

cf. Eq. (5.20). The latter result is obtained for $f = 3$ light flavors, and the range of c_{HT} has been estimated to be $c_{HT} \approx -0.025$ to $+0.03\,\mathrm{GeV}^2$ [84,85,402]. For recent reviews, see [371,464,358] and references therein. Additional renormalon contributions to the perturbative 3-loop result in Eq. (5.92) have been studied as well but their size seems to be small in the relevant perturbative region, $Q^2 \gtrsim 1\,\mathrm{GeV}^2$. For a review, see [257] and references therein. Disregarding the small nonperturbative contribution for $Q^2 > 1\,\mathrm{GeV}^2$, the Bjorken sum rule (5.91) is in reasonable agreement with experiments: According to Table 2, SLAC(E143) finds

$$\Gamma_1^p(Q^2) - \Gamma_1^n(Q^2) = 0.164 \pm 0.017 \tag{5.93}$$

at $Q^2 = 3\,\mathrm{GeV}^2$, to be compared with the predicted [r.h.s. of (5.91)] $\Gamma_1^p(Q^2) - \Gamma_1^n(Q^2) = 0.187 \pm 0.002$ at the same Q^2, using $\alpha_s/\pi = 0.076 \pm 0.010$. The most recent CERN (SMC) result is [28]

$$\Gamma_1^p(Q^2) - \Gamma_1^n(Q^2) = 0.195 \pm 0.029 \tag{5.94}$$

at $Q^2 = 10\,\mathrm{GeV}^2$, where the theoretical prediction is $\Gamma_1^p(Q^2) - \Gamma_1^n(Q^2) = 0.193 \pm 0.002$, using $\alpha_s/\pi = 0.061 \pm 0.004$. A more detailed comparison between theory and experiment can be found, for example, in [574,258,48].

Finally, it should be kept in mind that the original small EMC result for Γ_1^p in Eq. (3.3) implied already dramatic consequences for Γ_1^n *prior* to the recent CERN and SLAC measurements of the neutron structure function g_1^n, by assuming the validity of the 'safe' Bjorken sum rule: Using Eq. (3.3) in (5.91) one anticipated

$$\Gamma_1^n(Q^2 \approx 10\,\mathrm{GeV}^2) = -0.067 \pm 0.018 \tag{5.95}$$

which, being in agreement with recent measurements in Table 2, is about ten(!) times larger than the naive pre-EMC Ellis–Jaffe expectation $\Gamma_{1,\mathrm{EJ}}^n \approx -0.008$ based on Eq. (5.15) in conjuction with the Bjorken sum rules. These predictions for Γ_1^n can be translated into Bjorken-x space,

$$g_1^n(x,Q^2) = g_1^p(x,Q^2) - \tfrac{1}{6}[\delta u_v(x,Q^2) - \delta d_v(x,Q^2)] \tag{5.96}$$

where $\delta q_v \equiv \delta q - \delta\bar{q}$. The small NLO contribution due to $\delta C_q(x)$ in Eq. (4.47) has been suppressed. In order to reproduce the strongly negative x-integrated result Eq. (5.95), it can be anticipated [310] from Eq. (5.96) that $g_1^n(x,Q^2)$ has to become strongly negative for $x \lesssim 0.1$, in contrast to

$g_{1,\mathrm{EJ}}^n$ which gives rise to an almost vanishing $\Gamma_{1,\mathrm{EJ}}^n$. It will become transparent from a detailed (x, Q^2)-dependent analysis of all present data in Section 6, that such expectations have been confirmed by the more recent CERN(SMC) and SLAC measurements.

5.5. The Drell–Hearn–Gerasimov sum rule

The DHG sum rule [231,291] is a prediction for Γ_1 at $Q^2 = 0$ and can be considered as giving qualitative information on the magnitude of higher twist effects in the region between $Q^2 = 0$ and the present high energy data.

It relates the spin-dependent scattering cross section of circularly polarized real photons by longitudinally polarized nucleons N to the anomalous magnetic moment of the nucleon. If we define

$$I_N(Q^2) \equiv 2\frac{M^2}{Q^2}\int_0^1 g_1^N(x, Q^2)\,\mathrm{d}x\ , \tag{5.97}$$

the statement of the DHG sum rule is

$$I_N(0) = -\kappa_N^2/4 \tag{5.98}$$

where M is the mass of the nucleon and κ_N its anomalous magnetic moment, $\mu_p = (1 + \kappa_p)\mu_B$ and $\mu_n = \kappa_n\mu_B$. κ_N is defined by the nucleon–photon coupling

$$\gamma^\alpha(\mathrm{i}\partial_\alpha - e_N A_\alpha) - (\kappa_N\mu_B/2)\sigma_{\alpha\beta}F^{\alpha\beta} \tag{5.99}$$

with $e_p = +e$ and $e_n = 0$ and from experiment one has $\kappa_p = 1.79$ and $\kappa_n = -1.91$.

The derivation of the DHG sum rule relies on the relation between g_1 and the photoabsorption cross sections, Eqs. (2.10) and (2.14), and on the dispersion relation for forward Compton scattering. In fact, the spin-flip part of the forward Compton scattering amplitude is proportional to $\int_0^\infty[\sigma_{1/2} - \sigma_{3/2}]\mathrm{d}\nu/\nu$ and, at low Q^2, is given by $-(2\pi^2\alpha/M^2)\kappa_N^2$ which is usually referred to as the Low-theorem [453].

Fig. 23 compares the result of the DIS data for $I_p(Q^2)$ and $I_n(Q^2)$, using the recent Q^2-independent LO results $\Gamma_1^p = 0.146$ and $\Gamma_1^n = -0.064$ [309] in Eq. (5.97), with the values at $Q^2 = 0$ from the DHG sum rule. Since perturbative LO and NLO QCD is fully operative for $Q^2 \gtrsim 1\,\mathrm{GeV}^2$ [309], as will be discussed in more detail in the next section, the most striking feature of this figure is the necessity of a tremendous Q^2-dependence (variation) of Γ_1^p and $\Gamma_1^p - \Gamma_1^n$ in the low-Q^2 region, $Q^2 < 1\,\mathrm{GeV}^2$: In particular, Γ_1^p must change sign between $Q^2 \approx 0$ and $Q^2 \approx 1\,\mathrm{GeV}^2$, and this must be due to some *strong* nonperturbative higher twist effect. A parametrization (but not an explanation) of this effect was suggested by [64] and later on improved by [151,539]. It turns out that such effects seem to be significantly larger than what one obtains on the basis of QCD sum rules. Most recent E143 measurements [6] at small Q^2 confirm these expectations as well as the trend depicted in Fig. 23. Reviews on this topic can be found in [371,99], for example.

Experiments are being planned to test the sum rule directly [139,264]. This is important because, among other things, there has been some criticism towards the argument that connects the spin structure function integral to the $Q^2 = 0$ integral in Eqs. (5.97) and (5.98) [392].

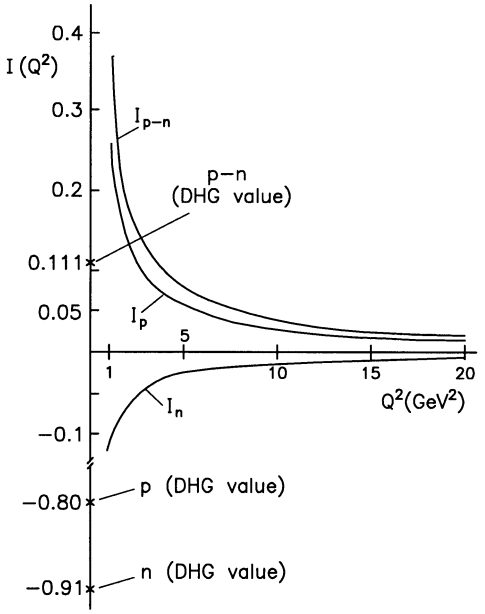

Fig. 23. DIS predictions for $I_{p,n}(Q^2)$ according to (5.97) using $\Gamma_1^p = 0.146$ and $\Gamma_1^n = -0.064$. These latter numbers are Q^2-independent in LO [309]. The DHG values refer to (5.98).

6. Polarized parton densities and phenomenological applications

6.1. Deep inelastic polarized lepton–nucleon scattering

Nowadays sophisticated phenomenological models describing the spin structure functions in LO and NLO QCD are used to interpret the experimental data. Before we discuss these models, we want to give a short historical overview about some simpler (and by now mostly obsolete) models that were discussed in the literature in the past, the Kuti–Weisskopf model [430], the Carlitz–Kaur model [159] and the Cheng–Fischbach [169,170] model.

When discussing the first moment of g_1 in Section 5.1 we have noted that in the SU(6) constituent picture the nucleon consists of three free quarks and its wave function is completely symmetric in spin and flavor indices. Squaring the SU(6) wave function one obtains the probabilites for an up or down quark with spin up or down and, from that, the SU(6) predictions $\Gamma_1^p = \frac{5}{54}$ and $\Gamma_1^n = 0$ according to (5.17). This prediction is clearly wrong except in that the proton is expected to have a larger positive asymmetry than the neutron with a very small asymmetry.

One of the first attempts to describe the nucleon in terms of a *relativistic* picture was the Kuti–Weisskopf model [430]. In this model the nucleon consists of three valence quarks described by the SU(6) wave function, allowing however for an x-dependent quark-density distribution, plus a core of an indefinite number of quark–antiquark pairs carrying vacuum quantum numbers and zero angular momentum. The model also postulated the existence of gluons carrying a fraction of the total momentum, the ratio of gluons to the quark–antiquark pairs being the only free

parameter of the model. At low x the core dominates while at high x only the valence quarks contribute to the scattering. The functional form of g_1 is given by

$$g_1(x) = \frac{5}{54}\frac{\Gamma(\gamma + 3(1-\alpha))}{\Gamma(1-\alpha)\Gamma(\gamma + 2(1-\alpha))} x^{-\alpha(0)}(1-x)^{-1+\gamma+2(1-\alpha(0))} \tag{6.1}$$

for the proton while for the neutron it is identically zero. Assuming that the behavior of structure functions near $x = 1$ is related to the elastic form factor one obtains $-1 + \gamma + 2(1 - \alpha(0)) = 3$. In their original work, Kuti and Weisskopf [430] considered $\alpha(0) \simeq 0.5$, as suggested by non-diffractive trajectories, which leads to an increase of the spin asymmetry at small x. This is in contradiction with the present correct view, cf. Section 4.4, and with experimental data. The normalization factor in Eq. (6.1) was chosen to fulfill the SU(6) predictions for the first moment sum rules. Therefore, just as SU(6), the model fails to explain the experimental data. Here, and in the other following pre-QCD approaches, the scale Q^2 at which Eq. (6.1) is expected to hold, cannot be specified except that $Q^2 \gg M^2$, as usual within the framework of the idealized 'impulse approximation'.

Later attempts [187] tried to improve the model by taking into account the difference between constituent and current quarks. The two are related by a Melosh transformation which is shown to be equivalent to a rotation in spin space [187]. The rotation angle θ is defined so as to fit the modified SU(6) formula $g_A/g_V = \frac{5}{3}\cos 2\theta$ to the experimental number, yielding $\cos 2\theta \approx 0.75$. The predictions for the spin asymmetry are

$$A_1^p = \left(\frac{19}{15} - \frac{16}{15}r(x)\right)\cos 2\theta, \qquad A_1^n = \left(\frac{2}{5r(x)} - \frac{3}{5}\right)\cos 2\theta \tag{6.2}$$

where $r(x) = F_2^n(x)/F_2^p(x)$ is the ratio of the unpolarized structure functions. In this model the prediction for Γ_1^p is even somewhat larger than that of the Ellis–Jaffe sum rule.

In another attempt to satisfy the Bjorken sum rule without completely abandoning the SU(6) picture of the nucleon, Babcock et al. [80] suggested to include perturbative estimates of the $q\bar{q}$ and gluon sea polarization. Furthermore, for the valence quarks the parametrization $\delta u(x) \simeq 0.44 u_v(x)$ and $\delta d(x) \simeq -0.35 d_v(x)$ was proposed. Since the authors oriented their results at the prediction of the Ellis–Jaffe sum rule, they are not in agreement with present data.

Most famous among the SU(6) inspired models for the polarized structure functions is certainly the Carlitz–Kaur model [159]. In this model the symmetry is broken by suggesting that the configuration, in which the non-interacting diquark system is in an isospin-1 state, is suppressed at high x relative to the isospin-0 case. This is quantified in terms of two functions, $I_0(x)$ and $I_1(x)$, describing the valence quark distributions, where the subscript refers to the isospin of the non-interacting system and which are obtained from unpolarized DIS data. At low x, the valence quarks are assumed to lose any memory of the parent spin orientation through interaction with the gluon sea. This is described in terms of a factor, called $\sin^2\theta(x)$, giving the probability that the quark will flip its spin through interactions with the sea. It is given by

$$\sin^2\theta(x) \equiv \frac{1}{2}\frac{H(x)N(x)}{H(x)N(x)+1}\ , \tag{6.3}$$

where $N(x)$ is the density of the gluon sea relative to the valence quarks and $H(x)$ is the probability of a spin-flipping interaction between valence quarks and gluons. The behavior of $N(x)$ for $x \to 1$ is suggested by dimensional counting rules and the behavior for $x \to 0$ by Regge theory, $N(x) \sim (1-x)^2/\sqrt{x}$. Assuming the x-independence of H, a measure of the dilution of the valence quark spin due to this interaction is then given by the spin dilution factor $\cos 2\theta(x) = H_0(1-x)^2/\sqrt{x}$. The polarized quark densities are given by

$$\delta u(x) = [u_v(x) - \tfrac{2}{3}d_v(x)]\cos 2\theta(x), \qquad \delta d(x) = -\tfrac{1}{3}d_v(x)\cos 2\theta(x)\ . \tag{6.4}$$

The only free parameter in the model is H_0. It is fixed by the Bjorken sum rule, $H_0 \approx 0.052$. Correspondingly, the spin dilution factor can be calculated. It is almost equal to 1 everywhere except at low values of x. Using Eq. (6.4), $\Gamma_1^{p,n}$ can be calculated and turn out to be essentially identical to the predictions of the Ellis–Jaffe sum rule. Furthermore, it should be noted that the d-quark spin density in Eq. (6.4) does not satisfy the perturbative QCD requirement $\delta d(x) \underset{x\to 1}{\sim} d_v(x)$.

In the Cheng–Fischbach model [169,170], later refined by Callaway and Ellis [156] and Cheng and Lai [171], it is simply assumed that the polarized quark distributions are related to the unpolarized ones via

$$\delta u_v(x) = \alpha(x)u_v(x), \qquad \delta d_v(x) = \beta(x)d_v(x)\ . \tag{6.5}$$

It is further assumed that $\alpha(x), \beta(x) \underset{x\to 1}{\sim} 1$ in order to take account of the argument that the valence quark at $x = 1$ remembers the spin of the parent nucleon. By contrast, the region near $x = 0$ is expected to be dominated by the sea so that the spin of the nucleon is no longer reflected by the valence quarks implying $\alpha(x), \beta(x) \underset{x\to 0}{\sim} 0$. Since Δd is negative, the boundary condition $\beta(x) \underset{x\to 1}{\sim} 1$ implies that $\delta d_v(x)$ changes sign as a function of x. Therefore, $\beta(x)$ was suggested to be of the form $\beta(x) = ((x-x_0)/(1-x_0))x^p$ so that the sign of $\delta d_v(x)$ flips at $x = x_0$. Furthermore, Cheng and Lai [171] have chosen $\alpha(x) = x^{0.26}$. Roughly, typical values of x_0 and p are of the order 0.5. These valence distributions alone cannot account for the experimental data which require in addition a large polarized sea quark and/or gluon density. In Ref. [171] an ansatz of the form $|\delta s(x)| = x^{\gamma_s}s(x)$, $|\delta g(x)| = x^{\gamma_g}g(x)$ was made. Since the data do not really fix $\delta s(x)$ and $\delta g(x)$ it was not possible to determine γ_s and γ_g from a fit.

Now we turn to more recent developments. According to the discussions and results presented in Sections 4.1, 4.2 and 5.1, it is straightforward to perform LO and NLO ($\overline{\text{MS}}$) QCD analyses of all presently available polarized DIS data on $g_1^{p,n}(x,Q^2)$. This affords the knowledge of appropriate input parton densities $\delta f(x,Q_0^2)$, $f = q, \bar{q}, g$, extracted (as far as possible) from present measurements at a conveniently chosen $Q^2 = Q_0^2$. The analyses can be performed either directly in Bjorken-x space or, more conveniently, in (Mellin) n-moment space where the RG evolution equations can be solved analytically as in Eqs. (4.60)–(4.64). During the past decade many LO analyses, partly supplemented by the NLO gluon anomaly in Eq. (4.46), (4.65) or (5.22), have been performed, e.g. [56,310,515,493,341,342,344,171,178,172,146,441], and more recently in [52,53,293,313,256,268,97,173,87,138,268]. With the recently completed calculation of all two-loop splitting function (anomalous dimensions) $\delta P_{ij}^{(1)}(x)$, $i,j = q,g$, in the $\overline{\text{MS}}$ factorization scheme [478,568,569], also fully consistent NLO ($\overline{\text{MS}}$) analyses became possible [309,551,294,9,270,

444,445,559]; alternative factorization schemes have been proposed as well for performing NLO analyses [88,48,9,31,446,367].

In general, the searched for parton densities $\delta f(x,Q^2)$ have to satisfy the fundamental positivity constraints (4.11) at any value of x and scale Q^2, as calculated by the unpolarized and polarized evolution equations, within the *same* factorization scheme. It is thus natural to perform polarized NLO analyzes in the $\overline{\rm MS}$ scheme where practically all unpolarized NLO parton densities have been analyzed and presented. Furthermore the total helicities, i.e. $n=1$ moments of $\delta f(x,Q^2)$ in Eq. (5.1), are constrained by the sum rules (5.8) and(5.9)

$$\Delta u + \Delta\bar{u} - \Delta d - \Delta\bar{d} = F + D = 1.2573 \pm 0.0028\ , \tag{6.6}$$

$$\Delta u + \Delta\bar{u} + \Delta d + \Delta\bar{d} - 2(\Delta s + \Delta\bar{s}) = 3F - D = 0.579 \pm 0.025\ , \tag{6.7}$$

which hold for the flavor $\mathrm{SU}(3)_f$ symmetric 'standard' scenario commonly used. It should be remembered that the flavor nonsinglet combinations $A_{3,8}$ in Eqs. (5.5) and (5.6) which appear in (6.6) and (6.7) are Q^2 independent also in NLO due to $\Delta P^{(1)}_{\mathrm{NS}-} = 0$ in (5.19).

As has been already discussed at the beginning of Section 5.1, there are serious objections to this latter full $\mathrm{SU}(3)_f$ symmetry (mainly due to $m_{u,d} \ll m_s$) which results in (6.7), in contrast to the unquestioned isospin $\mathrm{SU}(2)_f$ symmetry ($m_u \simeq m_d$) which gives rise to (6.6). A plausible (but extreme) alternative to the full $\mathrm{SU}(3)_f$ symmetry is a 'valence' scenario [450,451,448] where $\mathrm{SU}(3)_f$ is (maximally) broken and which is based on the assumption that the flavor-changing hyperon β-decay data fix only the total helicities of valence quarks $\Delta q_v(Q^2) \equiv \Delta q - \Delta\bar{q}$:

$$\Delta u_v(Q_0^2) - \Delta d_v(Q_0^2) = F + D = 1.2573 \pm 0.0028\ , \tag{6.8}$$

$$\Delta u_v(Q_0^2) + \Delta d_v(Q_0^2) = 3F - D = 0.579 \pm 0.025 \tag{6.9}$$

at some appropriately chosen input scale $Q^2 = Q_0^2$. Note that $\Delta q_v(Q^2)$ depends (marginally) on Q^2 in NLO due to $\Delta P^{(1)}_{\mathrm{NS}+} \neq 0$ in (5.19).

In the 'standard' $\mathrm{SU}(3)_f$ symmetric scenario we need $\Delta s = \Delta\bar{s} < 0$ in $\Gamma_1^{p,n}$ in Eq. (5.14) or (5.18) in order to comply with recent experiments (cf. Table 2), i.e. in order to obtain a reduction of the Ellis–Jaffe expectation $\Gamma^{p,n}_{1,\mathrm{EJ}}$, Eq. (5.15), based on A_3 and A_8 which are entirely fixed by Eqs. (6.6) and (6.7), respectively. [Remember that $\Delta g(Q^2)$ decouples from $\Gamma_1^{p,n}$ in (5.18) in NLO ($\overline{\rm MS}$) due to $\Delta C_g = 0$.] In the 'valence' scenario we can do even with $\Delta s = \Delta\bar{s} \simeq 0$ since here only the valence contribution to A_8 is fixed (apart from minor Q^2 dependent effects in NLO) by Eq. (6.9), with the entire A_3 still being fixed by (6.8) due to the assumption $\Delta\bar{u} = \Delta\bar{d} \equiv \Delta\bar{q}$ (which is again violated by minor Q^2 dependent effects in NLO). This gives in LO for Γ_1 in (5.4)

$$\Gamma_1^{p,n} = \pm\tfrac{1}{12}(F+D) + \tfrac{5}{36}(3F-D) + \tfrac{1}{18}(10\Delta\bar{q} + \Delta s + \Delta\bar{s}) \tag{6.10}$$

and a similar relation holds in NLO [309]. Thus, in contrast to Eq. (5.14), a light polarized sea $\Delta\bar{q} < 0$ will account for a reduction of $\Gamma_1^{p,n}$ *even* for the extreme $\mathrm{SU}(3)_f$ broken choice $\Delta s = \Delta\bar{s} = 0$!

Turning to the determination of the polarized LO and NLO parton distributions $\delta f(x,Q^2)$ it is helpful to consider some reasonable theoretical constraints concerning the sea and gluon densities, in particular in the relevant small-x region where only rather scarce data exist at present (in contrast to unpolarized DIS): apart from the rather general Regge constraints in Eq. (4.102) for $x \to 0$, color coherence of the gluon couplings at $x \simeq 0$, i.e. equal partition of the hadron's

momentum among its partons, implies for the gluon and sea densities [145,144]

$$\delta f(x,Q_0^2)/f(x,Q_0^2) \sim x \quad \text{as } x \to 0 \ , \tag{6.11}$$

and arguments based on helicity retention properties of perturbative QCD of valence densities at large-x imply [145,144,193]

$$\delta q_v(x,Q_0^2) \sim q_v(x,Q_0^2) \quad \text{as } x \to 1 \ . \tag{6.12}$$

The scale Q_0 at which these relations are supposed to hold remains unspecified. Although not strictly compelling, Eqs. (6.11) and (6.12) are expected [145,144] to hold at some 'intrinsic' bound-state-like scale ($Q_0^2 \lesssim 1\,\mathrm{GeV}^2$, say), but certainly not at much larger purely perturbative scales $Q_0^2 \gg 1\,\mathrm{GeV}^2$. Despite such 'guidelines', presently available scarce polarization data on $A_1(x,Q^2) \simeq g_1(x,Q^2)/F_1(x,Q^2)$, Eq. (2.14), constrain the polarized parton densities rather little, which holds in particular for $\delta g(x,Q^2)$ [309,313,294,88]. The determination of the polarized valence densities is less ambiguous. In order to avoid, as far as possible, pure guesses for the input densities $\delta f(x,Q_0^2)$, it has been suggested in [309,313] to employ the unpolarized valence-like input densities $f(x,Q_0^2)$ at $Q_0^2 = \mu^2 \simeq 0.3\,\mathrm{GeV}^2$, properly modified so as to comply with polarized DIS data, with the positivity inequalities (4.11) for $Q^2 \geq \mu^2$ and with the constraints (6.11) and (6.12). Subject to these requirements the following general ansatz for the LO and NLO polarized parton densities has been employed [309,9]:

$$\begin{aligned}
\delta q_v(x,\mu^2) &= N_{q_v} x^{a_{q_v}} q_v(x,\mu^2) \ , \\
\delta \bar{q}(x,\mu^2) &= N_{\bar{q}} x^{a_{\bar{q}}} (1-x)^{b_{\bar{q}}} \bar{q}(x,\mu^2) \ , \\
\delta s(x,\mu^2) &= \delta \bar{s}(x,\mu^2) = N_s \delta \bar{q}(x,\mu^2) \ , \\
\delta g(x,\mu^2) &= N_g x^{a_g} (1-x)^{b_g} g(x,\mu^2) \ ,
\end{aligned} \tag{6.13}$$

where the LO and NLO unpolarized input densities $f(x,\mu^2)$ at $\mu^2_{\mathrm{LO}} = 0.23\,\mathrm{GeV}^2$ and $\mu^2_{\mathrm{NLO}} = 0.34\,\mathrm{GeV}^2$, respectively, refer to the recent GRV valence-like densities [319]. It should be noted that employing valence-like gluon and sea input densities [i.e. $xg(x,\mu^2) \sim x^a$, $x\bar{q}(x,\mu^2) \sim x^{a'}$ with a, $a' > 0$ as $x \to 0$] allows for a *parameter-free* calculation of parton densities and DIS structure functions in the small-x region ($x \lesssim 10^{-2}$) at $Q^2 > \mu^2$ which is entirely based on the QCD dynamics [314,315,319]. The *perturbatively stable* LO/NLO predictions turned out to be in excellent agreement with all DESY-HERA measurements up to now [11,38,40,220,222,223].

The resulting fit parameters N_i, a_i, b_i for the 'standard' and 'valence' scenarios in LO and NLO can be found in [309] where appropriate simple parametrizations of the rather complicated QCD evolutions have also been given. The LO and NLO results for the asymmetries $A_1^{p,d}(x,Q^2)$ measured up to now, as discussed in Section 3, are presented in Fig. 24 for the 'standard' scenario. The results for the 'valence' scenario are very similar. In both cases the LO and NLO results are perturbatively stable and almost indistinguishable. The expected Q^2 dependence of $A_1(x,Q^2)$ is shown in Fig. 25 and compared with recent SLAC-E143 and SMC data. [The difference between the LO and NLO results in the small-Q^2 region is mainly due to different LO ($\mu^2_{\mathrm{LO}} = 0.23\,\mathrm{GeV}^2$) and NLO ($\mu^2_{\mathrm{NLO}} = 0.34\,\mathrm{GeV}^2$) input scales.] It should be emphasized that $A_1 \simeq g_1/F_1$ is in general expected to be Q^2 *dependent* as soon as gluon and sea densities become relevant, due to the very different polarized and unpolarized splitting functions $\delta P_{ij}^{(0,1)}(x)$ and $P_{ij}^{(0,1)}(x)$, respectively (except

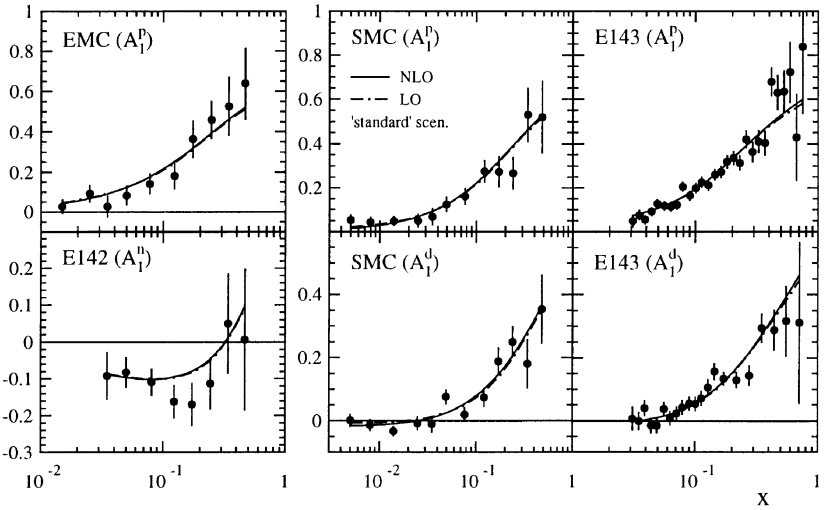

Fig. 24. Comparison of LO and NLO results for $A_1(x, Q^2)$ as obtained [309] from the fitted inputs at $Q^2 = \mu^2_{\mathrm{LO,NLO}}$ for the 'standard' scenario, Eqs. (6.6) and (6.7), with present data [490,77,20,17,18,65,2–4,23–25]. The Q^2 values adopted here correspond to the different values quoted by the experiments for each data point starting at $Q^2 \gtrsim 1\,\mathrm{GeV}^2$ at the lowest available x-bin.

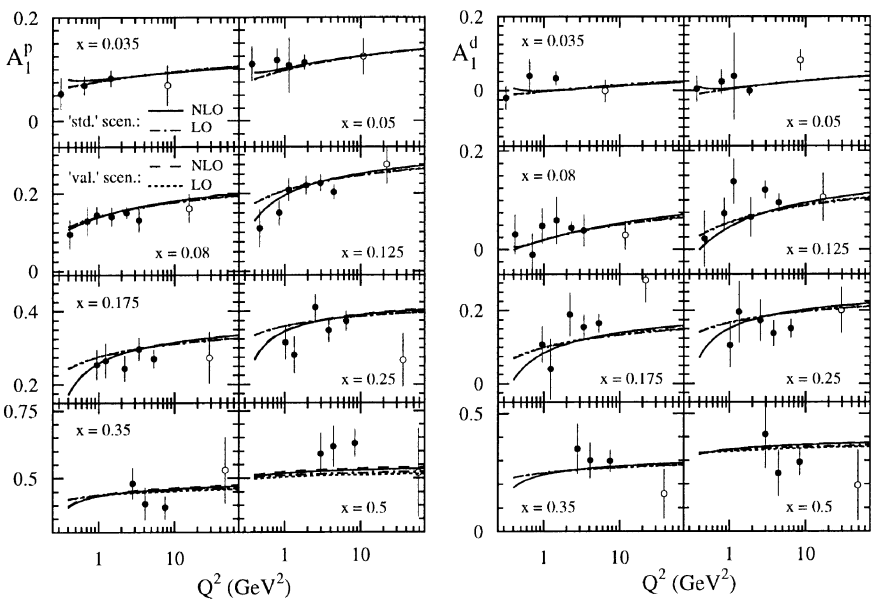

Fig. 25. The Q^2 dependence of $A_1^{p,d}(x, Q^2)$ as predicted by LO and NLO QCD evolutions [309] at various fixed values of x, compared with recent SLAC-E143 [2,4] (solid circles) and SMC data [25,17,18,20] (open circles).

for $\delta P_{qq}^{(0)} = P_{qq}^{(0)}$ which dominates, apart from marginal differences in the relevant NLO NS splitting functions, in the large-x region). Moreover, the smaller x the stronger becomes the dependence of the exactly calculated $A_1(x, Q^2)$ on the precise form of the input at $Q^2 = \mu^2$ [313]. For practical purposes, however, such ambiguities are irrelevant since $A_1 \simeq g_1/F_1 \simeq 2x\,g_1/F_2 \to 0$ as $x \to 0$ is already unmeasurably small (of the order 10^{-3}) for $x \lesssim 10^{-3}$. Thus the small-x region is unlikely to be accessible experimentally for $g_1(x, Q^2)$, in contrast to the situation for the unpolarized $F_{1,2}(x, Q^2)$. It is furthermore interesting to note that the approximate asymptotic ($x \to 0$) DLL expression (4.110) for $A_1(x, Q^2)$ does not even quantitatively reproduce the exact LO results for $A_1(x, Q^2)$ for $x \geq 10^{-3}$ [313]. It is therefore misleading to use the simple asymptotic DLL formulae (4.107)–(4.110) for quantitative estimates [93,94,263].

The structure functions $g_1^{p,n}(x, Q^2)$ and g_1^d, given by the relation (3.6), can now be extracted using Eqs. (2.14) and (2.18) where one usually neglects the subleading contributions proportional to γ^2. These results are shown in Figs. 26 and 27. The reason why the LO results are partly larger by more than about 10% than the NLO ones is mainly due to the LO approximation $R = 0$ in Eq. (2.19), as used in [309]. Some of the EMC and E143 asymmetry data [490,77,78,2,4] have been analysed by assuming A_1^p to be independent of Q^2. This can be partly responsible [309] for these 'data' falling somewhat below the NLO predictions in the small-x region, despite the excellent fits to A_1^p in Fig. 24. The predictions for the NLO parton distributions at the input scale $Q^2 = \mu_{\rm NLO}^2 = 0.34\,\mathrm{GeV}^2$ in Eq. (6.13) are shown in Fig. 28 and compared with the reference unpolarized NLO dynamical input densities of [319] which satisfy of course the positivity requirement (4.11) as is obvious from Eq. (6.13). The LO predictions are similar [309]. It should be noted that the strange densities correspond to $N_s = 1$ in (6.13) for the SU(3)$_f$ symmetric 'standard' scenario, whereas to

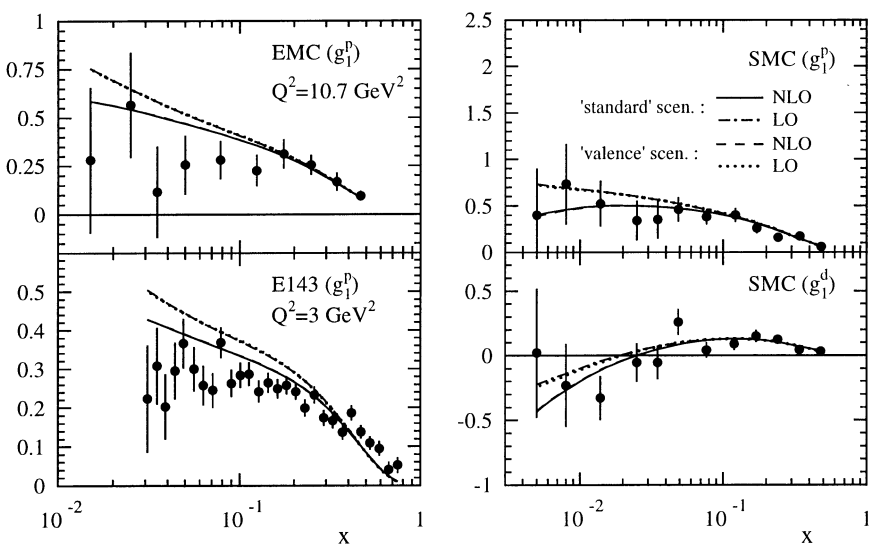

Fig. 26. Comparison of the 'standard' and 'valence' LO and NLO results [309] with the data for $g_1^{p,d}(x, Q^2)$ [490,77,78,17,18,20,65,2–4,23–25,28]. The SMC data correspond to different $Q^2 \gtrsim 1\,\mathrm{GeV}^2$ for $x \geq 0.005$, as do the theoretical results.

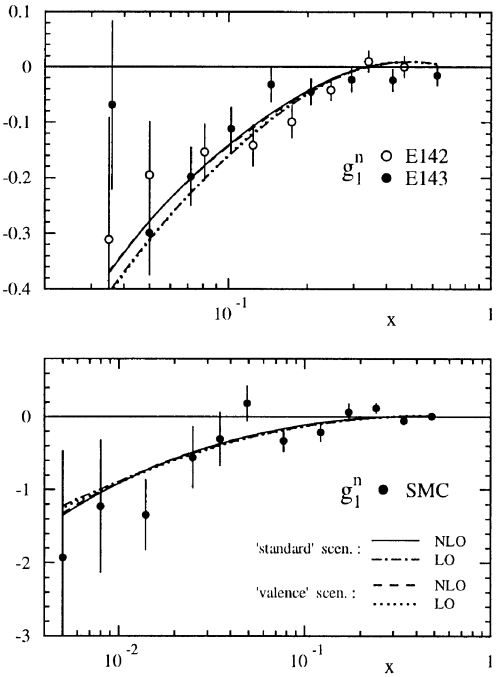

Fig. 27. Same as in Fig. 26 but for $g_1^n(x, Q^2)$. The E142 and E143 data [65,3] correspond to an average $\langle Q^2 \rangle = 2$ and $3\,\mathrm{GeV}^2$, respectively, and the theoretical predictions correspond to a fixed $Q^2 = 3\,\mathrm{GeV}^2$.

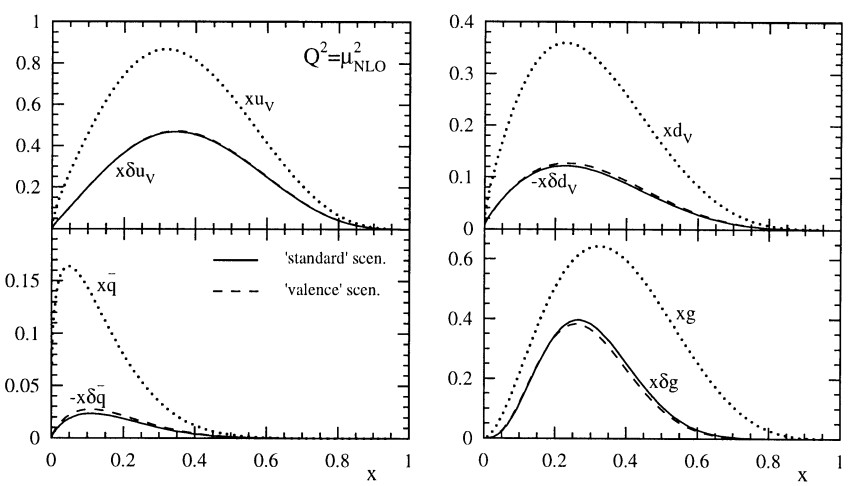

Fig. 28. Comparison of the fitted 'standard' and 'valence' input NLO($\overline{\mathrm{MS}}$) densities at $Q^2 = \mu^2_{\mathrm{NLO}} = 0.34\,\mathrm{GeV}^2$, according to Eq. (6.13) [309], with the unpolarized dynamical input densities of [319].

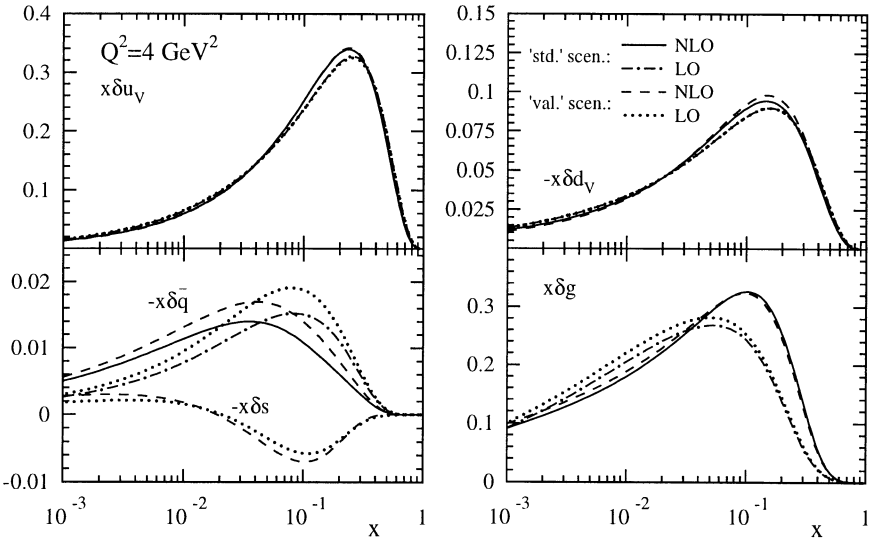

Fig. 29. The polarized LO and NLO($\overline{\text{MS}}$) densities at $Q^2 = 4\,\text{GeV}^2$ as obtained from the input densities at $Q^2 = \mu^2_{\text{LO,NLO}}$ as shown in Fig. 28 for the NLO. In the 'standard' scenario, δs coincides with the curves shown for $\delta\bar{q}$ in LO and NLO due to the SU(3)$_f$ symmetric input which is only marginally broken in NLO for $Q^2 > \mu^2_{\text{NLO}}$.

$N_s = 0$ for the SU(3)$_f$ broken 'valence' scenario [309]. The corresponding polarized densities at $Q^2 = 4\,\text{GeV}^2$, as obtained from these inputs at $Q^2 = \mu^2$ for the two scenarios in LO and NLO, are shown in Fig. 29. It is interesting to note that, within the radiative approach with its longer Q^2-evolution 'distance' starting at the low input scale μ^2 in Eq. (6.13), a *finite* (negative) strange polarized sea input $\delta s(x,\mu^2)$ is *always* required by present data for the 'standard' scenario. This holds true even if one uses (somewhat inconsistently in NLO) the 'off-shell' $\delta\widetilde{C}_g$ in Eqs. (4.46) or (4.65) which corresponds to $\Delta\widetilde{C}_g = \frac{1}{2}$, giving rise to Eq. (5.22), in contrast to $\Delta C_g^{\overline{\text{MS}}} = 0$. The shape of the polarized gluon densities δg presented in Figs. 30 and 31 is constained rather little by present asymmetry data [309,313,294]: Equally agreeable fits can be obtained for a fully saturated [inequality (4.11)] gluon input $\delta g(x,\mu^2) = g(x,\mu^2)$ as well as for the less saturated $\delta g(x,\mu^2) = xg(x,\mu^2)$. A purely dynamical [310] input $\delta g(x,\mu^2) = 0$ is also compatible with present data, but such a choice seems to be unlikely in view of $\delta\bar{q}(x,\mu^2) \neq 0$; it furthermore results in an unphysical steep [310] $\delta g(x,Q^2 > \mu^2)$, being mainly concentrated in the very small-x region $x < 0.01$, as in the corresponding case [314,296] for the unpolarized parton distributions in disagreement with experiment. The resulting NLO gluon densities $\delta g(x,Q^2)$ at $Q^2 = 4\,\text{GeV}^2$ which originate from these extreme inputs are compared in Fig. 30 with our 'fitted δg' curve of Fig. 29 obtained for the 'valence' scenario. Present data allow even for a partly negative $\delta g(x, 4\,\text{GeV}^2)$ [294] and specific model calculations can accommodate even a negative $\Delta g(4\,\text{GeV}^2)$ [312,376]. It turns out that $\delta g(x,Q^2)$ is somewhat less ambiguous if only the more global quantities δq_{NS}, $\delta\Sigma$ and δg are used for analyzing present data [88], instead of trying to delineate the individual parton densities.

An alternative analysis of polarized structure functions has been performed by Gehrmann and Stirling [294]. This was done in the same spirit as the unpolarized analysis [468], namely the

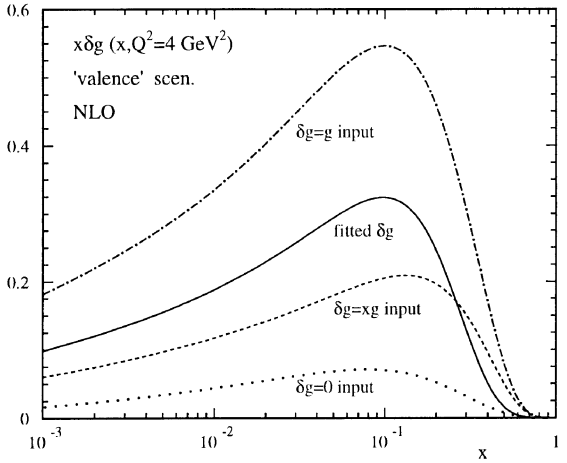

Fig. 30. The experimentally allowed range of NLO polarized gluon densities at $Q^2 = 4\,\mathrm{GeV}^2$ for the 'valence' scenario with differently chosen $\delta g(x, \mu^2_{\mathrm{NLO}})$ inputs. The 'fitted δg' curve is identical to the one in Fig. 29. Very similar results are obtained if $\delta g(x, \mu^2_{\mathrm{NLO}})$ is varied accordingly within the 'standard' scenario as well as in an LO analysis [309,313].

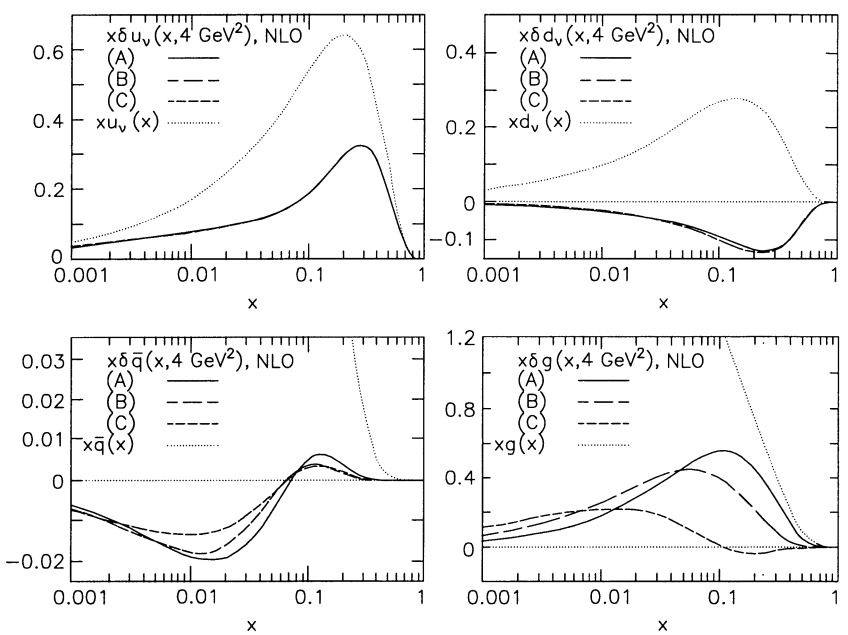

Fig. 31. NLO polarized and unpolarized parton distributions at $Q_0^2 = 4\,\mathrm{GeV}^2$ according to [294].

polarized parton distributions were chosen to be of the general form

$$x\delta f(x,Q_0^2) = \eta_f A_f x^{a_f}(1-x)^{b_f}(1+\gamma_f x+\rho_f\sqrt{x}) \tag{6.14}$$

for $f = u_v, d_v, \bar{q}, g$ at the starting scale $Q_0^2 = 4\,\mathrm{GeV}^2$. The normalization factors

$$A_f = \left[\left(1+\gamma_f\frac{a_f}{a_f+b_f+1}\right)\frac{\Gamma(a_f)\Gamma(b_f+1)}{\Gamma(a_f+b_f+1)} + \rho_f\frac{\Gamma(a_f+0.5)\Gamma(b_f+1)}{\Gamma(a_f+b_f+1.5)}\right]^{-1} \tag{6.15}$$

are determined by the condition that the first moments of $\delta f(x,Q_0^2)$ are given by η_f. The parameters $\eta_f, a_f, b_f, \gamma_f$ and ρ_f for $f = u_v$ and d_v were determined by LO and NLO fits to recent data. For the sea, an $SU(3)_f$ symmetric antiquark polarization was assumed (just as in the 'standard' scenario [309] as discussed above, e.g. Eq. (6.13) with $N_s = 1$). For $\delta g(x,Q_0^2)$, which is hardly constrained by the data (cf. Fig. 30), three alternative parametrizations were employed, a hard and a soft distribution (A and B) with the spin aligned with that of the parent proton and a distribution (called C) with the spin anti-aligned. All three choices give equally good descriptions of the structure function data, but would be relatively easy to discriminate if data on polarized gluon initiated processes like $\gamma^{(*)}g \to c\bar{c}$ or $qg \to \gamma q$ were available. In all cases the first moment $\eta_g = 1.9$ was chosen which is obtained in LO by attributing *all* the violation of the Ellis–Jaffe sum rule to a large gluon polarization. This number is in the same ballpark as if determined from an NLO analysis of the experimental data ($\Delta g(Q_0^2) = 1.5 \pm 0.5$ [88] and Eq. (6.16) and Tables 3 and 4 below), but with a large error. A summary of the fitted and chosen parameters together with the χ^2 of the fit can be found in Table 2 of [294]. The NLO polarized parton distributions at $Q_0^2 = 4\,\mathrm{GeV}^2$ for gluon scenarios A, B and C are shown in Fig. 31. It should be emphasized that present polarization data can be fitted even with a negative δg in the large-x region, as shown in Fig. 31, which refers to a more extreme choice than the ones depicted in Fig. 30. Furthermore, the LO GRV 94 [319] and the NLO MRS-A' [468] parton densities have been chosen as reference distributions, which are necessary for comparing with the positivity constraints (4.11), and are also shown in Fig. 31. The resulting fits for $g_1^{p,n,d}(x,Q^2)$ are similar in quality [294] as the ones shown in Figs. 26 and 27.

Finally let us turn to the first moments (total polarizations) $\Delta f(Q^2)$ in Eq. (5.1) of the polarized parton densities $\delta f(x,Q^2)$ and the resulting $\Gamma_1^{p,n}(Q^2)$. It should be recalled that, in contrast to the LO, the first moments of the NLO (anti)quark densities do renormalize, i.e. are Q^2 dependent, due to the nonvanishing of the 2-loop $\Delta P_{qq}^{(1)}$ and $\Delta P_{\mathrm{NS}+}^{(1)}$ in (5.19). Let us discuss the two scenarios in turn:

(i) In the 'standard' scenario the input densities in (6.13), being constrained by (6.6) and (6.7), imply in LO [309]

$$\begin{aligned} &\Delta u_v = 0.9181, \qquad \Delta d_v = -0.3392\,, \\ &\Delta\bar{q} = \Delta s = \Delta\bar{s} = -0.0587\,, \\ &\Delta g(\mu_{\mathrm{LO}}^2) = 0.362, \quad \Delta g(4\,\mathrm{GeV}^2) = 1.273, \quad \Delta g(10\,\mathrm{GeV}^2) = 1.570\,, \end{aligned} \tag{6.16}$$

which result in $\Delta\Sigma = 0.227$. This gives

$$\Gamma_1^p = 0.1461, \qquad \Gamma_1^n = -0.0635 \tag{6.17}$$

Table 3
First moments of polarized NLO parton densities $\delta f(x,Q^2)$ and of $g_1^{p,n}(x,Q^2)$ as predicted in the 'standard' scenario [309]. Note that the marginal differences for $\Delta\bar{q}$ and Δs indicate the typical amount of dynamical $SU(3)_f$ breaking generated by the RG Q^2-evolution to $Q^2 > \mu^2_{\rm NLO}$

$Q^2(\mathrm{GeV})^2$	Δu_v	Δd_v	$\Delta\bar{q}$	$\Delta s = \Delta\bar{s}$	Δg	$\Delta\Sigma$	Γ_1^p	Γ_1^n
$\mu^2_{\rm NLO}$	0.9181	− 0.3392	− 0.0660	− 0.0660	0.507	0.183	0.1136	− 0.0550
1	0.915	− 0.338	− 0.067	− 0.068	0.961	0.173	0.124	− 0.061
4	0.914	− 0.338	− 0.068	− 0.068	1.443	0.168	0.128	− 0.064
10	0.914	− 0.338	− 0.068	− 0.069	1.737	0.166	0.130	− 0.065

in reasonable agreement with present data (Table 2). The NLO results are shown in Table 3 which are in even better agreement with experiments (Table 2).

(ii) In the 'valence' scenario the input densities in (6.13), being constrained by (6.8) and (6.9), imply in LO [309]

$$\begin{aligned} &\Delta u_v = 0.9181, \qquad \Delta d_v = -0.3392\ , \\ &\Delta\bar{q} = -0.0712, \qquad \Delta s = \Delta\bar{s} = 0\ , \\ &\Delta g(\mu^2_{\rm LO}) = 0.372, \quad \Delta g(4\,\mathrm{GeV}^2) = 1.361, \quad \Delta g(10\,\mathrm{GeV}^2) = 1.684 \end{aligned} \tag{6.18}$$

which result in $\Delta\Sigma = 0.294$. Apart from this maximal $SU(3)_f$ breaking, these results are similar to the 'standard' ones in (6.16) and yield

$$\Gamma_1^p = 0.1456, \qquad \Gamma_1^n = -0.0639 \tag{6.19}$$

on account of (6.10). The NLO results are shown in Table 4.

These results for the total helicities (first moments) are similar to the ones observed in other recent LO and NLO analyzes [294,88,9].

Due to the similarity of the LO and NLO results in both scenarios, it is obviously impossible to distinguish experimentally between the 'standard' ($SU(3)_f$ symmetric) and 'valence' ($SU(3)_f$ maximally broken) scenario. In both scenarios the Bjorken sum rule (5.86) manifestly holds due to the constraints (6.6) and (6.8). Furthermore, the observed total helicities carried by the valence quarks, Δu_v and Δd_v, are compatible with the ones obtained very recently from semi-inclusive spin asymmetry measurements [27], cf. Section 6.5, which yielded $\Delta u_v = 1.01 \pm 0.24$ and $\Delta d_v = -0.57 \pm 0.25$ at $\langle Q^2\rangle \simeq 10\,\mathrm{GeV}^2$. It is also very interesting to note that our optimal fit results shown above favor a sizeable total gluon helicity $\Delta g(10\,\mathrm{GeV}^2) \simeq 1.7$, despite the fact that $\Delta g(Q^2)$ decouples from the full $(0 \le x \le 1)$ first moment $\Gamma_1(Q^2)$ in (5.18) in the $\overline{\rm MS}$ scheme (since $\Delta C_g^{\overline{\rm MS}} = 0$). This implies that for any experimentally relevant analysis (where $0.01 \lesssim x < 1$), the NLO $\delta g(x,Q^2)$ in Eq. (4.47), for example, plays an important role almost regardless of the value of the full first moment of $\delta C_g(x)$. The importance of $\delta g(x,Q^2)$ also holds in LO where δg does not directly appear in $g_1(x,Q^2)$, Eq. (4.5), but enters only via the RG evolution equations.

This large $\overline{\rm MS}$ result for $\Delta g(Q^2)$ is also comparable with the weaker constraint (5.85) obtained in the off-shell scheme (where $\Delta C_g = -\frac{1}{2}$) which is not too surprising since the RG solutions (5.81) and (5.83) differ only to $\mathcal{O}(\alpha_s)$. Furthermore one can be tempted to reinterpret our $\overline{\rm MS}$ results for

Table 4
The first moments (total helicities) as in Table 3, but for the maximally $SU(3)_f$ broken 'valence' scenario [309]

$Q^2(\mathrm{GeV})^2$	Δu_v	Δd_v	$\Delta\bar{q}$	$\Delta s = \Delta\bar{s}$	Δg	$\Delta\Sigma$	Γ_1^p	Γ_1^n
μ^2_{NLO}	0.9181	−0.3392	−0.0778	0	0.496	0.268	0.1142	−0.0544
1	0.915	−0.338	−0.080	-2.5×10^{-3}	0.982	0.252	0.124	−0.061
4	0.914	−0.338	−0.081	-3.5×10^{-3}	1.494	0.245	0.128	−0.064
10	0.914	−0.338	−0.081	-3.8×10^{-3}	1.807	0.244	0.130	−0.065

$\Delta\Sigma(Q^2)$ in terms of $\Delta\Sigma_{\mathrm{off}}$ in Eq. (5.26), by assuming that $\Delta g(Q^2)$ in the off-shell scheme is similar to our $\overline{\mathrm{MS}}$ results. This gives

$$\Delta\Sigma_{\mathrm{off}} \simeq 0.33\ (0.42) \tag{6.20}$$

according to the results for the 'standard' ('valence') scenario in Table 3 (Table 4). Thus the sizeable $\Delta g(Q^2)$ implies a sizeable amount of total helicity of singlet quark densities, $\Delta\Sigma_{\mathrm{off}}$, which comes close to the naive expectation $\Delta\Sigma_{\mathrm{off}} \simeq A_8 \simeq 0.6$ in Eq. (5.27) in contrast to $\Delta\Sigma(Q^2)$ in the $\overline{\mathrm{MS}}$ scheme.

Finally, it is very interesting to observe that at the low input scales $Q^2 = \mu^2_{\mathrm{LO,NLO}} = 0.23, 0.34\,\mathrm{GeV}^2$ the nucleon's spin is dominantly carried just by the total helicities of quarks and gluons

$$\tfrac{1}{2}\Delta\Sigma(\mu^2_{\mathrm{LO[NLO]}}) + \Delta g(\mu^2_{\mathrm{LO[NLO]}}) \simeq 0.5\ [0.6] \tag{6.21}$$

according to Eqs. (6.16) and (6.18), and Tables 3 and 4. Thus the helicity sum rule (1.1) implies that

$$L_z(\mu^2_{\mathrm{LO,NLO}}) \simeq 0\ . \tag{6.22}$$

The approximate vanishing of this latter nonperturbative angular momentum, being built up from the intrinsic k_T carried by partons, is intuitively expected for low bound-state-like scales (but *not* for $Q^2 \gg \mu^2$) implying that the spin of the nucleon is carried solely by quarks and gluons, Eq. (6.21), i.e. there is no 'spin surprise' whatsoever. At smaller distances, i.e. for $Q^2 \gg \mu^2_{\mathrm{LO,NLO}}$, this picture will break down since gluon and $q\bar{q}$ production off the initial partons will increase their k_T which in turn gives rise to a finite orbital angular momentum carried by quarks and gluons, $L_z(Q^2) = L_q(Q^2) + L_g(Q^2)$ [529,530,381,505]. Clearly a finite $L_z(Q^2)$ is required to reconcile, for example $\frac{1}{2}\Delta\Sigma(Q^2) + \Delta g(Q^2) \simeq 1.8$ at $Q^2 = 10\,\mathrm{GeV}^2$ (Table 3), with the sum rule (1.1). The relevant RG Q^2-evolution equations for the quark and gluon angular momenta $L_q(Q^2)$ and $L_g(Q^2)$ have been written down recently in LO [401]:

$$\frac{\mathrm{d}}{\mathrm{d}t}\begin{pmatrix} L_q(Q^2) \\ L_g(Q^2) \end{pmatrix} = \frac{\alpha_s(Q^2)}{2\pi}\begin{pmatrix} -\frac{4}{3}C_F & \frac{f}{3} \\ \frac{4}{3}C_F & -\frac{f}{3} \end{pmatrix}\begin{pmatrix} L_q(Q^2) \\ L_g(Q^2) \end{pmatrix} + \frac{\alpha_s(Q^2)}{2\pi}\begin{pmatrix} -\frac{2}{3}C_F & \frac{f}{3} \\ -\frac{5}{6}C_F & -\frac{11}{2} \end{pmatrix}\begin{pmatrix} \Delta\Sigma(Q^2) \\ \Delta g(Q^2) \end{pmatrix}, \tag{6.23}$$

where the second inhomogeneous term was first studied in [505] with $\Delta\Sigma$ and Δg evolving according to (5.2). The solution of (6.23) is straightforward:

$$L_q(Q^2) = -\frac{1}{2}\Delta\Sigma + \frac{1}{2}\frac{3f}{16+3f} + \left[L_q(Q_0^2) + \frac{1}{2}\Delta\Sigma - \frac{1}{2}\frac{3f}{16+3f}\right]L^{2(16+3f)/9\beta_0}\,, \tag{6.24}$$

$$L_g(Q^2) = -\Delta g(Q^2) + \frac{1}{2}\frac{16}{16+3f} + \left[L_g(Q_0^2) + \Delta g(Q_0^2) - \frac{1}{2}\frac{16}{16+3f}\right]L^{2(16+3f)/9\beta_0} \tag{6.25}$$

with $L \equiv \alpha_s(Q^2)/\alpha_s(Q_0^2)$ and $\Delta\Sigma \equiv \Delta\Sigma(Q_0^2) = \Delta\Sigma(Q^2)$ in LO. The last Eq. (6.25) demonstrates explicitly that the large gluon helicity $\Delta g(Q^2)$ as obtained above at large $Q^2 > \mu^2$ is canceled by an equally large, but negative, gluon orbital momentum. Asymptotically ($Q^2 \to \infty$) the solutions (6.24) and (6.25) become particularly simple

$$L_q + \tfrac{1}{2}\Delta\Sigma = \tfrac{1}{2}\,3f/(16+3f), \qquad L_g + \Delta g = \tfrac{1}{2}\,16/(16+3f)\,. \tag{6.26}$$

Thus the partition of the nucleon spin between quarks and gluons eventually follows the well-known partition of the quark and gluon momenta in the nucleon [338,339,295]. If the Q^2 evolution is slow, then Eq. (6.26) predicts that quarks carry less than about 50% of the nucleon spin even at low momenta [cf. Eqs. (6.16) and (6.18)].

It should be mentioned that, although $L_z = L_q + L_g$ can be theoretically formally formulated in a consistent covariant way [381,376,174], there appears to be no direct experimental test of the size as well as of the sign of $L_z(Q^2)$, or more ideally of the separate components $L_q(Q^2)$ and $L_g(Q^2)$. The possible measurement of azimuthal distributions has been proposed [180,477] but these are only sensitive to some average $\langle k_T^2 \rangle$ of rotating constituents in a polarized nucleon target.

More recently, Ji [395,396] has suggested to use deeply virtual Compton scattering (DVCS) $\gamma^*(Q^2)p \to \gamma p'$ in the limit of vanishing momentum transfer $t = (p' - p)^2$, in order to get direct information about the gauge invariant combinations $J_q = \frac{1}{2}\Delta\Sigma + L_q$ and $J_g = \Delta g + L_g$ appearing in the spin sum rule (1.1): $\frac{1}{2} = J_q(Q^2) + J_g(Q^2)$. In this limit, $J_{q,g} = \frac{1}{2}[A_{q,g}(0) + B_{q,g}(0)]$ where $A_{q,g}(t)$ and $B_{q,g}(t)$ are the 'Dirac' and 'Pauli' form factors of the quark and gluon energy-momentum tensor [395,398,498] (which are analogously defined as the well known form factors of the electromagnetic vector current). The form factors $A_q(t)$ and $B_q(t)$ are then related via sum rules to the $n = 2$ moments (Bjorken-x averages) of the structure functions of the *non*forward (or *off*-forward) DVCS. Although the extrapolation $t \to 0$, required to obtain $J_{q,g}$, is difficult [397,497,426] (if at all possible), rough estimates result in a DVCS cross section at $-t < 1\,\mathrm{GeV}^2$ above 1 pb at CEBAF and DESY–Hermes kinematics [397,563].

6.2. Heavy quark production in polarized DIS and in photoproduction

In the previous sections we have realized, among other things, the enormous difficulties to extract the polarized gluon distribution and in particular its first moment from inclusive deep inelastic data. These problems have been anticipated several years ago by theoretical studies [55,241,158,50], and they are in fact not surprising in view of the well-known subtleties having occurred in all attempts to determine the unpolarized gluon density in unpolarized DIS experiments during the past two decades.

A popular way out of this dilemma is the study of semi-inclusive cross sections, and in particular of charm production, because the production of heavy quark hadrons is triggered in leading order by the photon–gluon fusion mechanism [$\gamma^*(\gamma)\delta g \to h\bar{h}$ with $h = b, c$] and is therefore sensitive to the gluon density inside the proton, whereas the heavy quark content of the proton is usually negligible, if it exists at all, at presently available Q^2-values. Due to its prominent decay mechanism, J/ψ production is the most distinct among the charmed events. In contrast to open charm production one faces here, however, the additional model dependence for bound-state production, such as the 'duality model' [281,346,403,298,300] (nowadays also called 'color evaporation' model) and the color-singlet model [162,111,82,83]. In the duality or 'soft color' treatment of color quantum numbers the cross section for bound charm production is given by

$$\sigma_{\text{onium}} = \frac{1}{9}\int_{2m_c}^{2m_D} \mathrm{d}m \frac{\mathrm{d}\sigma_{c\bar{c}}}{\mathrm{d}m}\,, \tag{6.27}$$

where $\mathrm{d}\sigma_{c\bar{c}}$ is computed perturbatively in LO and NLO due to $\gamma^* g \to c\bar{c}$, etc. (or due to $q\bar{q} \to c\bar{c}$, $gg \to c\bar{c}$, etc., for hadronically produced quarkonia), since here the color singlet property of the J/ψ is ignored at the perturbative stage of the calculation. The subsequent hadronization of the color singlet state is then assumed to be characterized by multiple (nonperturbative) soft gluon emissions, i.e. the treatment of color is, on the average, statistical with the factor $\frac{1}{9}$ representing the statistical probability that the $3 \times \bar{3}$ charm pair is asymptotically in a color singlet state. Alternatively, in the color-singlet model the color singlet property of the produced onium states (J/ψ, etc.) is enforced already at short distances, $\Delta x \sim m_\psi^{-1}$, by the emission of a perturbative (octet) gluon off the produced charm quark. It is this latter assumption which casts doubt on the color-singlet model since it does not seem logical to enforce perturbatively the color-singlet property of the onia at short distances, given that there remains practically an infinite time for soft gluons to readjust the color of the $c\bar{c}$ pair before it appears as an asymptotic J/ψ or, alternatively, $D\bar{D}$ state. In other words, it is hard to imagine that a color singlet state formed at a range m_ψ^{-1}, automatically survives to form a J/ψ. Indeed, the duality ('color evaporation') treatment has received renewed attention and appears to be the favorite mechanism of heavy quarkonia production [58,235,526,290,527] (or a variant of it which differs in its nonrelativistic treatment of the nonperturbative long-distance part of the $c\bar{c}$ matrix elements which obey simple 'velocity-scaling' laws with respect to the relative velocity β of the $c\bar{c}$; this allows for a systematic expansion in $\alpha_s(2m_c)$ and β [129].) The reason for this revival is that some data on the production of ψ- and Υ-states disagree with the simple minded color-singlet model predictions; occasionally by well over one order of magnitude as in the case of ψ' production at the Fermilab Tevatron [140]. Thus it seems to be more appropriate to study and delineate the relevant quarkonia production mechanism using unpolarized reactions first, instead of using a particular model to get access to $\delta g(x, Q^2 \approx m_{J/\psi}^2)$ via polarized deep inelastic (or photon) production of J/ψ's [304,305,340,404,325,546]. This statement is even more true for (diffractive) elastic J/ψ production where some very speculative models exist [142,516,517,447]. They are based on a two-gluon exchange but it is not clear whether the square of the polarized gluon density $\delta g(x, Q^2 \approx m_{J/\psi}^2)$ or some independent two-gluon correlation function appears in the cross section formula.

Therefore, from the theoretical point of view a much cleaner signal for the gluon density in heavy quark production is open charm production, although experimentally it has worse statistics due to

the difficulties in identifying D-mesons. Instead of the deep inelastic process one may as well look at photoproduction, because the mass of the charm quark forces the process to take place in the perturbative regime. The advantage of photoproduction over DIS is its larger cross section. Several fixed target experiments, HERMES at DESY [57], COMPASS at CERN [106] and a new facility at SLAC [73] are being developed to measure the polarized gluon distribution via photoproduction.

In leading order the inclusive polarized deep inelastic open charm production cross section is given by, using Eq. (2.7) or (2.41)

$$\frac{\mathrm{d}^2\Delta\sigma_c}{\mathrm{d}x\,\mathrm{d}y} = \frac{\mathrm{d}^2}{\mathrm{d}x\,\mathrm{d}y}\frac{1}{2}(\sigma^{\leftarrow}_{\Rightarrow} - \sigma^{\leftarrow}_{\Leftarrow}) \approx \frac{4\pi\alpha^2}{Q^2}(2-y)g_1^c(x,Q^2) \tag{6.28}$$

where [577,311]

$$g_1^c(x,Q^2) = \frac{\alpha_s(\mu_F^2)}{9\pi}\int_{(1+4m_c^2/Q^2)x}^{1}\frac{\mathrm{d}x'}{x'}\delta g(x',\mu_F^2)\delta C_c\left(\frac{x}{x'},Q^2\right) \tag{6.29}$$

is the charm contribution to the polarized structure function g_1 and where

$$\delta C_c(z,Q^2) = (2z-1)\ln((1+\beta)/(1-\beta)) + (3-4z)\beta \tag{6.30}$$

is the partonic matrix element due to $\gamma^*\delta g \to c\bar{c}$. Note that the renormalization scale of α_s in (6.29) has been set equal to the factorization scale μ_F appearing in δg and that one usually takes $\mu_F = 2m_c$. Furthermore, $\beta = \sqrt{1-4m_c^2/\hat{s}}$ where $\hat{s} = (p+q)^2 = Q^2(1-z)/z$ is the Mandelstam variable of the subprocess. By combining these formulae with the unpolarized cross section one can obtain the polarization asymmetry $A^c = \mathrm{d}\Delta\sigma^c/\mathrm{d}\sigma^c$. If one plugs in the drastically differing LO polarized gluon densities of [309] and the oscillating GS–C density of [294] which are for convenience compared to each other in Fig. 32, one obtains the results for $g_1^c(x,Q^2)$ and the deep-inelastic charm asymmetry $A^c = g_1^c/F_1^c$ shown in Fig. 33 at $Q^2 = 10\,\mathrm{GeV}^2$ [311,553,554]. (Note that the corresponding NLO densities are shown in Figs. 30 and 31 at $Q^2 = 4\,\mathrm{GeV}^2$.) It should further be noted that the dashed curve in Fig. 33a corresponds, at $x \approx 0.01$, to about 10% of the full g_1^p which implies that a fairly accurate high statistics experiment would be required in order

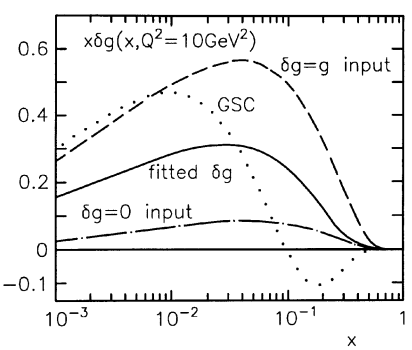

Fig. 32. Polarized gluon densities at $Q^2 = 10\,\mathrm{GeV}^2$ ($\approx 4m_c^2$) of the four LO sets used in this subsection. The dotted curves refers to set C of [294] whereas the other densities are taken from [313] as described in Section 6.1.

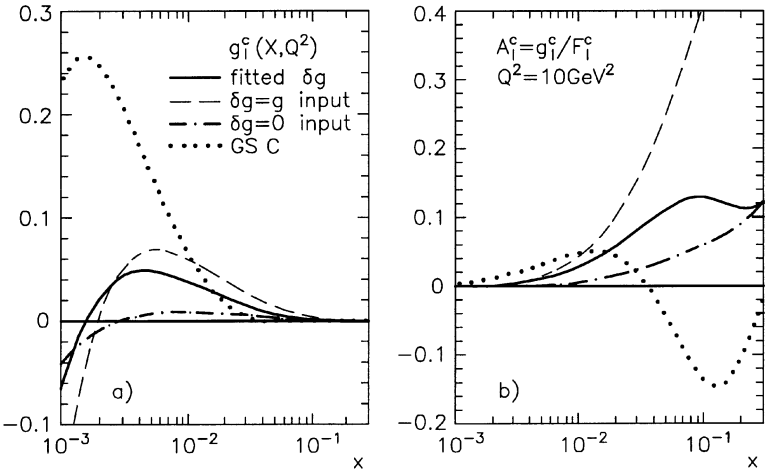

Fig. 33. Charm contribution g_1^c to g_1 at $Q^2 = 10\,\mathrm{GeV}^2$ for the four gluon distributions of Fig. 32, calculated according to Eq. (6.29) using $\mu_F = 2m_c$ with $m_c = 1.5\,\mathrm{GeV}$ [553,554].

to extract $\delta g(x,\mu_F^2)$ from g_1^c. The size of A_1^c in Fig. 33b in the large-x region, $x > 0.01$, is deceptive since here the individual g_1^c and $F_1^c = (F_2^c - F_L^c)/2x$ [308] rapidly decrease as a result of the threshold condition $\beta \geq 0$. Realistically, A_1^c is of the order of 5% at $x \simeq 0.01$ where g_1^c is also sizable as shown in Fig. 33. For $x \lesssim 0.005$, which could be reached at the HERA $\vec{e}\vec{p}$ collider, the situation is even less favorable, since $g(x,\mu_F^2)$ becomes much larger than $\delta g(x,\mu_F^2)$ as $x \to 0$ and A_1^c is correspondingly small. Furthermore, the contribution δC_c in (6.30) from the polarized subprocess $\gamma^* g \to c\bar{c}$ changes sign towards the HERA small-x region, so that A_1^c is further suppressed, cf. Fig. 33, and becomes probably unmeasurable below $x \simeq 0.005$. It should be noted that this latter oscillation of δC_c causes the strong increase of g_1^c in the region of very small x, as shown by the dotted curve in Fig. 33a, via the convolution with the peculiarly oscillating polarized gluon density GS–C of Fig. 32. The relevant asymmetry A_1^c in Fig. 33b remains negligible due to the enormously increasing unpolarized gluon density for $x \to 0$.

We now turn to the case of *photo*production of charm. It is straightforward to obtain from the above expressions (6.28)–(6.30) the inclusive open charm photoproduction cross section by taking the simultaneous limits $Q^2 \to 0$ and $z \to 0$ while keeping $Q^2/z \approx \hat{s}$ fixed:

$$\Delta\sigma_{\gamma p}^c(s_\gamma) = \frac{4\pi\alpha\alpha_s(\mu_F^2)}{9s_\gamma}\int_{4m_c^2/s_\gamma}^1 \frac{\mathrm{d}x'}{x'}\delta g(x',\mu_F^2)\left(3\beta - \ln\frac{1+\beta}{1-\beta}\right) \tag{6.31}$$

where $\beta = \sqrt{1 - 4m_c^2/\hat{s}}$ and $\hat{s} = x's_\gamma$. This integrated cross section depends only on the total proton–photon energy $s_\gamma = (P+q)^2$ which for a fixed target experiment is given by $s_\gamma = 2ME_\gamma$ where E_γ is the photon energy. By varying the photon energy it is in principle possible to explore the x-dependence of δg. Very high photon energies correspond to small values of x. However, as we shall see later, it is not trivial to obtain the first moment of δg from the cross section, Eq. (6.31). The expected polarization asymmetry is given as a function of $\sqrt{s_\gamma}$ in Fig. 34 for various possible forms

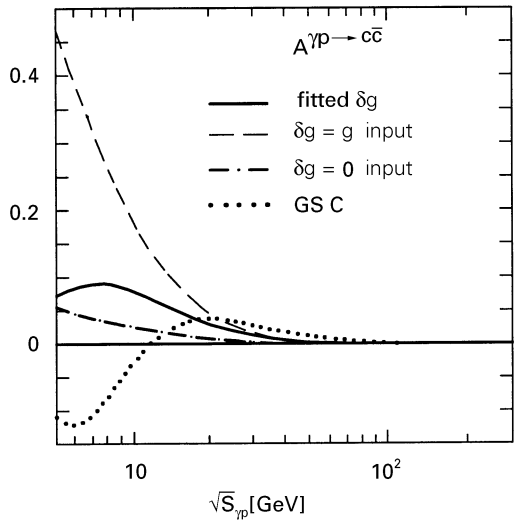

Fig. 34. Longitudinal spin asymmetry for the total charm photoproduction cross section calculated according to Eq. (6.31), using $\mu_F = 2m_c$ with $m_c = 1.5\,\text{GeV}$, for the four polarized gluon densities shown in Fig. 32 [553,554].

of $\delta g(x,\mu_F^2)$. It is clearly seen that it becomes rapidly smaller towards higher energies due to the two reasons disussed above [oscillation of the parton matrix element and singular behavior of $g(x,4m_c^2)$]. Thus the *total* charm cross section and the asymmetry become unmeasurably small at HERA energies, $\sqrt{s_\gamma} \sim 200\,\text{GeV}$, to be reached with a possible future doubly polarized $\vec{e}\vec{p}$ collider [553,554]. On the other hand, it seems more feasible that the total asymmetry in $\gamma p \to c\bar{c}$ can be measured at smaller energies, $\sqrt{s_\gamma} \lesssim 20\,\text{GeV}$, where future polarized fixed-target experiments like COMPASS [106] will be performed.

It should be noted that the choice of scale μ_F in δg in Eqs. (6.29) and (6.31) is not certain: probably $2m_c$ is a reasonable choice but it might as well be $\sqrt{s_\gamma}$ or any number in between. This uncertainty reflects our ignorance about the magnitude of the higher order correction and could be resolved if a higher order calculation of these cross sections will be performed. The same statement holds true for the argument of α_s. Therefore, in the equations presented below the scale of δg and α_s will be chosen to be more general, μ_F and μ_R, respectively. It turns out that the variation of the cross sections when one varies μ_F and μ_R is larger ($\sim 20\%$) than that of the asymmetries ($\leq 5\%$) so that one may speculate that the higher order corrections to A^c are small. However, to prove this conjecture a higher order calculation is necessary.

Eq. (6.31) was obtained after integration over the charm quark production angle $\hat{\theta}$ (in the gluon–photon cms). If one is interested in the p_T distribution or wants to introduce a p_T-cut, it is appropriate to keep the $\hat{\theta}$ dependence in the fully differential cross section [286,553,554]

$$\frac{\mathrm{d}^2\Delta\sigma^c_{\gamma p}}{\mathrm{d}x'\mathrm{d}\cos\hat{\theta}} = \frac{e_c^2\alpha_s(\mu_R^2)}{16\hat{s}}\delta g(x',\mu_F^2)\beta\left\{2\frac{\hat{t}^2+\hat{u}^2-2m_c^2\hat{s}}{\hat{t}\hat{u}} + 4m_c^2\frac{\hat{t}^3+\hat{u}^3}{\hat{t}^2\hat{u}^2}\right\} \tag{6.32}$$

where $\hat{s} = x's_\gamma$, $\hat{t} = -(\hat{s}/2)(1-\beta\cos\hat{\theta})$ and $\hat{u} = -(\hat{s}/2)(1+\beta\cos\hat{\theta})$. It is possible to make a transformation to the transverse momentum of the charmed quark by using $p_T^2 = (\hat{s}/4 - m_c^2)\sin^2\hat{\theta}$:

$$\Delta\sigma^c_{\gamma p}(p_{T\text{cut}}) = \frac{e_c^2\alpha_s(\mu_R)}{16 s_\gamma}\int_{4m_c^2/s_\gamma}^1 \frac{dx'}{x'}\delta g(x',\mu_F^2)\frac{\beta}{\hat{s}/4-m_c^2} \times \int_{p_{T\text{cut}}^2}^{\hat{s}/4-m_c^2} \frac{dp_T^2}{\sqrt{1-(p_T^2/(\hat{s}/4-m_c^2))}}\left[2m_c^2\frac{\hat{s}}{\hat{t}\hat{u}} - \frac{\hat{t}}{\hat{u}} - \frac{\hat{u}}{\hat{t}} - 2m_c^2\left(\frac{\hat{t}}{\hat{u}^2}+\frac{\hat{u}}{\hat{t}^2}\right)\right]. \tag{6.33}$$

There are several good reasons to study the p_T distribution. First of all and in general, it gives more information than the inclusive cross section. Secondly and in particular, it can be shown that the integrated photoproduction cross section, Eq. (6.31), as well as the corresponding DIS charm production cross section in (6.28) are not sensitive to the first moment of δg. The sensitivity is strongly increased, however, if a p_T-cut of the order of $p_T \geq 1\,\text{GeV}$ is introduced, see below. Last but not least, it is experimentally reasonable and often necessary to introduce a p_T-cut.

Let us dwell on the first moment discussion for a moment. It is true that the first moment is only one among an infinite set of moments and the most interesting quantity to know is the full x-dependence of $\delta g(x,Q^2)$ at a given Q^2. However, as was shown in Section 5, the first moment Δg certainly has its significance, firstly because it enters the fundamental spin sum rule (1.1) and secondly because it gives the contribution within the proton to the γ_5 anomaly, $\langle PS|\bar{q}\gamma_\mu\gamma_5 q|PS\rangle = (\Delta q - (\alpha_s/2\pi)\Delta g)S_\mu$, within the proton. In massless DIS it is straightforward to find out what the contribution of the first moment to the cross section is. One can apply the convolution theorem (4.23) to see that the contribution of Δg is given by the first moment of the parton matrix element, i.e. by the $n=1$ gluonic Wilson coefficient, cf. Eq. (4.62). If masses are involved, like m_c, the answer to this question is somewhat more subtle. Since the cross section is not any more a convolution of the standard form, (4.14), one can formally write the integrals in (6.29) and (6.31) as $\int_\xi^1 (dx'/x')\delta g(x',\mu_F^2)H(\xi/x',Q^2)$ where $\xi = (1+(4m_c^2/Q^2))x$ for DIS charm production and $\xi = 4m_c^2/S_\gamma$ for photoproduction ($Q^2=0$) of charm. Now one can apply the convolution theorem by integrating this expression over ξ and the first moment $\int_0^1 dz\, H(z,Q^2)$ gives essentially the contribution from $\Delta g(\mu_F^2)$. By integrating Eqs. (6.30) and (6.31) it turns out that both for the inclusive charm DIS and photoproduction the corresponding quantities $\int_0^1 dz\, H(z,Q^2)$ identically vanish [577,311,304,305]. This can be traced back to the small-p_T behavior of the (perturbative) partonic cross section (Wilson coefficient) for $\gamma^* g \to c\bar{c}$ which cancels the contribution of the large-p_T region in $\int_0^1 dz\, H(z,Q^2)$ [462,565,566]. It is not really a surprise in view of the structure of the anomaly in massive QCD [cf. the discussion after Eq. (5.39) and the appendix of [433]]. Since the integrals $\int_0^1 dz\, z^{n-1}H(z,Q^2)$ keep being small in a neighborhood of $n=1$ one may conclude from this that these cross sections are not suited for determining the first moment of δg. Fortunately, the situation changes if one includes a p_T-cut of greater than 1 GeV. In that case the sensitivity to $\delta g(x,\mu_F^2)$ is reestablished because the small-p_T behavior of the matrix element for $\gamma g \to c\bar{c}$ does not cancel the contribution of the large-p_T region any more [436].

The formulae presented in Eqs. (6.31)–(6.33) were obtained for strictly real photons $Q^2=0$. This is a reasonable approximation for the projected fixed target experiment (photoproduction) but may be improved, if one is interested in operating the HERA ep collider also with polarized high-energy protons. In that case the Weizsäcker–Williams approximation may be introduced [286,553,554] to account for the tail of the photon propagator. The Weizsäcker–Williams approximation is also

advantageous because tagging of the electron, needed for the extraction of the cross section at fixed photon energy would reduce the cross section too strongly. On the basis of the Weizsäcker–Williams approximation one may go on to include a possible resolved photon contribution to the cross section described by polarized photon structure functions $\delta f^{\gamma}(x,\mu_F^2)$ with $f=q,g$ [322,324,320,555]. These quantities are completely unmeasured so far and could, in the 'maximal' scenario, contribute up to 20% of the cross section [553,554]. The polarized lowest order cross section for producing a charm quark with transverse momentum p_T and cms-rapidity η then is

$$\frac{d^2\Delta\sigma_{ep}^c}{dp_T d\eta} = 2p_T \sum_{f^e,f} \int_{\rho e^{-\eta}/(1-\rho e^{\eta})}^1 dx_e x_e \delta f^e(x_e,\mu_F^2) x_p \delta f(x_p,\mu_F^2) \frac{1}{x_e-\rho e^{-\eta}} \frac{d\Delta\hat{\sigma}}{d\hat{t}}\,, \tag{6.34}$$

where $\rho \equiv m_T/\sqrt{s}$ with $m_T \equiv \sqrt{p_T^2+m_c^2}$ and $x_p \equiv x_e \rho e^{\eta}/(x_e-\rho e^{-\eta})$. The sum runs over all relevant parton species. δf^e are effective polarized parton densities in the longitudinally polarized electron defined by

$$\delta f^e(x_e,\mu_F^2) = \int_{x_e}^1 \frac{dy}{y} \Delta P_{\gamma/e}(y) \delta f^{\gamma}\left(x_{\gamma}=\frac{x_e}{y},\mu_F^2\right), \tag{6.35}$$

where $\Delta P_{\gamma/e}$ is the polarized Weizsäcker–Williams spectrum

$$\Delta P_{\gamma/e}(y) = \frac{\alpha}{2\pi}\left[\frac{1-(1-y)^2}{y}\right] \ln\frac{Q_{max}^2(1-y)}{m_e^2 y^2}\,, \tag{6.36}$$

and the same cuts as in the unpolarized case should be used, $Q_{max}^2 = 4\,\mathrm{GeV}^2$ and the y-cuts $0.2 \le y \le 0.85$ [221]. The cross section, Eq. (6.34), can be transformed to the more relevant HERA laboratory frame by a simple boost which implies $\eta \equiv \eta_{cms} = \eta_{LAB} - \frac{1}{2}\ln(E_p/E_e)$, where we have counted positive rapidity in the proton forward direction. The spin-dependent differential LO subprocess cross sections $d\Delta\hat{\sigma}/d\hat{t}$ for the resolved processes $gg \to c\bar{c}$ and $q\bar{q} \to c\bar{c}$ with $m_c \neq 0$ can be found in [198,409]. The dominant direct ('unresolved') contribution derives from $\delta f^{\gamma}(x_{\gamma},\mu_F^2) \equiv \delta(1-x_{\gamma})$ in (6.35) with the corresponding polarized cross sections for the direct subprocess $\gamma g \to c\bar{c}$ being readily obtained from that for $gg \to c\bar{c}$ by dropping the nonabelian (s-channel) part and multiplying by $2N_c e_c^2 \alpha/\alpha_s(\mu_F^2)$ where $e_c = 2/3$. Note that the resolved photon contributions are relevant mainly for (real) photoproduction and that they are appreciable only at very high energies $\sqrt{s_{\gamma}} \ge 100\,\mathrm{GeV}$. Furthermore, there are experimental techniques to separate the resolved part from the direct photon contribution, see e.g. [273]. Fig. 35 shows results for the p_T and η_{LAB} distributions obtained for the four different polarized gluon densities in Fig. 32 for $E_p = 820\,\mathrm{GeV}$ and $E_e = 27\,\mathrm{GeV}$ [553,554]. The curve denoted by 'resolved' is an estimated upper limit for the resolved photon contribution. It is negligibly small unless p_T becomes very small. Also shown are the corresponding asymmetries A^c which are much larger than for the total cross section if one goes to p_T of about 10–20 GeV. Furthermore, the asymmetries are sensitive to the size and shape of the polarized gluon distribution used. Included in the asymmetry plots are the expected statistical errors δA^c at HERA which can be estimated from

$$\delta A = 1/P_e P_p \sqrt{\mathscr{L}\sigma\varepsilon}\,, \tag{6.37}$$

where P_e, P_p are the beam polarizations, $\mathscr{L}$ is the integrated luminosity and ε the charm detection efficiency, estimated to be $P_e * P_p = 0.5$, $\mathscr{L} = 100\,\mathrm{pb}^{-1}$ and $\varepsilon = 0.15$.

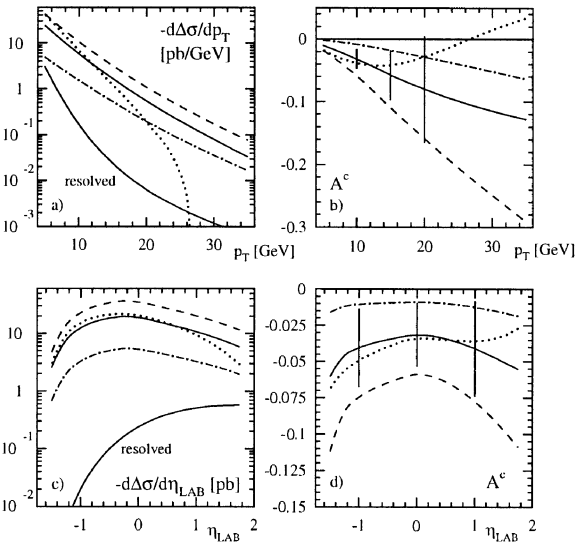

Fig. 35. p_T- and η_{LAB}-dependence of the (negative) polarized charm-photoproduction cross section and asymmetry in ep-collisions at HERA [553,554]. The considered kinematic regions are $-1 \le \eta_{LAB} \le 2$ for the p_T-distribution and $p_T > 8\,\text{GeV}$ for the η_{LAB}-distribution. The various curves correspond to the various polarized gluon densities in Fig. 32. For comparison, the 'resolved' contribution to the cross section, calculated with the 'fitted' δg in Fig. 32 and the 'maximally' saturated set of polarized photonic parton densities, is shown by the lower solid curves.

6.3. Heavy quark production in hadronic collisions

Hadronic heavy quark production proceeds via the (so far available) LO subprocesses

$$\delta g \delta g \to h\bar{h}, \quad \delta q \delta \bar{q} \to h\bar{h}\,, \tag{6.38}$$

and appears to be a very sensitive and presumably the most realistic test of $\delta g(x,\mu_F^2)$, since δg enters 'quadratically' and the $\delta q \delta \bar{q}$ contribution is small [205,229,198,409]. Here the polarized $\vec{p}\vec{p}$ RHIC collider ($\sqrt{s} = 50$–$500\,\text{GeV}$) with high luminosity ($\mathscr{L} \gtrsim 10^{32}\,\text{cm}^{-2}\,\text{s}^{-1}$) will play a decisive role [148,585]. The differential cross sections for the subprocesses in Eq. (6.38) are given by [198]

$$\frac{\mathrm{d}}{\mathrm{d}\hat{t}}\Delta\hat{\sigma}^{gg\to h\bar{h}} \equiv \frac{\mathrm{d}}{\mathrm{d}\hat{t}}\frac{1}{2}(\hat{\sigma}_{++}^{gg\to h\bar{h}} - \hat{\sigma}_{+-}^{gg\to h\bar{h}}) = \frac{\pi\alpha_s^2}{8\hat{s}^2}\left(\frac{3}{\hat{s}^2} - \frac{4}{3\tilde{t}\tilde{u}}\right)\left[\tilde{t}^{\,2} + \tilde{u}^2 - \frac{2m_h^2\hat{s}}{\tilde{t}\tilde{u}}(\tilde{t}^2 + \tilde{u}^2)\right], \tag{6.39}$$

$$\frac{\mathrm{d}}{\mathrm{d}\hat{t}}\Delta\hat{\sigma}^{q\bar{q}\to h\bar{h}} = -\frac{\mathrm{d}}{\mathrm{d}\hat{t}}\hat{\sigma}^{q\bar{q}\to h\bar{h}} = -\frac{\pi\alpha_s^2}{3\hat{s}^2}\frac{4}{3}\frac{\tilde{t}^2 + \tilde{u}^2 + 2m_h^2\hat{s}}{\hat{s}^2}\,, \tag{6.40}$$

where $\pm$ refers to the helicity of the incoming partons, $\alpha_s = \alpha_s(\mu_F^2)$ and $\tilde{t} \equiv \hat{t} - m_h^2$, $\tilde{u} \equiv \hat{u} - m_h^2$, i.e. $\hat{s} + \tilde{t} + \tilde{u} = 0$. By integrating with respect to $\tilde{t}$ the total cross sections are then easily obtained:

$$\Delta\hat{\sigma}^{gg\to h\bar{h}}(\hat{s},\mu_F^2) = \frac{\pi\alpha_s^2}{16\hat{s}}\left[2\left(3\beta^2 - \frac{17}{3}\right)\ln\frac{1+\beta}{1-\beta} + 5\beta(5-\beta^2)\right], \tag{6.41}$$

$$\Delta\hat{\sigma}^{q\bar{q}\to h\bar{h}}(\hat{s},\mu_F^2) = -\hat{\sigma}^{q\bar{q}\to h\bar{h}}(\hat{s},\mu_F^2) = -\frac{\pi\alpha_s^2}{9\hat{s}}\frac{4}{3}\beta(3-\beta^2) \tag{6.42}$$

with $\beta^2 = 1 - 4m_h^2/\hat{s}$. The unpolarized differential and total cross sections for $gg \to h\bar{h}$ are well known [298], with the latter being given by

$$\hat{\sigma}^{gg\to h\bar{h}}(\hat{s},\mu_F^2) \equiv \frac{1}{2}(\hat{\sigma}_{++}^{gg\to h\bar{h}} + \hat{\sigma}_{+-}^{gg\to h\bar{h}})$$

$$= \frac{\pi\alpha_s^2}{16\hat{s}}\left[\left(11 - 6\beta^2 + \frac{1}{3}\beta^4\right)\ln\frac{1+\beta}{1-\beta} + \frac{1}{3}\beta(31\beta^2 - 59)\right]. \tag{6.43}$$

A NLO analysis of the polarized cross section $\Delta\hat{\sigma}^{ij}$ for heavy quark production is unfortunately still missing.

For not too small polarized gluon densities, the total polarized cross section for heavy quark production ($4m_h^2 \le \hat{s} \le s$) is dominated by the gg-initiated subprocess, because the contribution from the subprocess $q\bar{q} \to h\bar{h}$ is marginal for large energies ($\sqrt{s} \gtrsim 50\,\mathrm{GeV}$). Although the latter can be easily implemented [198], we give here for simplicity only the result for the former cross section:

$$\Delta\sigma_{pp}^h(s) = \int_{4m_h^2}^s \mathrm{d}\hat{s}\int \mathrm{d}x_1\,\mathrm{d}x_2\;\delta g(x_1,\mu_F^2)\delta g(x_2,\mu_F^2)\Delta\hat{\sigma}^{gg\to h\bar{h}}(\hat{s},\mu_F^2)\delta(\hat{s} - x_1x_2s)$$

$$= \int_{4m_h^2/s}^1 \mathrm{d}x_1 \int_{4m_h^2/sx_1}^1 \mathrm{d}x_2\;\delta g(x_1,\mu_F^2)\delta g(x_2,\mu_F^2)\Delta\hat{\sigma}^{gg\to h\bar{h}}(x_1x_2s,\mu_F^2)$$

$$= \int_{4m_h^2/s}^1 \frac{\mathrm{d}\tau}{\tau}\Delta\hat{\sigma}^{gg\to h\bar{h}}(\tau s,\mu_F^2)\Phi_{gg}(\tau,\mu_F^2)\,, \tag{6.44}$$

where the polarized gluon luminosity (flux) is given by

$$\Phi_{gg}(\tau,\mu_F^2) = \tau\int_\tau^1 \frac{\mathrm{d}x_1}{x_1}\delta g(x_1,\mu_F^2)\delta g\left(\frac{\tau}{x_1},\mu_F^2\right). \tag{6.45}$$

The relevant spin–spin asymmetry is defined by

$$A_{pp}^h(s) = \Delta\sigma_{pp}^h(s)/\sigma_{pp}^h(s)\,, \tag{6.46}$$

where the unpolarized cross section is analogous to the polarized cross section, Eq. (6.44), with $g(x,\mu_F^2)$ appearing instead of $\delta g(x,\mu_F^2)$ and the unpolarized partonic cross section (6.43) has to be used instead of $\Delta\hat{\sigma}$. The typical scale to be used in (6.44) is again $\mu_F \approx 2m_h$. For the production of heavy quarkonia (J/ψ, Υ, etc.) one proceeds in the same way except that in Eq. (6.44) the region of integration has to be taken as $4m_c^2 \le \hat{s} \le 4m_D^2$ or $4m_b^2 \le \hat{s} \le 4m_B^2$, instead of $4m_h^2 \le \hat{s} \le s$. However, one faces here the additional bound-state model dependence as discussed in the previous section [205,229]. The expected asymmetries (6.46) for total charm and bottom production at typical RHIC energies are shown in Fig. 36 for the various possible forms of $\delta g(x,\mu_F^2)$ shown in Fig. 32. Although the asymmetries are very sensitive to the polarized gluon density $\delta g(x,4m_h^2)$, they become relatively small at top RHIC energies, with A_{pp}^b being almost an order of magnitude larger than A_{pp}^c. It seems that realistic measurements of δg will be possible preferably at medium RHIC

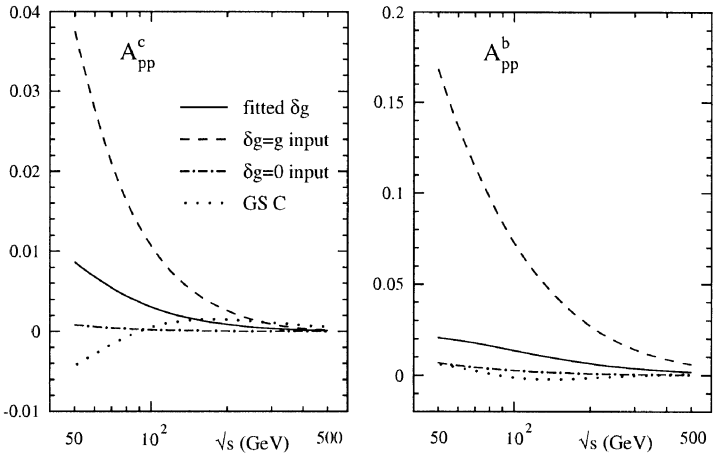

Fig. 36. Asymmetries for the total charm and bottom hadroproduction, according to Eq. (6.46), at RHIC energies using $m_c = 1.5\,\text{GeV}$ and $m_b = 4.5\,\text{GeV}$, for the four polarized gluon densities shown in Fig. 32.

energies, $\sqrt{s} \lesssim 100\,\text{GeV}$, or at future HERA-$\vec{N}$ energies, $\sqrt{s} \approx 40\,\text{GeV}$ (for a recent review see [423], and references therein). It should be noted, however, that the introduction of a p_T-cut, as discussed in the previous section for charm photoproduction [553,554,436], could result in sizeably larger asymmetries at high energies.

6.4. High p_T jets in high energy lepton–nucleon collisions

A possible way to distinguish the spin-dependent parton distributions is to study jet production at HERA operated in the polarized mode [158,56,311]. The idea is based on the fact that the parton subprocesses $\gamma^* q \to gq$ and $\gamma^* g \to q\bar{q}$ lead to a different large-p_T behavior so that the contributions from $\delta q(x, \mu_F^2)$ and from $\delta g(x, \mu_F^2)$ might be distinguished. The undetermined QCD renormalization/factorization scale μ_F is taken to be $\mu_F^2 = Q^2$, although a choice like $\mu_F = p_T$ is equally feasible. Unfortunately, at CERN (SMC), SLAC and DESY (Hermes) jet cross sections are difficult to measure because the signatures are minute at small $\sqrt{s}$. Furthermore, it turns out that the polarization asymmetries for jet production even at HERA ($\sqrt{s} \approx 300\,\text{GeV}$) are not too large, and in view of the statistical error obtained for luminosities $\mathscr{L} \sim 100\,\text{pb}^{-1}$, cf. Eq. (6.37) with $\varepsilon \sim 1$, one should not be too optimistic that $\delta g(x, \mu_F^2)$ can be determined from such measurements. This situation will obviously improve for integrated luminosities $\mathscr{L} \sim 500\,\text{pb}^{-1}$ as may be optimistically expected at a future fully polarized HERA $\vec{e}\vec{p}$ collider [219,224,124]. An overview of the physics issues will be given in the following.

The result for $\langle g_1^p \rangle$ when written differentially in $\lambda = 4p_T^2/Q^2$ is

$$\frac{\mathrm{d}}{\mathrm{d}\lambda}\int_0^1 \mathrm{d}x\, g_1^p(x, Q^2, \lambda) = \frac{\alpha_s(\mu_R^2)}{4\pi}\sum_q e_q^2[C_F M_q(\lambda)(\Delta q + \Delta\bar{q})(\mu_F^2) + T_R M_g(\lambda)\Delta g(\mu_F^2)] \tag{6.47}$$

with $C_F = 4/3$ and $T_R = 1/2$, and where the functions $M_q(\lambda)$ and $M_g(\lambda)$ are given by

$$M_q(\lambda) = \frac{\frac{11}{8}\lambda + \frac{13}{4} + \frac{2}{\lambda}}{(1+\lambda)^{3/2}} \ln \frac{\sqrt{1+\lambda}+1}{\sqrt{1+\lambda}-1} - \frac{12+11\lambda}{4\lambda(1+\lambda)}, \tag{6.48}$$

$$M_g(\lambda) = \frac{\lambda - 2}{2(1+\lambda)^2} - \frac{\lambda(4+\lambda)}{4(1+\lambda)^{5/2}} \ln \frac{\sqrt{1+\lambda}+1}{\sqrt{1+\lambda}-1}. \tag{6.49}$$

As usual, one takes $\mu_R^2 = \mu_F^2 = Q^2$. The important point to observe is [56] that $M_g(\lambda)$ gives a negative contribution which, for a large positive $\Delta g \sim 3$ would be the dominant contribution in Eq. (6.47). However, this derivation is strongly idealized, because the negative M_g gets a large contribution from the small-x region where measurements become difficult due to the large unpolarized cross section. Imposing a cut $x \geq x_0$ on the x-integration [311], typically $x_0 = Q^2/2ME_l$ with $x_0 \leq x \leq (1+\lambda)^{-1}$, the negative signal from M_g is drastically reduced so that it is doubtful that this effect can be used to determine Δg.

Instead of using a cut one can directly verify this finding by a study of the distribution $\mathrm{d}g_1^p(x, Q^2, \lambda)/\mathrm{d}\lambda$ as a function of x and λ [311]. The result is shown in Fig. 37. It can be seen that only for $x \leq 0.001$ a clear negative signal in the perturbatively safe region $p_T \gtrsim 4\,\mathrm{GeV}$ develops. This feature has nothing to do with the particular $\delta g(x, Q^2)$ and $\delta q(x, Q^2)$ chosen for this plot, but is a consequence of the structure of the perturbative parton matrix element.

So far in this subsection we have discussed the determination of the first moment Δg. Now we turn to the directly measurable x-dependent densities like $\delta g(x, \mu_F^2)$. In general, the cross section for polarized deep inelastic electron proton scattering with several partons in the final state

$$e_{\Rightarrow}^-(l) + p_{\Rightarrow}(P) \to e^-(l') + \text{remnant}(p_r) + \text{parton } 1(p_1) + \cdots + \text{parton } n(p_n) \tag{6.50}$$

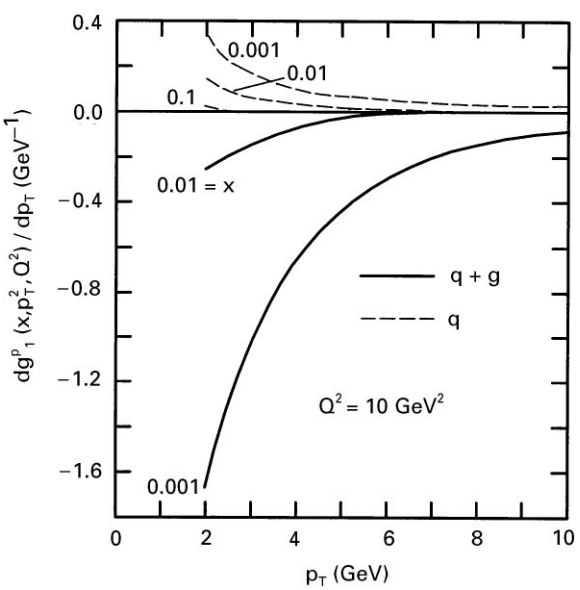

Fig. 37. p_T depencence of $g_1^p(x, p_T^2, Q^2)$ for various values of x at $Q^2 = 10\,\mathrm{GeV}^2$ [311].

is generically given by

$$\mathrm{d}\Delta\sigma^{\mathrm{had}}_{n\text{-jet}} = \sum_f \int \mathrm{d}x_f\, \delta f(x_f,\mu_F^2)\, \mathrm{d}\Delta\hat{\sigma}^f(p = x_f P, \alpha_s(\mu_R^2), \mu_R^2, \mu_F^2)\,, \tag{6.51}$$

where the sum runs over incident partons $f = q, \bar{q}, g$ which carry a fraction x_f of the proton momentum. $\Delta\hat{\sigma}^f$ denotes the partonic cross section from which collinear initial state singularities are factorized out (in a next-to-leading order calculation) and included in the scale-dependent parton densities δf. A natural scale for multi-jet production in DIS may be $\mu_R^2 = \mu_F^2 = 1/4\ (\sum_j p_{\mathrm{T}}^B(j))^2$, with the average $p_{\mathrm{T}}^B(j)$ being defined in the Breit frame by $2E_j^2(1-\cos\theta_{jP})$, where the subscripts j and P denote the jet and proton. Results about this cross section including HO effects can be found in [479,265]. If the jets are defined in a modified JADE scheme, the theoretical uncertainties of the two-jet cross section can be very large due to higher order effects. These uncertainties are smaller for the cone algorithm, which is defined in the laboratory frame. In this algorithm the distance $\Delta R = \sqrt{(\Delta\eta)^2 + (\Delta\phi)^2}$ between two partons decides whether they should be recombined to a single jet. Here the variables are the pseudo-rapidity η and the azimuthal angle ϕ. Partons with $\Delta R < 1$ are recombined. Furthermore, a cut on the jet transverse momenta of $p_{\mathrm{T}}(j) > 5\,\mathrm{GeV}$ in the lab frame and in the Breit frame was imposed. Using the polarized parton densities (set A) of [293] it was found [265] that the LO polarized dijet cross section $\Delta\sigma$(2-jet) is $-45\,\mathrm{pb}$ at HERA energies ($\sqrt{s} \approx 300\,\mathrm{GeV}$). This negative result for the polarized dijet cross section is entirely due to the boson–gluon fusion process, which is negative for $x \lesssim 0.025$ and its contribution to the total polarized dijet cross section is $-53\,\mathrm{pb}$. The contribution from the quark initiated subprocess is positive over the whole kinematical range and contributes with 8 pb to the resulting dijet cross section. With these numbers one obtains a rather small average asymmetry of ≈ -0.015. To obtain these numbers, polarizations of 70% for both the electron and the proton beams have been assumed. Note, however, that the shape of the polarized gluon density is hardly (or even not at all) constrained by currently available DIS data, in particular for small x. Alternative parametrizations of the polarized gluon distributions in the small-x region, which are still consistent with all present data [293,309], can lead to asymmetries which are a factor two larger. Although the dijet events are in principle sensitive to this lower x range, the resulting numbers for the asymmetries are in general small because of the dominance of the unpolarized gluon density in the small-x region.

Reducing the proton beam energy to 410 GeV, instead of the nominal 820 GeV, does not improve the signal, although the mean value of y is higher. The asymmetry signal increases only for a few points around $x > 0.1$, since a lower incident energy probes slightly higher values of x [479,265].

One may also have a look at large-p_{T} jet photoproduction [553,554]. In that case the generic cross section formula for the production of a single jet with transverse momentum p_{T} and rapidity η is similar to that in (6.34), the sum now running over all properly symmetrized $2 \to 2$ subprocesses for the direct ($\gamma b \to cd$) and resolved ($ab \to cd$) cases. The corresponding differential helicity-dependent LO subprocess cross sections can be found in [80] for the case that only light flavors are involved. One may neglect the charm content of the nucleon and consider charm only contributing as a final state via $\gamma g \to c\bar{c}$ (for the direct part) and $gg \to c\bar{c}$, $q\bar{q} \to c\bar{c}$ (for the resolved part).

Just as for the case of heavy quark photoproduction it turns out that the resolved photon contributions are at most subdominant (in the 'maximal' scenario studied by [553,554]), if not negligible. As these authors have found, the 'direct' cross sections are fairly large over the whole rapidity range, and also as a funtion of p_T, and sensitive to the shape and size of $\delta g(x, p_T^2)$ with, unfortunately, not too sizeable asymmetries as compared to the statistical errors for $\mathscr{L} = 100\,\mathrm{pb}^{-1}$. A measurement of δg thus appears to be possible under the imposed conditions only if luminosities exceeding $100\,\mathrm{pb}^{-1}$ can be reached.

6.5. Semi-inclusive polarization asymmetries

A straightforward idea to study polarized DIS in more detail is to analyze semi-inclusive cross sections. Heavy quark production as discussed in Sections 6.2 and 6.3 is an example for this. Another possibility is to tag for light quark hadrons, like the pions, kaons or protons, in order to obtain information on the spin flavor content of the nucleon, i.e. consider the process

$$\vec{e} + \vec{p} \to e' + H + X \ . \tag{6.52}$$

The charged hadrons H most suited for this analysis are mainly $\pi^{\pm}$ and $K^{\pm}$ but also p and $\bar{p}$ may be interesting [27,30,13]. Recently, π^0 production has been used as well for extracting $\delta s(x, Q^2)$ [79]. In particular, one can compare cross sections of hadrons with positive and negative electric charge to obtain additional information. In the unpolarized case and within the framework of the LO-QCD quark parton model the cross section is given by

$$\frac{1}{\sigma}\frac{\mathrm{d}\sigma^{\pm}}{\mathrm{d}z} = \frac{\sum_{q,H} e_q^2 q(x, Q^2) D_q^H(z, Q^2)}{\sum_q e_q^2 q(x, Q^2)} \ , \tag{6.53}$$

where σ is the inclusive cross section and one is considering the production of hadrons $H^{\pm}$. The fragmentation function $D_q^H(z, Q^2)$ represents the probability that a struck quark with flavor q fragments into a hadron H carrying fractional momentum z of the parent (= struck) quark q (see, for example, [45,509]). In NLO the cross section in (6.53) does not factorize in x and z anymore, but instead one has more complicated double convolution integrals over parton densities, fragmentation functions and Wilson coefficients [49,288].

In the polarized case one may define asymmetries $A_1^{\pm}$, similar to the inclusive asymmetry, Eq. (2.10), namely

$$A_1^{\pm} = (\sigma_{1/2}^{\pm} - \sigma_{3/2}^{\pm})/(\sigma_{1/2}^{\pm} + \sigma_{3/2}^{\pm}) \ . \tag{6.54}$$

In analogy to (6.53) these semi-inclusive asymmetries in LO-QCD are given by

$$A_1^{\pm}(x, z, Q^2) = \frac{\sum_{q,H} e_q^2 \delta q(x, Q^2) D_q^H(z, Q^2)}{\sum_{q,H} e_q^2 q(x, Q^2) D_q^H(z, Q^2)} \ . \tag{6.55}$$

This result holds under the (to some extent questionable) assumption that the fragmentation functions do not depend on the quark helicity [278,190]. The idea then is to take the $q(x, Q^2)$ and the $D_q^H(z, Q^2)$ from other (unpolarized) experimental data and use the measurement of $A_1^{\pm}$ to

determine the $\delta q(x,Q^2)$. By using different targets (proton, deuteron and ^{3}He) one measures different linear combinations of the $\delta q(x,Q^2)$ according to Eq. (6.55). For example, the deuteron cross section is considered the sum of the proton and neutron cross section, corrected by the D-state factor $1-\frac{3}{2}w_D$, as will be discussed in Section 6.10. Because of isospin symmetry the asymmetries for proton and neutron are related by exchange of up and down quarks and antiquarks. To increase the statistics, the LO relation (6.55) is sometimes integrated over the measured z-domain [27], i.e. $D_q^H(Q^2)=\int_{0.2}^1 \mathrm{d}z\, D_q^H(z,Q^2)$ is used in (6.55) instead of $D_q^H(z,Q^2)$.

One may take higher order QCD corrections to Eq. (6.55) into account. The NLO corrections to the denominator of the asymmetry are well known [49,288], and the NLO corrections to the numerator have been calculated too [177,269]. In the $\overline{\mathrm{MS}}$ scheme, where the anomalous gluon contribution is hidden in the definition of the singlet quarks $\Delta\Sigma$, the NLO corrections turn out to be much smaller than the present experimental accuracy. Furthermore, present measurements [27] do not involve the small-x region $x\lesssim 0.005$.

If one considers the production of the 6 charged hadrons $\pi^\pm$, $K^\pm$, p and $\bar{p}$ from 3 quarks and 3 antiquarks, there are in principle 36 independent fragmentation functions. Among these the fragmentation functions of strange quarks into pions can be neglected. The fragmentation functions of nonstrange quarks into pions can be obtained, for example, from EMC measurements [70] by using charge conjugation and isospin symmetry. The number of independent fragmentation functions can be further reduced by assumptions like $D_d^{(K^-=\bar{u}s)}=D_{\bar{d}}^{(K^-=\bar{u}s)}$ and $D_s^{(K^-=\bar{u}s)}=D_d^{(\pi^-=\bar{u}d)}$ for unfavored and favored fragmentations, respectively, so that finally the number of independent quark fragmentation functions is 6. In addition, there are the three gluon fragmentation functions $D_g^H(z,Q^2)$ which in LO enter only via the evolution equations, whereas in NLO they enter the cross sections and asymmetries (6.55) directly.

The quark fragmentation functions together with the unpolarized parton densities and a measurement of the spin asymmetries of proton and deuteron and/or ^{3}He serve as input to determine all the valence and sea quark densities $\delta q_v(x,Q^2)=\delta q(x,Q^2)-\delta\bar{q}(x,Q^2)$ and $\delta q_{\mathrm{sea}}(x,Q^2)=2\delta\bar{q}(x,Q^2)$ $(q=u,d,s)$. If one measures the spin asymmetries in certain x-bins, there is for each x-bin a system of linear equations for the six unknown spin distributions. The weight of the strange quark distributions in these equations is marginal, so that they cannot be determined. Recently, however, asymmetries for $\pi^0=\frac{1}{2}(\pi^+ + \pi^-)$ production off a ^{3}He target have been measured [79] which allow the extraction of $\delta s/s$ according to a suggestion of [278]. Although the statistics is still inferior, there is an indication that $\delta s(x,Q^2)$ turns negative for $x\lesssim 0.1$ and vanishes at larger values of x as theoretically anticipated. The statistical errors of present polarized experiments are so large that the power of the method can be increased by the additional assumption $\delta\bar{u}(x,Q^2)=\delta\bar{d}(x,Q^2)\equiv\delta\bar{q}(x,Q^2)$. Finally, one is left with 3 unknown functions $\delta u_v(x,Q^2), \delta d_v(x,Q^2)$ and $\delta\bar{q}(x,Q^2)$. These have been determined in a recent analysis by the SMC collaboration [27] for 12 x-bins between 0.005 and 0.48 and assuming Q^2-independence of the asymmetries. Their results show that at the present stage this method is not really accurate enough for a quantitative analysis. Typical errors are about 50% or larger. However, in future this method will be certainly very fruitful to discriminate between the polarized up and down and sea quark contribution. A check on the consistency of the procedure is possible by using the relation

$$g_1^p(x,Q^2)-g_1^n(x,Q^2)=\tfrac{1}{6}[\delta u_v(x,Q^2)-\delta d_v(x,Q^2)]+\mathrm{O}(\delta\bar{u}-\delta\bar{d})+(\mathrm{HO}-\mathrm{QCD})\,. \tag{6.56}$$

The l.h.s. of this equation is obtained from inclusive data while the r.h.s. can be obtained from the semi-inclusive asymmetries. In addition, the assumptions $\delta\bar{u}(x,Q^2) = \delta\bar{d}(x,Q^2)$ and the smallness of the HO corrections can be checked.

An alternative procedure, in case of pions, has been suggested by [278]. These authors consider the asymmetry

$$A_{\text{mixed}} = \frac{(\sigma^+_{1/2} - \sigma^-_{1/2}) - (\sigma^+_{3/2} - \sigma^-_{3/2})}{(\sigma^+_{1/2} - \sigma^-_{1/2}) + (\sigma^+_{3/2} - \sigma^-_{3/2})} , \tag{6.57}$$

where 'mixed' refers to the combination $\pi^+ - \pi^-$ of $\pi^\pm$ production, for example, and which has a simple expression in terms of up- and down-quark densities,

$$A_{\text{mixed}} = \frac{4\delta u_v - \eta\delta d_v}{4u_v - \eta d_v} . \tag{6.58}$$

For the combination $\pi^+ - \pi^-$ the fragmentation functions cancel and thus $\eta = 1$. If, however, the hadrons are not identified, as in the SMC experiment [27], the factor η has to be evaluated by averaging the relevant fragmentation functions and is found to be about 0.5 for $z > 0.2$. This method, however, is not as simple as it looks, because the spectrometer acceptance is different for positive and negative hadrons and the ratio of these acceptances does not cancel in the asymmetries, Eq. (6.57). Still one can measure this ratio and correct for the acceptance difference. Finally, the quark distributions δu_v and δd_v obtained this way should be in agreement with the distributions obtained from $A_1^\pm$.

There is the possibility to obtain information on δs by looking at processes with fast kaons ($K^- = \bar{u}s$) in the final state [190]. These have a high probability to contain the initial struck quark, i.e. a fast kaon can be a signal for a s or $\bar{u}$ quark struck by the photon. Observation of the corresponding polarization asymmetry $A_{1,\text{fast}}^{K^-}$ is a signature of the existence of a polarized s resp. $\bar{u}$ sea. However, there are strong systematic uncertainties in such an experiment because some contribution will arise from $s\bar{s}$ pairs created in the photon–gluon fusion process.

Polarization asymmetries for semi-inclusive pion production have been measured from doubly longitudinally polarized (anti)proton–proton collisions at the Fermilab SPF [14] resulting in $A_{LL}^{\pi^\circ} \approx 0$ for $1 \lesssim p_T^{\pi^\circ} \lesssim 4\,\text{GeV}$ at $E^p_{\text{beam}} = 200\,\text{GeV}$, i.e. $\sqrt{s} = 20\,\text{GeV}$. It should be pointed out that this result does not necessarily imply a vanishing [14,500,501] gluon polarization Δg, but is equally consistent with a large $\Delta g \approx 3$–6 [572]. A clean distinction between a large and a small Δg scenario could be achieved, if it were possible to perform such a semi-inclusive experiment at, say, $\sqrt{s} \approx 100\,\text{GeV}$ with $p_T^{\pi^\circ} \gtrsim 5\,\text{GeV}$ [572].

6.6. Information from elastic neutrino–proton scattering

(Quasi)-elastic neutrino–proton scattering ($\nu p \to \nu p$) is mediated by the exchange of the Z boson. Since the parity violating Z-quark coupling involves $\gamma_\mu\gamma_5$, the *unpolarized* cross section will depend on the proton matrix element of the axial vector current. As will be shown below this offers in particular the possibility to measure a combination of the strange quark matrix $\langle p|\bar{s}\gamma_\mu\gamma_5 s|p\rangle$ and the anomalous gluon component. Theoretical aspects of this process have been reviewed in [407] and more recently in [42]. A very readable experimental paper on the subject is [39]. New neutrino

experiments like CHORUS, NOMAD, ICARUS, MINOS, COSMOS, etc., [481] aimed to search for neutrino oscillations are taking data or are under preparation and could also be used to get information on the NC neutrino (and antineutrino) elastic scattering on protons.

The one-nucleon matrix element of the hadronic neutral current has the form

$$\langle p'|J_\mu^Z|p\rangle = \bar{u}(p')\left[\gamma_\mu F_V^Z(Q^2) + \frac{\mathrm{i}}{2M}\sigma_{\mu\nu}q^\nu F_M^Z(Q^2) + \gamma_\mu\gamma_5 G_A^Z(Q^2)\right]u(p)\ . \tag{6.59}$$

As will be explained now, F_V^Z, F_M^Z and G_A^Z can be written as linear combinations of normalized matrix elements ('form factors') of the following $U_3 \times U_3$ quark currents:

$$V_\mu^a = \bar{q}\gamma_\mu T^a q, \quad V_\mu^0 = \tfrac{1}{3}\bar{q}\gamma_\mu q\ , \tag{6.60}$$

$$A_\mu^a = \bar{q}\gamma_\mu\gamma_5 T^a q, \quad A_\mu^0 = \tfrac{1}{3}\bar{q}\gamma_\mu\gamma_5 q\ . \tag{6.61}$$

Heavy quark contributions (c, b, t) to polarized structure functions turn out to be notoriously small [407,311], even if they are calculated on the basis of massless RG equations [407]. The normalized form factors are defined according to

$$\langle N(p')|V_\mu^{0,8}|N(p)\rangle = \bar{u}(p')\left[F_1^{0,8}(Q^2)\gamma_\mu + F_2^{0,8}(Q^2)\frac{\mathrm{i}\sigma_{\mu\nu}q^\nu}{2M}\right]u(p)\ , \tag{6.62}$$

$$\langle N(p')|V_\mu^{3}|N(p)\rangle = \bar{u}(p')\left[F_1^{3}(Q^2)\gamma_\mu + F_2^{3}(Q^2)\frac{\mathrm{i}\sigma_{\mu\nu}q^\nu}{2M}\right]\tau_3 u(p)\ , \tag{6.63}$$

$$\langle N(p')|A_\mu^{0,8}|N(p)\rangle = G_1^{0,8}(Q^2)\bar{u}(p')\gamma_\mu\gamma_5 u(p)\ , \tag{6.64}$$

$$\langle N(p')|V_\mu^{3}|N(p)\rangle = G_1^{3}(Q^2)\bar{u}(p')\gamma_\mu\gamma_5\tau_3 u(p)\ . \tag{6.65}$$

The four vector form factors $F_{1,2}^{3,8}$ can be measured in electromagnetic scattering. At $Q^2 = 0$ they are given in terms of the anomalous magnetic moments κ_N of the nucleons by

$$F_1^3(0) = \tfrac{1}{2}, \quad F_2^3(0) = \tfrac{1}{2}(\kappa_p - \kappa_n)\ , \tag{6.66}$$

$$F_1^8(0) = \tfrac{1}{2}\sqrt{3}, \quad F_2^8(0) = \tfrac{1}{2}\sqrt{3}(\kappa_p + \kappa_n)\ . \tag{6.67}$$

The $Q^2 \to 0$ limit of F_1^0 is the baryon number,

$$F_1^0(0) = 1\ . \tag{6.68}$$

The nonsinglet axial vector form factors $G_1^{3,8}$ at zero momentum transfer are related to the constants F and D introduced in hyperon semileptonic decays, cf. Eqs. (5.10) and (5.11),

$$G_1^3(0) = \frac{1}{2}(F + D) = \frac{1}{2}\frac{g_\mathrm{A}}{g_\mathrm{V}}, \quad G_1^8(0) = \frac{1}{\sqrt{12}}(3F - D)\ . \tag{6.69}$$

One is left with two singlet form factors undetermined at $Q^2 \to 0, F_2^0(0)$ and $G_1^0(0)$. $F_2^0(0)$ is the 'anomalous baryon number magnetic moment'. $G_1^0(0)$ is the singlet axial current form factor

relevant to spin physics. Both F_2^0 and G_1^0 can be measured in elastic neutral current scattering. In the naive parton model $G_1^0(0)$ can be expressed by the singlet polarized quark density $\Delta\Sigma$ introduced in Section 5. As discussed in detail in Section 5, higher order QCD corrections may introduce, within certain schemes, an anomalous gluon contribution.

Since the hadronic neutral current is a linear combination of the $U_3 \times U_3$ currents V_μ^a and A_μ^a,

$$J_\mu^Z = \sum_{a=0,3,8} (v_a V_\mu^a + a_a A_\mu^a) \,, \tag{6.70}$$

its matrix element Eq. (6.59) and thus the form factors F_V^Z, F_M^Z and G_A^Z appearing on the r.h.s. of Eq. (6.59) can be given as linear combinations of the normalized form factors $F_{1,2}^{0,3,8}$ and $G_1^{0,3,8}$,

$$F_V^Z = \sum_{a=0,3,8} v_a F_1^a, \quad F_M^Z = \sum_{a=0,3,8} v_a F_2^a, \quad G_A^Z = \sum_{a=0,3,8} a_a G_1^a \,. \tag{6.71}$$

To lowest order the coefficients v_a and a_a are determined by the vector and axial vector couplings of the Z to the quarks and given by

$$v_0 = -\tfrac{1}{2}, \quad v_3 = 1 - 2\sin^2\theta_W, \quad v_8 = (1/\sqrt{3})(1 - 2\sin^2\theta_W) \,, \tag{6.72}$$

$$a_0 = \tfrac{1}{2}, \quad a_3 = -1, \quad a_8 = -1/\sqrt{3} \,. \tag{6.73}$$

The impact of these results, and in particular of the last relation in Eq. (6.71), on spin physics is as follows: In the naive (i.e. non-QCD) parton model there is no Q^2 dependence and one can identify the axial vector form factors with combinations of first moments of polarized parton densities, for $f = 3$ active flavors,

$$\begin{aligned} G_1^0 &= \tfrac{1}{3}[\Delta(u+\bar{u}) + \Delta(d+\bar{d}) + \Delta(s+\bar{s})] \,, \\ G_1^3 &= \tfrac{1}{2}[\Delta(u+\bar{u}) - \Delta(d+\bar{d})] \,, \\ G_1^8 &= (1/\sqrt{12})[\Delta(u+\bar{u}) + \Delta(d+\bar{d}) - 2\Delta(s+\bar{s})] \,. \end{aligned} \tag{6.74}$$

If these results are combined to G_A^Z in Eq. (6.71), one finds that G_A^Z measures the following combination of first moments:

$$G_A^Z = -\tfrac{1}{2}[\Delta(u+\bar{u}) - \Delta(d+\bar{d}) - \Delta(s+\bar{s})] \,. \tag{6.75}$$

This is an important result because it shows that (quasi)-elastic neutral current processes allow to determine a linear combination of first moments of polarized parton densities, which is independent and different of what is measured in polarized deep inelastic electroproduction.

Higher order QCD, QED and quark mass corrections to this result have been estimated by [407] to be small. There is some effect from the renormalization group running of a_0 between the scale $< 1\,\mathrm{GeV}$ at which the hadronic matrix elements are defined and the scale m_Z at which the couplings are given. The effect of this running can be summarized as effectively replacing $a_0 = \frac{1}{2}$ by $a_0 \approx 0.48$. The running of the other couplings can be neglected to a good approximation.

The discussion so far seems to imply that elastic neutrino scattering is an extremely elegant method to determine the spin of the proton. Unfortunately, the above discussion is not the whole story. The point is that to fit neutrino-hadron scattering data one needs the form factors at $Q^2 \neq 0$ and there is a significant Q^2-dependence due to the finite extension of the proton. The exact Q^2-dependence of the form factors being unknown, a dipole approximation of the form $\sim (1 + Q^2/M_D^2)^{-2}$ is usually applied. In these expressions new phenomenological parameters M_D (different for each form factor) appear, which have to be determined experimentally. This uncertainty in the Q^2-dependence reduces the potential of the method very much [39,188]. Recently, a method has been suggested by [42] to reduce this sensitivity on the poorly known (non-strange) axial form factor and increase the accuracy and sensitivity to the strange axial form factor (Δs) by considering a certain combination of neutral and charged current neutrino and antineutrino cross sections, namely the asymmetry

$$A_N(Q^2) = \frac{(\mathrm{d}\sigma/\mathrm{d}Q^2)_{\nu N}^{\mathrm{NC}} - (\mathrm{d}\sigma/\mathrm{d}Q^2)_{\bar{\nu} N}^{\mathrm{NC}}}{(\mathrm{d}\sigma/\mathrm{d}Q^2)_{\nu n}^{\mathrm{CC}} - (\mathrm{d}\sigma/\mathrm{d}Q^2)_{\bar{\nu} p}^{\mathrm{CC}}} \,. \tag{6.76}$$

In principle, it should be possible to obtain information about the proton spin from the investigation of the quasi-elastic CC processes $\nu_\mu + n \to \mu^- + p$ and $\bar{\nu}_\mu + p \to \mu^+ + n$. However, the existing CC data are not accurate enough to compete with the NC elastic scattering data [289]. These and other suggestions are awaiting the experimental tests. For example, a measurement of G_1^0 in elastic scattering of unpolarized electrons off unpolarized protons might be feasible, because the forward backward asymmetry of the electrons in the cms is determined by the γ-Z interference terms and these in turn are proportional to G_1^0.

6.7. The OPE and QCD parton model for g_3 and g_{4+5}

In Section 2.4 the 'kinematics' of polarized charged and neutral current processes has been introduced and the structure functions $g_{3,4,5}$ have been defined. In this section we want to discuss the parton model and the phenomenological consequences of polarization effects involving charged and neutral currents. Further information can be found in the literature [211,432,571,388,508,472–474,393,62]. The first reference [211] is an old review and summarizes the theoretical articles [489,218,37,410,154] from before the startup of the CERN experiments. Just as for g_1 the naive parton model can be applied as a first approximation, whenever longitudinally polarized leptons probe longitudinally polarized protons ($P_\mu = MS_\mu$) at high energies (much larger than Λ_{QCD}). Under this condition the relevant structure functions in the hadronic tensor Eq. (2.31) are g_3 and $g_{4+5} := g_4 + g_5$.

Let us first consider neutrino nucleon scattering $\nu p \to l^- X$ which proceeds via W^+ exchange. (Analogously, for antineutrino scattering, $\bar{\nu} N \to l^+ X$ refers to the charged W^- current.) The results can also be taken over rather directly to the charged current reactions $l^+ p \to \bar{\nu} X$. Neutrinos couple to d-type quarks and to $\bar{u}$-type antiquarks so that the densities of these partons will appear in the structure functions. In principle, one has also to take into account the proper CKM mixing occuring at the charged current vertex. However, if one considers the contributions of 4 flavors (u, d, s and c), one always encounters the factor $\cos^2\theta_c + \sin^2\theta_c = 1$. One can get the parton model expressions for g_3 and g_{4+5} by an explicit calculation of the lowest order processes and by

comparing it to the general form of the hadron tensor (2.28)

$$g_1^{\nu N}(x,Q^2) = \delta d(x,Q^2) + \delta s(x,Q^2) + \delta\bar{u}(x,Q^2) + \delta\bar{c}(x,Q^2)\ , \tag{6.77}$$

$$g_3^{\nu N}(x,Q^2) = -[\delta d(x,Q^2) + \delta s(x,Q^2) - \delta\bar{u}(x,Q^2) - \delta\bar{c}(x,Q^2)]\ , \tag{6.78}$$

$$g_{4+5}^{\nu N}(x,Q^2) = 2xg_3^{\nu N}(x,Q^2)\ , \tag{6.79}$$

where the index νN always implies W^+ exchange. One obtains the corresponding formulae for $\bar{\nu}N$ (W^- exchange) by the flavor interchanges $d \leftrightarrow u$ and $s \leftrightarrow c$. The contribution of $g_{4-5}^{\nu N}$ to the cross section vanishes in the framework of the QCD improved parton model.

Some remarks are in order. Due to the charge conjugation property of γ_5 the antiquarks always appear with an opposite sign in g_3 and g_{4+5} as compared to g_1. As discussed in Section 5, the sum

$$\int_0^1 \mathrm{d}x(g_1^{\nu N} + g_1^{\bar{\nu}N})(x,Q^2) = \Delta\Sigma - f\frac{\alpha_s}{2\pi}\Delta g(Q^2) \tag{6.80}$$

is a measure of the axial vector singlet current matrix element and its measurement would be a nice way to verify the value of $\Delta\Sigma - f(\alpha_s/2\pi)\Delta g$ without recurrence to the low energy determination of the matrix elements A_3 and A_8. In contrast to g_1, the structure functions g_3 and g_{4+5} measure solely nonsinglet combinations of parton densities (just as F_3 in unpolarized DIS), so that they do not get a contribution from the gluon densitiy. They can yield informations of the following type: For example, by scattering on an isoscalar target one could find out, how large the polarized strange quark sea is

$$(g_3^{\nu N} - g_3^{\bar{\nu}N})_p(x,Q^2) + (g_3^{\nu N} - g_3^{\bar{\nu}N})_n(x,Q^2) = 2(\delta c + \delta\bar{c} - \delta s - \delta\bar{s})(x,Q^2)\ . \tag{6.81}$$

Other combinations have been studied in [472–474,62]. Furthermore, it should be mentioned that the treatment of the charm quark contributions to the above structure functions in terms of a massless intrinsic density $\delta c(x,Q^2) = \delta\bar{c}(x,Q^2)$ is controversial. It is more appropriate to calculate the heavy quark contributions to neutral and charged current processes perturbatively via the subprocess $W^+ g \to c\bar{s}$ [571], for example.

Just as F_1 and F_2 in unpolarized DIS, g_3 and g_{4+5} are related by a Callan–Gross-like relation, Eq. (6.79), originally derived by [228]. This relation will be violated beyond the leading order of QCD, except in the case of neutral currents where g_3 and g_{4+5} do not receive a gluonic contribution to $O(\alpha_s)$ [432,571]. Further new relations analogous to the Wandzura–Wilczek relation for g_2 (cf. [576] and Section 8.1) have been recently derived from a study of the twist-2 and twist-3 OPE [121,122].

The close relationship between unpolarized and polarized DIS in the limit $Q^2 \to \infty$, in which only longitudinal polarization survives, becomes very transparent within the OPE. In the high energy limit one can stick to the leading twist-2 operators, and the OPE for the hadronic tensor reads

$$W_{\mu\nu}^{\nu N} = \mathrm{i}\varepsilon_{\mu\nu\lambda\sigma}q^\lambda \sum_n \left(\frac{2}{Q^2}\right)^n q_{\mu_1}\ldots q_{\mu_{n-1}} \sum_i (R_i^{\sigma\mu_1\ldots\mu_{n-1}} E_i^n + Q_i^{\sigma\mu_1\ldots\mu_{n-1}} C_i^n)$$
$$+ \left(-g_{\mu\nu} + \frac{q_\mu q_\nu}{q^2}\right)\sum_n \left(\frac{2}{Q^2}\right)^n q_\sigma q_{\mu_1}\ldots q_{\mu_{n-1}} \sum_i (R_i^{\sigma\mu_1\ldots\mu_{n-1}} V_i^n + Q_i^{\sigma\mu_1\ldots\mu_{n-1}} X_i^n)$$

$$+\left(-g_{\mu\sigma}+\frac{q_\mu q_\sigma}{q^2}\right)\left(-g_{\nu\mu_1}+\frac{q_\nu q_{\mu_1}}{q^2}\right)$$

$$\times 2\sum_n\left(\frac{2}{Q^2}\right)^{n-1} q_{\mu_2}\ldots q_{\mu_{n-1}}\sum_i\left(R_i^{\sigma\mu_1\cdots\mu_{n-1}}W_i^n+Q_i^{\sigma\mu_1\cdots\mu_{n-1}}Y_i^n\right), \tag{6.82}$$

where R_i are the operators relevant for polarized scattering (Eqs. (4.72) and (4.73)) and Q_i are the corresponding operators for unpolarized scattering (essentially the same as Eqs. (4.72) and (4.73) but without a γ_5). $E_i^n, C_i^n, V_i^n, X_i^n, W_i^n$ and Y_i^n are the corresponding Wilson coefficients. For example, E_i^n is related to the structure function g_1, C_i^n to the structure function F_3, etc. More precisely, one has [508]

$$\int_0^1 \mathrm{d}x\, x^{n-1}F_1(x,Q^2)=\sum_i b_n^i X_i^n(Q^2/\mu^2,\alpha_s),\quad n=1,3,5,\ldots\ , \tag{6.83}$$

$$\int_0^1 \mathrm{d}x\, x^{n-2}F_2(x,Q^2)=2\sum_i b_n^i Y_i^n(Q^2/\mu^2,\alpha_s),\quad n=1,3,5,\ldots\ , \tag{6.84}$$

$$\int_0^1 \mathrm{d}x\, x^{n-1}F_3(x,Q^2)=\frac{1}{2}\sum_i b_n^i C_i^n(Q^2/\mu^2,\alpha_s),\quad n=1,3,5,\ldots\ , \tag{6.85}$$

$$\int_0^1 \mathrm{d}x\, x^{n-1}g_1(x,Q^2)=\frac{1}{2}\sum_i a_n^i E_i^n(Q^2/\mu^2,\alpha_s),\quad n=1,3,5,\ldots\ , \tag{6.86}$$

$$\int_0^1 \mathrm{d}x\, x^{n-1}g_3(x,Q^2)=\sum_i a_n^i V_i^n(Q^2/\mu^2,\alpha_s),\quad n=1,3,5,\ldots\ , \tag{6.87}$$

$$\int_0^1 \mathrm{d}x\, x^{n-2}g_{4+5}(x,Q^2)=2\sum_i a_n^i W_i^n(Q^2/\mu^2,\alpha_s),\quad n=1,3,5,\ldots\ , \tag{6.88}$$

where the $a_n^i(b_n^i)$ are the matrix elements for a (un)polarized proton, cf. Eq. (4.74). From these equations the Callan–Gross relations are apparent, because in leading order all Wilson coefficients are equal to 1. For more details we refer the reader to [508,121,122].

Let us now turn to neutral current exchange where the description is similar, although somewhat complicated by the γZ-interference. In LO the parton model predictions for the structure functions are

$$g_1^{\gamma Z}(x,Q^2)=\sum_q e_q v_q(\delta q+\delta\bar{q})(x,Q^2)\ , \tag{6.89}$$

$$g_3^{\gamma Z}(x,Q^2)=\sum_q e_q a_q(\delta q-\delta\bar{q})(x,Q^2)\ , \tag{6.90}$$

$$g_1^{ZZ}(x,Q^2)=\frac{1}{2}\sum_q (v_q^2+a_q^2)(\delta q+\delta\bar{q})(x,Q^2)\ , \tag{6.91}$$

$$g_3^{ZZ}(x,Q^2)=\sum_q v_q a_q(\delta q-\delta\bar{q})(x,Q^2)\ , \tag{6.92}$$

where v_q and a_q are the vector and axialvector coupling of the quark flavor q to the Z^0, $v_u = \frac{1}{2} - \frac{4}{3}\sin^2\theta_W$, $a_u = \frac{1}{2}$, $v_d = -\frac{1}{2} + \frac{2}{3}\sin^2\theta_W$ and $a_d = -\frac{1}{2}$, cf. Section 2.4. Furthermore, one has $g_{4+5}^{\gamma Z,ZZ} = 2xg_3^{\gamma Z,ZZ}$ and g_1^{γ} as before, cf. Eq. (4.5). NLO contributions can be found in [271,432,472–474,571,557]. For comparison let us include here the corresponding LO relations for the unpolarized structure functions, namely $F_1^{\gamma Z,ZZ} = \sum_q (e_q v_q, v_q^2 + a_q^2)(q + \bar{q})$, $F_3^{\gamma Z,ZZ} = 2\sum_q (e_q a_q, v_q a_q)(q - \bar{q})$ and $F_2^{\gamma Z,ZZ} = 2xF_1^{\gamma Z,ZZ}$. For the charged current processes $l^+ N \to \bar{\nu} X$ one can take over the expressions for $g_1^{\nu N}$, etc., from above, Eqs. (6.77)–(6.81).

6.8. Single-spin asymmetries and handedness

Single spin asymmetries $A_L = (\sigma_{\Rightarrow} - \sigma_{\Leftarrow})/(\sigma_{\Rightarrow} + \sigma_{\Leftarrow})$ are asymmetries that arise if only one of the external particles is longitudinally (or transversally) polarized. In deep inelastic lepton–nucleon scattering at $Q^2 \ll m_Z^2$ all single-spin asymmetries vanish – at least within the framework of the (twist-2) parton model – and the same holds true for many processes at RHIC, like direct photon, heavy quark or jet production. Still, there are circumstances under which nonvanishing single-spin asymmetries arise. For instance, many authors have tried to derive single-spin asymmetries from higher twist effects like the intrinsic transverse momentum of the partons within hadrons [534,535,195,196,132,240,494,495,435,237,560,76,59–61,423]. Such considerations have been triggered by several experiments which have shown that single-spin asymmetries can indeed be large both in semi-inclusive $pp^{\uparrow} \to \pi X$ [15,16,22] and exclusive $pp^{\uparrow} \to pp$ [67,157,209] reactions. These ideas go beyond the perturbative QCD (twist-2) parton model and are more difficult to test than the parton model inspired predictions which usually lead to double-spin asymmetries. Another example of single-spin asymmetries is the possibility to determine the spin of final state particles, like the handedness of jets. All these ideas and approaches will be discussed at the end of this section. We shall start the discussion with a leading, twist-2 source of single-spin asymmetries which is due to weak interactions, i.e. the presence of parity violating couplings in processes in which $W^{\pm}$ and Z^0 are involved. In such processes the γ_5 from the polarized particle and the γ_5 from the axial vector coupling combine in the matrix element to give a nonvanishing single-spin asymmetry even within the ordinary parton model. This point will be discussed first in this section because it can lead to drastic effects and, at RHIC, is an independent way to determine the polarized parton densities.

Let us recall that in unpolarized proton scattering the production of W's via $pp \to W^{\pm} X$ is sensitive to the form of the antiquark distributions, because the dominant contribution to the cross section comes from the quark-antiquark fusion reactions $u\bar{d} \to W^+$ and $\bar{u}d \to W^-$. The same holds true for polarized scattering where at least one of the protons is polarized. The corresponding single-spin asymmetry is given by

$$A_L^{PV} = \frac{\sigma_{\Rightarrow} - \sigma_{\Leftarrow}}{\sigma_{\Rightarrow} + \sigma_{\Leftarrow}} = \frac{\delta u(x_1, m_W^2)\bar{d}(x_2, m_W^2) - (u \leftrightarrow \bar{d})}{u(x_1, m_W^2)\bar{d}(x_2, m_W^2) + (u \leftrightarrow \bar{d})} \,. \tag{6.93}$$

Note that for kinematical reasons A_L^{PV} depends only on $y = \ln x_1/x_2$ because one has $x_1 = (m_W/\sqrt{S})e^{y}$ and $x_2 = (m_W/\sqrt{S})e^{-y}$. Eq. (6.93) is a crude LO approximation but it shows how sensitive one is to the polarized antiquark densities. A phenomenological analysis on the basis of this formula has been presented in [137,541] for the RHIC machine parameters chosen to be

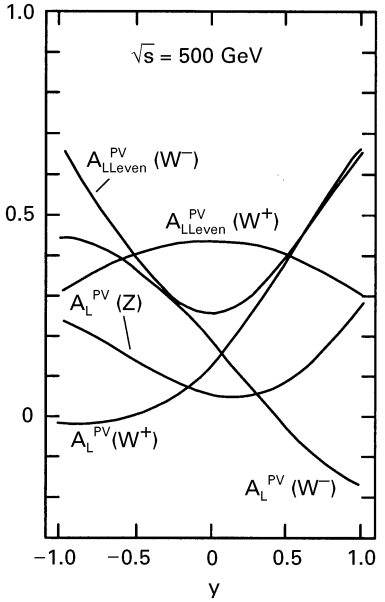

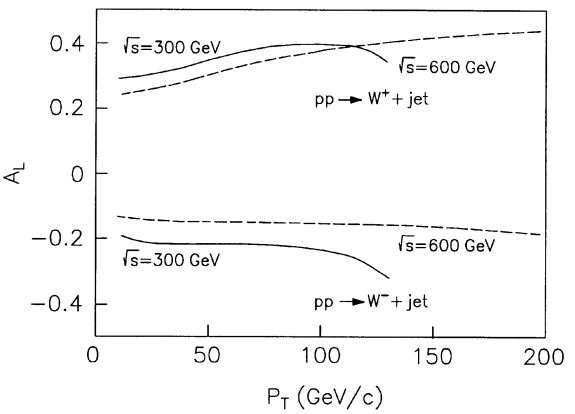

Fig. 38. The parity-violating spin asymmetries for $W^{\pm}$ and Z^0 production as a function of y under RHIC conditions [137]. The curves correspond to a suggested choice of the sea quark polarizations, cf. Ref. [135].

Fig. 39. The parity-violating single-spin asymmetries in $pp \to W^{\pm} + \text{jet}$ at $y = 0$ as a function of p_T under RHIC conditions. The results are taken from Ref. [136].

$\sqrt{s} = 0.5$ TeV, $L = 2 \times 10^{32}\,\text{cm}^{-2}\,\text{s}^{-1}$ and a polarization of 70%. The resulting single-spin asymmetries are shown in Fig. 38 as a function of y. In Ref. [136] the analysis has been extended to processes like $pp \to W^{\pm} + \text{jet} + X$. The corresponding single-spin asymmetries are shown in Fig. 39 as a function of p_T. Later on, a Monte Carlo study including collinear gluon bremsstrahlung has been carried out in [519]. The full NLO-QCD calculation has been performed in [579].

In principle, there are two other parity-violating asymmetries which can be measured if both protons are polarized, namely

$$A^{PV}_{\text{LLeven}}(y) = (\sigma^{\Leftarrow}_{\Leftarrow} - \sigma^{\Rightarrow}_{\Rightarrow})/(\sigma^{\Leftarrow}_{\Leftarrow} + \sigma^{\Rightarrow}_{\Rightarrow}) \tag{6.94}$$

and

$$A^{PV}_{\text{LLodd}}(y) = (\sigma^{\Leftarrow}_{\Rightarrow} - \sigma^{\Rightarrow}_{\Leftarrow})/(\sigma^{\Leftarrow}_{\Rightarrow} + \sigma^{\Rightarrow}_{\Leftarrow}) \tag{6.95}$$

Note that if parity is conserved one has $\sigma_{a,b} = \sigma_{-a,-b}$ and $\sigma_a = \sigma_{-a}$ so that all these asymmetries, including A^{PV}_L, vanish. In the parity violating $W^{\pm}$ production process they are given in leading order by [137]

$$A^{PV}_{\text{LLeven}}(y) = \frac{[\delta u(x_1, m_W^2)\bar{d}(x_2, m_W^2) - u(x_1, m_W^2)\delta\bar{d}(x_2, m_W^2)] - [u \leftrightarrow \bar{d}]}{[u(x_1, m_W^2)\bar{d}(x_2, m_W^2) - \delta u(x_1, m_W^2)\delta\bar{d}(x_2, m_W^2)] + [u \leftrightarrow \bar{d}]} \tag{6.96}$$

and

$$A_{\mathrm{LLodd}}^{PV}(y) = \frac{[u(x_1, m_W^2)\delta\bar{d}(x_2, m_W^2) + \delta u(x_1, m_W^2)\bar{d}(x_2, m_W^2)] - [u \leftrightarrow \bar{d}]}{[u(x_1, m_W^2)\bar{d}(x_2, m_W^2) + \delta u(x_1, m_W^2)\delta\bar{d}(x_2, m_W^2)] + [u \leftrightarrow \bar{d}]} \tag{6.97}$$

with the property $A_{\mathrm{LLeven}}^{PV}(y) = A_{\mathrm{LLeven}}^{PV}(-y)$ and $A_{\mathrm{LLodd}}^{PV}(y) = -A_{\mathrm{LLodd}}^{PV}(-y)$ and again sensitive to the polarized sea.

Results for these asymmetries are included in Fig. 38, obtained under the assumptions of Ref. [137]. These authors have suggested that one should make the approximation $|\delta u(x_1)\delta\bar{d}(x_2)| \ll u(x_1)\bar{d}(x_2)$. In that case the three asymmetries are not independent quantities any more but $A_{\mathrm{LLeven}}^{PV}(y)$ and $A_{\mathrm{LLodd}}^{PV}(y)$ can be expressed in terms of $A_{\mathrm{L}}^{PV}(y)$ and $A_{\mathrm{L}}^{PV}(-y)$. Whether this approximation is reasonable or not will be shown in future. In any case, among the three, A_{L}^{PV} is certainly the most interesting one because it will have the smallest statistical error. This is true despite the fact that the single-spin asymmetry will be smaller in absolute magnitude than the double-spin asymmetries by roughly a factor of 2.

Similar considerations as for W-production apply for Z-production at RHIC. One may also consider the Z-contribution to the Drell–Yan process $pp \to \gamma^*, Z^* \to \mu^+\mu^-$ which is relevant for large invariant masses of the $\mu^+\mu^-$ pair. There have been studies of large-p_{T} W [136] (and also large-p_{T} Z^* [442,443] and large-p_{T} jet production) induced by the higher order processes $q_i\bar{q}_j \to Wg$ and $q_ig \to q_jW$, where $i \neq j$ denotes the quark flavor. Let us discuss now qualitatively the significance of these processes for the determination of the polarized gluon density $\delta g(x, \mu_F^2)$ where μ_F may be roughly chosen as $\mu_F^2 \approx (p_{\mathrm{T}}^2 + m_W^2)/4$. If the beams are polarized and the initial partons are carrying a given helicity, one has for the Compton-type scattering process $q_i(h)g(\lambda) \to q_jW$ the parton level cross section

$$\frac{\mathrm{d}\hat{\sigma}}{\mathrm{d}\hat{t}} = \frac{\pi\alpha\alpha_s}{12\sin^2\theta_W \hat{s}^3\hat{u}}(h-1)(c_2\lambda + c_1(1-\lambda)) , \tag{6.98}$$

where $c_1 = (\hat{s} - m_W^2)^2 + (\hat{u} - m_W^2)^2$ and $c_2 = 2(\hat{u} - m_W^2)^2$. For $\bar{q}_i(h)g(\lambda) \to \bar{q}_jW$ the same formula holds but with $h \to -h$ and $\lambda \to -\lambda$. The resulting parton level single-spin asymmetries are $\hat{a}_{\mathrm{L}}^{PV} = 1$ for polarized quarks and $\hat{a}_{\mathrm{L}}^{PV} = 1 - (c_2/c_1)$ for polarized gluons. Since the last quantity is rather small on average [136], the single hadron helicity asymmetry will be dominated by polarized quarks and is not very sensitive to δg.

If it were possible to determine the polarization of the outgoing photon or jet, one would have nonvanishing single-spin asymmetries in processes without parity violation. Namely, one could study processes like $q + \vec{g} \to q + \vec{\gamma}$ or $q + \vec{g} \to \vec{q} + g$, etc., either at RHIC or one could use the energetic unpolarized proton beams of the Tevatron $\bar{p}p$ or HERA ep colliders ($E_p \approx 1\,\mathrm{TeV}$) to be scattered off a polarized fixed proton target. In the former case one would have to measure the circular polarization of the final state photon. This is quite difficult. It could be done either by selective absorbtion using a polarized detector [210] or by making use of the fact that in high energy photon induced showers the longitudinal polarization is conserved to a good degree of accuracy [471,323]. In the latter case an unpolarized quark collides with a polarized gluon and one would have to measure the polarization of the outgoing quark jet. It has been speculated [485,236,214,238,133] that information about the polarization of the initiating parton, i.e. the outgoing quark, can be obtained from the 'handedness' of a jet. As will be discussed below, present

experimental data show unfortunately so far no evidence for this concept to be relevant. Here handedness is defined as follows: consider the triple product of vectors $S := \boldsymbol{t}\cdot(\boldsymbol{k}_1 \times \boldsymbol{k}_2)$ where $\boldsymbol{t}$ is a unit vector along the jet axis, and $\boldsymbol{k}_1$ and $\boldsymbol{k}_2$ are the momenta of two particles in the jet chosen by some definite prescription, e.g. the two fastest particles. The jet is defined as left(right)-handed if S is negative(positive). For an ensemble of jets the handedness is defined as the asymmetry in the number of left- and right-handed jets, $H := (N_{S<0} - N_{S>0})/(N_{S<0} + N_{S>0})$. It can then be asserted that $H = \alpha P$ where P is the average polarization of the underlying partons in the ensemble of jets and α is the 'analyzing power' of the handedness method.

In order to obtain information about $\delta g(x, \mu_F^2)$ from processes like $p + \vec{p} \to j\vec{e}t + X$ one needs to know the value of α. It has been attempted [1] to determine α from jet production at SLD where a polarized Z-boson decays into two jets originating from a $q\bar{q}$ pair. The quark and antiquark in a Z^0 decay have opposite helicities. The SM predicts $P_{u,c} \approx 0.67$ and $P_{d,s,b} \approx 0.94$ for the average polarizations of quark flavors so that the quarks are produced predominantly left-handed and the antiquarks predominantly right-handed. In order to observe a net polarization in an ensemble of jets from Z^0 decays it is necessary to distinguish quark jets from antiquark jets. This separation can be achieved at SLC where Z^0 bosons are produced in collisions of highly longitudinally polarized electrons with unpolarized positrons. In this case the SM predicts a large difference in polar angle distributions between quarks and antiquarks. Unfortunately, no evidence for handedness was found by the SLD collaboration [1]. This negative result seems to imply that the connection between the polarization of the hard partons before the fragmentation and the orientation of the final state hadrons is very loose and washed out by confinement effects.

Instead of producing and delineating a polarized photon, Drell–Yan dilepton production has been suggested as a probe for polarized densities: here either the polarization of one of the final leptons in $p\vec{p} \to \gamma^* X \to \mu^+\vec{\mu}^- X$ has to be measured [199], or the angular distribution of the produced lepton pair [160] as a polarimeter for the virtual intermediate photon.

Similarly, instead of producing a polarized jet (quark), semi-inclusive polarized single-particle (e.g. $\vec{\Lambda}$) production has been suggested and analyzed as well. Either $e^+\vec{e}^- \to \vec{\Lambda}X$ [152] or $l\vec{p} \to l\vec{\Lambda}X$ [377,454,455,412], where in the latter case a longitudinally polarized lepton beam instead of a polarized nucleon target could do as well as a sensitive probe of $\delta g(x, Q^2)$. Here the (time-like) polarized fragmentation functions $\delta D_f^A(z, Q^2)$, $f = q, \bar{q}, g$ also enter, which are defined in analogy to the space-like polarized parton densities. Theoretically, these processes have been studied rather thoroughly during the past few years, not only in LO, but in NLO as well [272,556].

Finally, we want to come back to higher twist contributions as a source of single (transverse) spin asymmetries A_N. Let us first discuss semi-inclusive reactions such as $pp^\uparrow \to \pi X$ and $pp^\uparrow \to \gamma X$. At present, there are basically three sources for a nonvanishing A_N:

(i) dynamical contributions, i.e. 'hard' partonic twist-3 scattering effects, which result from a short distance part calculable in perturbative QCD combined with a long distance part related to quark–gluon correlations [240,494,495,560];

(ii) intrinsic k_T effects in parton distribution functions which, being nonperturbative universal nucleon properties, give rise to twist-3 contributions when convoluted with the hard partonic cross sections. Such contributions are usually referred to as 'Sivers effect' [534,535,59,483, 484,424];

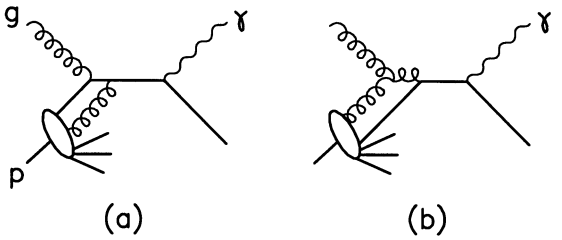

Fig. 40. Sample twist-3 quark-gluon correlation diagrams corresponding to fermionic (a) and gluonic (b) pole contributions which give rise to a nonvanishing single-spin asymmetry in hadronic direct-photon production.

(iii) intrinsic k_T effects in the parton fragmentation functions which is known as 'Collins' or 'sheared jet' effect [195,196,483,484,76].

A typical example for dynamical quark–gluon correlation contributions (i) to direct-γ production is depicted in Fig. 40. They give rise to $A_N^\gamma \neq 0$ and correspond to fermionic (quark) pole [240] and/or gluonic pole [494,495,247] dominance in the calculation of the twist-3 partonic scattering cross sections. Clearly, single-spin asymmetries for direct-γ production are not 'contaminated' by possible intrinsic k_T effects in fragmentation functions (iii), but k_T effects in parton densities (ii) could also be relevant besides (i). In the latter case (ii) one expects that the number of quarks with longitudinal momentum fraction x and transverse intrinsic motion $\boldsymbol{k}_T$ depends, on account of soft gluon interactions between initial state partons, on the transverse spin direction of the parent nucleon, so that the 'quark distribution analysing power' $N_q(\boldsymbol{k}_T) \equiv (f_{q/N^\uparrow}(x,\boldsymbol{k}_T) - f_{q/N^\downarrow}(x,\boldsymbol{k}_T))/(f_{q/N^\uparrow}(x,\boldsymbol{k}_T) + f_{q/N^\downarrow}(x,\boldsymbol{k}_T))$ can be different from zero. Similar soft interactions in the final (fragmentation) state may give rise to the 'Collins effect' (iii); it simply amounts to say that the number of hadrons h (say, pions) resulting from the fragmentation of a transversely polarized quark, with longitudinal momentum fraction z and transverse momentum $\boldsymbol{k}_T$, depends on the quark spin orientation. That is, one expects the 'quark fragmentation analyzing power' $A_q(\boldsymbol{k}_T) \equiv (D_{h/q^\uparrow}(z,\boldsymbol{k}_T) - D_{h/q^\downarrow}(z,\boldsymbol{k}_T))/(D_{h/q^\uparrow}(z,\boldsymbol{k}_T) + D_{h/q^\downarrow}(z,\boldsymbol{k}_T))$ to be different from zero, where, by parity invariance, the quark spin should be orthogonal to the $q-h$ plane. Notice also that time-reversal invariance does not forbid such a quantity to be nonvanishing because of the (necessary) soft interactions of the fragmenting quark with external strong fields, i.e. because of final state interactions. This idea has been applied [76] to the computation of the single-spin asymmetries observed in $pp^\uparrow \to \pi X$ [15,16,22]. As mentioned above, both $A_q(\boldsymbol{k}_T)$ and $N_q(\boldsymbol{k}_T)$ are leading twist quantities which, when convoluted with the elementary cross sections and integrated over, give twist-3 contributions to the single-spin asymmetries.

Each of the above mechanisms might be present and important in understanding twist-3 contributions. It is then important to study possible ways of disentangling these different contributions in order to be able to assess the importance of each of them. We discuss now single-spin asymmetries for various processes $AB^\uparrow \to CX$. To obtain a complete picture one needs to consider nucleon–nucleon interactions together with other processes, like lepton–nucleon scattering which might add valuable information too. For each of them one should discuss the possible sources of higher twist contributions, distinguishing, according to the above discussion, between those

originating from the hard scattering and those originating either from the quark fragmentation or distribution analyzing power [61,60,423]:

- $pN^{\uparrow} \to hX$: all kinds of higher twist contributions may be present; this asymmetry *alone* could not help in evaluating the relative importance of the different terms;
- $pN^{\uparrow} \to \gamma X$, $pN^{\uparrow} \to \mu^{+}\mu^{-}X$, $pN^{\uparrow} \to jets + X$: no fragmentation process is involved and one remains with possible sources of nonzero single-spin asymmetries in the hard scattering (i) or the quark distribution analyzing power due to an intrinsic k_{T} (ii);
- $lN^{\uparrow} \to hX$: a single-spin asymmetry can originate either from hard scattering (i) or from k_{T} effects in the fragmentation function (iii), but not in the distribution functions, as soft initial state interactions are suppressed by powers of α_s;
- $lN^{\uparrow} \to \gamma X$, $\gamma N^{\uparrow} \to \gamma X$, $lN^{\uparrow} \to \mu^{+}\mu^{-}X$, $lN^{\uparrow} \to jets + X$: a single-spin asymmetry in any of these processes may only be due to higher-twist dynamical hard scattering effects (i).

In the following we want to concentrate on some specific processes, in order to see to what extent valuable information can be obtained from measuring single-spin asymmetries at RHIC and at the future HERA-$\vec{N}$ (where we specifically refer to the 'phase I' program, i.e. to polarized fixed target experiments with an unpolarized beam; 'phase II' refers to a polarized proton beam as well [423]). One example is semi-inclusive $\pi^{\pm,0}$ production by $p^{\uparrow}p$ collisions which is known to exhibit surprisingly large single-spin asymmetries at 200 GeV. This was measured a few years ago by the E704 Collaboration using a transversely polarized beam [15,16,22]. For any kind of pions the asymmetry shows a considerable rise above $x_F > 0.3$, i.e. in the fragmentation region of the polarized nucleon. It is positive ($> 20\%$) for both π^{+} and π^{0} mesons, while it has the opposite sign for π^{-} mesons. The charged pion data were taken in the $0.2 < p_{\mathrm{T}} < 2\,\mathrm{GeV}$ range and it was found that the asymmetry is larger for $p_{\mathrm{T}} > 1\,\mathrm{GeV}$ than for $p_{\mathrm{T}} < 1\,\mathrm{GeV}$. Theoretical approaches as to the interpretation of these data have been put forward in [534,535,132,237,76,59]. The authors of Refs. [60,423] have examined to what accuracy this asymmetry could be measured at HERA-$\vec{N}$. They have shown that it would be possible to quantitatively determine the p_{T} dependence of the asymmetry up to p_{T} values of about 10 GeV.

Another example is to measure the single transverse spin asymmetry in inclusive direct photon production, $pp^{\uparrow} \to \gamma X$. Since this process proceeds without fragmentation, i.e. the photon carries directly the information from the hard scattering process, it measures a combination of initial k_{T} effects and hard scattering twist-3 processes [240,494,495,247]. The first and only results up to now were obtained by the E704 Collaboration [21] showing an asymmetry compatible with zero within large errors for $2.5 < p_{\mathrm{T}} < 3.1\,\mathrm{GeV}$ in the central region $|x_F| < 0.15$. Again, the authors of Refs. [60,423] have examined to what accuracy this asymmetry could be measured at HERA-$\vec{N}$. The contributions of the gluon-Compton scattering ($qg \to \gamma q$) and quark-antiquark annihilation ($q\bar{q} \to \gamma g$) were compared to the background photons that originate mainly from π^{0} and η decays. It turns out that a good sensitivity δA_N^{γ} of about 0.05 can be maintained up to $p_{\mathrm{T}} < 8\,\mathrm{GeV}$. For increasing transverse momentum the annihilation subprocess and the background photons are becoming less essential.

Thirdly, the single-spin asymmetry in Drell–Yan production, $pp^{\uparrow} \to l\bar{l}X$, at small transverse momenta was calculated [347] in the framework of twist-3 perturbative QCD at HERA-$\vec{N}$ energies. The resulting asymmetry does not exceed 2% and depends strongly on the kinematical domain. It should be noted that asymmetries of the size of a few percent represent the canonical

order of magnitude for single-spin asymmetries induced by twist-3 perturbative QCD effects, and that one may expect larger values only under very special circumstances. Note also, that such asymmetries on the few percent level are difficult to measure, even with sufficiently small statistical errors, since the systematic errors originating mainly from beam and target polarization measurements constitute a severe limit.

Recently, it has been suggested [435] that deep inelastic Compton scattering $lp \to l\gamma X$, where either the incoming lepton or proton are polarized, might lead to appreciable and well-measurable single-spin asymmetries in the small-x region. The idea is that intrinsic k_T and absorptive effects of the strong interactions lead to a complex phase in the vertex between the incoming quark and the prompt photon. This phase, in turn, induces a single-spin asymmetry.

Finally, it should be remembered that large spin effects in proton–proton elastic scattering, $pp^{\uparrow} \to pp$, have been discovered many years ago [67,157,209] with proton beam energies of 24 and 28 GeV. The single-spin asymmetry was found significantly different from zero for transverse momenta of the outgoing protons larger than 2 GeV. The transverse single-spin asymmetry in elastic pp scattering at HERA-$\vec{N}$ and RHIC energies has been calculated in a dynamical model that leads to spin-dependent pomeron couplings [328]. The predicted asymmetry is about 0.1 for $p_T^2 = 4$–$5\,\mathrm{GeV}^2$ with a projected statistical error of 0.01–0.02 for HERA-$\vec{N}$, i.e. a significant measurement of the asymmetry can be performed to test the spin dependence of elastic pp scattering at high energies. Although we do not have any detailed quantitative theoretical understanding of elastic single-spin asymmetries for the time being [133], it should be emphasized that, apart from possible helicity nonconserving effects occurring in the hadronic wave function, one expects at least qualitatively a *non*vanishing elastic single-spin asymmetry due to degenerate multiple Regge exchanges which give rise to different phases in different helicity amplitudes (see, e.g., [537] for a recent review).

6.9. Structure functions in DIS from polarized hadrons and nuclei of arbitrary spin

Shortly after the measurement of g_1^p at CERN there were several proposals to investigate spin effects in other nuclear targets. Most prominent among them are of course the deuteron (with spin $J = 1$) and Helium-3 ($J = \frac{1}{2}$), because they are used to determine g_1^n, but there are other potentially polarizable nuclei as well, like $^7\mathrm{Li}(J = \frac{3}{2})$, $^{10}\mathrm{B}(J = 3)$ and $^{27}\mathrm{Al}(J = \frac{5}{2})$. In those higher spin configurations additional structure functions arise which are in principle measureable, although they are typically smaller than the unpolarized structure functions, because polarization dependent effects arise only from the unpaired nucleons in the nucleus and are therefore suppressed as $1/A$. Furthermore, it should be noted that all these new structure functions would vanish for free nucleons. Thus, such experiments offer the possibility to confirm the spin structure of nucleons, and at the same time to obtain new information on nuclear binding effects.

Among the new structure functions originally studied and defined by [380,361,507,508] there are some which have a simple description within the parton model (like g_1 for the nucleons) and there are others which vanish in the parton model (i.e., appear only in higher orders of QCD like F_L or are of higher twist like g_2 for the nucleons). Those with a parton model interpretation can be described in terms of parton densities $q_{\pm}^{JM}(x, Q^2)$ which give the probability to find a quark with momentum fraction x and helicity $\pm\frac{1}{2}$ in a spin-J target with spin M along the z-axis, at some scale Q^2. Measuring the cross section for an unpolarized target determines the averaged quark

distribution

$$q^J(x,Q^2) = \frac{1}{2J+1}\sum_{M=-J}^{J} q^{JM}(x,Q^2)\ . \tag{6.99}$$

Because of QCD parity invariance one has $q_{\pm}^{JM} = q_{\mp}^{J,-M}$ so that only $2J+2$ $(2J)$ of the $4J+2$ $(4J)$ polarized parton densities are independent. (The numbers in brackets hold for half integer J.) It is appropriate to introduce combinations[8]

$$F_1^{JM} = \tfrac{1}{2}(q_+^{JM} + q_-^{JM})\ , \tag{6.100}$$

$$g_1^{JM} = \tfrac{1}{2}(q_+^{JM} - q_-^{JM})\ , \tag{6.101}$$

because in the Bjorken limit the cross sections on targets with spin (JM) probed with helicity $\pm\frac{1}{2}$ electrons can be written as

$$\frac{\mathrm{d}\frac{1}{2}(\sigma_+^{JM} + \sigma_-^{JM})}{\mathrm{d}x\,\mathrm{d}y} = \frac{8\pi\alpha^2\mathscr{M}E}{Q^4}[y^2x + 2x(1-y)]F_1^{JM}(x,Q^2) \tag{6.102}$$

and

$$\frac{\mathrm{d}\frac{1}{2}(\sigma_+^{JM} - \sigma_-^{JM})}{\mathrm{d}x\,\mathrm{d}y} = \frac{8\pi\alpha^2\mathscr{M}E}{Q^4}y(2-y)xg_1^{JM}(x,Q^2) \tag{6.103}$$

with $\mathscr{M}$ denoting the target mass.

Up to now we have introduced $2J+2$ $(2J)$ quark densities for (half)integer J corresponding to $2J+2$ $(2J)$ naive parton model structure functions. In addition, there are $4J$ $(4J+1)$ functions which get contributions either from higher twist operators or from HO QCD so that one has altogether $6J+2$ $(6J+1)$ independent structure functions for integer (half integer) spin, as will be shown after Eq. (6.106). For example, for $J=\frac{1}{2}$ there are F_1, $F_2 - 2xF_1$, g_1 and g_2, among them F_1 and g_1 of leading and $F_2 - 2xF_1$ of higher order in QCD, and g_2 being a higher twist contribtuion. For $J=1$ one has $F_1, F_2 - 2xF_1$, b_1, $b_2 - 2xb_1$, g_1, g_2, b_3 and b_4. In the naive quark parton approximation the only nonzero structure functions are F_1, g_1, b_1 and b_3. For example, b_1 can be measured by scattering an unpolarized electron beam from a polarized deuteron target with the target spin directed parallel to the direction of the incident electron beam and arranged in each of its $m_I = +1, 0, -1$ substates,

$$b_1(x,Q^2) = \sum_q e_q^2[F_1^{1,+1}(x,Q^2) + F_1^{1,-1}(x,Q^2) - 2F_1^{1,0}(x,Q^2)]\ . \tag{6.104}$$

[8] Instead of Eqs. (6.100) and (6.101) it is sometimes more convenient to define 'multipole' structure functions $[JL] := \sum_{M=-J}^{J}(-1)^{J-M}(JMJ-M|L0)q_+^{JM}$ where $(JMJ-M|L0)$ are the Clebsch–Gordan coefficients. These function can be measured using (un)polarized leptons for odd (even) L. They are particularly useful if the relative motion of nucleons inside the nucleus is to be considered. Furthermore, it should be noted that the first $L-1$ moments of these functions vanish.

In general, all b_i can be measured using unpolarized lepton beams. Furthermore, they all arise from nuclear binding effects and are not present for a system of free nucleons. One has $b_1 = 0$ if the spin-1 target consists of two spin $\frac{1}{2}$ constituents at rest, or in relative s-wave, and thus one expects $b_1(deuteron) \approx 0$, because the relative motion of the nucleons in the deuteron is nonrelativistic. In contrast one expects a large b_1^ρ because the quarks in the ρ-meson move relativistically [380,361]. Furthermore, an interesting sum rule for b_1 has been derived which is related to the electric quadrupole moment of the spin-1 target and to its polarized sea-quark content [189].

It is possible to write down the general hadron tensor for a spin-1 target

$$W_{\mu\nu} = -F_1 g_{\mu\nu} + F_2 \frac{P_\mu P_\nu}{P\cdot q} - b_1 r_{\mu\nu} + \frac{b_2}{6}(s_{\mu\nu} + t_{\mu\nu} + u_{\mu\nu}) + \frac{b_3}{2}(s_{\mu\nu} - u_{\mu\nu}) + \frac{b_4}{2}(s_{\mu\nu} - t_{\mu\nu})$$

$$+ \frac{ig_1}{P\cdot q}\varepsilon_{\mu\nu\lambda\sigma} q^\lambda s^\sigma + \frac{ig_2}{(P\cdot q)^2}\varepsilon_{\mu\nu\lambda\sigma} q^\lambda (P\cdot q s^\sigma - s\cdot q P^\sigma) \tag{6.105}$$

and to obtain the cross section from it. In Eq. (6.105) we have defined $r_{\mu\nu} = (g_{\mu\nu}/(P\cdot q)^2)(q\cdot\mathscr{E}^* q\cdot\mathscr{E} - \frac{1}{3}\kappa(P\cdot q)^2)$ with $\kappa = 1 + 4x^2\mathscr{M}^2/Q^2$, $s_{\mu\nu} = (2P_\mu P_\nu/(P\cdot q)^3)(q\cdot\mathscr{E}^* q\cdot\mathscr{E} - \frac{1}{3}\kappa \times (P\cdot q)^2)$, $t_{\mu\nu} = (1/2(P\cdot q)^2)(q\cdot\mathscr{E}^* P_\mu \mathscr{E}_\nu + q\cdot\mathscr{E}^* P_\nu \mathscr{E}_\mu + q\cdot\mathscr{E} P_\mu \mathscr{E}_\nu^* + q\cdot\mathscr{E} P_\nu \mathscr{E}_\mu^* - \frac{4}{3} P\cdot q P_\mu P_\nu)$ and $u_{\mu\nu} = (1/P\cdot q)(\mathscr{E}_\mu^* \mathscr{E}_\nu + \mathscr{E}_\nu^* \mathscr{E}_\mu + \frac{2}{3}\mathscr{M}^2 g_{\mu\nu} - \frac{2}{3} P_\mu P_\nu)$. $\mathscr{E}_\mu$ is the polarization 4-vector of the spin-1 target, i.e. it fulfills $P\cdot\mathscr{E} = 0$ and $\mathscr{E}\cdot\mathscr{E} = -\mathscr{M}^2$ and $s^\sigma \equiv (-i/\mathscr{M}^2)\varepsilon^{\sigma\alpha\beta\tau}\mathscr{E}_\alpha^*\mathscr{E}_\beta P_\tau$.

Instead of this cumbersome approach one may gain more physical insight by studying the various amplitudes appearing in the forward Compton helicity matrix elements. Namely, just as for the spin-$\frac{1}{2}$ target the optical theorem relates the hadron tensor for arbitrary spin to the imaginary part of the forward Compton scattering amplitude which in turn can be expressed in terms of helicity amplitudes. Let $A_{mM,m'M'}$ denote the imaginary part of the forward Compton helicity amplitude for $\gamma_m + \text{target}_M \to \gamma_{m'} + \text{target}_{M'}$,

$$A^J_{mM,m'M'} = \varepsilon^{*\mu}_{m'} W^{JM'M}_{\mu\nu} \varepsilon^\nu_m \ , \tag{6.106}$$

where ε^ν_m, $m = \pm 1, 0$, are the photon polarization vectors. *All* the structure functions like b_1, b_4, etc., discussed before can be expressed as linear combinations of these amplitudes. The $A^J_{mM,m'M'}$ are easily enumerated. Angular momentum conservation requires that the total helicity is conserved, $m + M = m' + M'$, which leaves $18J + 1$ independent helicity amplitudes. Time reversal invariance requires $A^J_{mM,m'M'} = A^J_{m'M',mM}$ which leaves $12J + 2$ independent amplitudes. Parity invariance requires $A^J_{mM,m'M'} = A^J_{-m-M,-m'-M'}$ so that one finally has the $6J + 2$ $(6J + 1)$ independent amplitudes, as mentioned before. Among them are diagonal transverse amplitudes $A^J_{\pm M,\pm M}$ which in the Bjorken limit correspond to the quark densities $q^{JM}_\pm$ introduced above: $A^J_{\pm M,\pm M} = q^{JM}_\pm$.

The amplitudes naturally arise when the hadron tensors $W^{JM'M}_{\mu\nu}$ are multiplied with the lepton tensor to form the cross section. To work that out in detail one has to expand the lepton tensor, Eq. (2.29), on the basis of virtual photon helicity eigenstates

$$L_{\mu\nu} = \frac{2Q^2}{\kappa y^2}\Big\{\lambda^2 \varepsilon_0^\mu \varepsilon_0^\nu + \frac{1}{2}(\lambda^2 + \kappa y^2)(\varepsilon_+^{\mu *}\varepsilon_+^\nu + \varepsilon_-^{\mu *}\varepsilon_-^\nu) - \frac{\lambda^2}{2}(\varepsilon_+^{\mu *}\varepsilon_-^\nu e^{2i\phi} + \varepsilon_-^{\mu *}\varepsilon_+^\nu e^{-2i\phi})$$

$$+\lambda\left(1-\frac{y}{2}\right)(\varepsilon_-^{\mu *}\varepsilon_0^{\nu}\mathrm{e}^{-\mathrm{i}\phi}+\varepsilon_0^{\mu}\varepsilon_-^{\nu}\mathrm{e}^{\mathrm{i}\phi}-\varepsilon_+^{\mu *}\varepsilon_0^{\nu}\mathrm{e}^{\mathrm{i}\phi}-\varepsilon_0^{\mu}\varepsilon_+^{\nu}\mathrm{e}^{-\mathrm{i}\phi})\Bigg\}$$

$$+\frac{2Q^2}{y\sqrt{\kappa}}\left\{\left(1-\frac{y}{2}\right)(\varepsilon_+^{\mu *}\varepsilon_+^{\nu}-\varepsilon_-^{\mu *}\varepsilon_-^{\nu})-\frac{\lambda}{2}(\varepsilon_-^{\mu *}\varepsilon_0^{\nu}\mathrm{e}^{-\mathrm{i}\phi}+\varepsilon_0^{\mu}\varepsilon_-^{\nu}\mathrm{e}^{\mathrm{i}\phi}+\varepsilon_+^{\mu *}\varepsilon_0^{\nu}\mathrm{e}^{\mathrm{i}\phi}+\varepsilon_0^{\mu}\varepsilon_+^{\nu}\mathrm{e}^{-\mathrm{i}\phi})\right\}, \tag{6.107}$$

where $\lambda^2=2(1-y)-(y^2/2)(\kappa-1)$ and ϕ is the azimuthal angle (measured with respect to the x-axis in the xy-plane) of the final lepton. The photon momentum is used as the spin quantization axis. Note that the first term ($\sim 2Q^2/\kappa y^2$) in Eq. (6.107) is spin-independent and the last term ($\sim 2Q^2/y\sqrt{\kappa}$) is the spin-dependent term.

The resulting expressions for the cross sections in terms of the helicity amplitudes are

$$\frac{\mathrm{d}\Sigma^{J\lambda'\lambda}}{\mathrm{d}x\,\mathrm{d}y\,\mathrm{d}\phi}=\frac{8\pi\alpha^2 MEx}{2\pi Q^4\kappa}\left\{\lambda^2\left(A^J_{0M,0M'}-\frac{1}{2}A^J_{+M,-M'}\mathrm{e}^{-2\mathrm{i}\phi}-\frac{1}{2}A^J_{-M,+M'}\mathrm{e}^{2\mathrm{i}\phi}\right)\right.$$

$$+\frac{1}{2}(\lambda^2+\kappa y^2)(A^J_{+M,+M'}+A^J_{-M,-M'})$$

$$\left.+\left(1-\frac{y}{2}\right)\lambda(A^J_{-M,0M'}\mathrm{e}^{\mathrm{i}\phi}+A^J_{0M,-M'}\mathrm{e}^{-\mathrm{i}\phi}-A^J_{+M,0M'}\mathrm{e}^{-\mathrm{i}\phi}-A^J_{0M,+M'}\mathrm{e}^{\mathrm{i}\phi})\right\}, \tag{6.108}$$

$$\frac{\mathrm{d}\Delta\Sigma^{J\lambda'\lambda}}{\mathrm{d}x\,\mathrm{d}y\,\mathrm{d}\phi}=\frac{8\pi\alpha^2 MEx}{2\pi Q^4\sqrt{\kappa}}\left\{y\left(1-\frac{y}{2}\right)(A^J_{+M,+M'}-A^J_{-M,-M'})-\frac{1}{2}y\lambda(A^J_{-M,0M'}\mathrm{e}^{\mathrm{i}\phi}+A^J_{0M,-M'}\mathrm{e}^{-\mathrm{i}\phi}\right.$$

$$\left.+A^J_{+M,0M'}\mathrm{e}^{-\mathrm{i}\phi}+A^J_{0M,+M'}\mathrm{e}^{\mathrm{i}\phi})\right\}. \tag{6.109}$$

These cross sections are not yet in a useful form because the helicities M and M' are defined w.r.t. the virtual photon direction which changes event by event. It is better to define cross sections for targets with definite helicites λ and λ' w.r.t. the incident beam direction. To transform between the 2 frames one has to perform an Euler rotation. The state $|J\lambda\rangle$ can be written in terms of $|JM\rangle$ as

$$|J\lambda\rangle=\sum_M \mathrm{e}^{\mathrm{i}(\lambda-M)\phi}d^J_{M\lambda}(\beta)|JM\rangle\,, \tag{6.110}$$

where $d^J_{M\lambda}(\beta)$ is the Wigner rotation matrix and (β) the angle between $\boldsymbol{q}$ and the incoming lepton direction $\boldsymbol{k}$. The cross sections for targets with definite polarizations in the lab frame can therefore be obtained from Eqs. (6.108) and (6.109) as

$$\frac{\mathrm{d}\sigma^{J\lambda'\lambda}}{\mathrm{d}x\,\mathrm{d}y\,\mathrm{d}\phi}=\sum_{M,M'}\frac{\mathrm{d}\Sigma^{J\lambda'\lambda}}{\mathrm{d}x\,\mathrm{d}y\,\mathrm{d}\phi}d^J_{M\lambda}(\beta)d^J_{M'\lambda'}(\beta)\mathrm{e}^{\mathrm{i}(\lambda-\lambda'+M'-M)\phi}\,, \tag{6.111}$$

$$\frac{\mathrm{d}\Delta\sigma^{J\lambda'\lambda}}{\mathrm{d}x\mathrm{d}y\mathrm{d}\phi}=\sum_{M,M'}\frac{\mathrm{d}\Delta\Sigma^{J\lambda'\lambda}}{\mathrm{d}x\mathrm{d}y\mathrm{d}\phi}d^J_{M\lambda}(\beta)d^J_{M'\lambda'}(\beta)\mathrm{e}^{\mathrm{i}(\lambda-\lambda'+M'-M)\phi}\,. \tag{6.112}$$

For more details see [361,380]. In those references models have been studied, like the bag model, to predict some of the 'new' nuclear structure functions F_1^{JM} and g_1^{JM}.

6.10. Nuclear bound state effects

In the previous section only the appearance of new structure functions in higher spin nuclei has been discussed. Another, probably even more important question is how the 'old' functions like g_1 are modified by nuclear effects, i.e. how much e.g. g_1^D deviates from $g_1^p + g_1^n$. This is a very important question because g_1^n cannot be determined directly but only through a measurement of g_1^D or $g_1(^3\mathrm{He})$. Let us start with the discussion of deuterium, for which a number of studies exists. The simplest and firmest theoretical approach to the deuteron is to approximate it as a free neutron and proton with polarization $1 - \frac{3}{2}w_D$, where w_D is the deuteron d-state probability. All other nuclear corrections are essentially small because they are suppressed by powers of $\boldsymbol{p}^2/M^2$ where $\boldsymbol{p}$ is the 3-momentum of the nucleon in the restframe of the nucleus. w_D can be calculated in NN potential models to be $w_D \approx 0.050 \pm 0.010$ [147,72]. There is a relatively large theoretical error in the prediction of w_D, because depending on which of the phenomenological potentials one uses one gets different answers. This theoretical error is by far the dominant source of uncertainty in the deuteron analysis, much larger than the $\mathrm{O}(\boldsymbol{p}^2/M^2)$ effects mentioned above. This is true except for the large-x region ($x \geq 0.8$) where large nuclear effects are known to be present for unpolarized scattering and expected for polarized scattering as well. It is not clear whether these effects are spin independent, in the sense that they drop out in the asymmetries $\sim g_1/F_1$, or not.

The fact that w_D is not precisely known may become a problem for future precision measurements of g_1^n because a variation of 2% in w_D corresponds to an error of roughly 10% in g_1^n. This is also the order of magnitude which other nuclear effects may have on the determination of g_1^n. To incorporate these effects there has been a sequence of papers ([475,476] and references therein, but see also the work of [582] to be discussed below) working in the impulse approximation, i.e. neglecting final state interactions. There may be final state interactions and related effects like final state pion exchange or nuclear shadowing, but these effects are usually assumed to be small for light nuclei and to some extent spin independent.

At first the so-called convolution model was applied to include nuclear binding and relativistic effects, and afterwards the effects of off-mass shellness of bound nucleons were studied. In the convolution model the free nucleon structure function is convoluted with the light cone momentum distribution of nucleons in the nucleus [512]

$$g_1^D(x,Q^2) = \sum_{N=n,p} \int_x^1 \frac{\mathrm{d}y}{y} \delta f_{N/D}(y) g_1^N\left(\frac{x}{y}, Q^2\right). \tag{6.113}$$

This formula holds in the Bjorken limit (infinite Q^2 and ν). For finite Q^2 there is a spectral representation which generalizes Eq. (6.113) [475,476,561]. It was found [562] that the convolution approach gives a result very close to the description with a constant factor $1 - \frac{3}{2}w_D$, at least for $x \leq 0.7$. Above 0.7 there are appreciable corrections to this factor which can become as large as 10%. The simple behavior for $x \leq 0.7$ is not modified when off-mass-shell corrections [475,476] are included but there are additional contributions at $x \geq 0.7$ (of up to 5%) which should be taken into

account. Although the nuclear effects are within the error bars of presently available data, they will be required in the high statistics E154 and HERMES experiments.

Now coming to ^{3}He, as a first approximation one may say that $g_1(^3\mathrm{He})$ directly gives g_1^n because the spins of the protons compensate each other due to the Pauli principle. This relies on the assumption that all nucleons are in a S wave. However, such a cancellation does not occur if other components of the three body wave function are considered. In Refs. [582,182,183] the question has been quantitatively discussed as to whether and to what extent the extraction of g_1^n from the asymmetry of the process $^3\vec{\mathrm{H}}\mathrm{e}(\vec{e},e')X$ could be hindered by nuclear effects arising from small wave function components of ^{3}He, as well as from Fermi motion and binding effects on DIS. The basic nuclear ingredient used in [182,183] is the spin-dependent spectral function of ^{3}He, which allows one to take into account at the same time Fermi motion and binding corrections. Of particular relevance are the up and down quark spectral functions $P^N_{\sigma\sigma' M}$, $N_{3+} \equiv P^N_{\frac{1}{2}\frac{1}{2}\frac{1}{2}}$ and $N_{3-} \equiv P^N_{-\frac{1}{2}-\frac{11}{22}}$, because the integral of their difference determines the nucleon polarizations $P_N^{(\pm)}$, $N = p,n$ [182,183]. These functions enter the so-called spectral representation of $g_1(^3\mathrm{He})$ as a function of g_1^N. Note that in the Bjorken limit this spectral representation goes over into Eq. (6.113).

In Ref. [582] the $^3\vec{\mathrm{H}}\mathrm{e}$ asymmetry has been calculated taking into account S' and D waves but considering only Fermi motion and omitting Q^2 dependent terms. Woloshyn used ^{3}He wave functions [35] calculated using the momentum space Faddeev equation, which are known to give a good description of the spin-averaged quasi-elastic data at medium energies. The extent to which the proton contribution to the spin asymmetry of ^{3}He can be neglected, can be envisaged by a look at the proton momentum distributions for spins parallel and antiparallel to the target, cf. Fig. 41 where they are plotted against the light cone momentum fraction. The spin dependence is seen to be quite small. Also shown in Fig. 41 are the corresponding curves for the neutron. The neutron curves answer the important question, how large the probability is of having a neutron with spin antiparallel to the nuclear spin. One sees that n_{3-} is very small as compared to n_{3+} but somewhat broader since it comes from components in the ^{3}He wave function with a larger high momentum tail than the dominant S-wave.

Fig. 42 shows typical results for $g_1(^3\mathrm{He})(x,Q^2)$ as compared to $g_1^n(x,Q^2)$ at some unknown (small) value of Q^2. The curves are given only up to $x \approx 0.9$ because above this value the calculation becomes unreliable. In fact, nuclear effects are expected to become much larger as $x \to 1$.

It is possible to summarize the effects of higher wave functions S' and D in ^{3}He by means of the following procedure: In a pure S wave state the nucleon polarizations are given by $P_n^{(+)} = 1$, $P_n^{(-)} = 0$ and $P_p^{(+)} = P_p^{(-)} = \frac{1}{2}$, whereas for a three-body wave function containing S, S' and D waves, one has

$$P_n^{(\pm)} = \tfrac{1}{2} \pm \tfrac{1}{2} \mp \Delta \,, \tag{6.114}$$

$$P_p^{(\pm)} = \tfrac{1}{2} \mp \Delta' \,, \tag{6.115}$$

where $\Delta = \frac{1}{3}[P_{S'} + 2P_D]$ and $\Delta' = \frac{1}{6}[P_D - P_{S'}]$. From world calculations on the three-body system one obtains, in correspondence with the experimental value of the binding energy of ^{3}He, $\Delta = 0.07 \pm 0.01$ and $\Delta' = 0.014 \pm 0.002$ [280]. Thus if the S' and D waves are considered and Fermi motion and binding effects are disregarded, one can write

$$g_1(^3\mathrm{He})(x,Q^2) = 2p_p g_1^p(x,Q^2) + p_n g_1^n(x,Q^2) \,, \tag{6.116}$$

$$A_{^3\vec{\mathrm{H}}\mathrm{e}} = 2f_p p_p A_{\vec{p}} + f_n p_n A_{\vec{n}} \,, \tag{6.117}$$

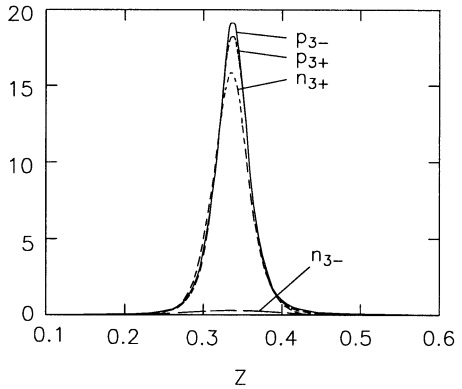

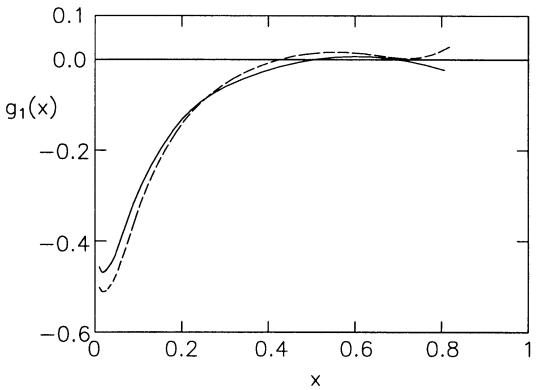

Fig. 41. Nucleon momentum distributions for spins parallel and antiparallel to a ^{3}He target, with z being the momentum fraction of the nucleon in the target, according to [582].

Fig. 42. $g_1(x)$ for neutron (dashed) and ^{3}He (solid curve) according to [582].

where $f_{p(n)}(x,Q^2) = F_2^{p(n)}(x,Q^2)/[2F_2^p(x,Q^2) + F_2^n(x,Q^2)]$ is the proton (neutron) dilution factor, $A_{\vec{p}(\vec{n})}(x,Q^2) = g_1^{p(n)}(x,Q^2)/F_1^{p(n)}(x,Q^2)$ is the proton (neutron) asymmetry and $p_{p(n)}$ are the effective nucleon polarizations

$$p_p = P_p^{(+)} - P_p^{(-)} = -0.028 \pm 0.004\ , \tag{6.118}$$

$$p_n = P_n^{(+)} - P_n^{(-)} = 0.86 \pm 0.02\ . \tag{6.119}$$

The above values correspond to Eqs. (6.114) and(6.115), while the spin-dependent spectral functions of [582,182,183] yield $p_p = -0.030$ and $p_n = 0.88$.

For future precision studies one will have to go even beyond those approximations, because there may be modifications due to the presence of the nuclear medium, like nuclear swelling and binding effects on the parton densities. These effects have recently been studied by [368] by depleting the parton densities of [309] at small Q^2 and evolving them according to the AP evolution equations. It turns out that these effects are far below the present experimental accuracy, but may be of some relevance for future precision measurements, in particular at small $x \leq 0.03$.

6.11. Direct photons and related processes in proton collisions using polarized beams

The most interesting prospect for polarized high energetic proton experiments is the possibility to determine $\delta g(x,\mu_F^2)$ from the process $\vec{p}\vec{p} \to \gamma X$ with a high energetic photon in the final state [248,135,112,341,342,171,201–203,331,297,136,148,471,345,541]. In unpolarized scattering hard photons are known to be a clean probe of the gluon distribution, because they can be directly detected, without undergoing fragmentation. Note that for physics beyond the standard model direct photon production is claimed to be a signal to probe compositeness. The observation of spin asymmetries in this reaction could help to disentangle the structure of new contact interactions [135].

On the parton level the process is induced in lowest order by the annihilation of light quarks $q\bar{q} \to \gamma g$ and by the Compton scattering $gq \to \gamma q$, and is strongly dependent on the magnitude of $\delta g(x, \mu_F^2)$ with $\mu_F \sim p_T^\gamma$. It may also be possible to determine $\delta g(x, \mu_F^2)$ from high-p_T jet production, but this process has a large background of quark-initiated events $qq \to partons$, and is therefore less sensitive to $\delta g(x, \mu_F^2)$. In Table 5 and Fig. 43 the parton level asymmetries for all the possible partonic $2 \to 2$ processes including direct photon production are shown as a function of the scattering angle in the parton-cms. The figure clearly shows that the photon processes are expected to give potentially large effects.

From a theoretical point of view it would also be interesting to study the production of high-p_T muon pairs in Drell–Yan processes involving off-shell photons, because they offer the possibility to obtain additional information, namely about the polarization of the final state. This information

Table 5
Tree-level partonic cross sections and asymmetries $\hat{a}_{LL}^{ij} = d\Delta\hat{\sigma}_{ij}/d\hat{\sigma}_{ij}$, including direct photon production processes [80,134]. A factor of $\pi\alpha_s^2/\hat{s}^2$ has been factored out of the jet cross sections and $\pi e_Q^2\alpha\alpha_s/\hat{s}^2$ has been factored out of the single-photon cross sections

	$\frac{d\hat{\sigma}_{ij}}{d\hat{t}}$	$\hat{a}_{LL}^{ij}$
$qq \to qq$	$\frac{4}{9}\left(\frac{\hat{s}^2+\hat{u}^2}{\hat{t}^2} + \frac{\hat{s}^2+\hat{t}^2}{\hat{u}^2} - \frac{2\hat{s}^2}{3\hat{t}\hat{u}}\right)$	$\frac{(\hat{s}^2-\hat{u}^2)/\hat{t}^2 + (\hat{s}^2-\hat{t}^2)/\hat{u}^2 - \frac{2}{3}\hat{s}^2/\hat{t}\hat{u}}{(\hat{s}^2+\hat{u}^2)/\hat{t}^2 + (\hat{s}^2+\hat{t}^2)/\hat{u}^2 - \frac{2}{3}\hat{s}^2/\hat{t}\hat{u}}$
$qq' \to qq'$	$\frac{4}{9}\frac{\hat{s}^2+\hat{u}^2}{\hat{t}^2}$	$\frac{\hat{s}^2-\hat{u}^2}{\hat{s}^2+\hat{u}^2}$
$q\bar{q} \to q'\bar{q}'$	$\frac{4}{9}\frac{\hat{t}^2+\hat{u}^2}{\hat{s}^2}$	-1
$q\bar{q} \to q\bar{q}$	$\frac{4}{9}\left(\frac{\hat{t}^2+\hat{u}^2}{\hat{s}^2} + \frac{\hat{s}^2+\hat{u}^2}{\hat{t}^2} - \frac{2\hat{u}^2}{3\hat{s}\hat{t}}\right)$	$\frac{(\hat{s}^2-\hat{u}^2)/\hat{t}^2 - (\hat{t}^2+\hat{u}^2)/\hat{s}^2 + \frac{2}{3}\hat{u}^2/\hat{s}\hat{t}}{(\hat{s}^2+\hat{u}^2)/\hat{t}^2 + (\hat{t}^2+\hat{u}^2)/\hat{s}^2 - \frac{2}{3}\hat{u}^2/\hat{s}\hat{t}}$
$q\bar{q} \to gg$	$\frac{32}{27}\frac{\hat{t}^2+\hat{u}^2}{\hat{t}\hat{u}} - \frac{8}{3}\frac{\hat{t}^2+\hat{u}^2}{\hat{s}^2}$	-1
$qg \to qg$	$\frac{\hat{s}^2+\hat{u}^2}{\hat{t}^2} - \frac{4}{9}\frac{\hat{s}^2+\hat{u}^2}{\hat{s}\hat{u}}$	$\frac{\hat{s}^2-\hat{u}^2}{\hat{s}^2+\hat{u}^2}$
$gg \to q\bar{q}$	$\frac{1}{6}\frac{\hat{t}^2+\hat{u}^2}{\hat{t}\hat{u}} - \frac{3}{8}\frac{\hat{t}^2+\hat{u}^2}{\hat{s}^2}$	-1
$gg \to gg$	$\frac{9}{2}\left(3 - \frac{\hat{s}\hat{u}}{\hat{t}^2} - \frac{\hat{s}\hat{t}}{\hat{u}^2} - \frac{\hat{t}\hat{u}}{\hat{s}^2}\right)$	$\frac{-3+2\hat{s}^2/\hat{t}\hat{u} + \hat{t}\hat{u}/\hat{s}^2}{3-\hat{s}\hat{u}/\hat{t}^2 - \hat{s}\hat{t}/\hat{u}^2 - \hat{t}\hat{u}/\hat{s}^2}$
$qg \to q\gamma$	$-\frac{1}{3}\left(\frac{\hat{s}}{\hat{u}} + \frac{\hat{u}}{\hat{s}}\right)$	$\frac{\hat{s}^2-\hat{u}^2}{\hat{s}^2+\hat{u}^2}$
$q\bar{q} \to \gamma g$	$\frac{8}{9}\left(\frac{\hat{t}}{\hat{u}} + \frac{\hat{u}}{\hat{t}}\right)$	-1

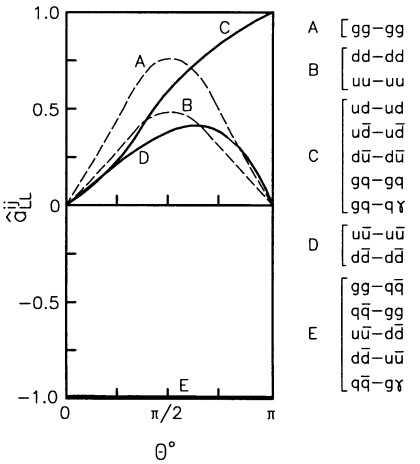

Fig. 43. Parton level asymmetries, including direct photon production processes as a function of the scattering angle in the parton-cms [134].

can be obtained, for example, from the angular distribution of the leptons [171,443,442]. For an interesting application of HO QCD to this process see [160]. The Drell–Yan process will be discussed later on in this subsection.

The observable to be measured in direct-γ production is the inclusive double-spin asymmetry

$$A_{LL}^{\gamma} = \frac{\sigma^{\Leftarrow}_{\Leftarrow} + \sigma^{\Rightarrow}_{\Rightarrow} - \sigma^{\Leftarrow}_{\Rightarrow} - \sigma^{\Rightarrow}_{\Leftarrow}}{\sigma^{\Leftarrow}_{\Leftarrow} + \sigma^{\Rightarrow}_{\Rightarrow} + \sigma^{\Leftarrow}_{\Rightarrow} + \sigma^{\Rightarrow}_{\Leftarrow}} \tag{6.120}$$

which reduces to

$$A_{LL}^{\gamma} = \frac{\sigma^{\Leftarrow}_{\Leftarrow} - \sigma^{\Leftarrow}_{\Rightarrow}}{\sigma^{\Leftarrow}_{\Leftarrow} + \sigma^{\Leftarrow}_{\Rightarrow}} \tag{6.121}$$

if parity is conserved. In Eqs. (6.120) and (6.121) it has been assumed that both protons are longitudinally polarized. More explicitly, this asymmetry is given by

$$A_{LL}^{\gamma} d\sigma = \sum_{i,j=q,\bar{q},g} \frac{1}{1+\delta_{ij}} \int dx\, dx' \{\delta f_i(x,\mu_F^2)\delta f_j'(x',\mu_F^2)\hat{a}_{LL}^{ij} d\hat{\sigma}_{ij} + (i \leftrightarrow j)\} \tag{6.122}$$

where $d\hat{\sigma}_{ij}$ and $d\sigma$ are the parton and hadron level cross sections for unpolarized direct-γ production,

$$d\sigma = \sum_{i,j=q,\bar{q},g} \frac{1}{1+\delta_{ij}} \int dx\, dx' \{f_i(x,\mu_F^2) f_j'(x',\mu_F^2) d\hat{\sigma}_{ij} + (i \leftrightarrow j)\} \ . \tag{6.123}$$

The prime refers to the second proton and f_i and f_j' are the parton densities in the two protons. $\hat{a}_{LL}^{ij}$ are the subprocess asymmetries, which along with the $d\hat{\sigma}_{ij}$ can be calculated in perturbative QCD, cf. Table 5 and Fig. 43. The product $d\Delta\hat{\sigma}_{ij} = \hat{a}_{LL}^{ij} d\hat{\sigma}_{ij}$ is much larger for the Compton subprocess than for the annihilation subprocess. This can be deduced from the explicit form of the

parton level cross sections and asymmetries in Table 5 and Fig. 43. The Compton subprocess has a positive $\hat{a}_{LL}^{i=g,j=q}$ and leads to a positive contribution to A_{LL}^{γ} which is proportional to δg. For the annihilation subprocess one has a negative $\hat{a}_{LL}^{ij}$. Since the Compton subprocess dominates on the parton level, one has usually a much smaller asymmetry A_{LL}^{γ} (positive or negative) if $\delta g(x,\mu_F^2)$ is small, in contrast to a large $\delta g(x,\mu_F^2)$. In the latter case one encounters large positive values of A_{LL}^{γ} up to 50%. In Fig. 44 A_{LL}^{γ} is shown as a function of the photon-p_T for the two scenarios of large and small δg. It is clearly seen that a measurement of A_{LL}^{γ} provides a valuable probe of $\delta g(x,\mu_F^2)$.

Higher order QCD corrections to the process $\vec{p}\vec{p} \to \gamma X$ involving polarized proton beams have been calculated by [201–204,331]. A particular feature is the appearance of the process $gg \to \gamma q\bar{q}$ whose contribution to the spin asymmetry is of the order of $[\delta g]^2$. The calculation has been performed in the framework of dimensional regularization, in which case special care is needed for the treatment of γ_5. In Refs. [201–203] the method of dimensional reduction was used and it was shown how to circumvent the problems with γ_5. In Ref. [331] the 't Hooft–Veltman scheme was used and the dependence of the cross section on isolation cuts has been examined carefully. Isolation cuts are needed in order to single out isolated direct hard photons from the background [332,330].

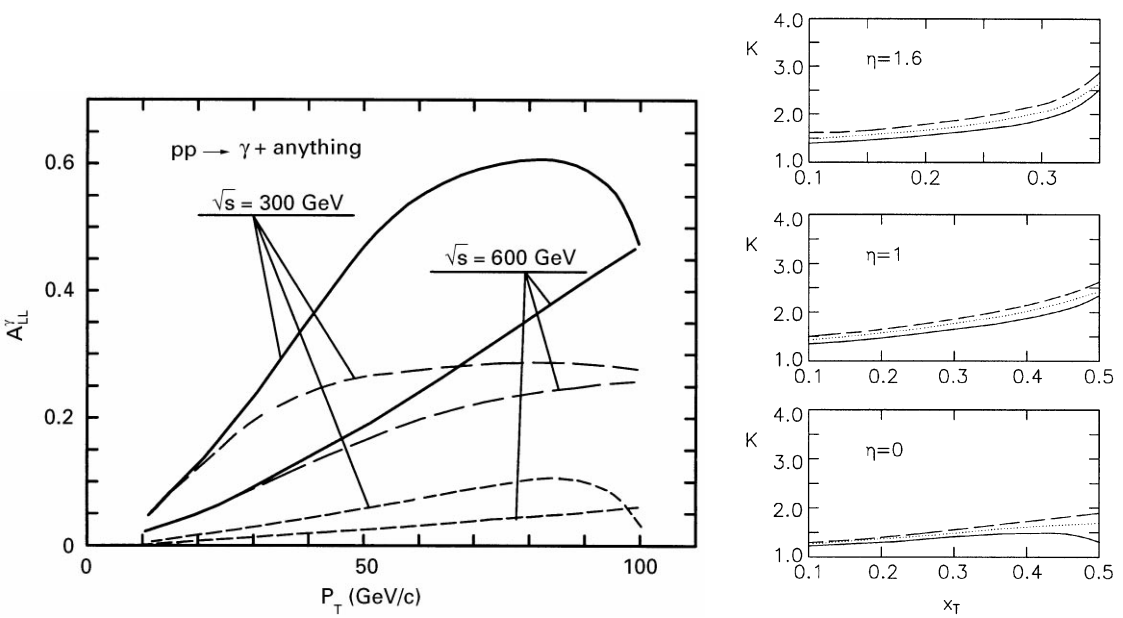

Fig. 44. A_{LL}^{γ} at 300 GeV pp beam energy with a large $\delta g(x,\mu_F^2)$ as a function of p_T at $\theta_{cm} = 45^\circ$ (upper solid curve) and $\theta_{cm} = 90^\circ$ (dashed curve). The lower short-dashed curve corresponds to a small $\delta g(x,\mu_F^2)$ at $\theta_{cm} = 90^\circ$. The factorization scale was chosen to be $\mu_F = p_T$. Analogous curves for $\sqrt{s} = 600$ GeV are also included [136].

Fig. 45. K-factor for direct γ-production in $\vec{p}\vec{p}$-collisions as a function of x_T [201–203]. The following parameters have been used: $\Lambda_{\overline{MS}} = 200$ MeV with 4 flavors and the parton distributions of Ref. [56] (set 1) with $\mu_F = p_T$. The three curves correspond to $\sqrt{s} = 38$(dashed), 100(dotted) and 500(solid) GeV.

The results of the calculation of Ref. [201–203] are shown in Fig. 45 in the form of the K-factor for the polarized cross section defined as the ratio of $K = (\mathrm{LO} + \mathrm{HO})/\mathrm{LO}$. The K-factors are shown as a function of $x_\mathrm{T} = 2p_\mathrm{T}/\sqrt{s}$ for various values of the rapidity η and $\sqrt{s}$. Note that for the p_T distribution one has the simple formula

$$\frac{\mathrm{d}(\Delta)\sigma}{\mathrm{d}p_\mathrm{T}^2} = \sum_{i,j=q,\bar{q},g} \frac{1}{1+\delta_{ij}} \int_{4p_\mathrm{T}^2/S}^1 \mathrm{d}x(\delta) f_i(x,p_\mathrm{T}^2) \int_{4p_\mathrm{T}^2/xS}^1 \mathrm{d}x'(\delta) f_j'(x',p_\mathrm{T}^2) \frac{\mathrm{d}(\Delta)\hat{\sigma}_{ij\to\gamma X}}{\mathrm{d}p_\mathrm{T}^2} \tag{6.124}$$

where $\mathrm{d}(\Delta)\hat{\sigma}/\mathrm{d}p_\mathrm{T}^2 = (\mathrm{d}(\Delta)\hat{\sigma}/\mathrm{d}\hat{t})\hat{s}/(\hat{t}-\hat{u})$ and $\mathrm{d}(\Delta)\hat{\sigma}/\mathrm{d}\hat{t}$ was given in Table 5. One finds in Fig. 45 that in all cases the HO corrections are positive and quite large, in particular at large x_T. Due to the quite large K-factors there is some ambiguity of the results concerning the unknown higher orders. However, this ambiguity is much smaller than the dependence on the input parton densities as has been discussed in [201–203] with a rather moderate gluon density as input. It should be kept in mind, however, that strictly speaking, there is a very subtle interplay between the magnitude of the K-factor in various schemes and the correct choice of the HO parton densities, the value of Λ, etc. Similar results have been obtained, using more recent polarized parton densities, for prompt photon production at a future fixed target HERA-$\vec{N}$ (phase II) experiment ($\sqrt{s} = 39$ GeV) [332] and at the RHIC collider ($\sqrt{s} = 50$–500 GeV) [330].

Instead of direct photon production one may consider production of W's or Z's balanced by a jet. These processes are very closely related because they involve analogous diagrams. The heavy vector bosons show the additional feature that spin asymmetries arise even if only one of the proton beams is polarized ('single-spin asymmetries'). This is due to the axialvector couplings involved and essentially a parity violating effect, as already discussed in Section 6.8. The corresponding single-spin asymmetry

$$A_\mathrm{L}^{W,Z} = (\sigma_\Rightarrow - \sigma_\Leftarrow)/(\sigma_\Rightarrow + \sigma_\Leftarrow) \tag{6.125}$$

involves products of polarized and unpolarized parton densities and would in principle be sensitive to $\delta g(x, m_W^2)$. It turns out, however, that the QCD matrix element for 'Compton' scattering of a polarized gluon on an unpolarized quark and associated production of a $W^\pm$ is very small, so that the single-spin asymmetries are not very suitable for the determination of $\delta g(x, m_W^2)$. They *are*, however, suitable for the determination of the various flavor contributions $\delta u(x, m_W^2)$ and $\delta d(x, m_W^2)$ to the proton spin. Recent analyses of these effects can be found in [519,135,137,541] where it is shown that the process $p\vec{p} \to W^\pm X$ at RHIC can lead to asymmetries around 50% with a large effect in the asymmetry for $p\vec{p} \to W^- X$ if $\delta\bar{u}(x, m_W^2)$ is small.

We now come to the Drell–Yan process [503,341,342,171,136,471,578,405,292]. We shall discuss here only the case of longitudinal polarization. The NLO corrections to the Drell–Yan process in transversely polarized hadron–hadron collisions have been analyzed in [200,573]. The longitudinal spin asymmetry $A_\mathrm{LL}^{\gamma^*} = \mathrm{d}\Delta\sigma/\mathrm{d}m_{ll}^2/\mathrm{d}\sigma/\mathrm{d}m_{ll}^2$ is defined in analogy to A_LL^γ but depends on the invariant mass of the produced lepton pair m_{ll}^2. The polarized and unpolarized cross sections are given by

$$\frac{\mathrm{d}(\Delta)\sigma}{\mathrm{d}m_{ll}^2} = (-)\frac{4\pi\alpha^2}{9sm_{ll}^2} \int \frac{\mathrm{d}x_1}{x_1}\frac{\mathrm{d}x_2}{x_2} \Bigg\{ \sum_{q=u,d,s} e_q^2(\delta) q(x_1, m_{ll}^2)(\delta)\bar{q}(x_2, m_{ll}^2)[\delta(1-z)$$

$$+\frac{\alpha_s(m_{ll}^2)}{2\pi}\theta(1-z)(\delta)c_{q\bar{q}}] + \frac{\alpha_s(m_{ll}^2)}{2\pi}\theta(1-z)(\delta)c_{qg}(z)(\delta)g(x_2,m_{ll}^2)$$

$$\times \sum_{q=u,d,s} e_q^2[(\delta)q(x_1,m_{ll}^2) + (\delta)\bar{q}(x_1,m_{ll}^2)]\Bigg\} + (1 \leftrightarrow 2) \tag{6.126}$$

where $z = m_{ll}^2/x_1 x_2 s$ and the coefficient functions $(\delta)c_{q\bar{q}}(z)$ and $(\delta)c_{qg}(z)$ for the relevant subprocesses are in the $\overline{\text{MS}}$-scheme given by [288,503,578,472–474,405,292]

$$c_{q\bar{q}}(z) = C_F\left\{\left(\frac{2}{3}\pi^2 - 8\right)\delta(1-z) + 4(1+z^2)\left(\frac{\ln(1-z)}{1-z}\right)_+ - 2\frac{1+z^2}{1-z}\ln z\right\}, \tag{6.127}$$

$$c_{qg}(z) = T_R\left[(2z^2-2z+1)\ln\frac{(1-z)^2}{z} - \frac{7}{2}z^2 + 3z + \frac{1}{2}\right], \tag{6.128}$$

$$\delta c_{q\bar{q}}(z) = -c_{q\bar{q}}(z)\,, \tag{6.129}$$

$$\delta c_{qg}(z) = -T_R\left[(2z-1)\ln\frac{(1-z)^2}{z} - \frac{3}{2}z^2 - z + \frac{5}{2}\right]. \tag{6.130}$$

It should be noted that the dominant $O(\alpha_s)$ contribution in Eq. (6.126) comes from the δ-function term in Eq. (6.127). It gives a large effect for the cross sections but not in the double-spin asymmetry $A_{LL}^{\gamma^*}$. The asymmetry is shown in Fig. 46 as a function of $\tau = m_{ll}^2/s$ for different parametrizations of $\delta g(x,m_{ll}^2)$ and $\delta s(x,m_{ll}^2)$. The asymmetries in Fig. 46 are of the same order of magnitude as for the direct photon process. In principle, one could expect that both the δg and the δs terms contribute about the same to the asymmetry. However, due to the smallness of $\delta c_{qg}(z)$ it turns out that the sea polarization plays a stronger role in $A_{LL}^{\gamma^*}$ than the gluon polarization. This is in contrast to the direct photon process which depends strongly on the polarization of the gluons.

Fig. 46 also shows that the Drell–Yan process could be very valuable to determine the strange sea polarization in the proton. A measurement of the sign of $A_{LL}^{\gamma^*}$ would already give information

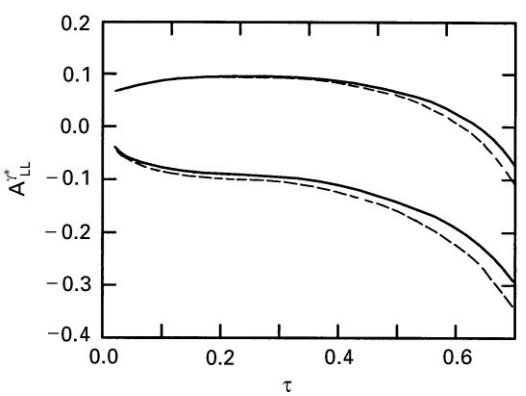

Fig. 46. Predicted Drell–Yan spin asymmetry as a function of $\tau = Q^2/s$ at $\sqrt{s} = 100$ GeV for large positive and large negative δs [171]. Dashed curves are the asymmetries without gluon contributions.

about the sign of δs. Unfortunately, the Drell–Yan process has a larger background than the direct photon production so that the expected statistical errors at RHIC are larger.

Finally, we want to add some remarks about the prospects of determining the polarized parton densities from jet production in hadronic collisions, in particular at RHIC [80,502,248,135,136,429, 178,500,501,230,541]. Quite in general many features of unpolarized jet production can be applied directly to the polarized case. For example, at low p_T the main contribution comes from gluon–gluon scattering so that this region is particularly suited for attempts to determine the (polarized) gluon density. Secondly, event rates and statistics are much larger than in direct photon production. A drawback is that the signatures are less clear as will be discussed below.

One has in principle the possibility to analyze single-jet production $\vec{p}\vec{p} \to JX$ as well as di-jet production $\vec{p}\vec{p} \to J_1 J_2 X$. The latter is more difficult but not impossible to analyze in a high-luminosity machine like RHIC. The single jet spin asymmetry can be calculated as a function of rapidity and transverse momentum of the jet from the ratio of the polarized and the unpolarized cross sections. These are given by

$$E\frac{\mathrm{d}(\Delta)\sigma}{\mathrm{d}^3 p} = \frac{1}{\pi}\sum_{i,j}\frac{1}{1+\delta_{ij}}\int_{x_{\min}}^{1}\mathrm{d}x_1\frac{2x_1x_2}{2x_1 - x_T e^{y}}\left[(\delta)f_i(x_1,\mu_F^2)(\delta)f_j(x_2,\mu_F^2)\frac{\mathrm{d}(\Delta)\hat{\sigma}_{ij}}{\mathrm{d}\hat{t}} + (i\leftrightarrow j)\right], \quad (6.131)$$

where $x_T = 2p_T/\sqrt{s}$, $x_{\min} = x_T e^{y}/(2 - x_T e^{-y})$ and $x_2 = x_1 x_T e^{-y}/(2x_1 - x_T e^{y})$. The explicit expressions for the parton cross sections can be found in Table 5 [80,134] and the corresponding parton level spin asymmetries are shown in Fig. 43. For all the dominant subprocesses the corresponding asymmetries $\hat{a}_{LL}^{ij}$ are positive, except for $q\bar{q}$ annihilation. This leads to positive values of the single jet double spin asymmetry $A_{LL}^{\mathrm{jet}} = \mathrm{d}\Delta\sigma/\mathrm{d}p_T/\mathrm{d}\sigma/\mathrm{d}p_T$ in the low p_T-range where the gluons dominate. The parton level spin asymmetries combine with suitable parton densities to give the proton asymmetries. These are shown in Fig. 47 as a function of p_T at two values of the beam energy for a $\delta g(x,\mu_F^2)$, $\mu_F \sim p_T$, with a small and with a large first moment $\Delta g(\mu_F^2)$ [136]. The significance of the small and intermediate p_T regime for the determination of δg is clearly exhibited. If $\Delta g(p_T^2)$ is large

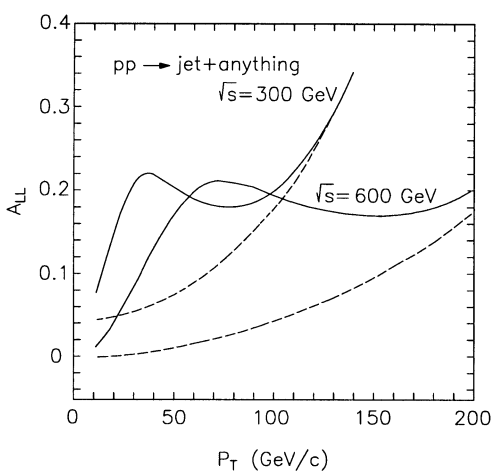

Fig. 47. Predicted spin asymmetries for single jet production as a function of the jet-p_T for a large (solid curve) and small (dashed curve) first moment $\Delta g(p_T^2)$ and two values of the RHIC beam energy [136].

one can easily have asymmetries of about 20% in the small p_T range. The relatively large RHIC luminosity $\mathscr{L} \sim 10^{32}\,\mathrm{cm}^{-2}\,\mathrm{s}^{-1}$ in combination with the large jet cross sections make the signal in principle large and will lead to small statistical errors [541]. The drawback of this method to determine $\delta g(x, p_T^2)$ is the large background of soft events in the small p_T region.

Let us now discuss 2-jet production. An observable to study is the distribution in the 2-jet invariant mass, $M_{JJ} = 2p_T \cosh(y^*)$, where $y^* = \frac{1}{2}(y_1 - y_2)$. It is given by

$$\frac{\mathrm{d}(\Delta)\sigma}{\mathrm{d}M_{JJ}} = \frac{M_{JJ}^3}{2s}\sum_{i,j}\int_{-Y}^{+Y}\mathrm{d}y_1\int_{y_m}^{y_M}\mathrm{d}y_2\frac{(\delta)f_i(x_1,\mu_F^2)(\delta)f_j(x_2,\mu_F^2)}{\cosh(y^*)}\frac{\mathrm{d}(\Delta)\hat{\sigma}_{ij}}{\mathrm{d}\hat{t}}\ , \tag{6.132}$$

where $x_{1,2} = \tau \mathrm{e}^{\pm(1/2)(y_1+y_2)}$, $y_m = \max(-Y, \log\tau - y_1)$ and $y_M = \min(-Y, -\log\tau - y_1)$. $Y \sim 1$ is a cutoff on the jet rapidity and τ is defined as $\tau = \sqrt{(4p_T^2/s)}\cosh^2(y^*)$. Numerical results for these distributions have been presented in [178,136]. They are shown in Fig. 48 as a function of the jet pair mass for two values of the proton energy and two choices of the polarized gluon density, a small $\delta g(x, M_{JJ}^2)$ (dashed curve) and a large one (solid curve). At intermediate values of the jet pair mass $M_{JJ} \sim 100$ GeV, they are even more sensitive to the magnitude of the polarized gluon density than the single jet p_T distribution but somewhat more difficult to measure. One may also examine di-jet production and higher order effects [230].

6.12. Spin-dependent structure functions and parton densities of the polarized photon

Structure functions $F_i^\gamma(x, Q^2)$ and parton densities $f^\gamma(x, Q^2)$, with $f = q, \bar{q}, g$, of unpolarized, i.e. helicity averaged, photons are theoretically well known (see, e.g. [303,316] and references therein) and experimentally rather well studied (see, e.g., [110,262] and references therein). In contrast to the (un)polarized hadronic parton densities studied so far, these densities obey *in*homogeneous evolution equations where the inhomogeneous LO and NLO terms $k_{i=q,g}^{(0,1)}(x)$ derive from the point-like splitting of the photon into quarks and gluons which can be calculated from first QED principles. In LO, $\gamma \to q\bar{q}$ gives rise to $k_q^{(0)}$, and $k_g^{(0)} = 0$. They are the so-called driving terms which

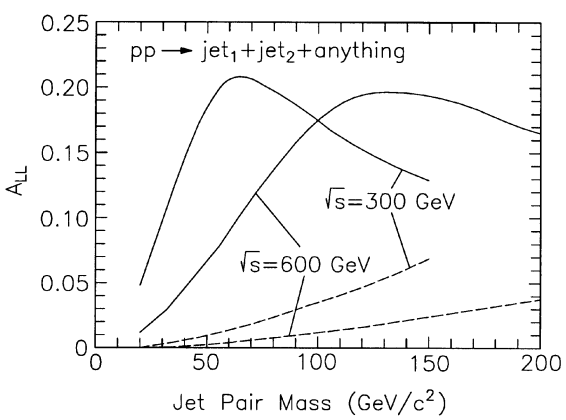

Fig. 48. Predicted asymmetries A_{LL} for dijet production as a function of the jet pair mass for two values of the proton energy and two choices of the polarized gluon density, a small $\delta g(x, M_{JJ}^2)$ (dashed curve) and a large one (solid curve) [136].

uniquely fix the 'point-like' (inhomogeneous) solution of the evolution equations for the parton densities of the photon, once a specific input scale Q_0^2 for $\alpha_s(Q_0^2)$ has been chosen. This is in contrast to the conventional 'hadronic' (homogeneous) part of the general solution, which derives from the common homogeneous evolution equations and which requires some nonperturbative hadronic (vector-meson-dominance oriented) input $f_{\rm had}^{\gamma}(x,Q_0^2)$.

In complete analogy to the helicity-averaged case $f^{\gamma}=f_{+}^{\gamma}+f_{-}^{\gamma}$, the spin-dependent parton densities of a longitudinally (more precisely, circularly) polarized photon are defined as [373,349,583,465]

$$\delta f^{\gamma}(x,Q^2)=f_{+}^{\gamma}(x,Q^2)-f_{-}^{\gamma}(x,Q^2) \tag{6.133}$$

with f_{+}^{γ} (f_{-}^{γ}) denoting the parton densities in the photon aligned (anti-aligned) with its helicity. As in Eq. (4.11), they satisfy the general positivity constraints

$$|\delta f^{\gamma}(x,Q^2)|\leq f^{\gamma}(x,Q^2)\ . \tag{6.134}$$

Similarly to Eq. (4.5), the polarized photon structure function is given by

$$g_1^{\gamma}(x,Q^2)=\frac{1}{2}\sum_q e_q^2[\delta q^{\gamma}(x,Q^2)+\delta\bar{q}^{\gamma}(x,Q^2)]+\mathrm{O}(\alpha_s,\alpha) \tag{6.135}$$

where the NLO (two-loop) contributions [555] have been suppressed. Note that $\delta q^{\gamma}=\delta\bar{q}^{\gamma}$ and $\delta q^{\gamma}=\mathrm{O}(\alpha/\alpha_s)$ in LO. In Bjorken x-space, these photonic parton densitites obey the following inhomogeneous LO evolution equations:

$$\frac{\mathrm{d}}{\mathrm{d}t}\delta q_{\rm NS}^{\gamma}(x,Q^2)=\frac{\alpha}{2\pi}\delta k_{\rm NS}^{(0)}(x)+\frac{\alpha_s(Q^2)}{2\pi}\delta P_{\rm NS}^{(0)}\otimes\delta q_{\rm NS}^{\gamma}\ , \tag{6.136}$$

$$\frac{\mathrm{d}}{\mathrm{d}t}\begin{pmatrix}\delta\Sigma^{\gamma}(x,Q^2)\\ \delta g^{\gamma}(x,Q^2)\end{pmatrix}=\frac{\alpha}{2\pi}\begin{pmatrix}\delta k_q^{(0)}\\ 0\end{pmatrix}+\frac{\alpha_s(Q^2)}{2\pi}\begin{pmatrix}\delta P_{qq}^{(0)} & 2f\delta P_{qg}^{(0)}\\ \delta P_{gq}^{(0)} & \delta P_{gg}^{(0)}\end{pmatrix}\otimes\begin{pmatrix}\delta\Sigma^{\gamma}\\ \delta g^{\gamma}\end{pmatrix}, \tag{6.137}$$

which are a straightforward generalization of Eqs. (4.12) and (4.19), taking into account the 'point-like' photon splitting $\gamma\to q$ which gives rise to the inhomogeneous terms: $\delta k_q^{(0)}=\delta P_{q\gamma}^{(0)}$ can be obtained, apart from obvious charge factors, from $\delta P_{qg}^{(0)}$ in (4.21) by multiplying it with $2fN_c/T_R$:

$$f(e_q^2-\langle e^2\rangle)^{-1}\delta k_{\rm NS}^{(0)}=\langle e^2\rangle^{-1}\delta k_q^{(0)}=6f(2x-1)\ , \tag{6.138}$$

where $\langle e^2\rangle\equiv f^{-1}\sum_q e_q^2$. Furthermore, $\delta k_g^{(0)}=\delta P_{g\gamma}^{(0)}=0$ has been used in (6.137). The LO equations (6.135)–(6.137) can be straightforwardly extended to NLO [555] where the $\mathrm{O}(\alpha\alpha_s)$ terms $\delta k_q^{(1)}$ and $\delta k_g^{(1)}$ derive from the $C_F T_f$ pieces of $2f\delta P_{qg}^{(1)}$ and $\delta P_{gg}^{(1)}$ in (A.4) and (A.6) in the Appendix, respectively, multiplied by fN_c/T_f.

The evolution equations (6.136) and (6.137) are most conveniently solved in Mellin n-moment space (cf. Eqs. (4.22) and (4.23)) where the solutions can be given analytically and one can easily keep track of the contributions stemming form different powers of α_s in order to avoid terms beyond the order considered. The inversion to Bjorken x-space is again straightforward with the help of (4.37). The general solution decomposes into

$$\delta f^{\gamma,n}(Q^2)=\delta f_{\rm PL}^{\gamma,n}(Q^2)+\delta f_{\rm had}^{\gamma,n}(Q^2) \tag{6.139}$$

with the 'point-like' (inhomogeneous) solution being given by

$$\delta q^{\gamma,n}_{\mathrm{NS,PL}}(Q^2) = \frac{4\pi}{\alpha_s(Q^2)}\,[1 - L^{1-(2/\beta_0)\delta P^{(0)n}_{\mathrm{NS}}}]\frac{1}{1-(2/\beta_0)\delta P^{(0)n}_{\mathrm{NS}}}\frac{\alpha}{2\pi\beta_0}\delta k^{(0)n}_{\mathrm{NS}}\ , \tag{6.140}$$

$$\begin{pmatrix}\delta\Sigma^{\gamma,n}_{\mathrm{PL}}(Q^2)\\ \delta g^{\gamma,n}_{\mathrm{PL}}(Q^2)\end{pmatrix} = \frac{4\pi}{\alpha_s(Q^2)}\,[1 - L^{1-(2/\beta_0)\delta\hat{P}^{(0)n}}]\frac{1}{1-(2/\beta_0)\delta\hat{P}^{(0)n}}\frac{\alpha}{2\pi\beta_0}\begin{pmatrix}\delta k^{(0)n}_q\\ 0\end{pmatrix} \tag{6.141}$$

and the 'hadronic' (homogeneous) solution given by

$$\delta q^{\gamma,n}_{\mathrm{NS,had}}(Q^2) = L^{-(2/\beta_0)\delta P^{(0)n}_{\mathrm{NS}}}\delta q^{\gamma,n}_{\mathrm{NS,had}}(Q^2_0) \tag{6.142}$$

$$\begin{pmatrix}\delta\Sigma^{\gamma,n}_{\mathrm{had}}(Q^2)\\ \delta g^{\gamma,n}_{\mathrm{had}}(Q^2)\end{pmatrix} = L^{-(2/\beta_0)\delta\hat{P}^{(0)n}}\begin{pmatrix}\delta\Sigma^{\gamma,n}_{\mathrm{had}}(Q^2_0)\\ \delta g^{\gamma,n}_{\mathrm{had}}(Q^2_0)\end{pmatrix}, \tag{6.143}$$

where $L(Q^2) \equiv \alpha_s(Q^2)/\alpha_s(Q^2_0)$. Note that the 'hadronic' solutions are formally identical to the usual ones in Eqs. (4.27) and (4.28) since they are derived from the homogeneous part of the evolution equations (6.136) and (6.137). The structure of these LO solutions can be straightforwardly extended to NLO [316,555] by using the techniques discussed in Section 4.2 being based on the (two-loop) evolution matrix in Eq. (4.56).

The new ingredient of these solutions is the 'point-like' component which is driven by the inhomogeneous (photon splitting) terms $\delta k^{(0)}_i$ in Eqs. (6.140) and (6.141), i.e. they uniquely determine the 'point-like' parton densities in the photon once an appropriate input scale Q^2_0 has been specified. This is in contrast to the hadronic components in (6.142) and (6.143) which require, as usual, also the specification of the input densities $\delta f^{\gamma}_{\mathrm{had}}(x,Q^2_0)$. In general, one expects the 'point-like' $\delta f^{\gamma}_{\mathrm{PL}}(x,Q^2)$ to be dominant in the large-x region since the $\delta k^{(0)}_i$ in (6.140) and (6.141) increase as $x \to 1$ according to (6.138). This is in contrast to the 'hadronic' $\delta f^{\gamma}_{\mathrm{had}}(x,Q^2)$ where the (VMD oriented) input $\delta f^{\gamma}_{\mathrm{had}}(x,Q^2_0) \sim (1-x)^a$ as $x \to 1$. Such expectations have been well established in the case of unpolarized photons [316,317,110,262]. For polarized photons, several model calculations have been performed for estimating $\delta f^{\gamma}(x,Q^2)$ in LO [373,349,583]. More recently, in order to obtain a somewhat more realistic estimate for the theoretical uncertainties in the experimentally entirely unknown δf^{γ}, two very different scenarios were considered in [322,324]: The 'minimal scenario' is characterized by the input

$$\delta f^{\gamma}_{\mathrm{had}}(x,\mu^2) = 0\ , \tag{6.144}$$

whereas the 'maximal scenario' is defined by the other extreme input

$$\delta f^{\gamma}_{\mathrm{had}}(x,\mu^2) = f^{\gamma}_{\mathrm{had}}(x,\mu^2)\ , \tag{6.145}$$

with $Q^2_0 \equiv \mu^2 = \mu^2_{\mathrm{LO}} = 0.25\,\mathrm{GeV}^2$ and the unpolarized LO GRV photon densities $f^{\gamma}_{\mathrm{had}}(x,\mu^2)$ have been taken from [317]. It should be mentioned that the range of such VMD inspired inputs can be further restricted [324] by using the sum rule

$$\int_0^1 \delta q^{\gamma}(x,Q^2)\,\mathrm{d}x = 0 \tag{6.146}$$

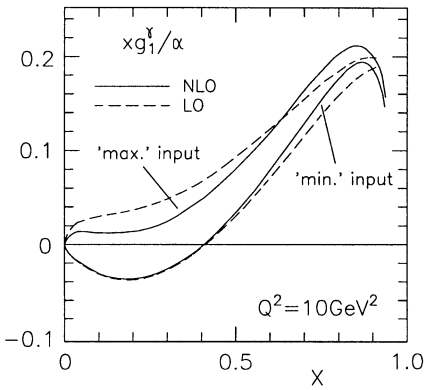

Fig. 49. LO and NLO expectations for g_1^γ according to the 'minimal' and 'maximal' inputs in Eqs. (6.144) and (6.145), respectively [555]. The results shown correspond to $f = 3$ flavors.

which derives from the vanishing of the first moment of g_1^γ due to the conservation of the electromagnetic current (gauge invariance) [243,98,487,279]. Note that the 'minimal' hadronic input (6.144) satisfies this sum rule automatically. Such inputs have also been implemented in NLO [555] and some typical expectations for g_1^γ are shown in Fig. 49. The strong increase in the large-x region is typical for the 'point-like' $\delta q_{\text{PL}}^\gamma$ as discussed above. The 'minimal' scenario is 'point-like' throughout the entire x-region due to the vanishing hadronic input in (6.144). The possible importance of the hadronic components in Eqs. (6.142) and (6.143) is illustrated by the 'maximal' scenario results in Fig. 49 which involve an additional hadronic component due to the input (6.145).

Several suggestions have been proposed to measure $\delta f^\gamma(x, Q^2)$ at polarized ep [321,322] and e^+e^- colliders [320]. It has been discussed already in Section 6.2 that these resolved photon contributions could amount up to 20% of the total charm production cross section at future $\vec{e}\vec{p}$ collisions [553,554]. The situation improves for photoproduction of jets at future $\vec{e}\vec{p}$ colliders ($\sqrt{s_{\gamma p}} \approx 200\,\text{GeV}$) where the much larger size of the resolved photon contributions to single-inclusive jet and, in particular, dijet production [553,554] could give rise to experimentally testable signatures of the parton densities of a polarized photon in the not too distant future.

7. Nonperturbative approaches to the proton spin

In Section 5 it was shown that the apparent smallness of the flavor singlet axial vector current matrix element is due either to a negative sea polarization or to a positive gluon polarization. However, no theoretical prediction for the value of this matrix element was presented. There are several nonperturbative approaches which try to remedy this situation [564,531,174,116] and lattice calculations have been attempted as well [459,326,213,287]. The well-established isotriplet Goldberger–Treiman (GT) relation

$$g_{\text{A}}^3(0) = \frac{\sqrt{2} f_\pi}{2M} g_{\pi_3 NN}, \quad f_\pi = 132\,\text{MeV}\ , \tag{7.1}$$

which fixes the axial coupling $g_A^3(0) = g_A = 1.2573 \pm 0.0028$ in terms of the strong coupling constant $g_{\pi_3 NN}$, has inspired [564,531] to generalize it to the isosinglet $U_A(1)$ case to see if one can learn something about the magnitude of $g_A^0 S_\mu \equiv \langle PS|\bar{\psi}\gamma_\mu\gamma_5\psi|PS\rangle$. [9]

Many discussions on the isosinglet GT relation were mainly motivated by the desire to understand why the g_A^0 inferred from the EMC experiment is so small ($g_A^0 \sim 0.15$, cf. Table 6) [167,282–285,523,96,564,531,194,350,389,117,164,242,260–262,575,452,532,488,245]. At first sight, the $U_A(1)$ GT relation seems not to be in the right ballpark, as the naive SU(6) quark-model prediction yields far too large a value $g_A^0 \approx 0.80$, because $g_{\eta_0 NN} = (\sqrt{6}/5) g_{\pi_3 NN}$. It was then suggested that the 'physical' η_0-nucleon coupling is composed of a bare coupling $g^{(0)}_{\eta_0 NN}$ and a coupling between the ghost field and the nucleon. In QCD the ghost field $G \equiv \partial_\mu K^\mu$, cf. (5.38), is necessary to solve the $U_A(1)$ problem. It mixes with the bare η_0 and is allowed to have a direct $U_A(1)$ invariant interaction g_{GNN} with the proton. Unfortunately, the definition of this coupling is not free of ambiguities. For example, it is sometimes assumed in the literature to be the coupling between the glueball and the nucleon. Furthermore, unlike in the case of $g_A^3(0)$, the predictive power of the $U_A(1)$ GT relation is partly lost by the mixing. In chirally invariant schemes (like the off-shell regularization discussed in Section 5) one may at least identify the term $(\sqrt{n_f} f_\pi/2M) g_{\eta_0 NN}$ with the total quark spin inside the proton $\Delta\Sigma_{\text{off}}$, cf. Section 5 [531].

It is interesting to obtain a scheme-independent relation. For the isotriplet GT relation this is possible because it holds irrespective of the light quark masses. For $m_\pi^2 \neq 0$ it may be derived from PCAC, while in the chiral limit $g_A^3(q^2)$ can be related to an isotriplet form factor which in turn receives nonvanishing pion pole contributions. By the same token it can be shown in the OZI limit that the isosinglet $U_A(1)$ GT relation [531,532]

$$g_A^0(0) = (\sqrt{3} f_\pi/2M) g^{(0)}_{\eta_0 NN} \tag{7.2}$$

remains totally scheme and mass independent. In Eq. (7.2) $g^{(0)}_{\eta_0 NN}$ is a bare unphysical coupling between η_0 and the nucleon. The η_0 is not a physical meson but constructed from the mass eigenstates via [523,96,174]

$$\begin{pmatrix} \pi_3 \\ \eta_8 \\ \eta_0 \end{pmatrix} = \begin{pmatrix} 1 & \theta_1 \cos\theta_3 + \theta_2 \cos\theta_3 & \theta_1 \sin\theta_3 - \theta_2 \cos\theta_3 \\ -\theta_1 & \cos\theta_3 & \sin\theta_3 \\ \theta_2 & -\sin\theta_3 & \cos\theta_3 \end{pmatrix} \begin{pmatrix} \pi_0 \\ \eta \\ \eta' \end{pmatrix}, \tag{7.3}$$

where $\theta_1 = -0.016$, $\theta_2 = -0.0085$ and $\theta_3 = -18.5^\circ$ are the mixing angles of the π–η system [245]. Consequently, the complete (= isotriplet + octet + singlet) GT relation in terms of physical coupling constants reads

$$\begin{aligned} g_A^3(0) = \frac{\sqrt{2} f_\pi}{2M} g_{\pi_3 NN} = \frac{\sqrt{2} f_\pi}{2M} [& g_{\pi NN} \pm g_{\eta' NN}(\theta_1 \sin\theta_3 - \theta_2 \cos\theta_3) \\ & \pm g_{\eta NN}(\theta_1 \cos\theta_3 + \theta_2 \sin\theta_3)] \,, \end{aligned} \tag{7.4}$$

[9] Note that in Section 5 a different notation was used, namely $A_0 S_\mu = \Delta\Sigma_{\text{on}} S_\mu = \langle PS|\bar{\psi}\gamma_\mu\gamma_5\psi|PS\rangle$ and $g_A^3(0) = g_A/g_V$. Further, in Section 6.6 an isotriplet form factor $G_1^3(Q^2)$ has been introduced which is normalized differently than $g_A^3(Q^2)$, namely $G_1^3(Q^2) = \frac{1}{2} g_A^3(Q^2)$.

$$g_A^8(0) = \frac{\sqrt{6}f_\pi}{2M} g_{\eta_8 NN} = \frac{\sqrt{6}f_\pi}{2M}(g_{\eta NN}\cos\theta_3 + g_{\eta' NN}\sin\theta_3 \mp g_{\pi NN}\theta_1)\ , \tag{7.5}$$

$$g_A^0(0) = \frac{\sqrt{3}f_\pi}{2M} g^{(0)}_{\eta_0 NN} = \frac{\sqrt{3}f_\pi}{2M}(g_{\eta' NN}\cos\theta_3 - g_{\eta NN}\sin\theta_3 \pm g_{\pi NN}\theta_2) + \cdots\ , \tag{7.6}$$

where the upper sign is for the proton and the lower sign for the neutron and the ellipses in the last relation are related to the ghost coupling to be discussed below.

Although the isosinglet GT relation is scheme invariant, the interpretation of the η_0 field is scheme dependent. When the $SU(6)$ quark model is applied to the coupling $g^{(0)}_{\eta_0 NN}$ the predicted g_A^0 is too large, $g_A^0 = 0.80$. This can be resolved by applying the $SU(6)$ model to the physical coupling $g_{\eta_0 NN}$ rather than to $g^{(0)}_{\eta_0 NN}$. One receives a two-component expression [531]

$$g_A^0(0) = \frac{\sqrt{3}f_\pi}{2M}\left(g_{\eta_0 NN} - \frac{1}{2\sqrt{3}} m^2_{\eta_0} f_\pi g_{GNN}\right) \tag{7.7}$$

where g_{GNN} is the coupling defined in the effective QCD nucleon Lagrangian

$$\mathscr{L} = \cdots + \frac{g_{GNN}}{4M}\partial^\mu GTr(\bar{N}\gamma_\mu\gamma_5 N) + \frac{\sqrt{3}}{f_\pi}(\partial K)\eta_0 + \cdots\ , \tag{7.8}$$

where $\partial K = (1/\sqrt{3})m^2_{\eta_0} f_\pi \eta_0 + \frac{1}{12} g_{GNN} m^2_{\eta_0} f_\pi \partial^\mu Tr(\bar{N}\gamma_\mu\gamma_5 N)$ is the anomaly with matrix element $\langle N|\partial K|N\rangle = \frac{1}{3}\langle N|\partial^\mu J^5_\mu|N\rangle = (1/\sqrt{3}) f_\pi g^{(0)}_{\eta_0 NN} = \frac{2}{3} M g_A^0(0)$.

In order to arrive at a small EMC-like g_A^0 one may now argue that there is a cancellation between the two terms of Eq. (7.7). This is reminiscent to the situation in the perturbative framework where a cancellation between $\Delta\Sigma$ and Δg was proposed to explain the spin EMC effect. However, there is no scheme independent identification between the various terms of the perturbative and nonperturbative approach.

Some authors have questioned [245] the $U(1)$ GT relation (7.7) but it seems that it survives as long one takes proper care of all the mixing effects. Still it should be stressed that until now no direct experimental confirmation exists, and in this sense it is one of the speculations from the realms of nonperturbative QCD. The point is that both sides of the relation are difficult to grab. The right-hand side (i.e. the low-energy couplings) cannot really be determined from low energy data, because g_{GNN} is not known.[10] Even the ηNN couplings are only known within large errors, cf. the discussion in [174]. For example, a determination of $g_{\eta' NN}$ using F, D and θ_3 values gives $g_{\eta' NN} = 3.4$ [175] whereas an estimate of the $\eta' \to 2\gamma$ decay rate through the baryon triangle contributions yields $g_{\eta' NN} = 6.3$ [81]. The analysis of the NN potential gives $g_{\eta' NN} = 7.3$ [233] while the forward NN scattering analyzed by dispersion relations gives $g_{\eta' NN} < 3$ [335]. On the other hand, the only chance to determine g_{GNN} is from the polarized DIS data via the $U(1)$ GT

[10] There is a conjecture, though no proof, that g_{GNN} is given by the quark sea contribution ('disconnected insertion'), $-(m^2_{\eta_0} f^2_\pi/4M) g_{GNN} = \Delta(u_s + \bar{u}) + \Delta(d_s + \bar{d}) + \Delta(s + \bar{s}) \approx 3\Delta(s + \bar{s})$ [174]. Furthermore, g_{GNN} could in principle be obtained from low-energy baryon–baryon scattering in which an additional $SU(3)$ singlet contact interaction arises from the ghost interaction but this is very difficult to measure [523].

relation. However, there is no direct identification between g_{GNN} and an observable defined in high-energy scattering. Therefore, the whole issue remains somehow speculative and undecided.

Another attempt to obtain information on the proton spin matrix elements from low energy meson properties was recently made by Birkel and Fritzsch [116]. They used the masses and properties of the axial vector mesons with quantum numbers $J^{PC} = 1^{++}$. The spectrum consists of the isoscalar mesons $f_1(1285)$, $f_1(1420)$ and $f_1(1510)$. After correcting for the mixing with the isovector $a_1(1260)$ and the strange isodoublet K_1, the f_1 mesons can be written as a linear combination of the three axial vector states $|N\rangle = (1/\sqrt{2})|\bar{u}u + \bar{d}d\rangle$, $|S\rangle = |\bar{s}s\rangle$ and an exotic gluonic meson state $|G\rangle$. The latter interpretation arises because within the $SU(3)$ multiplets one expects only two isoscalar mesons f_i. A relatively large mixing is found between the N, S and G state, and this is due largely to the effect of the anomaly and reminiscent of what happens in the case of pseudoscalar mesons [116]. On the basis of this analysis one may use the idea of 'axial vector' dominance to get information on the proton spin matrix element. The basic relation is

$$\langle P|\bar{q}\gamma_\mu\gamma_5 q|P\rangle = \sum_A \frac{\langle 0|\bar{q}\gamma_\mu\gamma_5 q|A\rangle\langle AP|P\rangle}{m_A^2 - k^2}\bigg|_{k^2=0} \tag{7.9}$$

where $\langle 0|\bar{q}\gamma_\mu\gamma_5 q|A\rangle$ denotes the transition element of the axial vector current between the vacuum and the axial vector meson A, and $\langle AP|P\rangle$ describes the coupling of the axial vector meson to the proton. The 4-momentum transfer is k. Using Eq. (7.9) one can relate $\Delta(u + \bar{u})$, $\Delta(d + \bar{d})$ and $\Delta(s + \bar{s})$ to the corresponding couplings of axial vector mesons. Without the gluonic state, a relatively large value of the flavor singlet quark spin contribution $\Delta\Sigma \approx 0.52$ is obtained. Inclusion of the gluonic state $\langle GP|P\rangle \neq 0$ leads to numbers of the order $\Delta\Sigma \approx 0.25$ in accordance with DIS data. However, just as in the U(1) Goldberger Treiman model there is a free parameter which has to be fixed, namely the coupling g_{GP} to the proton defined by $\langle GP|P\rangle = \mathrm{i}g_{GP}\bar{u}(P)\gamma_\nu\gamma_5 u(P)\varepsilon^\nu$ where ε^ν is the polarization vector of the gluonic state. It is hard to determine g_{GP} experimentally. The above number $\Delta\Sigma \approx 0.25$ corresponds to the choice $g_{GP} = 19$.

A more general method to obtain nonperturbative results on the proton spin matrix elements is lattice gauge theory. After the 1987 EMC spin surprise, several attempts were made to compute Δg and $\langle PS|\bar{\psi}\gamma_\mu\gamma_5\psi|PS\rangle$ using lattice QCD. A first direct calculation of $\Delta\Sigma$ was made in [459] but without final results. Successful lattice computations in the quenched approximation were published recently [213,287,326]. A more ambitious program of computing the polarized structure functions g_1 and g_2 is also feasible and encouraging early results were reported in [326]. In Refs. [213,287], the scheme and gauge invariant matrix elements $\langle PS|\bar{\psi}\gamma_\mu\gamma_5\psi|PS\rangle$ were calculated. The results are shown in Table 6 and compared to the experimental data, although one should keep in mind that the computation of sea quark contributions might be questionable in a quenched calculation. Varying the quark masses it was found in [287] that a considerable amount of the sea contributions is mass independent and therefore must be induced by gluons through the ABJ anomaly. This is in accord with arguments based on perturbative QCD and presented in Section 5. However, for a direct lattice computation of Δg one would need gauge configurations on a sizeable lattice not available so far. It is hoped that lattice results for Δg will be available in the near future. The most recent improvement in this field is the implementation of an improved action by the DESY/HLRZ collaboration [115], i.e. of a systematic procedure for the removal of all terms linear in the lattice spacing a from the lattice observables [558,456,457] which reduces the cutoff errors

Table 6
Axial couplings and quark spin content of the proton from lattice calculations according to [174]. Note that the 'experimental' singlet results are model and scheme dependent and the stated numbers refer to an average of recent LO and NLO($\overline{\text{MS}}$) analyses. In the off-shell scheme one obtains [48], for example, $g_A^0 = 0.45(9)$; see, however, Ref. [9]

	[213]	[287]	Experiment
g_A^0	0.25(12)	0.18(10)	0.22(6)
g_A^3	1.20(10)	0.985(25)	1.2573(28)
g_A^8	0.61(13)	—	0.579(25)
$\Delta(u+\bar{u})$	0.79(11)	0.638(54)	0.80(3)
$\Delta(d+\bar{d})$	−0.42(11)	−0.347(46)	−0.46(3)
$\Delta(s+\bar{s})$	−0.12(1)	−0.109(30)	−0.12(3)
F	0.45(6)	0.382(18)	0.459(8)
D	0.75(11)	0.607(14)	0.798(8)

order by order in a, yielding a better extrapolation towards the continuum limit [115]. This O(a) improved lattice theory yields, for example, $\Delta u_v = 0.841(52)$ and $\Delta d_v = -0.245(15)$, in reasonable agreement with DIS experiments (cf. Section 6.1 and Ref. [9]).

There are also attempts to explain the smallness of g_A^0, i.e. of $\Delta\Sigma$, by invoking the Skyrme model [143,255,518,184,185,114]. Here one argues [143,255] that the quark singlet contribution $\Delta\Sigma$ is suppressed by $1/N_c$ while $\Delta(q+\bar{q}) = \text{O}(1)$ for each separate flavor, and a similar suppression should hold for $\Delta g(Q^2)$. Besides the fact that the precise relation between the Skyrme model and QCD is somewhat unclear, in particular in connection with Δg, this explanation has been questioned within the Skyrme model itself [518,184,185,114,381].

Alternatively, QCD sum rules [109,179] result in a similarly small total singlet spin contribution $g_A^0 = 0.1$–0.2 [343,354]. Again, a distinction between the individual $\Delta\Sigma$ and Δg contributions cannot be obtained.

Very promising appears to be the chiral soliton approach towards the structure of the nucleon within the effective chiral theory [226,227,580] which allows for the calculation of the *full* x-dependence of the structure functions and the parton densities from first principles, in contrast to just their nth moments as obtained in the nonperturbative approaches discussed so far. The relevance and influence of the instanton vacuum on low-energy QCD observables has been emphasized in particular by Diakonov et al. [226,227] who calculated unpolarized (spin-averaged) and polarized valence and sea input densities from first principles at the typical scale which is set by the inverse average instanton size $\bar{\rho}$, i.e. $Q_0^2 \approx \bar{\rho}^{-2} \approx 0.36\,\text{GeV}^2$. The instanton size remains the only free parameter in the calculation, and its inverse serves as an UV cutoff of the nonrenormalizable effective chiral field theory. What makes this approach quite promising is the fact that it predicts [226,227], besides the valence densities, a *valence*-like input (unpolarized) sea density in the small-x region at $Q_0^2 = 0.3$–$0.4\,\text{GeV}^2$, which forms the basic ingredient for understanding and predicting all small-x unpolarized DIS HERA-data [11,38,40,220,222,223] from first principles, i.e. pure (parameter-free) QCD dynamics [316,318,319]. So far, the polarized sea and the (un)polarized gluon input densities have not been calculated. It is in particular the valence-like gluon densities [319,309], being $1/N_c$ 'suppressed', which have to come out sizeable at $Q_0^2 = 0.3$–$0.5\,\text{GeV}^2$.

Otherwise the chiral soliton approach does not refer to a perturbative (twist-2) input scale reachable by perturbative RG evolutions, but instead would refer to some nonperturbative input quark scale which cannot be reached by perturbative evolutions. Nevertheless, for the time being, the chiral soliton approach appears to be a realistic model of nonperturbative QCD which might eventually link, from first principles, the confining regime to the perturbative sector.

It should be stressed that only future (dedicated) experiments can ultimately decide about the physical reality of the various theoretical ideas and scenarios discussed so far. It should be kept in mind, however, that all realistic experiments are of course sensitive to the explicit x-dependence of the polarized parton densities $\delta f(x,Q^2)$ and in most cases are not directly related to their first moments $\Delta f(Q^2)$.

8. Transverse polarization

8.1. The structure function g_2

For pure photon exchange the complete polarization part of the hadron tensor is antisymmetric and given by, cf. (2.1),

$$W^A_{\mu\nu} = \mathrm{i}\frac{M}{Pq}\varepsilon_{\mu\nu\rho\sigma}q^\rho\left\{S^\sigma g_1(x,Q^2) + \left(S^\sigma - \frac{Sq}{Pq}P^\sigma\right)g_2(x,Q^2)\right\}. \tag{8.1}$$

For longitudinal polarization and at Q^2 much larger than M^2 the g_1-piece gives the dominant contribution, with g_2 being suppressed by a factor x^2M^2/Q^2 according to (2.7). However, for a nucleon transversely polarized with respect to the beam direction, $W^A_{\mu\nu}$ is proportional to $(xM/Q)(g_1+g_2)$, so that g_1 and g_2 enter with equal coefficients but the whole contribution is down by a factor xM/Q with respect to g_1 in the longitudinally polarized case. This can again be derived from the inclusive, fully differential cross section Eq. (2.7). Therefore g_2 being measured at SLAC and DESY will have much less accuracy than g_1. Furthermore, it is really the combination $g_T \equiv g_1 + g_2$ which is the 'transverse spin structure function' although, for obvious reasons, one usually refers just to g_2 [375].

Since g_2 is related to a transverse polarization, it is not easy to find a partonic interpretation [45,383,348]: in a transversely polarized nucleon, the quark spin operator projected along the nucleon spin, $\Sigma_T = \gamma_0\gamma_5 \not{S}_T$ with $\not{S}_T \sim \gamma_1$, does not commute with the free quark Hamiltonian $H_0 = \alpha_z p_z$ and thus there exists no energy eigenstate $|p_z\rangle$ such that $\Sigma_T|p_z\rangle = \lambda_T|p_z\rangle$. Therefore, Σ_T is a 'bad' operator and depends on the dynamics. Nevertheless, a transverse-spin *average* for quarks can still be defined in the nucleon and it is just $g_T \equiv g_1 + g_2$ which is sensitive to the quark–gluon interactions – a clear sign that no simple parton interpretation can be made for it [375,382]. This is in contrast to the longitudinally polarized nucleon, where the quark helicity operator $\Sigma_{||} = \gamma_0\gamma_5\not{S}_{||}$, with $\not{S}_{||} \sim \gamma_3$, commutes with H_0 and thus $g_1(x)$ measures directly the quark helicity distribution. It should be further noted, that g_2 vanishes [45,382] for a free (massless or massive) quark, i.e. for a pointlike nucleon, and thus g_2 cannot be expressed as an incoherent sum over free on-shell partons. The partons must be interacting and/or virtual in order to contribute to g_2. Therefore, g_2 will serve as a unique probe of 'higher twist' (twist $\equiv$ dimension-spin $= 3$) as well.

Regardless of the difficulties with a partonic interpretation, g_2 itself consists of a twist-2 (g_2^{WW}) and a twist-3 ($\bar{g}_2$) contribution,

$$g_2 = g_2^{WW} + \bar{g}_2 \tag{8.2}$$

both of which can a priori contribute the same order of magnitude. The twist-2 contribution g_2^{WW} is the so-called 'Wandzura–Wilczek' piece [576] which will be discussed first: In leading twist-2, the same operators in Eqs. (4.72) and (4.73) contribute to g_1 and g_2; therefore one has, through the optical theorem [375,382],

$$\int_0^1 dx\ x^{n-1} g_2^{WW}(x,Q^2) = -\frac{1}{2}\frac{n-1}{n}\sum_i M_i^n E_i^n(Q^2/\mu^2,\alpha_s), \quad n = 1,3,5,\ldots \tag{8.3}$$

By comparing this with the corresponding equation for g_1, (4.75), one obtains [576]

$$\int_0^1 dx\ x^{n-1}\left[\frac{n-1}{n} g_1(x,Q^2) + g_2^{WW}(x,Q^2)\right]^{\text{twist-2}} = 0\ . \tag{8.4}$$

This can be inverted to Bjorken-x space to give

$$g_2^{WW}(x,Q^2) = -g_1(x,Q^2) + \int_x^1 \frac{dy}{y} g_1(y,Q^2)\ , \tag{8.5}$$

which is the so-called Wandzura–Wilczek relation [576]. This twist-2 expectation for g_2 and the present experimental results on g_1 are shown in Fig. 50. Note that the twist-2 Wandzura–Wilczek piece g_2^{WW} of g_2 obeys automatically the so-called Burkhardt–Cottingham sum rule [153], $\int_0^1 g_2^{WW}(x,Q^2)\,dx = 0$, which follows from Eqs. (8.4) or (8.5) and to which we shall return below.

It is a unique feature of g_2 that the higher twist term $\bar{g}_2$ in (8.2) is not suppressed by inverse powers of Q^2 and thus could in principle be equally important as the twist-2 contributions g_2^{WW} discussed so far. It should, however, be kept in mind that $\bar{g}_2$ vanishes for ultrarelativistic on-shell quarks where $S^\sigma \sim P^\sigma$, i.e. in this case there are not enough four vectors to form the

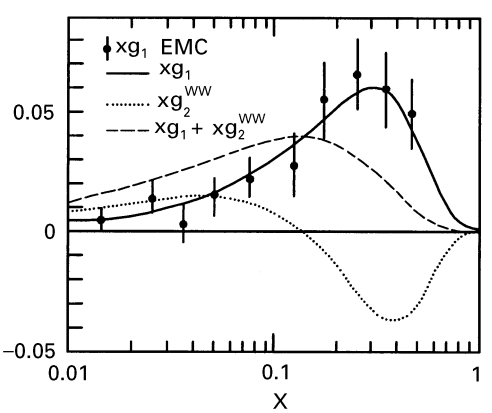

Fig. 50. Twist-2 expectations for the structure function $g_2^{WW}(x,Q^2 = 10\,\text{GeV}^2)$, using a parametrization of the EMC data (solid curve) [77,78] on $g_1^p(x,Q^2 = 10\,\text{GeV}^2)$, according to the Wandzura–Wilczek relation (8.5).

required antisymmetric combination in (8.1). Furthermore, one might naively expect $\bar{g}_2$ to be small because nonrelativistic corrections, being of the order m_q/M or m_q/Λ, are small for light quarks. Future experiments will prove to what extent this is actually the case. A considerable twist-3 contribution, however, might be due to the off-shellness of interacting quarks with virtuality k^2 where k^2/Λ^2 is not small [533,46,47,375,382]. On the other hand, within the covariant relativistic parton model approach it has been argued [374] that the quark virtuality k^2 is expected to be not sizeable and therefore deviations from the Wandzura–Wilczek relation (8.5) should be small. In the following we shall explain this argument, because it allows to get some physical insight into the properties of g_2. As a straightforward generalization of the unpolarized case [301], the covariant parton model expression for the antisymmetric part (8.1) of the hadron tensor is given by a convolution over the struck parton's momentum in the 'hand bag' diagram,

$$W^A_{\mu\nu}(q,P,S) = \sum_{s=\pm} \int \mathrm{d}^4k\, f_s(P,k,S) w^A_{\mu\nu,s}(q,k)\delta[(k+q)^2 - m^2]\ , \tag{8.6}$$

where f_s is some Lorentz-invariant hadronic wave function. The antisymmetric tensor for the parton–photon interaction is given by

$$w^A_{\mu\nu,\pm} = \tfrac{1}{4}\,\mathrm{tr}[(1 \mp \gamma_5 \not{n})(\not{k} + m)\gamma_\mu(\not{k} + \not{q} + m)\gamma_\nu] - (\mu \leftrightarrow \nu) = \pm\, \mathrm{i}m\varepsilon_{\mu\nu\alpha\beta} q^\alpha n^\beta \tag{8.7}$$

with n^β being the off-shell parton spin vector, $k\cdot n = 0$, $n^2 = -1$. Defining

$$\tilde{f}(P\cdot k, k^2) = -\frac{M}{k\cdot S}\frac{m}{\sqrt{k^2 - M^2k^4/(P\cdot k)^2}}(f_+ - f_-)\ , \tag{8.8}$$

a comparison of Eqs. (8.6) and (8.1) yields [374]

$$g_1(x) = \frac{\pi x}{8}\int \mathrm{d}k^2\, \mathrm{d}k_T^2\, \tilde{f}\left(x + \frac{k^2 + k_T^2}{xM^2}, k^2\right)\left(1 - \frac{k^2 + k_T^2}{x^2M^2}\right)\left(1 - \frac{2k^2}{x^2M^2 + k^2 + k_T^2}\right), \tag{8.9}$$

$$g_T(x) \equiv g_1(x) + g_2(x) = \frac{\pi x}{8}\int \mathrm{d}k^2\, \mathrm{d}k_T^2\, \tilde{f}\left(x + \frac{k^2 + k_T^2}{xM^2}, k^2\right)\frac{k_T^2}{x^2M^2} \tag{8.10}$$

for a longitudinally and transversely polarized photon, respectively. The last equation, (8.10), immediately proves that a finite transverse polarization result g_T can arise only for a nonvanishing parton transverse momentum $k_T^2 \neq 0$. Therefore, the EMC observation of a nonvanishing value of $\int_0^1 g_1(x)\,\mathrm{d}x$ is direct evidence for $k_T^2 \neq 0$ (via the Burkhardt–Cottingham sum rule $\int_0^1 g_2(x)\,\mathrm{d}x = 0$, to be discussed below). Furthermore, the second factor in parentheses in the integrand of Eq. (8.9) proportional to $2k^2$ violates the Wandzura–Wilczek sum rule and explicitly describes higher-twist corrections ($\bar{g}_2$) to it. In the absence of this term one easily derives from (8.9) and (8.10)

$$\frac{\mathrm{d}}{\mathrm{d}x}\,[g_1(x) + g_2(x)] = -\frac{1}{x}g_1(x) \tag{8.11}$$

and hence the Wandzura–Wilczek sum rule (8.5). There seems to be not much room for a sizeable $k^2 \neq 0$ since the first term in parentheses in the integrand of Eq. (8.9) gives rise to a zero for $g_1(x)$ if $k^2 + k_T^2 \approx x^2M^2$. The lack of experimental evidence for such a zero suggests that $k^2 + k_T^2 \ll x^2M^2$.

Ignoring the possibility that $k^2 < 0$ contributes appreciably, the second factor in parentheses in (8.9) is essentially unity, giving thus only small corrections to the Wandzura–Wilczek sum rule. It should be noted that $g_T(x)$ in Eq. (8.10) gets no additional off-mass-shell correction, besides from the one entailed in $\tilde{f}$, and that a measurement of g_1 gives a direct estimate [374] of the mean intrinsic k_T of partons as a function of x, in complete analogy with the unpolarized case [301].

Unfortunately, it must be noted that the scale Q^2, at which these results are supposed to hold, remains undetermined within the covariant parton model [301]. Therefore, these results have only a qualitative rather than a quantitative character. Furthermore, and more importantly, the virtuality k^2 alone is not a reliable measure for the importance of all possible twist-3 contributions to g_2, because of the appearance of additional twist-3 operators which describe quark–gluon correlations and explicitly quark-mass-dependent operators. These operators will now be discussed in some detail: In the OPE approach to g_2 the higher twist terms are determined by a tower of operators whose number increases with increasing moments. Therefore, Eqs. (8.3)–(8.5) are incomplete due to the neglect of $\bar{g}_2$ in (8.2), and in principle significant modifications of Fig. 50 might be expected. The modifications $\bar{g}_2$ due to higher twist can be described in terms of matrix elements of the following twist-3 operators [414,533,382,417,418]:

$$R_F^{\sigma\mu_1\cdots\mu_{n-1}} = \frac{\mathrm{i}^{n-1}}{n}\left[(n-1)\bar{\psi}\gamma_5\gamma^\sigma D^{\{\mu_1}\cdots D^{\mu_{n-1}\}}\psi - \sum_{l=1}^{n-1}\bar{\psi}\gamma_5\gamma^{\mu_l}D^{\{\sigma}D^{\mu_1}\cdots D^{\mu_{l-1}}D^{\mu_{l+1}}\cdots D^{\mu_{n-1}\}}\psi\right], \tag{8.12}$$

$$R_{m_q}^{\sigma\mu_1\cdots\mu_{n-1}} = \mathrm{i}^{n-2}\bar{\psi}m_q\gamma_5\gamma^\sigma D^{\{\mu_1}\cdots D^{\mu_{n-2}}\gamma^{\mu_{n-1}\}}\psi\ , \tag{8.13}$$

$$R_k^{\sigma\mu_1\cdots\mu_{n-1}} = \frac{1}{2n}(V_k - V_{n-1-k} + U_k + U_{n-1-k})\ , \tag{8.14}$$

where m_q in (8.13) represents the quark mass (matrix) and $\{\ \}$ means symmetrization over the Lorentz indices; furthermore, the flavor structure (λ_a) for the quark fields ψ has been suppressed for simplicity and the appropriate subtraction of trace terms is always implied in order to render the resulting operators traceless, i.e. of definite spin. The operators in (8.14) contain explicitly the gluon field strength $G_{\mu\nu}$ and its dual tensor $\tilde{G}_{\mu\nu} = \frac{1}{2}\varepsilon_{\mu\nu\alpha\beta}G^{\alpha\beta}$ and are given by

$$V_k = \mathrm{i}^n g S\bar{\psi}\gamma_5 D^{\mu_1}\cdots G^{\sigma\mu_k}\cdots D^{\mu_{n-2}}\gamma^{\mu_{n-1}}\psi\ ,$$

$$U_k = \mathrm{i}^{n-3} g S\bar{\psi}D^{\mu_1}\cdots\tilde{G}^{\sigma\mu_k}\cdots D^{\mu_{n-2}}\gamma^{\mu_{n-1}}\psi\ ,$$

where S means symmetrization over μ_i and g is the QCD coupling constant. It is a well-known fact [533,46,47,375,382,417,418] that these operators (8.12)–(8.14) are not independent and related through the 'equation of motion' operator

$$R_{\mathrm{eq}}^{\sigma\mu_1\cdots\mu_{n-1}} = \mathrm{i}^{n-2}\frac{n-1}{2n}S[\bar{\psi}\gamma_5\gamma^\sigma D^{\mu_1}\cdots D^{\mu_{n-2}}\gamma^{\mu_{n-1}}(\mathrm{i}\not{D} - m_q)\psi$$
$$+\ \bar{\psi}(\mathrm{i}\not{D} - m_q)\gamma_5\gamma^\sigma D^{\mu_1}\cdots D^{\mu_{n-2}}\gamma^{\mu_{n-1}}\psi]\ . \tag{8.15}$$

Making use of the identities $D_\mu = \frac{1}{2}\{\gamma_\mu, \not{D}\}$ and $[D_\mu, D_\nu] = gG_{\mu\nu}$ one can obtain the following relation for the twist-3 operators:

$$R_F^{\sigma\mu_1\cdots\mu_{n-1}} = \frac{n-1}{n} R_{m_q}^{\sigma\mu_1\cdots\mu_{n-1}} + \sum_{k=1}^{n-2} (n-1-k) R_k^{\sigma\mu_1\cdots\mu_{n-1}} + R_{\rm eq}^{\sigma\mu_1\cdots\mu_{n-1}} \ . \tag{8.16}$$

Leaving aside the Q^2 dependence for the time being, the moments of g_2 are given by

$$\int_0^1 {\rm d}x\, x^{n-1} g_2(x,Q^2) = \frac{1}{2}\frac{n-1}{n}(d_n - a_n), \quad n = 3,5,7,\ldots \tag{8.17}$$

which represents the generalization of the pure twist-2 relation (8.3) and where the contribution from the twist-2 operators is summarized in $a_n = \sum_i M_i^n E_i^n$ and d_n is the matrix element of the sum of all twist-3 operators contributing to the nth moment of g_2. Note that this formula is only true if one formally keeps R_F in the operator basis because the matrix element d_n is defined by

$$\langle P,S|R_F^{\sigma\mu_1\cdots\mu_{n-1}}|P,S\rangle = -\frac{n-1}{n} d_n (S^\sigma P^{\mu_1} - S^{\mu_1} P^\sigma) P^{\mu_2}\cdots P^{\mu_{n-1}} \ . \tag{8.18}$$

If one eliminates R_F from the basis via Eq. (8.16), the matrix elements of the operators R_{m_q}, R_k and $R_{\rm eq}$ will appear. Note further that there is *no* relation (8.17) for the first moment $n = 1$, because there is no twist-3 operator for $n = 1$. This is in contrast to g_1 whose first moment is fixed in the operator product expansion by the matrix element of the axial vector singlet current (cf. Section 5).

Combining Eq. (8.17) with the analogous pure twist-2 relation (4.75) for g_1,

$$\int_0^1 {\rm d}x\, x^{n-1} g_1(x,Q^2) = \frac{1}{2} a_n \ , \tag{8.19}$$

it has become customary to extract the pure twist-3 matrix element d_n:

$$d_n(Q^2) = 2\int_0^1 {\rm d}x\, x^{n-1}\left[g_1(x,Q^2) + \frac{n}{n-1} g_2(x,Q^2)\right] = 2\frac{n}{n-1}\int_0^1 {\rm d}x\, x^{n-1}\bar{g}_2(x,Q^2) \ , \tag{8.20}$$

where the latter equality follows from Eqs. (8.2) and (8.4). Being pure twist-3, $d_n(Q^2)$ is a direct probe of nonpartonic effects such as quark–gluon correlations. In other words, it is a direct measure of deviations from the (twist-2) Wandzura–Wilczek relation (8.5). Several experimental attempts at CERN (SMC [19]) and SLAC (E143 [5], E154 [8]) to observe such deviations by measuring $g_2^{p,n,d}(x,Q^2)$ via $A_{\rm T}$ in (2.13) did not result in any statistically relevant twist-3 contribution ($\bar{g}_2$) to g_2, i.e. present data are in agreement with the twist-2 Wandzura–Wilczek prediction derived from (8.5), $g_2(x,Q^2) \approx g_2^{\rm WW}(x,Q^2)$, at presently attainable values of Q^2. Qualitatively, the observed tendency is that $g_2^p(x,Q^2)$ is positive in the region of smaller x and negative in the region of larger x values, in agreement with the twist-2 Wandzura–Wilczek expectations [5] (cf. Fig. 50). More specifically, present measurements imply, for example, for the third $n = 3$ moment $d_3(Q^2 \approx 5\ {\rm GeV}^2)$ in Eq. (8.20) the following results [5,8]:

$$\begin{aligned} d_3^p &= (5.4 \pm 5.0)\times 10^{-3} \quad \text{(E143)} \ , \\ d_3^d &= (3.9 \pm 9.2)\times 10^{-3} \quad \text{(E143)} \ , \\ d_3^n &= (-10 \pm 15)\times 10^{-3} \quad \text{(E154, SLAC average)} \ . \end{aligned} \tag{8.21}$$

Comparing these results with bag model expectations [550,402,542–544], $d_3^p \approx (6 \text{ to } 18)\times 10^{-3}$, $d_3^d \approx (3 \text{ to } 7)\times 10^{-3}$ and $d_3^n \approx (-2.5 \text{ to } 0.3)\times 10^{-3}$ or with those obtained from QCD sum rules

[84,85,548], $d_3^p \approx (-9 \text{ to } 0)\times 10^{-3}$, $d_3^d \approx (-22 \text{ to } -8)\times 10^{-3}$ and $d_3^n \approx (-40 \text{ to } -15)\times 10^{-3}$, it becomes clear that for the time being there is no possibility to distinguish between different models.

As a side remark, it should be noted that the matrix elements d_n appear also in higher twist corrections to g_1. For example, the first moment of g_1 has an expansion [246,402]

$$\int_0^1 \mathrm{d}x\, g_1(x,Q^2) = \frac{1}{2}a_1 + \frac{M^2}{9Q^2}(a_3 + 4d_3 + 4f_3) + \mathrm{O}\left(\frac{M^4}{Q^4}\right). \tag{8.22}$$

The higher twist corrections in this result are not completely fixed by a_3 and d_3, but there is another matrix element f_3 of a twist-4 operator involved, defined by

$$\sum_i e_q^2 \langle PS|\bar{q}g\tilde{G}_{\alpha\beta}\gamma^\beta q|PS\rangle = 2M^2 f_3 S_\alpha\ . \tag{8.23}$$

This twist-4 matrix element f_3 has been estimated [84,85,246,400], partly from a QCD sum rule approach, with similar uncertainties as the above estimates of d_3.

There have been attempts to calculate also $g_2(x,Q^2)$ in the bag model [382,550,542–544]. The bag model does not contain gluon fields explicitly, but the boundary of the bag-confined quarks simulates the binding effect coming from quark–gluon and gluon–gluon interactions. Hence, the structure function g_2 calculated in the bag model includes higher twist effects and measures possibly large twist-3 matrix elements comparable in size to the twist-2 ones. Indeed, sizeable departures from the Wandzura–Wilczek relation [550] have been noted in an extended version of the MIT bag model [525]. They are mainly induced by the noncovariance of the relativistic bag model, which originates from the implementation of the bag boundary in the equation of motion. This is in spite of the fact that the average parton virtuality in the bag is small, from which one might erroneously conclude that $\bar{g}_2 \approx 0$ according to the covariant parton model discussed above. The predictions for g_2 [550] are shown in Fig. 51. It should, however, be emphasized that the results of such bound-state models are expected to hold at some nonperturbative bound-state scale, typically $Q^2 \sim \Lambda^2$. Strictly speaking, it is therefore not even possible to use these predictions as an input for an evolution to a larger scale $Q^2 \gtrsim 1\,\mathrm{GeV}^2$, unless one arbitrarily chooses the bag bound-state scale $Q^2 \gg \Lambda^2$, from where a perturbative evolution could be started. In order to demonstrate the importance of different scale effects, the EMC prediction for the twist-2 g_2^{WW} at $Q^2 \approx 10\,\mathrm{GeV}^2$ is taken from Fig. 50 and shown in Fig. 51 as well. The difference between the bag and EMC prediction is indeed very large, indicating that expectations from bound-state models are not very relevant for actual deep inelastic measurements. This is not very surprising since the bag predictions for g_1 [382] and for unpolarized structure functions [525] also disagree with actual deep inelastic measurements. Therefore, the large bag model prediction for $\bar{g}_2$ appears to be not too relevant for future experiments. In fact, other models [461,463,521] based on the light-cone quark model [234] give substantially different predictions for $g_2(x)$ than Fig. 51. According to these models, g_2 and $\bar{g}_2$ could also become strongly negative (of the order of -1) for $x < 0.1$. Therefore, it should be reemphasized that it is very important to check experimentally first the Wandzura–Wilczek relation (8.5) and then to extract $\bar{g}_2 \equiv g_2 - g_2^{\mathrm{WW}}$, despite the fact that present experiments [5,8,19] are, within large errors, consistent with a vanishing $\bar{g}_2(x,Q^2)$.

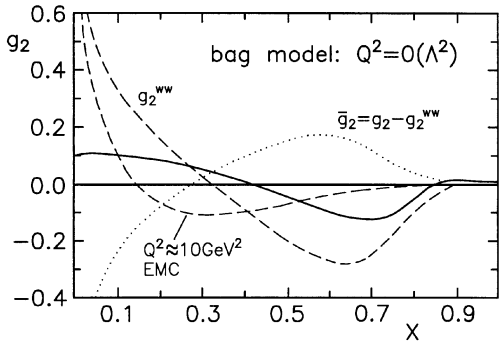

Fig. 51. Predictions for g_2 [550] of an extended (one-gluon exchange) version of the MIT bag model [525] using a bag radius $R = 0.7$ fm and spin-singlet and -triplet intermediate diquark masses of 0.56 and 0.8 GeV. The EMC prediction for g_2^{WW} of Fig. 50 is also shown.

We have already noted that for the first moment of g_2 there is no twist-3 operator within the light-cone OPE. This is a hint, though no proof, of the so-called 'Burkhardt–Cottingham (BC) sum rule' [153]

$$\int_0^1 \mathrm{d}x\, g_2(x, Q^2) = 0 \ . \tag{8.24}$$

This relation can be derived as a superconvergence relation based on Regge asymptotics (see [375] for a review). Recently, it has been shown by an explicit calculation that it is fulfilled in higher-order QCD [51,416]. The (more general but also more questionable) Regge proof was derived by considering the asymptotic behavior of the virtual Compton helicity amplitude A_2 related to g_2,

$$g_2(x, Q^2) = \frac{\nu^2}{2\pi M^4} \mathrm{Im}\, A_2(q^2, \nu) \ , \tag{8.25}$$

where $\nu \equiv P \cdot q$. The first moment of g_2 is given in terms of A_2 as

$$\int_0^1 \mathrm{d}x\, g_2(x, Q^2) = \frac{Q^2}{2\pi M^4} \int_{-q^2/2}^{\infty} \mathrm{d}\nu'\, \mathrm{Im}\, A_2(q^2, \nu') \ . \tag{8.26}$$

Combining Cauchy's theorem with crossing symmetry one finds the following dispersion relation for A_2:

$$A_2(q^2, \nu) = \frac{2}{\pi} \nu \int_{-q^2/2}^{\infty} \frac{\mathrm{d}\nu'}{\nu'^2 - \nu^2} \mathrm{Im}\, A_2(q^2, \nu') \ . \tag{8.27}$$

Burkhardt and Cottingham argue that all known Regge singularities contributing to A_2 have an intercept $\alpha(0)$ less than zero. This is equivalent to the statement that A_2 falls off to zero stronger than $1/\nu$ as $\nu \to \infty$ (more precisely $\sim \nu^{\alpha(0)-1}$ modulo logarithms). This implies that one can take the limit $\nu \to \infty$ under the ν' dispersion integral and obtains

$$A_2(q^2, \nu) \approx -\frac{2}{\pi \nu} \int_{-q^2/2}^{\infty} \mathrm{d}\nu'\, \mathrm{Im}\, A_2(q^2, \nu') \tag{8.28}$$

which is compatible with the rapid Regge fall-off only if the integral vanishes. Thus (8.26) implies the BC sum rule (8.24).

The derivation raises some questions. For example, Heimann [353] has argued that there might be contributions from multi-pomeron cuts which invalidate the assumption of intercept less than zero and would imply a highly singular behavior $g_2(x) \to x^{-2}$ as $x \to 0$ so that the first moment integral would not even converge. On the other hand, Regge cuts with branch points at $\alpha(0) \geq 0$ or specific nonpolynomial residue $J = 0$ fixed poles in Compton amplitudes [166,375] could invalidate the BC sum rule by terms of order at most $1/Q^2$. It is, therefore, possible that the BC sum rule might be restored asymptotically, as $Q^2 \to \infty$, because the residues of the Pomeron cuts fall off at $Q^2 \to \infty$. Apart from such an 'exotic' situation, the BC sum rule (8.24) appears to be very robust and is most probably true [375,382]. Furthermore, in the framework of perturbative QCD there is no indication of a violation of the BC sum rule [51,416] so that we believe that it is probably valid at sufficiently high Q^2. It should be emphasized again that the light-cone OPE per se is *non*-committal about the BC sum rule since the twist-3 operators with mixed symmetry in (8.12)–(8.14) need at least two (antisymmetrized) indices ($n > 1$) which implies the validity of Eq. (8.17) only for $n > 1$. We would need the $n \to 1$ continuation of the twist-3 matrix element d_n: if d_n is less singular than $(n-1)^{-1}$ as $n \to 1$, the BC sum rule (8.24) would hold, as one might naively expect; it would not hold if $d_n \sim (n-1)^{-1}$ for $n \to 1$ (but on the other hand we know that the twist-2 matrix element a_1 in (8.19) is not singular because the $n = 1$ moment of g_1 is finite). It is clearly important to check the validity of the BC sum rule experimentally – as far as possible. Present measurements at an average Q^2 of 3–5 GeV^2 imply [5,8]

$$\int_{0.03}^{1} \mathrm{d}x\, g_2^p(x,Q^2) = -0.013 \pm 0.028, \quad \int_{0.014}^{1} \mathrm{d}x\, g_2^n(x,Q^2) = 0.06 \pm 0.15\ , \tag{8.29}$$

which are consistent with (8.24) but certainly not conclusive. It would nevertheless be very interesting if the BC sum rule were not true, because this would imply a nonconventional behavior of twist-3 operators ($d_n \sim (n-1)^{-1}$) or the importance of long-range effects [382,463,461,521].

Another interesting, but less problematic sum rule concerns the valence content of g_1 and g_2 [239,244]

$$\int_0^1 \mathrm{d}x\, x[g_1(x,Q^2) + 2g_2(x,Q^2)]^{\text{valence}} = 0 \tag{8.30}$$

which amounts to the vanishing of all twist-3 contributions to the second ($n = 2$) moment of g_2. Apart from the fact that this sum rule can be independently derived from the OPE [122], there is also a wealth of similar sum rules between structure functions in the electroweak sector (see [121,122] and references therein) which are unfortunately beyond the experimental reach for the time being.

Let us finally come to the logarithmic scaling violations to Eq. (8.17), in particular the Q^2-evolution of $\bar{g}_2(x,Q^2)$ is theoretically unknown and in general an unsolved intricate problem, because the number of independent twist-3 operators increases with n [68,149,150,504]. Thus, the dimension of the anomalous dimension matrix becomes larger with increasing n and therefore there exist no Altarelli–Parisi-type evolution equations. Anomalous dimensions and coefficient functions for g_2 have been calculated, see [399,418] and earlier references quoted therein, but for

principal reasons a satisfactory physical model to predict $\bar{g}_2(x,Q^2)$ does not exist. There have been attempts [44], to which we shall return below, to construct practical approximations to the Q^2 evolution in the large-n limit ($x \to 1$) as well as in the limit $N_c \to \infty$. Unfortunately, the very large-x region and probably also the large N_c limit are experimentally not very relevant. The latter just gives an indication that the effect of the Q^2 evolution of $\bar{g}_2(x,Q^2)$ might be large throughout the whole x-region [550]. Furthermore, a parton inspired picture involves two-parton 'correlation functions' $C(x_1,x_2)$, where two partons (with Bjorken x_1 and x_2) split from the proton at the same time and interact with the photon (see, e.g., [461,560]). However, these functions are as undetermined as the matrix elements of the higher twist operators.

At the end of this section we want to discuss the operator mixing and its effects on the Q^2-evolution and the coefficient functions for the simple case of $n = 3$. The coefficient functions at the tree level and the anomalous dimensions for the operators depend separately upon the choice of the independent operator basis. But the Q^2 evolution of the moments of g_2 does of course not depend on it. In the case $n = 3$ there are four operators with the constraint

$$R_F = \tfrac{2}{3}R_m + R_1 + R_{\rm eq} \ , \tag{8.31}$$

where the Lorentz indices of operators are omitted. One may choose the operators R_F, R_m, and R_1 as independent operators and eliminate the 'EOM' operator $R_{\rm eq}$. One then gets the following renormalization matrix for the composite operators:

$$\begin{pmatrix} R_F \\ R_1 \\ R_m \\ R_{\rm eq1} \end{pmatrix}_{\rm R} = \begin{pmatrix} Z_{11} & Z_{12} & Z_{13} & Z_{14} \\ Z_{21} & Z_{22} & Z_{23} & Z_{24} \\ 0 & 0 & Z_{33} & 0 \\ 0 & 0 & 0 & Z_{44} \end{pmatrix} \begin{pmatrix} R_F \\ R_1 \\ R_m \\ R_{\rm eq1} \end{pmatrix}_{B} , \tag{8.32}$$

where the Z_{ij} can be calculated in dimensional regularization and are of form $Z_{ij} = \delta_{ij} + (1/\varepsilon)(g^2/16\pi^2)z_{ij}$ with $D = 4 - 2\varepsilon$. A straightforward but tedious calculation gives [417,418]

$$\begin{aligned} z_{11} &= \tfrac{7}{6}C_F + \tfrac{3}{8}N_c, & z_{12} &= -\tfrac{3}{2}C_F + \tfrac{21}{8}N_c \ , \\ z_{13} &= 3C_F - \tfrac{1}{4}N_c, & z_{14} &= -\tfrac{3}{8}N_c \ , \\ z_{21} &= \tfrac{1}{6}C_F - \tfrac{1}{8}N_c, & z_{22} &= -\tfrac{1}{2}C_F + \tfrac{25}{8}N_c \ , \\ z_{23} &= -\tfrac{1}{3}C_F + \tfrac{1}{12}N_c, & z_{24} &= \tfrac{1}{8}N_c \ , \\ z_{33} &= 6C_F, & z_{44} &= 0 \ . \end{aligned} \tag{8.33}$$

$R_{\rm eq1}$ is a gauge non-invariant 'equation of motion' operator

$$R_{\rm eq1}^{\sigma\mu_1\mu_2} = {\rm i}\tfrac{1}{3}S[\bar{\psi}\gamma_5\gamma^\sigma\partial^{\mu_1}\gamma^{\mu_2}({\rm i}\not{\partial} - m_q)\psi + \bar{\psi}({\rm i}\not{\partial} - m_q)\gamma_5\gamma^\sigma\partial^{\mu_1}\gamma^{\mu_2}\psi] \tag{8.34}$$

which comes into play when renormalizing the operators in (8.31). Although this operator is gauge noninvariant, it may be chosen to appear in the operator basis because it vanishes by the equation of motion. The above results in Eq. (8.34) satisfy the equalities [417]

$$\begin{aligned} &z_{11} + z_{12} = z_{21} + z_{22}, \quad \tfrac{2}{3}z_{11} + z_{13} = \tfrac{2}{3}z_{21} + z_{23} + \tfrac{2}{3}z_{33}, \\ &z_{13} - \tfrac{2}{3}z_{12} = z_{23} - \frac{2}{3}z_{22} + \tfrac{2}{3}z_{33} \ . \end{aligned} \tag{8.35}$$

What happens if one chooses R_1, R_m, $R_{\rm eq}$ and $R_{\rm eq1}$, and eliminates R_F? Using (8.31) and the relations (8.35) one gets the renormalization matrix

$$\begin{pmatrix} R_1 \\ R_m \\ R_{\rm eq} \\ R_{\rm eq1} \end{pmatrix}_R = \begin{pmatrix} Z_{21}+Z_{22} & \frac{2}{3}Z_{21}+Z_{23} & Z_{21} & Z_{24} \\ 0 & Z_{33} & 0 & 0 \\ 0 & 0 & Z_{11}-Z_{21} & Z_{14}-Z_{24} \\ 0 & 0 & 0 & Z_{44} \end{pmatrix} \begin{pmatrix} R_1 \\ R_m \\ R_{\rm eq} \\ R_{\rm eq1} \end{pmatrix}_B . \tag{8.36}$$

This choice of basis was adopted, for example, in [44] in their approximate calculation of anomalous dimensions in the large N_c limit:

$$\bar{\gamma}^n_{\rm NS} = 4N_c\left(\sum_{j=1}^{n}\frac{1}{j} - \frac{1}{4} - \frac{1}{2n}\right) \tag{8.37}$$

valid for large n, i.e. for large values of x close to 1. It should be noted that this anomalous dimension differs substantially from the one naively obtained by ignoring the operator mixing as was done in the early days [356,520,36,37,414,415,68]. In that approximation the evolution equation for the moments of the twist-3 contribution $\bar{g}_2$ to g_2 in Eq. (8.2) reads

$$\int_0^1 {\rm d}x\, x^{n-1}\bar{g}_2(x,Q^2) = \left\{\frac{\alpha_s(Q^2)}{\alpha_s(Q_0^2)}\right\}^{\bar{\gamma}^n_{\rm NS}/2\beta_0}\int_0^1 {\rm d}x\, x^{n-1}\bar{g}_2(x,Q_0^2) \tag{8.38}$$

with β_0 given in (4.13). This Q^2 evolution has been quantitatively studied in [550] and used by [5] to compare bound-state model predictions, e.g. in Fig. 51, with experimental results, such as the ones in (8.21), at larger values of Q^2.

8.2. *Transverse chiral-odd* (‘*transversity*’) *structure functions*

In analogy to the unpolarized and polarized structure functions F_1 and g_1, the ‘transversity’ structure function [499,414,150,75,206,383,384,506] is, in LO, formally given by (cf. Eq. (4.5))

$$h_1(x,Q^2) = \frac{1}{2}\sum_q e_q^2[\delta_{\rm T}q(x,Q^2) + \delta_{\rm T}\bar{q}(x,Q^2)] \tag{8.39}$$

where, similarly to Eqs. (4.1) and (4.2),

$$\delta_{\rm T}\overset{(-)}{q}(x,Q^2) \equiv \overset{(-)}{q}{}^{\uparrow}(x,Q^2) - \overset{(-)}{q}{}^{\downarrow}(x,Q^2) \tag{8.40}$$

describes the (anti)quark ‘transversity’ distribution with $\overset{(-)}{q}{}^{\uparrow}$ ($\overset{(-)}{q}{}^{\downarrow}$) being the probability of finding a (anti)quark in a transversely polarized proton with spin parallel (antiparallel) to the proton spin. The transverse polarization of a quark entering an interaction kernel is obtained by using $u(p,s)\bar{u}(p,s) = -\not{p}\not{s}\gamma_5$ for its spinor $u(p,s)$ with $s\cdot p = 0$. The $\delta_{\rm T}\overset{(-)}{q}$ are related to the tensor current $\bar{q}\,{\rm i}\sigma^{\mu\nu}\gamma_5 q$ which is chiral (and charge conjugation) *odd*, i.e. measure correltions between left- and

right-handed quarks, $q_L \leftrightarrow q_R$, induced for example by nonperturbative condensates $\langle \bar{q}_L\, q_R \rangle$ in the nucleon. Thus, unlike in the familiar case of the $q(x,Q^2)$ and $\delta q(x,Q^2)$, there is no gluonic transversity density at leading twist [379,391,540]. Together, $q, \delta q$ and $\delta_T q$ provide a complete description of quark momentum and spin at leading twist as can be seen generically from a spin-density matrix representation in the quark- and nucleon-helicity basis,

$$\mathscr{F}(x,Q^2) = \tfrac{1}{2}q(x,Q^2)I\otimes I + \tfrac{1}{2}\delta q(x,Q^2)\sigma_3\otimes\sigma_3 + \tfrac{1}{2}\delta_T q(x,Q^2)(\sigma_+\otimes\sigma_- + \sigma_-\otimes\sigma_+)\,. \tag{8.41}$$

Thus the $\delta_T^{(-)} q\,(x,Q^2)$ are leading twist-2 densities and *complete* the twist-2 sector of nucleonic parton distributions, and are therefore in principle as interesting as the familiar $f(x,Q^2)$ and $\delta f(x,Q^2)$. Unfortunately, the $\delta_T^{(-)} q$ densities are experimentally more difficult to access and entirely unknown so far. (Although the name 'transversity' is fairly universal, the notation is not. In addition to $\delta_T q$, notations such as h_1^q, h_T, $\Delta_T q$, $\Delta_1 q$, δq, etc., are common as well [499,206,383, 384,75]).

It should be remembered that the common unpolarized and longitudinally polarized quark densities q and δq, respectively, considered up to now are related to the matrix elements of vector and axial–vector currents, $\bar{q}\gamma_\mu q$ and $\bar{q}\gamma_\mu\gamma_5 q = \bar{q}_L\gamma_\mu\gamma_5 q_L + \bar{q}_R\gamma_\mu\gamma_5 q_R$, respectively, which preserve chirality, i.e. are chiral-*even* ($q_L \to q_L, q_R \to q_R$) in contrast to the chiral-odd $\delta_T q$. Thus, the transverse spin structure function $g_T = g_1 + g_2$ (or g_2) of the previous Section 8.1, which preserves chirality, must not be confused with h_1 which flips chirality. We have seen that for g_2, arising from transversally polarized nucleons, the cross section picks up a factor of $M/\sqrt{Q^2}$ because in these processes the nucleon helicity changes but the quark chirality does not change in the hard scattering subprocess [383,384,148]. Therefore it is obviously not possible to measure the chiral-odd transversity structure function $h_1(x,Q^2)$ in usual ep inclusive DIS which, apart from small quark mass corrections, gives always rise to chiral-even transitions ($\gamma^* q_L \to q_L$, etc.), i.e. to $F_{1,2}$ and $g_{1,2}$. The chiral-even transitions are illustrated in Fig. 52 where the quark lines leaving and entering the nucleon are of a single chirality. This is so because the photons and gluons participating in the hard scattering process have a vector-like interaction with the massless quark. Thus in lowest order only two independent quark-nucleon amplitudes enter the description of DIS: the sum in Fig. 53 over chirality gives the unpolarized structure function F_1 (or F_2), whereas the difference gives the structure function g_1 of longitudinal polarization.

On the other hand, in hadronic collisions, the chirality of the quark lines leaving and entering a given nucleon need not be the same, as illustrated in Fig. 54. This is due to nonperturbative condensates $\langle \bar{q}_L q_R \rangle \neq 0$ which break the chiral symmetry of the QCD vacuum as well as of the

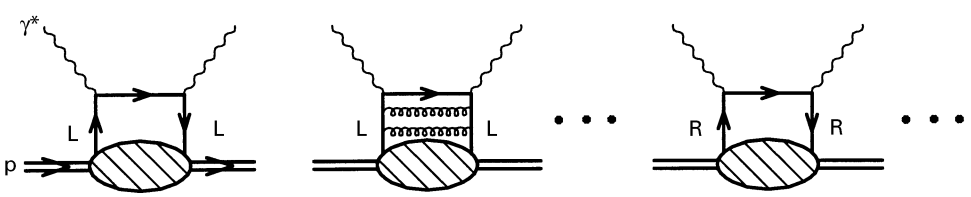

Fig. 52. Chiral (even) structure of deep inelastic scattering.

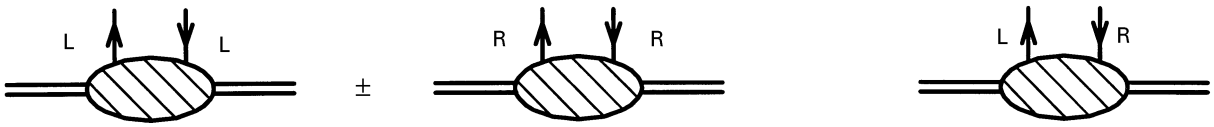

Fig. 53. Left- and right-handed chiral even quark distributions as measured in DIS whose sum and difference give $F_1(x,Q^2)$ and $g_1(x,Q^2)$, respectively.

Fig. 54. Chiral (odd) flip distribution which gives the 'transversity' structure function $h_1(x,Q^2)$.

nucleon structure due to bound state effects [383,384,148]. The corresponding new leading twist-2 structure function is referred to as $h_1(x,Q^2)$ in (8.39). Its interpretation is obscure in the chiral basis, but is revealed by using the transverse projection operators $P_{\Uparrow\Downarrow} = \frac{1}{2}(1 \pm \gamma_5 \not{S}_T)$ instead of $P_{R,L} = \frac{1}{2}(1 \pm \gamma_5)$, cf. Eq. (1.3). Here the transversely polarized nucleon and quarks are classified as eigenstates of the transversely projected Pauli–Lubanski spin operator $\gamma_5 \not{S}_T$ (which is the more familiar form proportional to $W_\mu = -\frac{1}{2}\varepsilon_{\mu\nu\rho\sigma}J^{\nu\rho}P^\sigma$), i.e. $\gamma_5 \not{S}_T u(P_z,S_T) = \pm u(P_z,S_T)$. In contrast to the transverse quark spin operator $\gamma_0\gamma_5\not{S}_T$ relevant for g_2 in the previous Section 8.1, the Pauli–Lubanski operator $\gamma_5\not{S}_T$ commutes with the free quark Hamiltonian $H_0 = \alpha_z p_z$, and therefore $h_1(x,Q^2)$ can be interpreted in terms of the quark-parton model as done in (8.39).

There are further subleading (twist-3) transversity distributions [383,384,483] such as h_2 which is the chiral-odd analog of g_2. There is, furthermore, a twist-3 chiral-odd scalar distribution $e(x,Q^2)$ related to the unit operator, i.e. measuring, via its first moment, the nucleon σ-term. More explicitly, the complete set of structure functions are defined by the light cone Fourier transform of nucleon matrix elements of quark bilocal operators as follows:

$$\int\frac{d\lambda}{2\pi}e^{i\lambda x}\langle PS|\bar{q}(0)\gamma_\mu q(\lambda n)|PS\rangle = 2[f_1^q(x,Q^2)p_\mu + M^2 f_4^q(x,Q^2)n_\mu]\,, \tag{8.42}$$

$$\int\frac{d\lambda}{2\pi}e^{i\lambda x}\langle PS|\bar{q}(0)\gamma_\mu\gamma_5 q(\lambda n)|PS\rangle = 2M[g_1^q(x,Q^2)p_\mu S\cdot n + g_T^q(x,Q^2)S_{T\mu} + M^2 g_3^q(x,Q^2)n_\mu S\cdot n]\,, \tag{8.43}$$

$$\int\frac{d\lambda}{2\pi}e^{i\lambda x}\langle PS|\bar{q}(0)q(\lambda n)|PS\rangle = 2Me^q(x,Q^2)\,, \tag{8.44}$$

$$\int\frac{d\lambda}{2\pi}e^{i\lambda x}\langle PS|\bar{q}(0)i\sigma_{\mu\nu}\gamma_5 q(\lambda n)|PS\rangle = 2[h_1^q(x,Q^2)(S_{T\mu}p_\nu - S_{T\nu}p_\mu) + h_L^q(x,Q^2)M^2(p_\mu n_\nu - p_\nu n_\mu)S\cdot n + h_3^q(x,Q^2)M^2(S_{T\mu}n_\nu - S_{T\nu}n_\mu)]\,, \tag{8.45}$$

which holds at some factorization scale Q^2, $h_L^q \equiv \frac{1}{2}h_1^q + h_2^q$, and in order to follow more closely the original notation [383,384] we have used $f_1^q \equiv q$, $g_1^q \equiv \delta q$, $h_1^q \equiv \delta_T q$, etc. Two light-like null-vectors ($p^2 = n^2 = 0$) have been introduced via the relation $P_\mu = p_\mu + (M^2/2)n_\mu$ with $p\cdot n = 1$, and the nucleon spin vector is decomposed as $S_\mu = S\cdot n p_\mu + S\cdot p n_\mu + S_{T\mu}$. The twist-4 contributions f_4^q, g_3^q and h_3^q will not be considered in the following.

The $\delta_T \overset{(-)}{q}$ and the longitudinal $\delta \overset{(-)}{q}$ densities are not entirely independent of each other since one clearly has $\overset{(-)}{q}_+ + \overset{(-)}{q}_- = \overset{(-)}{q}^{\uparrow} + \overset{(-)}{q}^{\downarrow}$ by rotational invariance, which implies the general positivity constraints [381,384]

$$|\delta_T \overset{(-)}{q}(x,Q^2)| \leq \overset{(-)}{q}(x,Q^2) \tag{8.46}$$

in complete analogy to (4.11). A second inequality has been derived by Soffer [538],

$$|\delta_T \overset{(-)}{q}(x,Q^2)| \leq \tfrac{1}{2}[\overset{(-)}{q}(x,Q^2) + \delta \overset{(-)}{q}(x,Q^2)] = \overset{(-)}{q}_+(x,Q^2)\ , \tag{8.47}$$

which has its origin in the positivity properties of helicity amplitudes. This latter inequality can also be derived in the context of the parton model [538,536,327].

Being a twist-2 quantity, where only fermions contribute, $h_1(x,Q^2)$, i.e. $\delta \overset{(-)}{q}_T(x,Q^2)$ obey a simple nonsinglet-type Altarelli–Parisi evolution equation. In LO it is similar to (4.12) and reads [75]

$$\frac{\mathrm{d}}{\mathrm{d}t}\delta_T \overset{(-)}{q}(x,Q^2) = \frac{\alpha_s(Q^2)}{2\pi}\delta_T P_{qq}^{(0)} \otimes \delta_T \overset{(-)}{q} \tag{8.48}$$

where $t = \ln Q^2/Q_0^2$ and

$$\delta_T P_{qq}^{(0)}(x) = C_F\left[\frac{2x}{(1-x)_+} + \frac{3}{2}\delta(1-x)\right] \tag{8.49}$$

with $C_F = \frac{4}{3}$. Alternatively, in Mellin n-moment space this RG evolution equation becomes similar to (4.24) and reads

$$\frac{\mathrm{d}}{\mathrm{d}t}\,\delta_T \overset{(-)}{q}{}^n(Q^2) = \frac{\alpha_s(Q^2)}{2\pi}\delta_T P_{qq}^{(0)n}\,\delta_T \overset{(-)}{q}{}^n(Q^2)\ , \tag{8.50}$$

where the nth moment is defined by Eq. (4.22) and the nth moment of (8.49) is given by

$$\delta_T P_{qq}^{(0)n} = C_F[\tfrac{3}{2} - 2S_1(n)] \tag{8.51}$$

with $S_1(n)$ being defined right after Eq. (4.26). The solution of (8.50) is straightforward and is formally identical to the one in (4.27). Recently, the calculation of the NLO two-loop splitting functions $\delta_T P_{qq\pm}^{(1)}(x)$ has been completed in the $\overline{\mathrm{MS}}$ factorization scheme [427,351,570] for the flavor combinations $\delta_T q_\pm \equiv \delta_T q \pm \delta_T \bar{q}$. The LO evolutions of the twist-3 distributions $e(x,Q^2)$ and $h_L(x,Q^2)$ in (8.44) and (8.45) have been studied as well recently [421,422,86,107].

Since the corresponding evolution kernels are entirely different for the $\overset{(-)}{q}(x,Q^2)$, $\delta \overset{(-)}{q}(x,Q^2)$ and $\delta_T \overset{(-)}{q}(x,Q^2)$ densities, the question immediately arises whether the Soffer inequality (8.47) is maintained when QCD is applied [327,406,90]. It turns out, however, that this inequality is preserved by LO [90] and NLO [570,470] QCD evolutions at any $Q^2 > Q_0^2$ provided it is valid at the input scale $Q^2 = Q_0^2$.

As stated above, the transversity distributions are experimentally entirely unknown so far. Being chiral odd, they cannot be directly determined from the common fully inclusive DIS process, i.e. $h_1(x,Q^2)$ is not directly measurable despite its formal definition in (8.39). One would need, for example, to measure a (single) transverse asymmetry in single transversely polarized *semi*-inclusive DIS $ep^{\uparrow\downarrow} \to eh^{\uparrow}X$ with $h = \Lambda$, jet, ... [74,75,195–197,394]. This requires, however, a (difficult) measurement of the transverse polarization of the final state $h^{\uparrow}$. Old ideas [485,241] have been revived [238,195–197,394] for determining the polarization of an outgoing quark (or gluon), in particular chiral-odd fragmentation functions, via the hadron distribution in the jet, for example. Perhaps a more feasible possibility has been suggested recently [385,378] to extract $\delta_{\mathrm{T}}q$ from DIS two-meson production, e.g. $ep^{\uparrow\downarrow} \to e\pi^{+}\pi^{-}X$ via a Collins-angle-like ϕ distribution [195,196] by measuring the observable $\boldsymbol{\pi}^{+} \times \boldsymbol{\pi}^{-} \cdot \boldsymbol{S}_{\mathrm{T}}$, i.e. the correlation of the normal to the plane formed by the three-momenta $\boldsymbol{\pi}^{\pm}$ with the nucleon's transverse spin. This, however, requires the cross section to be held fully differential to avoid averaging the meson–meson final state interaction phase to zero. It is conceivable that HERMES and (in the not too distant future) COMPASS can perform such measurements.

A more natural way to search for transversity densities is in doubly transversely polarized hadron–hadron initiated reactions like $p^{\uparrow}p^{\uparrow\downarrow} \to \mu^{+}\mu^{-}, \gamma, jj, c\bar{c}, \ldots X$ [499,75,383,384,148,206, 390,573,200,405,406,570,386,469,470,91,513]. Here the chirality changing densities (cf. Fig. 54) appear automatically in the initial states without extra suppressions as illustrated for Drell–Yan dilepton production in Fig. 55. The expected double transverse asymmetries A_{TT} turn out, however, to be prohibitively small, $A_{\mathrm{TT}} \ll A_{\mathrm{LL}}$ (typically, smaller by about an order of magnitude), i.e. much smaller than the doubly longitudinally polarized asymmetries (inlcuding the DIS A_1 and A_2) considered thus far. Single transverse asymmetries A_{T} measured in reactions like $pp^{\uparrow\downarrow} \to j^{\uparrow}X$ might be sizeable (about 10%) [552], but require again a delicate measurement of the polarizations of the outgoing quarks and gluon via the hadron distribution in the final jet $j^{\uparrow}$. Such experiments could be performed at HERA-$\vec{N}$(phase I) and RHIC. Whereas these purely transverse asymmetries A_{TT} and A_{T} measure solely $\delta_{\mathrm{T}}\overset{(-)}{q}$, a mixed longitudinal-transverse asymmetry A_{LT}, down by a factor M/Q, gives access to $h_{\mathrm{L}}(x,Q^2) \equiv \frac{1}{2}h_1 + h_2$ provided g_1 and $g_{\mathrm{T}} = g_1 + g_2$ are known [383,384,390]. It should be noted that most of these processes have been analyzed in LO-QCD, with the exception of transversely polarized Drell–Yan dimuon production which has been already extended to the NLO within different factorization schemes [573,200,405,570,470].

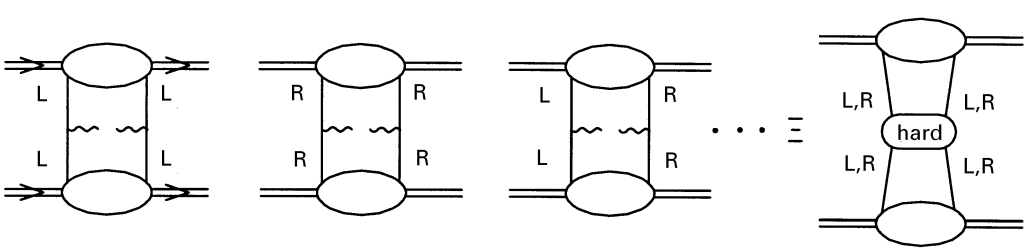

Fig. 55. Chiral structure of hadronic Drell–Yan production of lepton pairs with invariant mass $Q^2 \equiv q^2 > 0$ produced by the virtual photons. Chirality flip ($R \leftrightarrow L$) occurs without suppression due to the two initial hadrons (nonperturbative bound states) involved in the process.

Due to the lack of any experimental information, all these studies and expectations for transverse asymmetries are based on theoretical model estimates for $\delta_T \overset{(-)}{q}$ and the other subleading transversity densities. In the nonrelativistic quark model, $\delta_T q(x,Q^2) = \delta q(x,Q^2)$ due to rotational invariance, whereas in the bag model [383,384,550,528] $\delta_T q(x,Q^2) \gtrsim \delta q(x,Q^2)$ in the medium to large x-region – both expectations hold presumably at some nonperturbative bound-state-like scale $Q^2 = \mathcal{O}(\Lambda^2)$. Somewhat smaller results, $\delta_T q(x,Q^2) \lesssim \delta q(x,Q^2)$, are obtained by a chiral chromodielectric confinement model [92] and by the chiral soliton approach [491] at $Q^2 \simeq 0.3\,\mathrm{GeV}^2$, and with QCD sum rules [372] at $Q^2 \gtrsim 1\,\mathrm{GeV}^2$. It seems that transversity densities are sizeable and not too different from the (longitudinal) helicity distributions. Anyway, $\delta_T q \neq \delta q$ ($h_1 \neq g_1$) directly probes relativistic effects in the wave function. In particular, h_1 could develop a very different small-x behavior as compared to g_1 [92,359,411,528].

There have also been attempts [384,352,538,524,92] to estimate the nucleon's 'tensor charge', i.e. the total transversity $\Delta_T q(Q^2)$ carried by quarks,

$$\int_0^1 [\delta_T q(x,Q^2) - \delta_T \bar{q}(x,Q^2)]\,\mathrm{d}x \equiv \Delta_T q(Q^2)\ , \tag{8.52}$$

which is a flavor nonsinglet valence quantity (quarks *minus* antiquarks, since the tensor current is C-odd) and measures a simple local operator analogous to the axial charge (cf. Eq. (5.33))

$$\langle PS|\bar{q}\mathrm{i}\sigma_{\mu\nu}\gamma_5 q|PS\rangle = (1/M)(S_\mu P_\nu - S_\nu P_\mu)\Delta_T q\ . \tag{8.53}$$

Unlike its vector and (NS) axial–vector equivalents, the tensor charge is not conserved in QCD, so it has an anomalous dimension at one loop. To understand the physical meaning of the tensor charge it is helpful to make a comparison between the chirally odd and even matrix elements in the rest frame of the nucleon, $P^\mu = (M,\mathbf{0})$ and $S^\mu = (0,\boldsymbol{S})$

$$\langle PS|\bar{q}\mathrm{i}\sigma_{i0}\gamma_5 q|PS\rangle = \langle PS|\bar{q}\Sigma_i q|PS\rangle = S_i\Delta_T q\ , \tag{8.54}$$

$$\langle PS|\bar{q}\gamma_i\gamma_5 q|PS\rangle = \langle PS|\bar{q}\gamma_0\Sigma_i q|PS\rangle = S_i\Delta(q+\bar{q})\ , \tag{8.55}$$

i.e. the spin operator related to axial current differs by an additional γ_0 from the expectation value of the Pauli–Lubanski 'transversity' operator. The above estimates imply [352,524,92] $\Delta_T\Sigma(Q^2) \equiv \Delta_T(u+d+s) = 0.6$ to 1 at Q^2 of about 5–10 GeV^2 which compares well with a recent lattice calculation [69], $\Delta_T\Sigma \simeq 0.6 \pm 0.1$. These results are intriguing since they seem to imply that the tensor charge behaves more like the 'naive' quark model expectation (5.16), $\Delta_T\Sigma = \Delta\Sigma^{SU(6)} = 1$, in contrast to the experimental result $\Delta\Sigma(Q^2) \simeq 0.2$ (cf. Table 3, for example) that quarks carry much less of the nucleon's spin than naively expected. Furthermore, one of the outstanding puzzles is how to obtain an independent measure of $\Delta_T q(Q^2)$ and thereby formulate a 'transversity sum rule' analogous to those that have been so helpful in the study of $\Delta(q+\bar{q})$ in connection with the spin of the proton.

Keeping in mind that we need the transversity densities $\delta_T \overset{(-)}{q}(x,Q^2)$, besides the more common $f(x,Q^2)$ and $\delta f(x,Q^2)$, for a complete understanding of the leading twist-2 sector of the nucleon's parton structure, we face the curious situation of having reached a remarkably advanced theoretical sophistication without having any experimental 'transversity' measurements whatsoever!

Note added. Very recently the calculation of the NLO contributions to polarized photoproduction of heavy quarks, $\vec{\gamma}\vec{p} \to c\bar{c}X$, as discussed in Section 6.2, has been completed [130,131]. As expected, among other things, the dependence of $\Delta\sigma^c_{\gamma p}$ in (6.31) on μ_F is considerably reduced in NLO.

Acknowledgements

One of us (E.R.) expresses his warmest thanks to M. Glück for numerous discussions and for a fruitful collaboration on various topics presented here during the past decade. He also thanks M. Stratmann and W. Vogelsang for their collaboration during the past years and for their help in preparing some of the figures presented. We are also grateful to G. Altarelli for some helpful and clarifying comments and discussions. Furthermore, B.L. would like to thank J. Bartels, H. Fritzsch, S. Forte, P. Gambino, M. Göckeler, Y. Koike, J. Kodaira, G. Piller, G. Ridolfi, P. Ratcliffe, M.G. Ryskin, A. Schaefer, J. Soffer and E. Steffens for comments and discussions in connection with this work. Finally we thank Mrs. H. Heininger, Mrs. R. Jurgeleit and Mrs. S. Laurent for their help in typing the manuscript and in preparing some of the figures.

This work has been supported in part by the 'Bundesministerium für Bildung, Wissenschaft, Forschung und Technologie', Bonn, as well as by the 'Deutsche Forschungsgemeinschaft'.

Appendix. Two-loop splitting functions and anomalous dimensions

In addition to the well-known LO (one-loop) polarized splitting functions [54] which are given in Eqs. (4.16) and (4.21), with their nth moment, as defined in (4.22), given in (4.26). For completeness we list here the results for the NLO (two-loop) splitting functions $\delta P^{(1)}_{ij}$ as recently calculated in [478,568,569]. As discussed in the text (Section 4, etc.), these calculations were done in the $\overline{\text{MS}}$ scheme. To deal with γ_5 and the ε-tensor, the HVBM scheme [due to its not fully anticommuting γ_5, additional finite renormalizations are required in order to guarantee the conservation of the flavor nonsinglet axial vector current, Eq. (4.93)] or equivalently the reading point method has been used. The flavor nonsinglet splitting functions in (4.49) are the same as for the unpolarized case [212]

$$\begin{aligned}
\delta P^{(1)}_{\text{NS}\pm}(x) &= P^{(1)}_{\text{NS}\pm}(x) = P^{(1)}_{qq}(x) \pm P^{(1)}_{q\bar{q}}(x) \\
&= C_F^2[-(2\ln x \ln(1-x) + \tfrac{3}{2}\ln x)\delta p_{qq}(x) - (\tfrac{3}{2} + \tfrac{7}{2}x)\ln x \\
&\quad - \tfrac{1}{2}(1+x)\ln^2 x - 5(1-x) + (\tfrac{3}{8} - \tfrac{1}{2}\pi^2 + 6\zeta(3))\delta(1-x)] \\
&\quad + C_F C_A[(\tfrac{1}{2}\ln^2 x + \tfrac{11}{6}\ln x + \tfrac{67}{18} - \tfrac{1}{6}\pi^2)\delta p_{qq}(x) + (1+x)\ln x + \tfrac{20}{3}(1-x) \\
&\quad + (\tfrac{17}{24} + \tfrac{11}{18}\pi^2 - 3\zeta(3))\delta(1-x)] \\
&\quad + C_F T_f[-(\tfrac{2}{3}\ln x + \tfrac{10}{9})\delta p_{qq}(x) - \tfrac{4}{3}(1-x) - (\tfrac{1}{6} + \tfrac{2}{9}\pi^2)\delta(1-x)] \\
&\quad \pm (C_F^2 - \tfrac{1}{2}C_F C_A)[2(1+x)\ln x + 4(1-x) + 2S_2(x)\delta p_{qq}(-x)] \; . \qquad \text{(A.1)}
\end{aligned}$$

Note that the '$\pm$' meaning of $\delta P_{\mathrm{NS}\pm}$ has been interchanged in [568,569]. The flavor-singlet splitting functions in (4.53) are given by [478,568,569] (see footnotes 3 and 5)

$$\delta P_{qq}^{(1)}(x) = \delta P_{\mathrm{NS}-}^{(1)}(x) + \delta P_{PS,qq}^{(1)}(x) \tag{A.2}$$

with

$$\delta P_{PS,qq}^{(1)}(x) = 2C_F T_f[1 - x - (1 - 3x)\ln x - (1 + x)\ln^2 x] , \tag{A.3}$$

and

$$\begin{aligned} 2f\delta P_{qg}^{(1)}(x) = {} & C_F T_f[- 22 + 27x - 9\ln x + 8(1 - x)\ln(1 - x) \\ & + \delta p_{qg}(x)(2\ln^2(1 - x) - 4\ln(1 - x)\ln x + \ln^2 x - \tfrac{2}{3}\pi^2)] \\ & + C_A T_f[2(12 - 11x) - 8(1 - x)\ln(1 - x) + 2(1 + 8x)\ln x \\ & - 2(\ln^2(1 - x) - \tfrac{1}{6}\pi^2)\delta p_{qg}(x) - (2S_2(x) - 3\ln^2 x)\delta p_{qg}(- x)] , \end{aligned} \tag{A.4}$$

$$\begin{aligned} \delta P_{qq}^{(1)}(x) = {} & C_F T_f[- \tfrac{4}{9}(x + 4) - \tfrac{4}{3}\delta p_{gq}(x)\ln(1 - x)] \\ & + C_F^2[- \tfrac{1}{2} - \tfrac{1}{2}(4 - x)\ln x - \delta p_{gq}(- x)\ln(1 - x) \\ & + (- 4 - \ln^2(1 - x) + \tfrac{1}{2}\ln^2 x)\delta p_{gq}(x)] \\ & + C_F C_A[(4 - 13x)\ln x + \tfrac{1}{3}(10 + x)\ln(1 - x) + \tfrac{1}{9}(41 + 35x) \\ & + \tfrac{1}{2}(- 2S_2(x) + 3\ln^2 x)\delta p_{gq}(- x) \\ & + (\ln^2(1 - x) - 2\ln(1 - x)\ln x - \tfrac{1}{6}\pi^2)\delta p_{gq}(x)] , \end{aligned} \tag{A.5}$$

$$\begin{aligned} \delta P_{gg}^{(1)}(x) = {} & - C_F T_f[10(1 - x) + 2(5 - x)\ln x + 2(1 + x)\ln^2 x + \delta(1 - x)] \\ & - C_A T_f[4(1 - x) + \tfrac{4}{3}(1 + x)\ln x + \tfrac{20}{9}\delta p_{gg}(x) + \tfrac{4}{3}\delta(1 - x)] \\ & + C_A^2[\tfrac{1}{3}(29 - 67x)\ln x - \tfrac{19}{2}(1 - x) + 4(1 + x)\ln^2 x - 2S_2(x)\delta p_{gg}(- x) \\ & + (\tfrac{67}{9} - 4\ln(1 - x)\ln x + \ln^2 x - \tfrac{1}{3}\pi^2)\delta p_{gg}(x) + (3\zeta(3) + \tfrac{8}{3})\delta(1 - x)] , \end{aligned} \tag{A.6}$$

where $C_F = 4/3$, $C_A = 3$, $T_f = fT_R = f/2$, $\zeta(3) \approx 1.202057$ and

$$\begin{aligned} & \delta p_{qq}(x) = \frac{2}{(1 - x)_+} - x - 1 , \\ & \delta p_{qg}(x) = 2x - 1, \quad \delta p_{gq}(x) = 2 - x , \\ & \delta p_{gg}(x) = \frac{1}{(1 - x)_+} - 2x + 1 , \end{aligned} \tag{A.7}$$

and the ' + ' description has obviously to be omitted for $\delta p_{ii}(-x)$. Furthermore,

$$S_2(x) = \int_{x/(1+x)}^{1/(1+x)} \frac{\mathrm{d}z}{z} \ln\left(\frac{1-z}{z}\right). \tag{A.8}$$

For relating the above results to those of [478] the following expression for $S_2(x)$ is needed:

$$S_2(x) = -2\mathrm{Li}_2(-x) - 2\ln x \ln(1+x) + \tfrac{1}{2}\ln^2 x - \tfrac{1}{6}\pi^2\,, \tag{A.9}$$

where $\mathrm{Li}_2(x)$ is the usual Dilogarithm [225]. The coefficient functions relevant for a consistent NLO($\overline{\mathrm{MS}}$) analysis of $g_1(x,Q^2)$ in (4.47) are given by Eqs. (4.41) and (4.42). It should be recalled that convolutions involving the $(\ )_+$ distributions can be conveniently calculated numerically with the help of Eq. (4.18).

The nth moments of these splitting functions, defined in (4.22), which are needed for the evolution equations (4.54) and (4.55) in Mellin-moment space, are as follows. The moments of the LO splitting functions, $\delta P_{ij}^{(0)n}$, are given in (4.26). The moments of the $\delta P_{\mathrm{NS}\pm}^{(1)}(x)$ in (A.1), being the same as for the unpolarized case [212,267] (see footnote 4), are

$$\begin{aligned}
-\delta P_{\mathrm{NS}\pm}^{(1)n} = {} & C_F^2\left[2\frac{2n+1}{n^2(n+1)^2}S_1(n) + 2\left(2S_1(n) - \frac{1}{n(n+1)}\right)\left(S_2(n) - S_2'\left(\frac{n}{2}\right)\right)\right. \\
& \left. + 3S_2(n) + 8\tilde{S}(n) - S_3'\left(\frac{n}{2}\right) - \frac{3n^3+n^2-1}{n^3(n+1)^3} - \frac{3}{8} \mp 2\frac{2n^2+2n+1}{n^3(n+1)^3}\right] \\
& + C_F C_A\left[\frac{67}{9}S_1(n) - \left(2S_1(n) - \frac{1}{n(n+1)}\right)\left(2S_2(n) - S_2'\left(\frac{n}{2}\right)\right)\right. \\
& - \frac{11}{3}S_2(n) - 4\tilde{S}(n) + \frac{1}{2}S_3'\left(\frac{n}{2}\right) \\
& \left. - \frac{1}{18}\frac{151n^4+236n^3+88n^2+3n+18}{n^3(n+1)^3} - \frac{17}{24} \pm \frac{2n^2+2n+1}{n^3(n+1)^3}\right] \\
& + C_F T_f\left[-\frac{20}{9}S_1(n) + \frac{4}{3}S_2(n) + \frac{2}{9}\frac{11n^2+5n-3}{n^2(n+1)^2} + \frac{1}{6}\right].
\end{aligned} \tag{A.10}$$

The moments of the flavor singlet splitting functions in (A.2)–(A.6) are given by [478,309] (see footnote 5)

$$\delta P_{qq}^{(1)n} = \delta P_{\mathrm{NS}-}^{(1)n} + \delta P_{PS,qq}^{(1)n} \tag{A.11}$$

with

$$-\delta P_{PS,qq}^{(1)n} = 2C_F T_f \frac{n^4+2n^3+2n^2+5n+2}{n^3(n+1)^3} \tag{A.12}$$

and

$$\begin{aligned}
-2f\delta P_{qg}^{(1)n} = {} & C_F T_f\left[2\frac{n-1}{n(n+1)}(S_2(n) - S_1^2(n)) + 4\frac{n-1}{n^2(n+1)}S_1(n)\right. \\
& \left. - \frac{5n^5+5n^4-10n^3-n^2+3n-2}{n^3(n+1)^3}\right]
\end{aligned}$$

$$+\ 2C_A T_f\left[\frac{n-1}{n(n+1)}\left(-S_2(n)+S_2'\left(\frac{n}{2}\right)+S_1^2(n)\right)-\frac{4}{n(n+1)^2}S_1(n)\right.$$
$$\left.-\frac{n^5+n^4-4n^3+3n^2-7n-2}{n^3(n+1)^3}\right], \tag{A.13}$$

$$-\delta P_{gq}^{(1)n}=4C_F T_f\left[-\frac{n+2}{3n(n+1)}S_1(n)+\frac{5n^2+12n+4}{9n(n+1)^2}\right]$$
$$+\ C_F^2\left[\frac{n+2}{n(n+1)}(S_2(n)+S_1^2(n))-\frac{3n^2+7n+2}{n(n+1)^2}S_1(n)\right.$$
$$\left.+\frac{9n^5+30n^4+24n^3-7n^2-16n-4}{2n^3(n+1)^3}\right]$$
$$+\ C_F C_A\left[\frac{n+2}{n(n+1)}\left(-S_2(n)+S_2'\left(\frac{n}{2}\right)-S_1^2(n)\right)+\frac{11n^2+22n+12}{3n^2(n+1)}S_1(n)\right.$$
$$\left.-\frac{76n^5+271n^4+254n^3+41n^2+72n+36}{9n^3(n+1)^3}\right], \tag{A.14}$$

$$-\delta P_{gg}^{(1)n}=C_F T_f\frac{n^6+3n^5+5n^4+n^3-8n^2+2n+4}{n^3(n+1)^3}$$
$$+\ 4C_A T_f\left[-\frac{5}{9}S_1(n)+\frac{3n^4+6n^3+16n^2+13n-3}{9n^2(n+1)^2}\right]$$
$$+\ C_A^2\left[-\frac{1}{2}S_3'\left(\frac{n}{2}\right)-2S_1(n)S_2'\left(\frac{n}{2}\right)+4\tilde{S}(n)+\frac{4}{n(n+1)}S_2'\left(\frac{n}{2}\right)\right.$$
$$+\frac{67n^4+134n^3+67n^2+144n+72}{9n^2(n+1)^2}S_1(n)$$
$$\left.-\frac{48n^6+144n^5+469n^4+698n^3+7n^2+258n+144}{18n^3(n+1)^3}\right], \tag{A.15}$$

where

$$S_k(n)\equiv\sum_{j=1}^{n}\frac{1}{j^k}\,, \tag{A.16}$$

$$S_k'\left(\frac{n}{2}\right)\equiv 2^{k-1}\sum_{j=1}^{n}\frac{1+(-)^j}{j^k}=\frac{1}{2}(1+\eta)S_k\left(\frac{n}{2}\right)+\frac{1}{2}(1-\eta)S_k\left(\frac{n-1}{2}\right), \tag{A.17}$$

$$\tilde{S}(n)\equiv\sum_{j=1}^{n}\frac{(-)^j}{j^2}S_1(j)=-\frac{5}{8}\zeta(3)+\eta\left[\frac{S_1(n)}{n^2}+\frac{\pi^2}{12}G(n)+\int_0^1 \mathrm{d}x\,x^{n-1}\frac{\mathrm{Li}_2(x)}{1+x}\right] \tag{A.18}$$

with $G(n) \equiv \psi((n+1)/2) - \psi(n/2)$, $\psi(z) = \mathrm{d}\ln\Gamma(z)/\mathrm{d}z$ and $\eta = \pm 1$ for $\delta P^{(1)n}_{\mathrm{NS}\pm}$ and $\eta = -1$ for the flavor singlet anomalous dimensions. The analytic continuations in n, required for the Mellin inversion of these sums to Bjorken-x space [cf. Eq. (4.37)], are well known [314,316] (see also [581]). The conventional anomalous dimensions $\delta\gamma^{(1)n}_{ij}$ are related to the $\delta P^{(1)n}_{ij}$ via $\delta\gamma^{(1)n}_{ij} = -8\delta P^{(1)n}_{ij}$ (cf. footnotes 1 and 5). The moments of the relevant $\overline{\mathrm{MS}}$ coefficient functions for $g^n_1(Q^2)$ are given in Eqs. (4.63) and (4.64). Finally, we list for completeness the first moments $\Delta P^{(1)}_{ij} \equiv \delta P^{(1)n=1}_{ij} = \int_0^1 \mathrm{d}x\, \delta P^{(1)}_{ij}(x)$ and the ones of the coefficient functions $\Delta C_i \equiv \delta C^{n=1}_i$:

$$\begin{aligned}
&\Delta P^{(1)}_{\mathrm{NS}-} = 0, \qquad \Delta P^{(1)}_{\mathrm{NS}+} = (C_F^2 - \tfrac{1}{2}C_F C_A)(\tfrac{13}{2} - \pi^2 + 4\zeta(3)) \,, \\
&\Delta P^{(1)}_{qq} = -3C_F T_f, \qquad \Delta P^{(1)}_{qg} = 0 \\
&\Delta P^{(1)}_{gq} = -\tfrac{9}{4}C_F^2 + \tfrac{71}{12}C_F C_A - \tfrac{1}{3}C_F T_f \\
&\Delta P^{(1)}_{gg} = \tfrac{17}{6}C_A^2 - C_F T_f - \tfrac{5}{3}C_A T_f \equiv \frac{\beta_1}{4}
\end{aligned} \tag{A.19}$$

and

$$\Delta C_q = -\tfrac{3}{2}C_F, \qquad \Delta C_g = 0 \,. \tag{A.20}$$

References

[1] K. Abe et al., (SLD Collab.), Phys. Rev. Lett. 74 (1994) 1512.
[2] K. Abe et al., (E143 Collab.), Phys. Rev. Lett. 74 (1995) 346, SLAC-PUB-6508.
[3] K. Abe et al., (E143 Collab.), Phys. Rev. Lett. 75 (1995) 25, SLAC-PUB-95-6734.
[4] K. Abe et al., (E143 Collab.), Phys. Lett. B 364 (1995) 61.
[5] K. Abe et al., (E143 Collab.), Phys. Rev. Lett. 76 (1996) 587, SLAC-PUB-95-6982.
[6] K. Abe et al., (E143 Collab.), Phys. Rev. Lett. 78 (1997) 815.
[7] K. Abe et al., (E154 Collab.), Phys. Rev. Lett. 79 (1997) 26.
[8] K. Abe et al., (E154 Collab.), Phys. Lett. B 404 (1997) 377.
[9] K. Abe et al., (E154 Collab.), Phys. Lett. B 405 (1997) 180.
[10] H. Abramowicz et al., (CDHSW Collab.), Z. Phys. C 15 (1982) 19.
[11] I. Abt et al., (H1 Collab.), Nucl. Phys. B 407 (1993) 515.
[12] K. Ackerstaff et al., (HERMES Collab.), Phys. Lett. B 404 (1997) 383.
[13] K. Ackerstaff et al., (HERMES Collab.), DESY 99-048, hep-ex/9906035 (1999).
[14] D.L. Adams et al., (E581/704 Collab.), Phys. Lett. B 261 (1991) 197.
[15] D.L. Adams et al., (E704 Collab.), Phys. Lett. B 264 (1991) 462.
[16] D.L. Adams et al., (E704 Collab.), Z. Phys. C 56 (1992) 181.
[17] D. Adams et al., (SM Collab.), Phys. Lett. B 329 (1994) 399.
[18] D. Adams et al., (SM Collab.), Phys. Lett. B 339 (1994) 332, Erratum.
[19] D. Adams et al., (SM Collab.), Phys. Lett. B 336 (1994) 125.
[20] D. Adams et al., (SM Collab.), Phys. Lett. B 357 (1995) 248.
[21] D.L. Adams et al., (E704 Collab.), Phys. Lett. B 345 (1995) 569.
[22] D.L. Adams et al., (E704 Collab.), Phys. Rev. D 53 (1996) 4747.
[23] D. Adams et al., (SM Collab.), Phys. Lett. B 396 (1997) 338.
[24] D. Adams et al., (SM Collab.), Phys. Rev. D 56 (1997) 5330.
[25] B. Adeva et al., (SM Collab.), Phys. Lett. B 302 (1993) 533.
[26] B. Adeva et al., (SM Collab.), Phys. Lett. B 320 (1994) 400.
[27] B. Adeva et al., (SM Collab.), Phys. Lett. B 369 (1996) 93.
[28] B. Adeva et al., (SM Collab.), Phys. Lett. B 412 (1997) 414.

[29] B. Adeva et al., (SM Collab.), Phys. Rev. D 58 (1998) 1 12 001.
[30] B. Adeva et al., (SM Collab.), Phys. Lett. B 420 (1998) 180.
[31] B. Adeva et al., (SM Collab.), Phys. Rev. D 58 (1998) 1 12 002.
[32] S.L. Adler, Phys. Rev. 143 (1966) 1144.
[33] S.L. Adler, Phys. Rev. 177 (1969) 2426.
[34] S.L. Adler, W.A. Bardeen, Phys. Rev. 182 (1969) 1517.
[35] I.R. Afnan, N.D. Birrell, Phys. Rev. C 16 (1977) 823.
[36] M.A. Ahmed, G.G. Ross, Phys. Lett. B 56 (1975) 385.
[37] M.A. Ahmed, G.G. Ross, Nucl. Phys. B 111 (1976) 441.
[38] T. Ahmed et al., (H1 Collab.), Nucl. Phys. B 439 (1995) 471.
[39] L.A. Ahrens et al., Phys. Rev. D 35 (1987) 785.
[40] S. Aid et al., (H1 Collab.), Nucl. Phys. B 470 (1996) 3.
[41] A. Airapetian et al., (HERMES Collab.), Phys. Lett. B 442 (1998) 484.
[42] W.M. Alberico, S.M. Bilenky, C. Giunti, C. Maieron, Z. Phys. C 70 (1996) 463.
[43] M.J. Alguard et al., (SLAC-Yale Collab., E80), Phys. Rev. Lett. 37 (1976) 1261.
[44] A. Ali, V.M. Braun, G. Hiller, Phys. Lett. B 226 (1991) 117.
[45] G. Altarelli, Phys. Rep. 81 (1982) 1.
[46] G. Altarelli, in: A. Zichichi (Ed.), Proceedings of the 27th International E. Majorana Summer School of Subnuclear Physics on 'The Challenging Questions', Erice, 1989, Plenum Press, New York, 1990, p. 33.
[47] G. Altarelli, in: W. Buchmüller, G. Ingelman (Eds.), Proceedings of the HERA-Workshop, Hamburg, 1991, DESY, 1992, Vol. I, p. 379.
[48] G. Altarelli, R.D. Ball, S. Forte, G. Ridolfi, Nucl. Phys. B 496 (1997) 337.
[49] G. Altarelli, R.K. Ellis, G. Martinelli, S.-Y. Pi, Nucl. Phys. B 160 (1979) 301.
[50] G. Altarelli, B. Lampe, Z. Phys. C 47 (1990) 315.
[51] G. Altarelli, B. Lampe, P. Nason, G. Ridolfi, Phys. Lett. B 334 (1994) 187.
[52] G. Altarelli, P. Nason, G. Ridolfi, Phys. Lett. B 320 (1994) 152.
[53] G. Altarelli, P. Nason, G. Ridolfi, Phys. Lett. B 325 (1994) 538, Erratum.
[54] G. Altarelli, G. Parisi, Nucl. Phys. B 126 (1977) 298.
[55] G. Altarelli, G.G. Ross, Phys. Lett. B 212 (1988) 391.
[56] G. Altarelli, W.J. Stirling, Particle World 1 (1989) 40.
[57] M. Amarian et al. (HERMES Collab.) HERMES 97-004, 1997.
[58] J.F. Amundson, O.J.P. Eboli, E.M. Gregores, F. Halzen, Phys. Lett. B 390 (1997) 323.
[59] M. Anselmino, M.E. Boglione, F. Murgia, Phys. Lett. B 362 (1995) 164.
[60] M. Anselmino et al., On the physics potential of polarized NN collisions at HERA, in: Proceedings of Workshop on Future Physics at HERA, Hamburg, 1996, p. 837.
[61] M. Anselmino et al., DESY-Zeuthen 96-04, 1996, unpublished.
[62] M. Anselmino, P. Gambino, J. Kalinowski, Z. Phys. C 64 (1994) 267.
[63] M. Anselmino, A. Efremov, E. Leader, Phys. Rep. 261 (1995) 1.
[64] M. Anselmino, B.L. Ioffe, E. Leader, Sov. J. Nucl. Phys. 49 (1989) 136.
[65] P.L. Anthony et al. (E142 Collab.), Phys. Rev. Lett. 71 (1993) 959; Phys. Rev. D 54 (1996) 6620.
[66] P.L. Anthony et al. (E155 Collab.), Phys. Lett. B 463 (1999) 339.
[67] J. Antille et al., Nucl. Phys. B 185 (1981) 1.
[68] I. Antoniadis, C. Kounnas, Phys. Rev. D 24 (1981) 505.
[69] S. Aoki, M. Doui, T. Hatsuda, Y. Kuramashi, Phys. Rev. D 56 (1997) 433.
[70] M. Arneodo et al. (EMC Collab.), Nucl. Phys. B 321 (1989) 541.
[71] R.G. Arnold et al., SLAC proposal E155, October 1993.
[72] R.G. Arnold, C.E. Carlson, F. Gross, Phys. Rev. C 21 (1980) 1426.
[73] R.G. Arnold et al., Preliminary Proposal to Measure Polarized Open Charm Photoproduction, Stanford, 1996.
[74] X. Artru, AIP Conf. Proc. 223 (1991) 176.
[75] X. Artru, M. Mekhfi, Z. Phys. C 45 (1990) 669.
[76] X. Artru, J. Czyzewski, I. Yabuki, Z. Phys. C 73 (1997) 527.

[77] J. Ashman et al. (EM Collab.), Phys. Lett. B 206 (1988) 364.
[78] J. Ashman et al. (EM Collab.), Nucl. Phys. B 328 (1989) 1 and references therein.
[79] H.R. Avakian, P. DiNezza et al. (HERMES Collab.), π^0 Electroproduction in DIS, Frascati Report, December 1996.
[80] J. Babcock, E. Monsay, D. Sivers, Phys. Rev. D 19 (1979) 1483.
[81] B. Bagchi, A. Lahiri, J. Phys. G 16 (1990) 239.
[82] R. Baier, R. Rückl, Nucl. Phys. B 218 (1983) 289.
[83] R. Baier, R. Rückl, Z. Phys. C 19 (1983) 251.
[84] I.I. Balitsky, V.M. Braun, A.V. Kolesnichenko, Phys. Lett. B 242 (1990) 245.
[85] I.I. Balitsky, V.M. Braun, A.V. Kolesnichenko, Phys. Lett. B 318 (1993) 648, Erratum.
[86] I.I. Balitsky, V.M. Braun, Y. Koike, K. Tanaka, Phys. Rev. Lett. 77 (1996) 3078.
[87] R.D. Ball, S. Forte, G. Ridolfi, Nucl. Phys. B 444 (1995) 287.
[88] R.D. Ball, S. Forte, G. Ridolfi, Phys. Lett. B 378 (1996) 255.
[89] D.P. Barber et al., Phys. Lett. B 343 (1995) 436.
[90] V. Barone, Phys. Lett. B 409 (1997) 499.
[91] V. Barone, T. Calarco, A. Drago, Phys. Rev. D 56 (1997) 527.
[92] V. Barone, T. Calarco, A. Drago, Phys. Lett. B 390 (1997) 287.
[93] J. Bartels, B.I. Ermolaev, M.G. Ryskin, Z. Phys. C 70 (1996) 273.
[94] J. Bartels, B.I. Ermolaev, M.G. Ryskin, Z. Phys. C 72 (1996) 627.
[95] J. Bartelski, R. Rodenberg, Phys. Rev. D 41 (1990) 2800.
[96] J. Bartelski, S. Tatur, Phys. Lett. B 265 (1991) 192.
[97] J. Bartelski, S. Tatur, Univ. Warsaw CAMK-95-288, 1992.
[98] S.D. Bass, Int. J. Mod. Phys. A 7 (1992) 6039.
[99] S.D. Bass, Mod. Phys. Lett. A 12 (1997) 1051.
[100] S.D. Bass, Mod. Phys. Lett. A 13 (1998) 791.
[101] S.D. Bass, Eur. Phys. J. A 5 (1999) 17.
[102] S.D. Bass, P.V. Landshoff, Phys. Lett. B 336 (1994) 537.
[103] S.D. Bass, B.L. Ioffe, N.N. Nikolaev, A.W. Thomas, J. Moscow Phys. Soc. 1 (1991) 317.
[104] G. Baum et al. (SLAC-Yale Collab.), Phys. Rev. Lett. 45 (1980) 2000.
[105] G. Baum et al. (SLAC-Yale Collab., E130), Phys. Rev. Lett. 51 (1983) 1135.
[106] G. Baum et al. (COMPASS Collab.), COMPASS Proposal, CERN/SPSLC 96-14, 1996.
[107] A.V. Belitsky, D. Müller, Nucl. Phys. B 503 (1997) 279.
[108] J.S. Bell, R. Jackiw, Nuovo Cim. A 51 (1969) 47.
[109] V.M. Belyaev, B.L. Ioffe, Ya.I. Kogan, Phys. Lett. B 151 (1985) 290.
[110] Ch. Berger, W. Wagner, Phys. Rep. 146 (1987) 1.
[111] E.L. Berger, D. Jones, Phys. Rev. D 23 (1981) 1521.
[112] E.L. Berger, J.W. Qiu, Phys. Rev. D 40 (1989) 778.
[113] A. Berera, Phys. Lett. B 293 (1992) 445.
[114] V. Bernard, U.G. Meissner, Phys. Lett. B 223 (1989) 439.
[115] C. Best et al., Hadron structure functions from lattice QCD, Talk presented at the DIS '97, Chicago, April 1997.
[116] M. Birkel, H. Fritzsch, Phys. Rev. D 53 (1996) 6195.
[117] M. Birse, Phys. Lett. B 249 (1990) 291.
[118] J.D. Bjorken, Phys. Rev. 148 (1966) 1467.
[119] J.D. Bjorken, Phys. Rev. D 1 (1966) 1376.
[120] B.B. Blinov et al. (E-880 Collab.), Phys. Rev. Lett. 73 (1994) 1621.
[121] J. Blümlein, N. Kochelev, Phys. Lett. B 381 (1996) 296.
[122] J. Blümlein, N. Kochelev, Nucl. Phys. B 498 (1997) 285.
[123] J. Blümlein, W.D. Nowak (Eds.), Proceedings of the Workshop on the 'Prospects of Spin Physics at HERA', DESY-Zeuthen, DESY 95-200, August 1995.
[124] J. Blümlein, A. DeRoeck, T. Gehrmann, W.D. Nowak (Eds.), Proceedings of the Workshop on 'Deep Inelastic Scattering off Polarized Targets: Theory meets Experiment', DESY-Zeuthen, DESY 97-200, September 1997.

[125] J. Blümlein, S. Riemersma, A. Vogt, Nucl. Phys. B Proc. Suppl. 51C (1996) 30.
[126] J. Blümlein, A. Vogt, Phys. Lett. B 370 (1996) 149.
[127] J. Blümlein, A. Vogt, Phys. Lett. B 386 (1996) 350.
[128] G.T. Bodwin, J. Qiu, Phys. Rev. D 41 (1990) 2755.
[129] G.T. Bodwin, E. Braaten, G.P. Lepage, Phys. Rev. D 51 (1995) 1125.
[130] I. Bojak, M. Stratmann, Phys. Lett. B 433 (1998) 411.
[131] I. Bojak, M. Stratmann, Nucl. Phys. B 540 (1999) 345.
[132] C. Boros, L. Zuo-Tang, M. Ta-Chung, Phys. Rev. Lett. 70 (1993) 1751.
[133] C. Bourrely, J. Soffer, E. Leader, Phys. Rep. 59 (1980) 95.
[134] C. Bourrely, F.M. Renard, J. Soffer, P. Taxil, Phys. Rep. 177 (1989) 320.
[135] C. Bourrely, J. Soffer, P. Taxil, Phys. Rev. D 36 (1987) 3373.
[136] C. Bourrely, J.P. Guillet, J. Soffer, Nucl. Phys. B 361 (1991) 72.
[137] C. Bourrely, J. Soffer, Phys. Lett. B 314 (1993) 132.
[138] C. Bourrely et al., Marseille CPT-96/PE.3327.
[139] N. deBotton, Proceedings of the Conference on High Energy Spin Physics, Bonn, 1990, p. 419.
[140] E. Braaten, S. Fleming, Phys. Rev. Lett. 74 (1995) 3327.
[141] P. Breitenlohner, D. Maison, Commun. Math. Phys. 52 (1977) 11, 39, 55.
[142] S.J. Brodsky, L. Frankfurt, J.F. Gunion, A.H. Mueller, M. Strikman, Phys. Rev. D 50 (1994) 3134.
[143] S.J. Brodsky, J. Ellis, M. Karliner, Phys. Lett. B 206 (1988) 309.
[144] S.J. Brodsky, M. Burkhardt, I. Schmidt, Nucl. Phys. B 441 (1995) 197.
[145] S.J. Brodsky, I. Schmidt, Phys. Lett. B 234 (1990) 144.
[146] F. Buccella, J. Soffer, Mod. Phys. Lett. A 8 (1993) 225.
[147] W.W. Buck, F. Gross, Phys. Rev. D 20 (1989) 2361.
[148] G. Bunce et al., Particle World 3 (1992) 1 and references therein.
[149] A.P. Bukhvostov, A.A. Kuraev, L.N. Lipatov, JETP Lett. 37 (1983) 482.
[150] A.P. Bukhvostov, A.A. Kuraev, L.N. Lipatov, Sov. Phys. JETP 60 (1984) 22.
[151] V.D. Burkert, B.L. Ioffe, Phys. Lett. B 296 (1992) 223.
[152] M. Burkardt, R.L. Jaffe, Phys. Rev. Lett. 70 (1993) 2537.
[153] H. Burkhardt, W.N. Cottingham, Ann. Phys. (NY) 56 (1970) 453.
[154] R.N. Cahn, F.C. Gilman, Phys. Rev. D 17 (1978) 1313.
[155] C.G. Callan, D.J. Gross, Phys. Rev. D 8 (1973) 4383.
[156] D.J.E. Callaway, S.D. Ellis, Phys. Rev. D 29 (1984) 567.
[157] P.R. Cameron et al. (E794 Collab.), Phys. Rev. D 32 (1985) 3070.
[158] R.D. Carlitz, J.C. Collins, A.H. Mueller, Phys. Lett. B 214 (1988) 229.
[159] R.D. Carlitz, J. Kaur, Phys. Rev. Lett. 38 (1977) 673.
[160] R.D. Carlitz, R.S. Willey, Phys. Rev. D 45 (1992) 2323.
[161] C.E. Carlson, W.-K. Tung, Phys. Rev. D 5 (1972) 721.
[162] C.H. Chang, Nucl. Phys. B 172 (1980) 425.
[163] M. Chanowitz, M. Furman I. Hinchliffe, Nucl. Phys. B 159 (1979) 225.
[164] K.T. Chao, J. Wen, H. Zeng, Phys. Rev. D 46 (1992) 5078.
[165] H.Y. Cheng, Chin. J. Phys. 29 (1991) 67.
[166] T.P. Cheng, W.K. Tung, Phys. Rev. Lett. 24 (1970) 851.
[167] T.P. Cheng, L.-F. Li, Phys. Rev. Lett. 62 (1989) 1441.
[168] T.P. Cheng, L.-F. Li, Phys. Lett. B 366 (1996) 365.
[169] H.Y. Cheng, E. Fischbach, Phys. Rev. D 19 (1979) 860.
[170] H.Y. Cheng, E. Fischbach, Phys. Rev. Lett. 52 (1984) 399.
[171] H.Y. Cheng, S.N. Lai, Phys. Rev. D 41 (1990) 91.
[172] H.Y. Cheng, C.F. Wai, Phys. Rev. D 46 (1992) 125.
[173] H.Y. Cheng, H.H. Liu, C.-Y. Wu, Taiwan Academia Sinica IP-ASTP-17-95.
[174] H.Y. Cheng, Lecture at the Xth Spring School on Particles and Fields, Taiwan; Int. J. Mod. Phys. A 11 (1996) 5109.

[175] H.Y. Cheng, Chin. J. Phys. 34 (1996) 738.
[176] H.Y. Cheng, Phys. Lett. B 427 (1998) 371.
[177] P. Chiappetta, J.Ph. Guillet, Z. Phys. C 32 (1986) 209.
[178] P. Chiappetta, G. Nardulli, Z. Phys. C 51 (1991) 435.
[179] C.B. Chiu, J. Pasupathy, S.L. Wilson, Phys. Rev. D 32 (1985) 1786.
[180] T.T. Chou, C.N. Yang, Nucl. Phys. B 107 (1976) 1.
[181] N. Christ, B. Hasslacher, A.H. Mueller, Phys. Rev. D 6 (1972) 3543.
[182] C. Ciofi degli Atti, S. Scopetta, E. Pace, G. Salme, Phys. Rev. C 48 (1993) R968.
[183] C. Ciofi degli Atti, E. Pace, G. Salme, Phys. Rev. C 51 (1995) 1108.
[184] G. Clement, J. Stern, Phys. Lett. B 220 (1989) 238.
[185] G. Clement, J. Stern, Phys. Lett. B 231 (1989) 471.
[186] F.E. Close, An Introduction to Quarks and Partons, Academic Press, New York, 1979.
[187] F.E. Close, Nucl. Phys. B 80 (1974) 269.
[188] F.E. Close, Phys. Rev. Lett. 64 (1990) 361.
[189] F.E. Close, S. Kumano, Phys. Rev. D 42 (1990) 2377.
[190] F.E. Close, R.G. Milner, Phys. Rev. D 44 (1991) 3691.
[191] F.E. Close, R.G. Roberts, Phys. Lett. B 316 (1993) 165.
[192] F.E. Close, R.G. Roberts, Phys. Lett. B 336 (1994) 257.
[193] F.E. Close, D. Sivers, Phys. Rev. Lett. 39 (1977) 1116.
[194] T.D. Cohen, M.K. Banerjee, Phys. Lett. B 230 (1989) 129.
[195] J.C. Collins, Nucl. Phys. B 394 (1993) 169.
[196] J.C. Collins, Nucl. Phys. B 396 (1993) 161.
[197] J.C. Collins, S.F. Heppelmann, G.A. Ladinsky, Nucl. Phys. B 420 (1994) 565.
[198] A.P. Contogouris, S. Papadopoulos, B. Kamal, Phys. Lett. B 246 (1990) 523.
[199] A.P. Contogouris, S. Papadopoulos, Phys. Lett. B 260 (1991) 204.
[200] A.P. Contogouris, B. Kamal, Z. Merebashvili, Phys. Lett. B 337 (1994) 169.
[201] A.P. Contogouris, B. Kamal, Z. Merebashvili, F.V. Tkachev, Phys. Lett. B 304 (1993) 329.
[202] A.P. Contogouris, B. Kamal, Z. Merebashvili, F.V. Tkachev, Phys. Rev. D 48 (1993) 4092.
[203] A.P. Contogouris, B. Kamal, Z. Merebashvili, F.V. Tkachev, Phys. Rev. D 54 (1996) 7081, Erratum.
[204] A.P. Contogouris, Z. Merebashvili, Phys. Rev. D 55 (1997) 2718.
[205] J.L Cortes, B. Pire, Phys. Rev. D 38 (1988) 3586.
[206] J.L Cortes, B. Pire, J.P. Ralston, Z. Phys. C 55 (1992) 409.
[207] K. Coulter et al. (HERMES proposal) DESY-PRC 90/01, 1990.
[208] K. Coulter et al. (HERMES proposal) DESY-PRC 93/06, 1993.
[209] D.G. Crabb et al., Phys. Rev. Lett. 65 (1990) 3241.
[210] N.S. Craigie, K. Hidaka, A. Penzo, J. Soffer, Nucl. Phys. B 204 (1982) 365.
[211] N.S. Craigie, K. Hidaka, M. Jacob, F.M. Renard, Phys. Rep. 99 (1984) 70.
[212] G. Curci, W. Furmanski, R. Petronzio, Nucl. Phys. B 175 (1980) 27.
[213] S.J. Dong, J.F. Lagae, K.F. Liu, Phys. Rev. Lett. 75 (1995) 2096.
[214] R.H. Dalitz, G.R. Goldstein, R. Marshall, Z. Phys. C 42 (1989) 441.
[215] T. DeGrand, Nucl. Phys. B 151 (1979) 485.
[216] Y.S. Derbenev, A.M. Kondratenko, Sov. Phys. Doklady 20 (1976) 562.
[217] Y.S. Derbenev et al., Particle Accelerators 8 (1978) 115.
[218] E. Derman, Phys. Rev. D 7 (1973) 2755.
[219] A. DeRoeck, T. Gehrmann, in: J. Blümlein, A. DeRoeck, T. Gehrmann, W.D. Nowak (Eds.), Proceedings of the Workshop on Deep Inelastic Scattering off Polarized Targets: Theory meets Experiment, DESY-Zeuthen, September 1997, DESY 97-200, p. 523.
[220] M. Derrick et al., (ZEUS Collab.), Phys. Lett. B 316 (1993) 412.
[221] M. Derrick et al., (ZEUS Collab.), Phys. Lett. B 348 (1995) 665.
[222] M. Derrick et al., (ZEUS Collab.), Z. Phys. C 65 (1995) 379.
[223] M. Derrick et al., (ZEUS Collab.), Z. Phys. C 69 (1996) 607.

[224] A. Deshpande, V.W. Hughes, J. Lichtenstadt, in: J. Blümlein, A. DeRoeck, T. Gehrmann, W.D. Nowak (Eds.), Proceedings of the Workshop on 'Deep Inelastic Scattering off Polarized Targets: Theory meets Experiment', DESY-Zeuthen, September 1997, DESY 97-200, p. 548.
[225] A. Devoto, D.W. Duke, Riv. Nuov. Cim. 7 (1984) 1.
[226] D. Diakonov, V. Petrov, P. Pobylitsa, M. Polyakov, C. Weiss, Nucl. Phys. B 480 (1996) 341.
[227] D. Diakonov, V. Petrov, P. Pobylitsa, M. Polyakov, C. Weiss, Phys. Rev. D 56 (1997) 4069.
[228] D.A. Dicus, Phys. Rev. D 5 (1972) 1367.
[229] M.A. Doncheski, R.W. Robinett, Phys. Lett. B 248 (1990) 188.
[230] M.A. Doncheski, R.W. Robinett, L. Weinkauf, Phys. Rev. D 44 (1991) 2717.
[231] S.D. Drell, A.C. Hearn, Phys. Rev. Lett. 16 (1966) 908.
[232] M. Düren, K. Rith, in: W. Buchmüller, G. Ingelman (Eds.), Proceedings of the HERA-Workshop, Hamburg 1991, Vol. I, DESY, 1992, p. 427.
[233] O. Dumbrajs et al., Nucl. Phys. B 216 (1983) 2755.
[234] Z. Dziembowski, J. Franklin, Phys. Rev. D 42 (1990) 905 and references therein.
[235] O.J.P. Eboli, E.M. Gregores, F. Halzen, Talk presented at the 26th International Symposium on Multiparticle Dynamics, Faro, Portugal, 1996, Univeristy of Madison Report MADPH-96-965.
[236] A.V. Efremov, Sov. J. Nucl. Phys. 28 (1978) 83.
[237] A.V. Efremov, V.M. Korotkiyan, O.V. Teryaev, Phys. Lett. B 348 (1995) 577.
[238] A.V. Efremov, L. Mankiewicz, N.A. Törnquist, Phys. Lett. B 284 (1992) 394.
[239] A.V. Efremov, O.V. Teryaev, Sov. J. Nucl. Phys. 39 (1984) 962.
[240] A.V. Efremov, O.V. Teryaev, Phys. Lett. B 150 (1985) 383.
[241] A.V. Efremov, O.V. Teryaev, Dubna Report E2-88-287; published in: X. Fischer et al. (Eds.), Proceedings of the International Hadron Symposium, Bechyne, Czechoslowakia, 1988, Czech. Academy of Science, Prague, 1989, p. 302.
[242] A.V. Efremov, J. Soffer, O.V. Teryaev, Nucl. Phys. B 346 (1990) 97.
[243] A.V. Efremov, O.V. Teryaev, Phys. Lett. B 240 (1990) 200.
[244] A.V. Efremov, O.V. Teryaev, E. Leader, Phys. Rev. D 55 (1997) 4307.
[245] A.V. Efremov, J. Soffer, N.A. Törnqvist, Phys. Rev. D 44 (1991) 1369.
[246] B. Ehrnsperger, A. Schäfer, L. Mankiewicz, Phys. Lett. B 323 (1994) 439.
[247] B. Ehrnsperger, A. Schäfer, W. Greiner, L. Mankiewicz, Phys. Lett. B 321 (1994) 121.
[248] M.B. Einhorn, J. Soffer, Nucl. Phys. B 274 (1986) 714.
[249] J. Ellis, R.A. Flores, Nucl. Phys. B 307 (1988) 883.
[250] J. Ellis, R.A. Flores, Phys. Lett. B 263 (1991) 259.
[251] J. Ellis, R.A. Flores, Nucl. Phys. B 400 (1993) 25.
[252] J. Ellis, R.A. Flores, S. Ritz, Phys. Lett. B 198 (1987) 393.
[253] J. Ellis, R.L. Jaffe, Phys. Rev. D 9 (1974) 1444.
[254] J. Ellis, R.L. Jaffe, Phys. Rev. D 10 (1974) 1669, Erratum.
[255] J. Ellis, M. Karliner, Phys. Lett. B 213 (1988) 73.
[256] J. Ellis, M. Karliner, Phys. Lett. B 313 (1993) 131.
[257] J. Ellis, M. Karliner, in: J. Blümlein, W.-D. Nowak (Eds.), Proceedings of the Workshop on the Prospects of Spin Physics at HERA, DESY-Zeuthen, August 1995, DESY 95-200, p. 3.
[258] J. Ellis, M. Karliner, Phys. Lett. B 341 (1995) 397.
[259] U. Ellwanger, Phys. Lett. B 259 (1991) 469.
[260] U. Ellwanger, B. Stech, Phys. Lett. B 241 (1990) 409.
[261] U. Ellwanger, B. Stech, Z. Phys. C 49 (1991) 683.
[262] M. Erdmann, The Partonic Structure of the Photon, Tracts in Modern Physics, Vol. 138, Springer, Berlin, 1997.
[263] B.I. Ermolaev, S.I. Manayenkov, M.G. Ryskin, Z. Phys. C 69 (1996) 259.
[264] A. Faessler (Ed.), Prog. Part. Nucl. Phys. 34 (1995).
[265] J. Feltesse, F. Kunne, E. Mirkes, Karlsruhe preprint TTP96-29 (1996).
[266] R.P. Feynman, Photon Hadron Interactions, W.A. Benjamin/Addison Wesley Pub., New York, 1972.
[267] E.G. Floratos, C. Kounnas, R. Lacaze, Nucl. Phys. B 192 (1981) 417.

[268] D. de Florian et al., Phys. Rev. D 51 (1995) 37.
[269] D. de Florian, C.A. Garcia Canal, R. Sassot, Nucl. Phys. B 470 (1996) 195.
[270] D. de Florian, O.A. Sampayo, R. Sassot, Phys. Rev. D 57 (1998) 5803.
[271] D. de Florian, R. Sassot, Phys. Rev. D 51 (1995) 6052.
[272] D. de Florian, R. Sassot, Nucl. Phys. B 488 (1997) 367.
[273] J.R. Forshaw, R.G. Roberts, Phys. Lett. B 319 (1993) 539.
[274] S. Forte, Phys. Lett. B 224 (1989) 189.
[275] S. Forte, Nucl. Phys. B 331 (1990) 1.
[276] S. Forte, in: J. Blümlein, A. DeRoeck, T. Gehrmann, W.D. Nowak (Eds.), Proceedings of the Workshop on 'Deep Inelastic Scattering off Polarized Targets: Theory meets Experiment', DESY-Zeuthen, September 1997, DESY 97-200, p. 122.
[277] C. Foudas et al., (CCFR Collab.), Phys. Rev. Lett. 64 (1990) 1207.
[278] L.L. Frankfurt, M.I. Strikman, L. Mankiewicz, A. Schäfer, E. Rondio, A. Sandacz, V. Papavassiliou, Phys. Lett. B 230 (1989) 141.
[279] A. Freund, L.M. Sehgal, Phys. Lett. B 341 (1994) 90.
[280] J.L. Friar, B.F. Gibson, G.L. Payne, A.M. Bernstein, T.T. Chupp, Phys. Rev. C 42 (1990) 2310.
[281] H. Fritzsch, Phys. Lett. B 67 (1977) 217.
[282] H. Fritzsch, Phys. Lett. B 229 (1989) 122.
[283] H. Fritzsch, Phys. Lett. B 242 (1990) 451.
[284] H. Fritzsch, Mod. Phys. Lett. A 5 (1990) 625, 1815.
[285] H. Fritzsch, Phys. Lett. B 256 (1991) 75.
[286] S. Frixione, G. Ridolfi, Phys. Lett. B 383 (1996) 227.
[287] M. Fukugita, Y. Kuramashi, M. Okawa, A. Ukawa, Phys. Rev. Lett. 75 (1995) 2092.
[288] W. Furmanski, R. Petronzio, Z. Phys. C 11 (1982) 293.
[289] G.T. Garvey, W.C. Louis, D.H. White, Phys. Rev. C 48 (1993) 761.
[290] R. Gavai et al., Int. J. Mod. Phys. A 10 (1995) 3043.
[291] S.B. Gerasimov, Sov. J. Nucl. Phys. 2 (1966) 430.
[292] T. Gehrmann, Nucl. Phys. B 498 (1997) 245.
[293] T. Gehrmann, W.J. Stirling, Z. Phys. C 65 (1995) 461.
[294] T. Gehrmann, W.J. Stirling, Phys. Rev. D 53 (1996) 6100.
[295] H. Georgi, H.D. Politzer, Phys. Rev. D 9 (1974) 416.
[296] M. Glück, R.M. Godbole, E. Reya, Z. Phys. C 41 (1989) 667.
[297] M. Glück, L.E. Gordon, E. Reya, W. Vogelsang, Phys. Rev. Lett. 73 (1994) 388.
[298] M. Glück, J.F. Owens, E. Reya, Phys. Rev. D 17 (1978) 2324.
[299] M. Glück, E. Reya, Phys. Rev. D 14 (1976) 3034.
[300] M. Glück, E. Reya, Phys. Lett. B 79 (1978) 453.
[301] M. Glück, E. Reya, Nucl. Phys. B 145 (1978) 24.
[302] M. Glück, E. Reya, Phys. Rev. D 25 (1982) 1211.
[303] M. Glück, E. Reya, Phys. Rev. D 28 (1983) 2749.
[304] M. Glück, E. Reya, Univ. Dortmund Report DO-TH 87/14, August 1987.
[305] M. Glück, E. Reya, Z. Phys. C 39 (1988) 569.
[306] M. Glück, E. Reya, Z. Phys. C 43 (1989) 679.
[307] M. Glück, E. Reya, Phys. Lett. B 270 (1991) 65.
[308] M. Glück, E. Reya, M. Stratmann, Nucl. Phys. B 422 (1994) 37.
[309] M. Glück, E. Reya, M. Stratmann, W. Vogelsang, Phys. Rev. D 53 (1996) 4775.
[310] M. Glück, E. Reya, W. Vogelsang, Nucl. Phys. B 329 (1990) 347.
[311] M. Glück, E. Reya, W. Vogelsang, Nucl. Phys. B 351 (1991) 579.
[312] M. Glück, E. Reya, W. Vogelsang, Phys. Rev. D 45 (1992) 2552.
[313] M. Glück, E. Reya, W. Vogelsang, Phys. Lett. B 359 (1995) 201.
[314] M. Glück, E. Reya, A. Vogt, Z. Phys. C 48 (1990) 471.
[315] M. Glück, E. Reya, A. Vogt, Z. Phys. C 53 (1992) 127.

[316] M. Glück, E. Reya, A. Vogt, Phys. Rev. D 45 (1992) 3986.
[317] M. Glück, E. Reya, A. Vogt, Phys. Rev. D 46 (1992) 1973.
[318] M. Glück, E. Reya, A. Vogt, Phys. Lett. B 306 (1993) 391.
[319] M. Glück, E. Reya, A. Vogt, Z. Phys. C 67 (1995) 433.
[320] M. Glück, M. Stratmann, W. Vogelsang, Phys. Lett. B 337 (1994) 373.
[321] M. Glück, W. Vogelsang, Z. Phys. C 53 (1992) 695.
[322] M. Glück, W. Vogelsang, Z. Phys. C 55 (1992) 353.
[323] M. Glück, W. Vogelsang, Phys. Lett. B 277 (1992) 515.
[324] M. Glück, W. Vogelsang, Z. Phys. C 57 (1993) 309.
[325] R.M. Godbole, S. Gupta, K. Sridhar, Phys. Lett. B 255 (1991) 120.
[326] M. Göckeler et al., Phys. Rev. D 53 (1996) 2317.
[327] G.R. Goldstein, R.L. Jaffe, X. Ji, Phys. Rev. D 52 (1995) 5006.
[328] S.V. Goloskokov, O.V. Selyugin, Phys. Atom. Nucl. 58 (1995) 1894.
[329] J.E. Goodwin et al., Phys. Rev. Lett. 64 (1990) 2779.
[330] L.E. Gordon, Nucl. Phys. B 501 (1997) 197.
[331] L.E. Gordon, W. Vogelsang, Phys. Rev. D 50 (1994) 1901.
[332] L.E. Gordon, W. Vogelsang, Phys. Lett. B 387 (1996) 629.
[333] M. Gourdin, Nucl. Phys. B 38 (1972) 418.
[334] J.C. Gregory et al. (PHENIX Collab.), PHENIX Preliminary Conceptual Design Report, BNL-PROPOSAL-R2, June 1992.
[335] W. Grein, P. Kroll, Nucl. Phys. A 338 (1980) 332.
[336] K. Griest, Phys. Rev. D 38 (1988) 2357.
[337] D.J. Gross, C.H. Llewellyn-Smith, Nucl. Phys. B 14 (1969) 337.
[338] D.J. Gross, F. Wilczek, Phys. Rev. D 8 (1973) 3633.
[339] D.J. Gross, F. Wilczek, Phys. Rev. D 9 (1974) 980.
[340] J.P. Guillet, Z. Phys. C 39 (1988) 75.
[341] S. Gupta, D. Indumathi, M.V.N. Murthy, Z. Phys. C 42 (1989) 493.
[342] S. Gupta, D. Indumathi, M.V.N. Murthy, Z. Phys. C 44 (1989) 356, Erratum.
[343] S. Gupta, M.V.N. Murthy, J. Pasupathy, Phys. Rev. D 39 (1989) 2547.
[344] S. Gupta, J. Pasupathy, J. Szwed, Z. Phys. C 46 (1990) 111.
[345] S. Güllenstern, P. Gornicki, L. Mankiewicz, A. Schäfer, Phys. Rev. D 51 (1995) 3305.
[346] F. Halzen, S. Matsuda, Phys. Rev. D 17 (1978) 1344.
[347] N. Hammon, O.V. Teryaev, A. Schäfer, Phys. Lett. B 390 (1997) 409.
[348] J.W. Harris et al. (STAR Collab.), Nucl. Phys. A 566 (1994) 277c.
[349] J.A. Hassan, D.J. Pilling, Nucl. Phys. B 187 (1981) 563.
[350] T. Hatsuda, Nucl. Phys. B 329 (1990) 376.
[351] A. Hayashigaki, Y. Kanazawa, Y. Koike, Phys. Rev. D 56 (1997) 7350.
[352] H. He, X. Ji, Phys. Rev. D 52 (1995) 2960.
[353] R.L. Heimann, Nucl. Phys. B 64 (1973) 429.
[354] E.M. Henley, W.Y.P. Hwang, L.S. Kisslinger, Phys. Rev. D 46 (1992) 431.
[355] The HERMES Charm Upgrade Program, HERMES 97-004.
[356] A.J.G. Hey, J.E. Mandula, Phys. Rev. D 5 (1972) 2610.
[357] A.J.G. Hey, Daresbury Lecture Notes, Vol. 13, 1974, unpublished.
[358] I. Hinchliffe, A. Kwiatkowski, Ann. Rev. Nucl. Part. Sci. 46 (1996) 609.
[359] M. Hirai, S. Kumano, M. Miyama, Comput. Phys. Commun. 111 (1998) 150.
[360] H. Hogaasen, F. Myhrer, Z. Phys. C 68 (1995) 625.
[361] P. Hoodbhoy, R.L. Jaffe, A. Manohar, Nucl. Phys. B 312 (1989) 571.
[362] G. 't Hooft, M. Veltman, Nucl. Phys. B 44 (1972) 189.
[363] G. 't Hooft, Phys. Rev. Lett. 37 (1976) 8.
[364] H. Huang et al., Phys. Rev. Lett. 73 (1994) 2982.
[365] E.W. Hughes et al. (1993) SLAC proposal E154, October 1993.

[366] E. Hughes, SLAC-PUB 6439: XXI SLAC Summer Institute on 'Spin Structure in High Energy Processes' (1993), SLAC-Report-444 (1994).
[367] S. Incerti, F. Sabatie (E155 Collab.) Saclay report PCCF-RI-9901 (1999).
[368] D. Indumathi, Phys. Lett. B 374 (1996) 193.
[369] G. Ingelman, A. De Roeck, R. Klanner, Proceedings of the Workshop on Future Physics at HERA, Hamburg, 1996.
[370] B.L. Ioffe, ITEP (Moscow) 61-94, talk at the 22nd ITEP Winter School of Physics, Moscow, 1994.
[371] B.L. Ioffe, ITEP (Moscow) 62-95, talk at the Workshop 'The Spin Structure of the Nucleon', Erice, 1995.
[372] B.L. Ioffe, A. Khodjamirian, Phys. Rev. D 51 (1995) 3373.
[373] A.C. Irving, D.B. Newland, Z. Phys. C 6 (1980) 27.
[374] J.D. Jackson, G.G. Ross, R.G. Roberts, Phys. Lett. B 226 (1989) 159.
[375] R.L. Jaffe, Comm. Nucl. Part. Phys. 19 (1990) 239.
[376] R.L. Jaffe, Phys. Lett. B 365 (1996) 359.
[377] R.L. Jaffe, Phys. Rev. D 54 (1996) 6581.
[378] R.L. Jaffe, Proceedings of the 'Workshop on DIS off Polarized Targets: Theory Meets Experiment', DESY-Zeuthen, September 1997, DESY 97-200, p. 167.
[379] R.L. Jaffe, A. Manohar, Phys. Lett. B 223 (1989) 218.
[380] R.L. Jaffe, A. Manohar, Nucl. Phys. B 321 (1990) 343.
[381] R.L. Jaffe, A. Manohar, Nucl. Phys. B 337 (1990) 509.
[382] R.L. Jaffe, X. Ji, Phys. Rev. D 43 (1991) 724.
[383] R.L. Jaffe, X. Ji, Phys. Rev. Lett. 67 (1991) 552.
[384] R.L. Jaffe, X. Ji, Nucl. Phys. B 375 (1992) 527.
[385] R.L. Jaffe, X. Jin, J. Tang, Phys. Rev. Lett. 80 (1998) 1166.
[386] R.L. Jaffe, N. Saito, Phys. Lett. B 382 (1996) 165.
[388] E. Jenkins, Nucl. Phys. B 354 (1991) 24.
[389] X. Ji, Phys. Rev. Lett. 65 (1990) 408.
[390] X. Ji, Phys. Lett. B 284 (1992) 137.
[391] X. Ji, Phys. Lett. B 289 (1992) 137.
[392] X. Ji, Phys. Lett. B 309 (1993) 187, references therein.
[393] X. Ji, Nucl. Phys. B 402 (1993) 217.
[394] X. Ji, Phys. Rev. D 49 (1994) 114.
[395] X. Ji, Phys. Rev. Lett. 78 (1997) 610.
[396] X. Ji, Plenary talk given at the 12th International Symposium on High-Energy Spin Physics, Amsterdam, September 1996, University of Maryland report 97-042 (1997).
[397] X. Ji, Phys. Rev. D 55 (1997) 7114.
[398] X. Ji, J. Phys. G 24 (1998) 1181.
[399] X. Ji, C. Chou, Phys. Rev. D 42 (1990) 3637.
[400] X. Ji, W. Melnitchouk, Phys. Rev. D 56 (1997) R1.
[401] X. Ji, J. Tang, P. Hoodbhoy, Phys. Rev. Lett. 76 (1996) 740.
[402] X. Ji, P. Unrau, Phys. Lett. B 333 (1994) 228.
[403] L.M. Jones, H.W. Wyld, Phys. Rev. D 17 (1978) 2332.
[404] P. Kalyniak, M.K. Sundaresan, P.J.S. Watson, Phys. Lett. B 216 (1989) 397.
[405] B. Kamal, Phys. Rev. D 53 (1996) 1142.
[406] B. Kamal, A.P. Contogouris, Z. Merebashvili, Phys. Lett. B 376 (1996) 290.
[407] D.B. Kaplan, A. Manohar, Nucl. Phys. B 310 (1988) 527.
[408] G. Karl, Phys. Rev. D 45 (1992) 247.
[409] M. Karliner, R.W. Robinett, Phys. Lett. B 324 (1994) 209.
[410] J. Kaur, Nucl. Phys. B 128 (1977) 219.
[411] R. Kirschner, L. Mankiewicz, A. Schäfer, L. Szymanowski, Z. Phys. C 74 (1997) 501.
[412] N.I. Kochelev, T. Morii, T. Yamanishi, Phys. Lett. B 405 (1997) 168.
[413] J. Kodaira, Nucl. Phys. B 165 (1979) 129.

[414] J. Kodaira, S. Matsuda, K. Sasaki, T. Uematsu, Nucl. Phys. B 159 (1979) 99.
[415] J. Kodaira, S. Matsuda, M. Muta, T. Uematsu, K. Sasaki, Phys. Rev. D 20 (1979) 627.
[416] J. Kodaira, S. Matsuda, T. Uematsu, K. Sasaki, Phys. Lett. B 345 (1995) 527.
[417] J. Kodaira, Y. Yasui, T. Uematsu, Phys. Lett. B 344 (1995) 348.
[418] J. Kodaira, Y. Yasui, K. Tanaka, T. Uematsu, Phys. Lett. B 387 (1996) 855.
[419] J.G. Körner, D. Kreimer, K. Schilcher, Z. Phys. C 54 (1992) 503.
[420] J. Kogut, L. Susskind, Phys. Rev. D 9 (1974) 3391.
[421] Y. Koike, K. Tanaka, Phys. Rev. D 51 (1995) 6125.
[422] Y. Koike, N. Nishiyama, Phys. Rev. D 55 (1997) 3068.
[423] V.A. Korotkov, W.-D. Nowak, ELFE Workshop, St. Malo, 1996, DESY 97-004 (1997).
[424] A. Kotzinian, Nucl. Phys. B 441 (1995) 234.
[425] A.D. Krisch, Phys. Rev. Lett. 63 (1989) 1137.
[426] P. Kroll, M. Schürmann, P.A.M. Guichon, Nucl. Phys. A 598 (1996) 435.
[427] S. Kumano, M. Miyama, Phys. Rev. D 56 (1997) R2504.
[428] J. Kunz, P.J. Mulders, S. Pollok, Phys. Lett. B 222 (1989) 481.
[429] Z. Kunszt, Phys. Lett. B 218 (1989) 243.
[430] J. Kuti, V.F. Weisskopf, Phys. Rev. D 4 (1971) 3418.
[431] C.S. Lam, B.A. Li, Phys. Rev. D 25 (1982) 683.
[432] B. Lampe, Phys. Lett. B 227 (1989) 469.
[433] B. Lampe, Z. Phys. C 47 (1990) 105.
[434] B. Lampe, Fortschr. Phys. 43 (1995) 673.
[435] B. Lampe, Phys. Lett. B 371 (1996) 317.
[436] B. Lampe, A. Ruffing, Munich preprint MPI-PhT/97-14, hep-ph/9703308.
[437] S.A. Larin, Phys. Lett. B 303 (1993) 113.
[438] S.A. Larin, Phys. Lett. B 334 (1994) 192.
[439] S.A. Larin, J.A.M. Vermaseren, Phys. Lett. B 259 (1991) 345.
[440] E. Leader, E. Predazzi, An Introduction to Gauge Theories and the 'New Physics', Cambridge University Press, Cambridge, 1982.
[441] E. Leader, K. Sridhar, Phys. Lett. B 295 (1992) 283.
[442] E. Leader, K. Sridhar, Phys. Lett. B 311 (1993) 324.
[443] E. Leader, K. Sridhar, Nucl. Phys. B 419 (1994) 3.
[444] E. Leader, A.V. Sidorov, D.B. Stamenov, Phys. Rev. D 58 (1998) 114028.
[445] E. Leader, A.V. Sidorov, D.B. Stamenov, Int. J. Mod. Phys. A 13 (1998) 5573.
[446] E. Leader, A.V. Sidorov, D.B. Stamenov, Phys. Lett. B 445 (1998) 232.
[447] E.M. Levin, A.D. Martin, R.G. Roberts, M.G. Ryskin, Durham, preprint DTP/95/96, 1995.
[448] J. Lichtenstadt, H.J. Lipkin, Phys. Lett. B 353 (1995) 119.
[449] H.J. Lipkin, Phys. Lett. B 230 (1989) 135.
[450] H.J. Lipkin, Phys. Lett. B 256 (1991) 284.
[451] H.J. Lipkin, Phys. Lett. B 337 (1994) 157.
[452] K.F. Liu, Phys. Lett. B 281 (1992) 141.
[453] F.E. Low, Phys. Rev. 96 (1954) 1428.
[454] W. Lu, B.-Q. Ma, Phys. Lett. B 357 (1995) 419.
[455] W. Lu, B.-Q. Ma, Phys. Lett. B 373 (1996) 223.
[456] M. Lüscher, P. Weisz, Commun. Math. Phys. 97 (1985) 59.
[457] M. Lüscher, P. Weisz, Commun. Math. Phys. 98 (1985) 433, Erratum.
[458] J.E. Mandula, Phys. Rev. Lett. 65 (1990) 1403.
[459] J.E. Mandula, M.C. Ogilvie, Phys. Lett. B 312 (1993) 327.
[460] L. Mankiewicz, Phys. Rev. D 43 (1991) 64.
[461] L. Mankiewicz, Z. Ryzak, Phys. Rev. D 43 (1991) 733.
[462] L. Mankiewicz, A. Schäfer, Phys. Lett. B 242 (1990) 455.
[463] L. Mankiewicz, A. Schäfer, Phys. Lett. B 265 (1991) 167.

[464] L. Mankiewicz, E. Stein, A. Schäfer, in: J. Blümlein, W.-D. Nowa (Eds.), Proceedings of the Workshop on the 'Prospects of Spin Physics at HERA', DESY-Zeuthen, August 1995, DESY 95-200, p. 201.
[465] A.V. Manohar, Phys. Lett. B 219 (1989) 357.
[466] A.V. Manohar, Phys. Rev. Lett. 66 (1991) 289.
[467] F. Martin, Phys. Rev. D 19 (1979) 1382.
[468] A.D. Martin, R.G. Roberts, W.J. Stirling, Phys. Lett. B 354 (1995) 155.
[469] O. Martin, A. Schäfer, Z. Phys. A 358 (1997) 429.
[470] O. Martin, A. Schäfer, M. Stratmann, W. Vogelsang, Phys. Rev. D 57 (1998) 3084.
[471] P.M. Mathews, R. Ramachandran, Z. Phys. C 53 (1992) 305.
[472] P.M. Mathews, V. Ravindran, Phys. Lett. B 278 (1992) 175.
[473] P.M. Mathews, V. Ravindran, Int. J. Mod. Phys. A 7 (1992) 6371.
[474] P.M. Mathews, V. Ravindran, Mod. Phys. Lett. A 7 (1992) 2695.
[475] W. Melnitchouk, G. Piller, A.W. Thomas, Phys. Lett. B 346 (1995) 165.
[476] W. Melnitchouk, G. Piller, A.W. Thomas, DOE-ER-40762-071, Adelaide Univ., 1996.
[477] T. Meng, J. Pan, Q. Xie, W. Zhu, Phys. Rev. D 40 (1989) 769.
[478] R. Mertig, W.L. van Neerven, Z. Phys. C 70 (1996) 637.
[479] E. Mirkes, C. Ziegler, Nucl. Phys. B 429 (1994) 93.
[480] L. Montanet et al., Particle Data Group, Phys. Rev. D 50 (1994) 1173.
[481] A. Morales, J. Morales, J.A. Villar (Eds.), Proceedings of the International Workshop on Theoretical and Phenomenological Aspects of Underground Physics (TAUP 95), Toledo, Nucl. Phys. (Proc. Suppl.) 48 (1996).
[482] D. Müller, O.V. Teryaev, Phys. Rev. D 56 (1997) 2607.
[483] P.J. Mulders, in: Proceedings of the Workshop on the Prospects of Spin Physics at HERA, DESY-Zeuthen, August 1995, DESY 95-200, p. 208.
[484] P.J. Mulders, R.D. Tangerman, Phys. Lett. B 352 (1995) 129.
[485] O. Nachtmann, Nucl. Phys. B 127 (1977) 314.
[486] E. Nappi et al. (SMC Letter of Intent) (1995) CERN/SPSLC 95-27.
[487] S. Narison, G.M. Shore, G. Veneziano, Nucl. Phys. B 391 (1993) 69.
[488] S. Narison, G.M. Shore, G. Veneziano, Nucl. Phys. B 433 (1995) 209.
[489] C. Nash, Nucl. Phys. B 31 (1971) 419.
[490] V. Papavassiliou (EM Collab.), in: O. Bartner (Ed.), Proceedings of the EPS Conference on High Energy Physics, Uppsala, 1987, Vol. I, p. 441.
[491] P.V. Pobylitsa, M.V. Polyakov, Phys. Lett. B 389 (1996) 350.
[492] H.D. Politzer, Phys. Rep. 14 (1974) 129.
[493] J. Qiu, G.P. Ramsey, D. Richards, D. Sivers, Phys. Rev. D 41 (1990) 65.
[494] J. Qiu, G. Sterman, Phys. Rev. Lett. 67 (1991) 2264.
[495] J. Qiu, G. Sterman, Nucl. Phys. B 378 (1992) 52.
[496] S.A. Rabinowitz et al. (CCFR Collab.), Phys. Rev. Lett. 70 (1993) 134.
[497] A.V. Radyushkin, Phys. Lett. B 380 (1996) 417.
[498] A.V. Radyushkin, Phys. Rev. D 56 (1997) 5524.
[499] J.P. Ralston, D.E. Soper, Nucl. Phys. B 152 (1979) 109.
[500] G.P. Ramsey, D. Richards, D. Sivers, Phys. Rev. D 37 (1988) 3140.
[501] G.P. Ramsey, D. Richards, D. Sivers, Phys. Rev. D 43 (1988) 2861.
[502] G. Ranft, J. Ranft, Nucl. Phys. B 165 (1980) 395.
[503] P. Ratcliffe, Nucl. Phys. B 223 (1983) 45.
[504] P. Ratcliffe, Nucl. Phys. B 264 (1986) 493.
[505] P. Ratcliffe, Phys. Lett. B 192 (1987) 180.
[506] P. Ratcliffe, Univ. Milano preprint MITH 91/18, 1991.
[507] V. Ravishankar, Phys. Lett. B 223 (1989) 225.
[508] V. Ravishankar, Nucl. Phys. B 374 (1992) 309.
[509] E. Reya, Phys. Rep. 69 (1981) 195.

[510] E. Reya, in: P.M. Zerwas, H.A. Kastrup (Eds.), 'QCD-20 Years Later', Aachen, 1992, World Scientific, Singapore, 1992, p. 272.
[511] E. Reya, Schladming lectures, 1993, Lecture Notes in Physics, Springer, Berlin, Vol. 426, p. 175.
[512] R.G. Roberts, The Structure of the Proton, Cambridge University Press, Cambridge, 1990.
[513] R.W. Robinett, Phys. Rev. D 45 (1992) 2563.
[514] T. Roser, Nucl. Instr. Meth. A 342 (1993) 343.
[515] G.G. Ross, R.G. Roberts, Rutherford Lab. RAL-90-062, unpublished.
[516] M.G. Ryskin, Z. Phys. C 57 (1993) 89.
[517] M.G. Ryskin, Phys. Lett. B 403 (1997) 335.
[518] Z. Ryzak, Phys. Lett. B 217 (1989) 325.
[519] A. Saalfeld, A. Schäfer, Phys. Rev. D 57 (1998) 3017.
[520] K. Sasaki, Prog. Theor. Phys. 54 (1975) 1816.
[521] A. Schäfer, Z. Phys. C 56 (1992) S179.
[522] D. Schaile, in: P.J. Bussey, I.G. Knowles (Eds.), Proceedings of the XXVII International Conference in High Energy Physics, Glasgow, July 1994, p. 27.
[523] J. Schechter, V. Soni, A. Subbaraman, H. Weigel, Mod. Phys. Lett. A 7 (1992) 1, and earlier work quoted therein.
[524] I. Schmidt, J. Soffer, Phys. Lett. B 407 (1997) 331.
[525] A.W. Schreiber, A.I. Signal, A.W. Thomas, Phys. Rev. D 44 (1991) 2653.
[526] G.A. Schuler, CERN-TH/95-75.
[527] G.A. Schuler, R. Vogt, Phys. Lett. B 387 (1996) 181.
[528] S. Scopetta, V. Vento, Phys. Lett. B 424 (1998) 25.
[529] L.M. Sehgal, Phys. Rev. 10 (1974) 1663.
[530] L.M. Sehgal, Phys. Rev. D 11 (1974) 2016, Erratum.
[531] G.M. Shore, G. Veneziano, Phys. Lett. B 244 (1990) 75.
[532] G.M. Shore, G. Veneziano, Nucl. Phys. B 381 (1992) 23.
[533] E.V. Shuryak, A.I. Vainshtein, Nucl. Phys. B 201 (1982) 141.
[534] D. Sivers, Phys. Rev. D 41 (1990) 83.
[535] D. Sivers, Phys. Rev. D 43 (1991) 261.
[536] D. Sivers, Phys. Rev. D 51 (1995) 4880.
[537] D. Sivers, Proceedings of the 'Workshop on DIS off Polarized Targets: Theory Meets Experiment', DESY-Zeuthen, September 1997, DESY 97-200, p. 383.
[538] J. Soffer, Phys. Rev. Lett. 74 (1995) 1292.
[539] J. Soffer, O.V. Teryaev, Phys. Rev. Lett. 70 (1993) 3373.
[540] J. Soffer, O.V. Teryaev, Phys. Rev. D 56 (1997) R1353.
[541] J. Soffer, J.M. Virey, Nucl. Phys. B 509 (1998) 297.
[542] X. Song, J.S. McCarthy, Phys. Rev. D 49 (1994) 3169.
[543] X. Song, J.S. McCarthy, Phys. Rev. D 50 (1994) 4718, Erratum.
[544] X. Song, Phys. Rev. D 54 (1996) 1955.
[545] X. Song, P.K. Kabir, J.S. McCarthy, Phys. Rev. D 54 (1996) 2108.
[546] K. Sridhar, E. Leader, Phys. Lett. B 295 (1992) 283.
[547] E. Steffens, K. Zapfe–Düren (1995) in: J. Blümlein, W.D. Nowak (Eds.), Proceedings of the Workshop on the 'Prospects of Spin Physics at HERA', DESY-Zeuthen, August 1995, DESY 95-200, p. 57.
[548] E. Stein, P. Gornicki, L. Mankiewicz, A. Schäfer, W. Greiner, Phys. Lett. B 343 (1995) 369.
[549] U. Stiegler, Phys. Rep. 277 (1996) 1.
[550] M. Stratmann, Z. Phys. C 60 (1993) 763.
[551] M. Stratmann in: J. Blümlein, A. De Roeck, T. Gehrmann, W.D. Nowak (Eds.), Proceedings of the Workshop on 'Deep Inelastic Scattering off Polarized Targets: Theory meets Experiment', DESY-Zeuthen, September 1997, DESY 97-200, p. 94.
[552] M. Stratmann, W. Vogelsang, Phys. Lett. B 295 (1992) 277.

[553] M. Stratmann, W. Vogelsang, in: G. Ingelman, A. De Roeck, R. Klanner (Eds.), Proceedings of the Workshop on Future Physics at HERA, Hamburg 1995/96, Vol. 2, p. 815.
[554] M. Stratmann, W. Vogelsang, Z. Phys. C 74 (1997) 641.
[555] M. Stratmann, W. Vogelsang, Phys. Lett. B 386 (1996) 370.
[556] M. Stratmann, W. Vogelsang, Nucl. Phys. B 496 (1997) 41.
[557] M. Stratmann, A. Weber, W. Vogelsang, Phys. Rev. D 53 (1996) 138.
[558] K. Symanzik, Nucl. Phys. B 226 (1983) 187, 205.
[559] S. Tartur, J. Bartelski, M. Kurzela, Univ. Warsaw Report, hep-ph/9903411, 1999.
[560] O.V. Teryaev, Proceedings of the Workshop on the Prospects of Spin Physics at HERA, DESY-Zeuthen, August 1995, DESY 95-200, p. 132.
[561] A.W. Thomas, Univ. Adelaide ADP-94-21/T161, 1994, invited talk at the 'SPIN 94' Conference, Bloomington, 1994.
[562] M.V. Tokarev, Phys. Lett. B 318 (1993) 559.
[563] M. Vanderhaeghen, P.A.M. Guichon, M. Guidal, Saclay Report, hep-ph/9905372, 1999.
[564] G. Veneziano, Mod. Phys. Lett. A 4 (1989) 1605.
[565] W. Vogelsang, Z. Phys. C 50 (1991) 275.
[566] W. Vogelsang, Diploma Thesis, University of Dortmund, 1990.
[567] W. Vogelsang, Ph.D. Thesis, University of Dortmund DO-TH 93/28, 1993, unpublished.
[568] W. Vogelsang, Phys. Rev. D 54 (1996) 2023.
[569] W. Vogelsang, Nucl. Phys. B 475 (1996) 47.
[570] W. Vogelsang, Phys. Rev. D 57 (1998) 1886.
[571] W. Vogelsang, A. Weber, Nucl. Phys. B 362 (1991) 3.
[572] W. Vogelsang, A. Weber, Phys. Rev. D 45 (1992) 4069.
[573] W. Vogelsang, A. Weber, Phys. Rev. D 48 (1993) 2073.
[574] R. Voss, Experiments on Polarized Deep Inelastic Scattering, invited talk at the Workshop on Deep Inelastic Scattering and QCD, Paris, April 1995 (CERN report).
[575] M. Wakamatsu, Phys. Lett. B 280 (1992) 97.
[576] S. Wandzura, F. Wilczek, Phys. Lett. B 72 (1977) 195.
[577] A.D. Watson, Z. Phys. C 12 (1982) 123.
[578] A. Weber, Nucl. Phys. B 382 (1992) 63.
[579] A. Weber, Nucl. Phys. B 403 (1993) 545.
[580] H. Weigel, L. Gamberg, H. Reinhardt, Phys. Lett. B 399 (1997) 287.
[581] T. Weigl, W. Melnitchouk, Nucl. Phys. B 465 (1996) 267.
[582] R.M. Woloshyn, Nucl. Phys. A 496 (1988) 749.
[583] Z. Xu, Phys. Rev. D 30 (1984) 1440.
[584] A. Yokosawa et al. (E581/704 Collab.), Fermilab Report 91 (1991) 10-17.
[585] A. Yokosawa, Argonne report ANL-HEP-CP-94-70 (1994), Proceedings of the 11th International Symposium on High Energy Spin Physics and Eighth International Symposium on Polarization Phenomena in Nuclear Physics, Indiana University, Bloomington.
[586] E.B. Zijlstra, W.L. van Neerven, Nucl. Phys. B 417 (1994) 61.